Novel findings to the function and mechanism of the major autolysin (Atl) in staphylococci and excretion of cytoplasmic proteins

Dissertation

der Mathematisch-Naturwissenschaftlichen Fakultät

der Eberhard Karls Universität Tübingen

zur Erlangung des Grades eines

Doktors der Naturwissenschaften

(Dr. rer. nat)

Vorgelegt von

Mulugeta Nega

aus Addis Abeba / Äthiopien

Tübingen

2020

Gedruckt mit Genehmigung der Mathematisch-Naturwissenschaftlichen Fakultät der Eberhard Karls Universität Tübingen.

Tag der mündlichen Qualifikation: 18.06.2020

Dekan:	Prof. Dr. Wolfgang Rosenstiel
1. Berichterstatter:	Prof. Dr. Friedrich Götz
2. Berichterstatter:	Prof. Dr. Andreas Peschel

† In memory of my late father Nega Zemene, who used to call me “Doktor”.

Table of contents

Abbreviations and symbols

Abbreviations

aa	Amino acids
Amp	Ampicillin
bp	Base pair
cw	Cell wall
Cy5	Cyanine dye (product name)
DNA	Deoxyribonucleic acid
DNase	Deoxyribonuclease
eDNA	extracellular DNA
EDTA	Ethylenediamine tetraacetic acid
FITC	Fluorescein isothiocyanate
g	Gram
GlcNac	N-acetyl glucosamine
GST	Glutathione-S-transferase
h	Hour
HPLC	High performance liquid chromatography
IPTG	Isopropyl-β-thiogalactoside
l	Litre
LTA	Lipoteichoic acid
k	Kilo
kb	Kilo-base
kDa	Kilo-dalton
M	Molar
m	Milli
min	Minute
MurNac	N-acetyl muramic acid
MW	Molecular weight
Ni-NTA	Nickel-nitrilotriacetic acid
PAGE	Polyacrylamide gel electrophoresis
PCR	Polymerase chain reaction
PGN	Peptidoglycan
PGH	Peptidoglycan hydrolase
rpm	Rotation per minute
RT	Room temperature
SAXS	Small angle X-ray scattering
SDS	Sodium dodecyl sulphate
sp.	Species
WT	Wild-type
WTA	Wall teichoic acid
PAM_3CSK_4	Palmitoyl-Cys((*RS*)-2,3-di(palmitoyloxy)-propyl)-OH
Nod1/2	Nucleotide-binding oligomerization domain 1/2
TLR	Toll like receptor

symbols

Å	Angstrom
°	Degree
Δ	Genetic mutation
μ	micro
%	Percent
L	Wavelength
::	insertion

Summary

The staphylococcal peptidoglycan (PGN) is a major and essential component of the cell wall. It is a dynamic structure that undergoes constant cycles of polymerization and hydrolysis which is carried out by transglycosylases/peptidases and PGN hydrolases. The major autolysin, Atl, is the most predominant PGN hydrolase in staphylococci. Though its structure and function have been studied extensively, little is known about the activity and interplay of its domains AmiA and GlcA during cell division and separation.

With this study, a highly resolved complex structure of the catalytic amidase domain of *S. aureus* Atl was elucidated. Moreover, its specific molecular ligand interaction mechanism and natural substrate specificity was resolved. Investigating the deletion mutants of both *AmiA* and *GlcA,* as well as *Atl* revealed that each of the enzymes plays a significant role in cell aggregation, proper septum formation and cell separation. Notably, loss of GlcA activity results in aberrant septum formation manifested by deformed and in part “kidney” like cell clusters. Despite a lowered peptidoglycan crosslinking, the Δ*atl*, Δ*amiA* und Δ*glcA* mutants were 10,000 to 100,000 times more tolerant to oxacillin than the parent strain.

For the first time, this work shows the activity of both AmiA and GlcA on their natural substrate, PGN. We found out that AmiA activity is specific to its host PGN while the naked glycan backbone is the natural substrate of GlcA. Our results revealed that the resolution of PGN during cell separation occurs in a defined order, in which AmiA first hydrolyzes the crosspeptides, followed by GlcA chewing back the naked glycan and releasing disaccharides. Additionally, we disproved the hitherto conclusion and showed that GlcA is not an *endo*- but an *exo*-β-N-acetylglucosaminidase.

One of the crucial steps in staphylococcal PGN biosynthesis is the addition of the five glycine residues to the stem peptide by the non-ribosomal peptidyl transferases FemA, FemB and FemX. In the second part of this thesis, we have examined the effects of a *femB* deletion and the consequent alteration of the cell wall structure of *S. carnosus* and its effect on the morphology, physiology and antibiotic susceptibility of the

organism. We have found out that shortening of the interpeptide bridge from five to three glycine residues poses a life-threatening problem for the organism leading to expanded cells, retarded growth, reduced peptidoglycan crosslinking, high susceptibility to cell wall antibiotics and surprisingly high secretion and release of proteins into the culture supernatant. This led us to further investigate the excretion pattern of cytoplasmic proteins in the pathogenic *S. aureus*. As a result, we were able to show that the main excretion of cytoplasmic proteins takes place at the septum mainly during the exponential growth phase and that they are significant factors in staphylococcal pathogenicity.

Zusammenfassung

Peptidoglycan (PGN) ist ein wichtiger und essenzieller Bestandteil der Zellwand von Staphylokokken. Es ist eine dynamische Struktur, die konstante Polymerisations- und Hydrolysezyklen durchläuft, die hauptsächlich von PGN-Transglycosylasen/ Peptidasen bzw PGN-Hydrolasen durchgeführt werden. Das Hauptautolysin Atl ist die prominente PGN-Hydrolase in Staphylokokken, deren Struktur und Funktion bereits ausführlich untersucht wurden. Trotzdem ist bisher wenig über die genaue Aktivität und das Zusammenspiel der Enzymdomänen AmiA und GlcA während der Zellteilung und -trennung bekannt.

Im Rahmen dieser Arbeit konnte die komplexe Struktur der katalytischen Amidasedomäne von *S. aureus* Atl hochaufgelöst dargestellt werden. Darüber hinaus wurden der spezifische Mechanismus der Wechselwirkung mit molekularen Liganden und die natürliche Substratspezifität aufgeklärt. Die Erzeugung und Untersuchung von *amiA*-, *glcA*- und *atl*-Deletionsmutanten ergab, dass jedes der zugehörigen Enzyme eine signifikante Rolle bei der Zellaggregation, der korrekten Septumbildung und der Zelltrennung spielt. Insbesondere führt der Verlust der GlcA-Aktivität zu einer aberranten Septumbildung, die sich in deformierten und teilweise „nierenähnlichen“ Zellclustern manifestiert. Trotz einer verringerten Peptidoglykanvernetzung waren die *Δatl*-, Δ*amiA*- und *ΔglcA*-Mutanten 10.000- bis 100.000-mal toleranter gegenüber Oxacillin als der Ausgangsstamm.

Diese Arbeit zeigt erstmalig die Wirkungsweise von AmiA und GlcA an ihrem natürlichen Substrat PGN. Wir konnten darlegen, dass AmiA spezifisch am Wirts-PGN agiert und der nackte Glykanstrang das natürliche Substrat von GlcA darstellt. Unsere Ergebnisse zeigen weiterhin, dass die Auflösung von PGN während der Zelltrennung in einer definierten Reihenfolge erfolgt, bei der zunächst von AmiA das Stammpeptid hydrolysiert wird und anschließend von GlcA das nackte Glykan zurückgeschnitten wird, so dass Disaccharide freigesetzt werden. Zusätzlich konnten wir zeigen, dass GlcA eine *exo*-beta-N-Acetylglucosaminidase ist und damit die bisherige Annahme, es handele sich um eine *endo*-beta-N-Acetylglucosaminidase, widerlegen.

Einer der wichtigen Schritte bei der PGN-Biosynthese von Staphylokokken ist die Anknüpfung der fünf Glycinreste an das Stammpeptid durch die nicht-ribosomalen Peptidyltransferasen FemA, FemB und FemX. Im zweiten Teil dieser Arbeit haben wir die Effekte einer *femB*-Deletion , insbesondere die daraus resultierende Veränderung der Zellwandstruktur von *S. carnosus* sowie deren Auswirkungen auf die Morphologie, Physiologie und Antibiotikasuszeptibilität untersucht. Wir konnten zeigen, dass die Verkürzung der Interpeptidbrücke von fünf auf drei Glycinreste ein lebensbedrohliches Problem für den Organismus darstellt und zu expandierten Zellen, verzögertem Wachstum, verringerter Peptidoglykanvernetzung und hoher Anfälligkeit für Zellwandantibiotika führt. Außerdem konnten wir, überraschenderweise deutlich höhere Mengen an sekretierten und freigesetzten cytoplasmatischen Proteinen im Kulturüberstand der untersuchten Mutanten nachweisen. Dies führte uns dazu, das Sekretionsmuster der cytoplasmatischen Proteine im pathogenen *S. aureus* näher zu untersuchen. Wir konnten zeigen, dass die Sekretion von cytoplasmatischen Proteinen überwiegend am Septum und hauptsächlich während der exponentiellen Wachstumsphase stattfindet und diese sekretierten Proteine wichtige Faktoren für die Pathogenität von Staphylokokken darstellen.

List of publications and personal contributions

Accepted publications

This thesis is based on the following publications and manuscripts.

Publication 1:

Büttner, F. M., Zoll, S., **Nega, M.**, Götz, F., & Stehle, T. (2014). Structure function analysis of *Staphylococcus aureus* amidase reveals the determinants of peptidoglycan recognition and cleavage. *J. Biol. Chem.* **289**, 11083-11094.

Personal contributions:

Experimental design, activity determination, substrate specificity analysis, HPLC method development and analysis, contribution to manuscript preparation.

Publication 2:

Nega, M., Dube, L., Kull, M., Ziebandt, A. K., Ebner, P., Albrecht, D., Krismer, B., Rosenstein, R., Hecker, M., & Götz, F. (2015) Secretome analysis revealed adaptive and non-adaptive responses of the *Staphylococcus carnosus* femB mutant. *Proteomics* **15**: 1268-1279.

Personal contributions:

Experimental design, cell wall isolation and purification, antimicrobial susceptibility determination, cell wall analysis, enzyme susceptibility determination, HPLC method development and analysis, manuscript preparation.

Publication 3:

Ebner, P., Prax, M., **Nega, M.**, Koch, I., Dube, L., Yu, W., Rinker, J., Popella, P., Flotenmeyer, M., & Götz, F. (2015) Excretion of cytoplasmic proteins (ECP) in *Staphylococcus aureus*. *Mol Microbiol* **97**: 775-789.

Personal contributions:

Peptidoglycan isolation preparation and digestion, peptidoglycan binding assay, LysM domain binding studies, PAGE analysis, contribution to manuscript preparation.

Publication 4:

Ebner, P., Rinker, J., Nguyen, M. T., Popella, P., **Nega, M.**, Luqman, A., Schittek, B., Di Marco, M., Stevanovic, S., & Götz F. (2016) Excreted Cytoplasmic Proteins Contribute to Pathogenicity in *Staphylococcus aureus*. *Infect Immun* **84**: 1672-1681.

Personal contributions:

Isolation and purification of recombinant Atl-amidase, Atl-N-acetylglucosaminidase and Atl-R1,2 repeat domains. Binding studies of Atl domains with FbaA and GapDH, contribution to manuscript preparation.

Publication 5:

Nega, M., Tribelli, P.M., Hipp, K. *et al.* New insights in the coordinated amidase and glucosaminidase activity of the major autolysin (Atl) in *Staphylococcus aureus*. *Commun Biol* **3,** 695 (2020). https://doi.org/10.1038/s42003-020-01405-2

Personal contributions:

Study design, experimental design, construction of all plasmids and mutants (except Atl complementation plasmid), all chromatographic analyses, MS analysis of disaccharides, purification of enzymes, enzyme-substrate digestion studies, manuscript preparation.

List of publications not included in this thesis

1. Pasztor L, Ziebandt AK, **Nega M**, Schlag M, Haase S, Franz-Wachtel M, Madlung J, Nordheim A, Heinrichs DE, Götz F: **Staphylococcal major autolysin (Atl) is involved in excretion of cytoplasmic proteins**. *J Biol Chem* 2010, **285**(47):36794-36803.

2. Volz T, **Nega M**, Buschmann J, Kaesler S, Guenova E, Peschel A, Rocken M, Götz F, Biedermann T: **Natural Staphylococcus aureus-derived peptidoglycan fragments activate NOD2 and act as potent costimulators of the innate immune system exclusively in the presence of TLR signals**. *FASEB J* 2010, **24**(10):4089-4102.

3. Muller-Anstett MA, Muller P, Albrecht T, **Nega M**, Wagener J, Gao Q, Kaesler S, Schaller M, Biedermann T, Götz F: **Staphylococcal peptidoglycan co-localizes with Nod2 and TLR2 and activates innate immune response via both receptors in primary murine keratinocytes**. *PLoS One* 2010, **5**(10):e13153.

4. Saising J, Dube L, Ziebandt AK, Voravuthikunchai SP, **Nega M**, Götz F: **Activity of gallidermin on Staphylococcus aureus and Staphylococcus epidermidis biofilms**. *Antimicrob Agents Chemother* 2012, **56**(11):5804-5810.

5. Krismer B, **Nega M**, Thumm G, Götz F, Peschel A: **Highly efficient Staphylococcus carnosus mutant selection system based on suicidal bacteriocin activation**. *Appl Environ Microbiol* 2012, **78**(4):1148-1156.

6. Towhid ST, **Nega M**, Schmidt EM, Schmid E, Albrecht T, Munzer P, Borst O, Götz F, Lang F: **Stimulation of platelet apoptosis by peptidoglycan from Staphylococcus aureus 113**. *Apoptosis* 2012, **17**(9):998-1008.

7. Bertsche U, Yang SJ, Kuehner D, Wanner S, Mishra NN, Roth T, **Nega M**, Schneider A, Mayer C, Grau T *et al*: **Increased cell wall teichoic acid production and D-alanylation are common phenotypes among daptomycin-resistant methicillin-resistant Staphylococcus aureus (MRSA) clinical isolates**. *PLoS One* 2013, **8**(6):e67398.

8. Chu YY, **Nega M**, Wolfle M, Plener L, Grond S, Jung K, Götz F: **A new class of quorum quenching molecules from Staphylococcus species affects communication and growth of gram-negative bacteria**. *PLoS Pathog* 2013, **9**(9):e1003654.

9. Krismer B, Liebeke M, Janek D, **Nega M**, Rautenberg M, Hornig G, Unger C, Weidenmaier C, Lalk M, Peschel A: **Nutrient limitation governs Staphylococcus aureus metabolism and niche adaptation in the human nose**. *PLoS Pathog* 2014, **10**(1):e1003862.

10. Schuster S, Yu W, **Nega M**, Chu YY, Zorn S, Zhang F, Götz F, Schreiber F: **The role of serum proteins in Staphylococcus aureus adhesion to ethylene glycol coated surfaces**. *Int J Med Microbiol* 2014, **304**(8):949-957.

11. Feng X, Hu Y, Zheng Y, Zhu W, Li K, Huang CH, Ko TP, Ren F, Chan HC, **Nega M** *et al*: **Structural and functional analysis of Bacillus subtilis YisP reveals a role of its product in biofilm production**. *Chem Biol* 2014, **21**(11):1557-1563.

12. Pozzi R, Coles M, Linke D, Kulik A, **Nega M**, Wohlleben W, Stegmann E: **Distinct mechanisms contribute to immunity in the lantibiotic NAI-107 producer strain Microbispora ATCC PTA-5024**. *Environ Microbiol* 2016, **18**(1):118-132.

13. Nguyen MT, Deplanche M, Nega M, Le Loir Y, Peisl L, Götz F, Berkova N: **Staphylococcus aureus Lpl Lipoproteins Delay G2/M Phase Transition in HeLa Cells**. *Front Cell Infect Microbiol* 2016, **6**:201.

14. Popella P, Krauss S, Ebner P, **Nega M**, Deibert J, Götz F: **VraH Is the Third Component of the Staphylococcus aureus VraDEH System Involved in Gallidermin and Daptomycin Resistance and Pathogenicity**. *Antimicrob Agents Chemother* 2016, **60**(4):2391-2401.

15. Luqman A, **Nega M**, Nguyen MT, Ebner P, Götz F: **SadA-Expressing Staphylococci in the Human Gut Show Increased Cell Adherence and Internalization**. *Cell Rep* 2018, **22**(2):535-545.

16. Ernst CM, Slavetinsky CJ, Kuhn S, Hauser JN, **Nega M**, Mishra NN, Gekeler C, Bayer AS, Peschel A: **Gain-of-Function Mutations in the Phospholipid Flippase MprF Confer Specific Daptomycin Resistance**. *mBio* 2018, **9**(6).

17. Reichert S, Ebner P, Bonetti EJ, Luqman A, **Nega M**, Schrenzel J, Sproer C, Bunk B, Overmann J, Sass P *et al*: **Genetic Adaptation of a Mevalonate Pathway Deficient Mutant in Staphylococcus aureus**. *Front Microbiol* 2018, **9**:1539.

18. Schlatterer K, Beck C, Hanzelmann D, Lebtig M, Fehrenbacher B, Schaller M, Ebner P, **Nega M**, Otto M, Kretschmer D *et al*: **The Mechanism behind Bacterial Lipoprotein Release: Phenol-Soluble Modulins Mediate Toll-Like Receptor 2 Activation via Extracellular Vesicle Release from Staphylococcus aureus**. *mBio* 2018, **9**(6).

19. Nguyen MT, Saising J, Tribelli PM, **Nega M**, Diene SM, Francois P, Schrenzel J, Sproer C, Bunk B, Ebner P *et al*: **Inactivation of farR Causes High Rhodomyrtone Resistance and Increased Pathogenicity in Staphylococcus aureus**. *Front Microbiol* 2019, **10**:1157.

Chapter I

Elucidation of the structure, activity and functional mechanism of the amidase and glucosaminidase domains of the major autolysin (Atl) of *Staphylococcus aureus*

Introduction

Staphylococcal cell wall

Staphylococcus aureus is a Gram-positive commensal bacterium that dwells on the human skin and in nasal passages. It is an important human pathogen causing hospital- and community-acquired infections, such as serious skin infections, endocarditis, osteomyelitis and toxic shock syndrome.

The cell wall of *S. aureus,* and bacteria in general, is a complex weave of macromolecular components holding the bacterial cell intact while enabling it to grow, divide and stay motile. It is an essential structure that protects the cell from mechanical damage, thermal and chemical change in the environment as well as internal and external osmotic rupture. The constituting macromolecules are mostly the peptidoglycan, teichoic acids, various polysaccharides and proteins. *S. aureus* has a typical Gram-positive cell envelope, which consists of a cytoplasmic membrane surrounded by a thick peptidoglycan layer. It is typically 20 to 30 nm thick and is characterized by short linear glycan strands of 5 to 25 disaccharide units [3] stacked to 20-40 layers and cross linked by peptides. The staphylococcus peptidoglycan is unique in that it shows a very high degree of cross-linking determined as a ratio of bridged peptides to the total amount of all peptide. It lies in general in the order of 80 to 90% and makes up to 40% of cell dry mass [1, 4]. In order for the bacteria to grow and divide, the peptidoglycan layer stays as a dynamic macromolecular structure undergoing constant cycles of polymerization and hydrolysis [5]. The staphylococcal

cell wall is not only essential for its survival and pathogenesis but is also a virulence factor during infection and primary target of a number of important cell wall acting antimicrobials.

Structure and biosynthesis of the staphylococcus peptidoglycan

Peptidoglycan of *S. aureus* is composed of a linear glycan polymer made up of repeating N-acetylmuramic acid (MurNAc) and N-acetylglucosamine (GlcNAc) linked via a β-1,4-linkage. The D-lactoyl group of each of the MurNAc is amide-linked to a pentapeptide unit unique to staphylococci. This stem peptide is composed of L-Ala-D-Glu-L-Lys-D-Ala-D-Ala where the α-carboxyl group of the D-glutamic acid is amidated [6, 7]. Neighboring stem peptides are cross-linked between the ε-amino group of L-Lys and the carboxyl group of D-Ala at position 4 of the next stem peptide via pentaglycine cross bridges detaching the D-Ala at position 5 by D,D-Decarboxylases in the process.

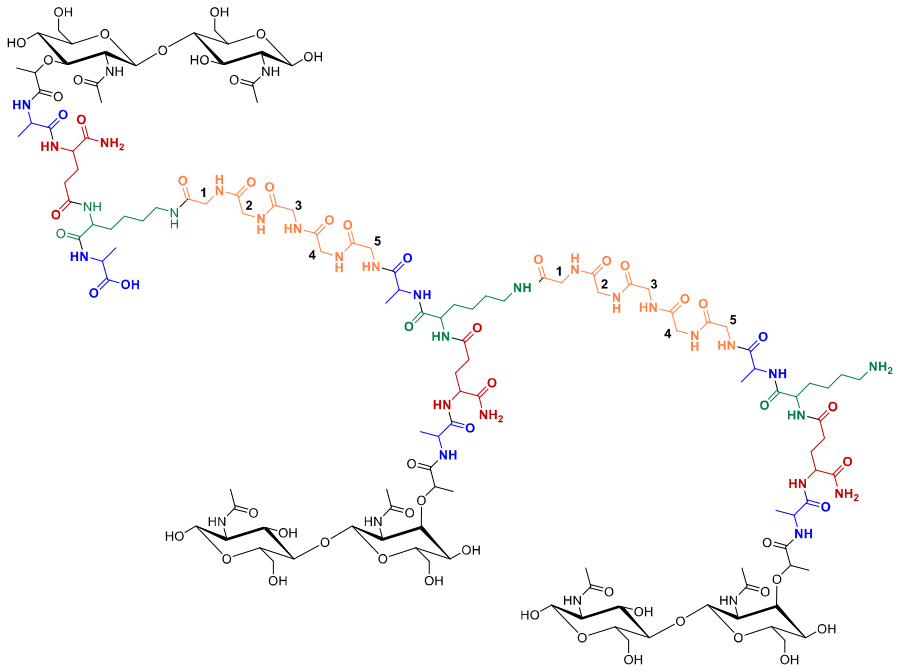

moiety. The stem peptide is further cross-linked between the ε-amino group of its L-Lys and the carboxyl group of D-Ala of the next stem peptide via a pentaglycine cross bridge. This interconnection of the glycan strands and cross-linked wall peptides makeup the three-dimensional exoskeletal network of peptidoglycan.

Staphylococcal PGN biosynthesis starts in the cytoplasm and proceeds in distinct enzymatic catalysis involving various substrates and steps (Fig. 2). The first step starts with the synthesis of glucosamine-6-phosphate (GlcN6P) by the aminotransferase GlmS through conversion of fructose-6- phosphate (F6P) into GlcN6P. GlcN6P is processed to *N*-acetylglucosamine uridyl diphosphate (UDP-GlcNAc) by the phosphoglucosamine mutase GlmM and the uridyltransferase GlmU [8] In the following step, MurA – catalyzes the transfer of enolpyruvate from phosphoenolpyruvate to the C3 hydroxyl of UDP-GlcNAc (Marquardt et al. 1992) whereas MurB reduces the C3 enolate to the lactate, resulting in formation of UDP-MurNAc [9].

Subsequently, the Mur ligases MurC, MurD and MurE sequentially add the amino acids L-Ala, D-Glu, and L-Lys to UDP-MurNAc. The last D-Ala-D-Ala dipeptide is made by the combined action of an L-Ala racemase, Alr, that converts L-Ala to D-Ala and a D-Ala-D-Ala ligase, Ddl, that binds the two amino acids, and is added by the MurF ligase to the UDP-tripeptide. In these steps, the Mur ligases use ATP to activate the amino acids and provide the necessary energy for coupling, since formation of peptide bonds is not a thermodynamically favorable reaction [10, 11]. The product, UDP-MurNAc-L-Ala-D-Glu-L-Lys-D-Ala-D-Ala, which is also known as Park's nucleotide is then linked to the lipid carrier undecaprenyl-diphosphate by MraY, the membrane translocase, yielding membrane-bound lipid I [12-14]. The membrane anchored Lipid I is then linked to UDP-GlcNAc by the membrane glycosyltransferase MurG resulting in the undecaprenyl-diphosphate-GlcNAc-MurNAc-pentapeptide, lipid II [15, 16].

In *S. aureus*, lipid II is further modified by the addition of five glycine residues catalyzed by the FemX, FemA and FemB proteins. These non-ribosomal peptidyl-transferases utilize glycyl-tRNA donors to sequentially add the five glycines to the PGN-lysyl side chain of lipid II. FemX adds the first glycine, FemA the next two and FemB adds last two glycyl units completing the pentapeptide side chain [17-20]. The Lipid II goes through further modification by amidation of the α-carboxylate of iso-glutamic acid at position 2 of the peptide chain. The enzymes involved in this modification are MurT and GatD [21, 22]. The final cytoplasmic step involves the translocation of Lipid II across the membrane which is accomplished by the flippase MurJ [23-25].

Once Lipid II translocation is accomplished and it is on the outside of the cell membrane, it is polymerized and crosslinked by a group of enzymes commonly known as penicillin binding proteins (PBP). *S. aureus* has four PBPs that polymerize the Lipid II units to peptidoglycan polymer. The N-terminal domain of each of PBP1, PBP2 and PBP3 harbors transglycosylase activity and polymerizes the MurNAc-GlcNac disaccharide of Lipid II to glycan chain. The C-terminal domain, which is also the penicillin binding domain, harbors transpeptidase activity and therefore catalyzes the transpeptidase activity between the pentaglycine bridge and the D-Ala at position 4 of the stem peptide. The decarboxylation of the last D-Ala-D-Ala is necessary for the cross linking to be completed and this is catalyzed by the PBP4, which is a carboxypeptidase with a D,D-carboxypeptidase activity [26].

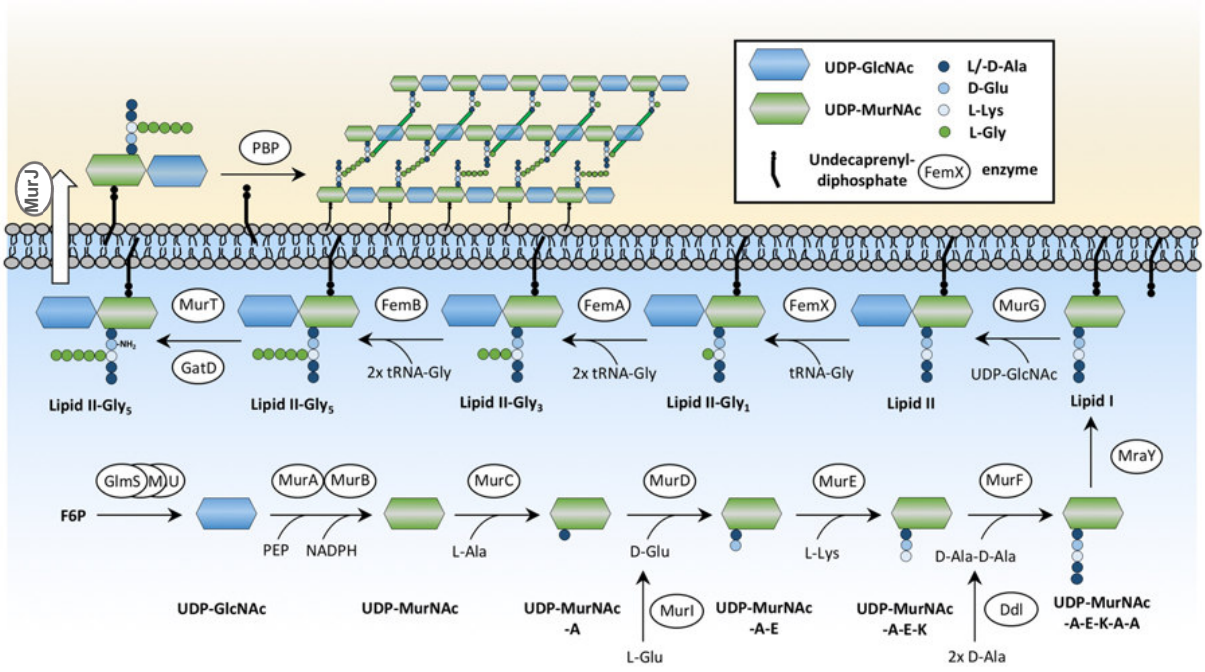

Figure 2. Peptidoglycan synthesis pathway of *S. aureus*. Peptidoglycan synthesis starts with glucosamine-6-phosphate (GlcN6P), a central metabolite controlling cell wall synthesis and glycolysis. It passes through many cytoplasmic and inner membrane bound steps involving a number of dedicated enzymes for each step. The assembled final building block, the Lipid II-Gly5 is then translocated to the outer membrane by a flippase and incorporated into the growing peptidoglycan polymer by transglycolsylases and transpeptidases known as penicillin binding proteins (PBPs). Image taken from Jarick, M. et al. The serine/threonine kinase Stk and the phosphatase Stp regulate cell wall synthesis in *Staphylococcus aureus*. *Sci Rep* **8,** 13693 (2018).

Staphylococcus Peptidoglycan hydrolases

The peptidoglycan layer is a dynamic macromolecular structure that undergoes through constant cycles of polymerization and hydrolysis to enable bacteria grow and divide [5]. The balance between degradation and polymerization is constantly controlled and maintained. This permanent peptidoglycan remodeling is carried out by cell wall (peptidoglycan) hydrolases. The activities of these cell wall hydrolases is therefore carefully regulated to maintain cell integrity or induce cell lysis. The physiological functions of cell wall hydrolases include the regulation of cell wall growth, the turnover of peptidoglycan during growth, the separation of daughter cells during cell division and autolysis [27]. Most bacteria therefore possess a range of peptidoglycan hydrolases, including lytic transglycosylases, amidases, glucosaminidases, or endopeptidases, that cleave bonds in the murein sacculus. In staphylococci, cell wall hydrolases have been studied extensively. They were classified as N-acetylglucosaminidases, N-acetylmuramoyl-L-alanine amidases, endopeptidases, and transglycosidases depending on their cleavage site. To date four N-acetylglucosaminidases, namely Atl-GlcA, SagA, SagB, and ScaH are characterized in *S. aureus.* They are described to be important for proper peptidoglycan build up and remodeling in the growth phase as well as septum formation and cell separation at the different stages of cell division. The glucosaminidase domain of the major autolysin Atl was described as an endo-acting β-1,4-glucoseaminidase responsible for daughter cell separation [28] whereas SagB was found to be responsible for shortening of newly synthesized glycan strands to their physiological length, thus ensuring flexibility during the cell elongation process [29, 30]. IsaA and SceD were described as lytic transglycosylases based on Sequence similarity to *E. coli* soluble lytic transglycosylase Slt, and demonstration of peptidoglycan hydrolase activity of purified proteins on peptidoglycan embedded in SDS-PAGE gels [31]. Similarly, three enzymes are described as amidases in *S. aureus*; the amidase domain of the major autolysin Atl-AmiA, SleI and LytN. The Atl-AmiA enzymatic activity was characterized by using mainly synthetic muropeptide substrates showing that it cuts the bond between the lactoyl moety of N-acetylmuramic acid and neighboring L-Ala. SleI containing a cell wall binding LysM and a catalytic domain, was characterized by comparing the HPLC and mass spectrometric analysis of the products of mutanolysin and mutanolysin/SleI digested peptidoglycan that it has an N-acetylmuramoyl-l-alanine amidase activity [32]. In the same way, LytN is composed of a cell wall binding LysM

and a catalytic CHAP domain. It was characterized to have both an N-acetylmuramoyl-L-alanine amidase and D-alanyl-glycine endopeptidase activities by analyzing its peptidoglycan digestion products using LC-MS [33]. Although these are some of the characterized proteins containing a CHAP domain, *Staphylococcus aureus* contains a set of more than ten different CHAP proteins that are not yet characterized. The CHAP domain, often in association with other domains that usually have cell wall binding or hydrolase functions, occurs mainly in cell wall hydrolases. It is therefore to be expected that there might be more proteins with an amidase function. The autolysin Aaa is also composed of LysM and CHAP domains. It contains three N-terminal LysM domains and a C-terminal CHAP domain. Its hydrolytic activity is not yet elucidated except that both the LysM and the CHAP domains were found to possess adhesive functions. LytM and Lss (lysostaphin) are two hydrolases that are known to act as glycyl-glycine endopeptidases cleaving within the pentaglycine interpeptide bridge [34, 35]. Interestingly, there is not any hydrolase found and described in the *S. aureus* genome that possesses an N-acetylmuramidase activity so far.

The staphylococcal major autolysin Atl

The staphylococcal major autolysin, Atl, is the most predominant peptidoglycan hydrolase and an important player in cell separation and daughter cell formation in staphylococci. Atl of S. aureus [36] and AtlE of Staphylococcus epidermidis [37] are quite similar in both sequence and domain organization. In both *S. aureus* and *S. epidermidis,* atl is flanked by the same genes. Investigation of the amino acid sequences of Atl proteins derived from 15 staphylococcal species representatives revealed that the overall organization of the bifunctional precursor protein consisting of the signal peptide, a propeptide (PP), the amidase (AmiA), six repeat sequences ($R1_{a,b}$, $R2_{a,b}$ and $R3_{a,b}$), and the N-acetylglucosaminidase (GlcA) was highly conserved in all of the species (Fig. 3). The most conserved domains being the enzyme domains AmiA and GlcA and the least-conserved; the PP and R regions [38]. Similarly, the three-domain enzyme Atl is roughly 137 kDa in size and is composed of a signal and pro-peptide as well as two catalytic domains; an N-terminal N-acetylmuramoyl-L-alanine amidase and a C-terminal β-N-acetylglucosaminidase [37, 39] (Fig. 3). These catalytic domains are separated by repeat domains that have cell wall binding functions [39]. The extracellular 62 kDa N-acetylmuramoyl-L-alanine amidase (AmiA) and 51

kDa β-N-acetylglucosaminidase (GlcA) are generated by extracellular proteolytic processing of the Atl forming a ring structure on the cell surface at the septal region for the next cell division site [28].

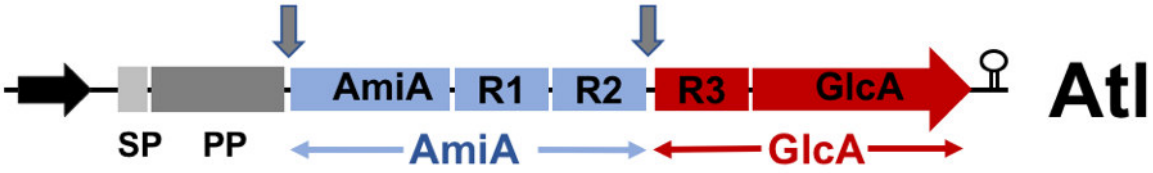

Figure 3. Organization of the domain structure of the *S. aureus* major autolysin (Atl). Atl is organized as a multidomain protein starting with the signal peptide (SP), followed by the propeptide (PP), the amidase (AmiA-R1R2) and the N-acetylglucosaminidase (R3-GlcA) domains. A certain proportion of Atl is post-translocationally processed as indicated by arrows. Structural analysis of the repeats R revealed that each repeat folds into two half-open β-barrel subunits connected by a linker [2]. The repeats represent LTA-binding domains that target the enzymes to the septum.

It has been already suggested that the two enzymes, AmiA and GlcA, which are involved in the partitioning of daughter cells after cell division, may be bound by a cellular component extending from the cell membrane, such as LTA [28]. The role of the propeptide (PP) has not been investigated so far except that it is not relevant for enzymatic activity of AmiA or GlcA. Most likely it is cleaved off by an extracellular protease. There are assumptions that it might play a role as an intra-molecular chaperone that facilitates the translocation of Atl as was shown for the staphylococcal lipases [40, 41].

The repeat domains of the Atl belong to the family of SH3b (bacterial SH3) domains that exhibit structural homology to the well-studied eukaryotic SH3 (Src Homology 3) domains. These cell wall binding domains comprise three repeat domains denoted $R1_{a,b}$, $R2_{a,b}$ and $R3_{a,b}$ (Fig. 3). In previous studies, based on sequence alignments, each of the two repeat units, a and b, were considered to be a single repeat domain [36, 37, 42]. However, structural studies showed that each repeat domain unit can further be subdivided in to smaller units that show higher homology to each other than the following repeat unit [43]. The function of the repeat domains is mainly to direct the corresponding amidase and N-acetylglucosaminidase towards the septum region that forms between dividing daughter cells [44]. Targeting of the repeats is based on an exclusion strategy mediated by wall teichoic acid and binding is very likely mediated by lipoteichoic acids (LTA) [43].

Cell wall turnover and recycling

The peptidoglycan layer is a dynamic macromolecular structure that undergoes through constant cycles of polymerization and hydrolysis. During this process a permanent turnover of peptidoglycan building blocks takes place. Kluj et al. recently reported the mechanism by which the glycan backbone is internalized and re-inserted in to the newly synthesized peptidoglycan in *S. aureus*. According to this mechanism, the MurNAc-GlcNAc disaccharide is released from PGN by the major autolysin Atl which is taken up and is concomitantly phosphorylated by a phosphotransferase system transporter MurP. The uptaken and phosphorylated disaccharide is intracellularly hydrolysed by the 6-phospho-N -acetylmuramidase, MupG to MurNac 6-phosphate and GlcNac which is further utilized and integrated by the PGN biosynthetic machinery. With such a mechanism, about 5% of the MurNac of the PGN in *S. aureus* per generation is recycled [45, 46]. These findings further cement the important function of Atl in cell wall recycling and biogenesis.

Peptidoglycan and host immune response

The innate immune system recognizes microbial products using germline-encoded receptors that initiate inflammatory responses to infection.
Immune cells detect microorganisms based on their unique molecules or pathogen-associated molecular patterns (PAMPs) that are recognized by multiple classes of pattern-recognition receptors (PRRs) that initiate inflammatory responses [47] The bacterial cell wall peptidoglycan is a prime example of a conserved pathogen-associated molecular pattern (PAMP) for which the innate immune system has evolved sensing mechanisms.

The polymer structure of PGN as well as its fragments are recognized as PAMPs by a number of pattern recognition receptors (PRRs) that are secreted, intracellularly expressed or expressed on the cell surface. In addition, proteins and lipoproteins that are associated with the peptidoglycan structure are recognized by the PRRs. Two PRRs are associated with recognition of peptidoglycan and its fragments; Toll like receptors (TLRs) and the nucleotide-binding oligomerization domain (NOD)-like receptors (NLRs). The role of TLRs in direct recognition of peptidoglycan has been controversial. Early studies identified peptidoglycan as a TLR2 ligand [48-50].

However, later studies showed that the TLR2-inducing activity of peptidoglycan was most likely to be due to cell wall lipoproteins and lipoteichoic acids (LTAs) that commonly co-purify with peptidoglycan [51].

In a previous work, we have addressed this question by using a strain of *S. aureus* deficient in diacylglyceryl transferase (lgt) and therefore fails to lipidate lipoproteins. Our results showed that lgt-deficient bacteria are poor activators of TLR2-expressing reporter cells and peptidoglycan monomers from these bacteria activate cells only in the presence of other defined TLR2 ligands such as PAM_3CSK_4. The most well-defined sensors of peptidoglycan are the cytosolic NLRs, NOD1 and NOD2, which are expressed by diverse cell types [52]. As cytosolic sensors, NOD1 and NOD2 must either detect bacteria that enter the cytosol, or peptidoglycan must be degraded to generate fragments that could be transported into the cytosol for these sensors to function. While NOD1 is activated mainly by DAP type gram negative peptidoglycan, NOD2 is activated by the Lys type gram positive peptidoglycan fragments. The minimal ligand for NOD1 is iE-DAP, a dipeptide composed of the D-Glu–mDAP residues of the peptide chain from mDAP-type peptidoglycans specific to Gram-negative bacteria. Similarly, the muramyl dipeptide of gram positive peptidoglycan, MDP, is defined as the minimal fragment of peptidoglycan that is a NOD2 ligand [53, 54]

Most of the Nod agonist activity produced by bacteria is found in the culture supernatant of growing bacteria [55]. The cell wall of bacteria is remodeled by hydrolases that degrade intact PGN into smaller fragments during cell growth and division, which are imported and recycled. It has been shown that mutants that are defective in the recycling of PGN fragments exhibit increased Nod1-dependent NF-κB activation [56]. These results suggest that Nod senses bacterial growth through the recognition of PGN fragments released by growing bacteria, most likely through degradation by cell wall hydrolases.

Aim of the study

The staphylococcal major autolysin, Atl is the most predominant peptidoglycan hydrolase in staphylococci. In addition to its role in cell division, several studies have identified the importance of the *atl* gene products in cell wall recycling, biofilm formation, host cell recognition and immune evasion. But there are still a number of unanswered questions that need to be answered. This dissertation deals with the further characterization of the major autolysin of *Staphylococcus aureus* (Atl) and its catalytic active components; the amidase AmiA, and N-acetylglucosaminidase, GlcA.

To determine the specificity of recognition and the mechanism of catalysis of the amidase AmiA, in cooperation with the department of biochemistry, work group of Prof. Thilo Stehle, we aim to resolve the crystal structures of the enzyme in the absence and presence of a substrate ligand and determine its substrate specificity with regard to different natural peptidoglycan structures.

Enzymatic activities of both the AmiA and GlcA are so far determined and described using either synthetic substrates or zymogram analysis with heat inactivated whole cells. We therefore aim to elucidate the substrate interaction, specificity and proper enzymatic mechanism of both the AmiA and GlcA using the natural substrate of both enzymes, staphylococcal peptidoglycan. Deletion of Atl showed impaired cell separation and formation of large clusters. We therefore aim to further elaborate the role played by AmiA and GlcA in cell division and separation of *S. aureus*. Furthermore, we aim to find out the effect of these enzymes on the antibiotic susceptibility or tolerance of *S. aureus*.

Results and discussion

Under this section, results of the following publications are summarized and discussed.

1. Büttner, F. M., Zoll, S., **Nega, M**., Gotz, F., and Stehle, T. (2014) Structure function analysis of *Staphylococcus aureus* amidase reveals the determinants of peptidoglycan recognition and cleavage. J*. Biol. Chem*. 289, 11083–11094. doi: 10.1074/jbc.M114.557306

2. **Nega, M.,** Tribelli, P.M., Hipp, K. *et al.* New insights in the coordinated amidase and glucosaminidase activity of the major autolysin (Atl) in *Staphylococcus aureus*. *Commun Biol* **3,** 695 (2020). https://doi.org/10.1038/s42003-020-01405-2

Crystal structure of the catalytic domain of *S. aureus* Atl amidase

Several hydrolytic enzymes ensure the plasticity of the staphylococcal cell wall by processing the complex PGN network. Of these the predominant one is the major autolysin Atl which is composed of two enzymes with hydrolytic activity, an amidase (AmiA) and a N-acetylglucosaminidase (GlcA), that cleave PGN at different locations.

The staphylococcal Atl domain organization is highly conserved in all of the species, with the amidase being the most conserved domain. To acquire knowledge about peptidoglycan (PGN) engagement and binding, the structure of the catalytic domain of AmiA (AmiA-cat) was solved to the atomic resolution of 1.12 Å. AmiA-cat features a mixed α/β-fold with a central, six-stranded β-sheet that is surrounded by seven helices. The active site is located in a well-defined binding cleft that is made up of two α-helices and loops. A catalytic zinc ion is coordinated by two histidine and one aspartate side chains (Fig. 4A).

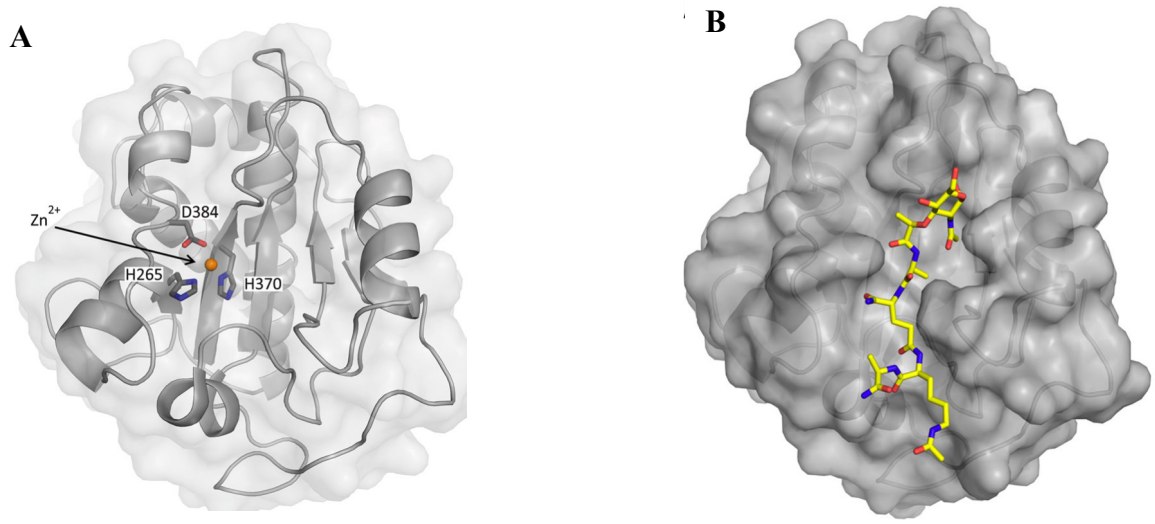

Figure 4. Structure of AmiA catalytic domain (AmiA-cat) with and without its ligand. A) Mixed α/β fold of unliganded AmiA-cat in a schematic representation with a transparent surface. The zinc ion (orange) and its coordinating residues (dark gray) are highlighted. B) AmiA-cat in complex with the ligand MurNAc tetrapeptide in the active site.

To establish the structural requirements of PGN recognition and the enzymatic mechanism of cleavage, as well as obtain data on the molecular interactions upon substrate binding, crystal structure of the catalytic domain of AmiA (AmiA-cat) in complex with a peptidoglycan-derived ligand was solved at a 1.55 Å resolution. For

this, the purified amidase catalytic domain, AmiA-cat, was EDTA treated to chelate the zinc ion and avoid possible ligand degradation. Modified Muramoyltetrapeptide (MurNAc-tetP) containing an amidated D-Ala and acetylated L-Lys was chosen as it approximates the natural ligand best. Binding of the ligand to AmiA-cat was successful, and a complex structure at 1.55 Å resolution with excellent statistics was obtained.

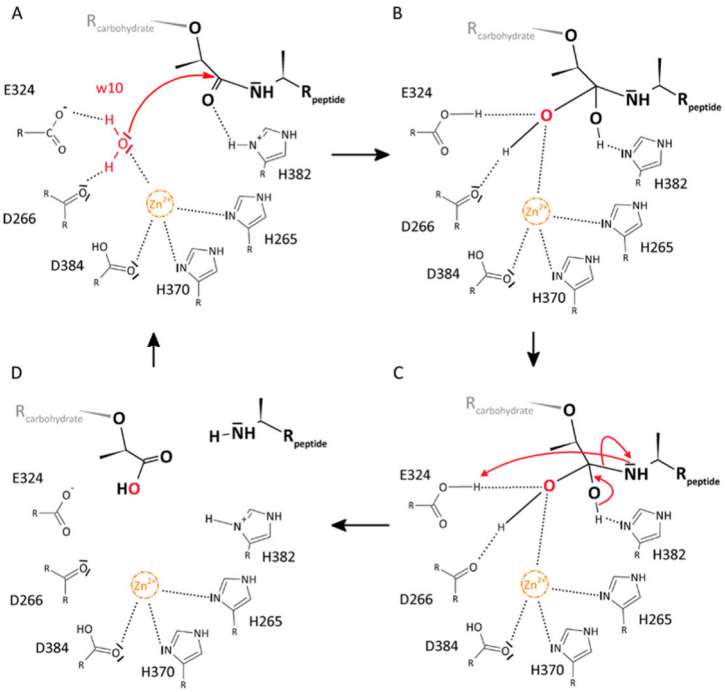

Figure 5. Proposed reaction mechanism of AmiA. **(A)** Water-10 (w10) is hydrogen-bonded to Asp-266 and Glu-324, and its free electron pairs face towards the scissile bond. Zn^{2+} is complexed by His-265, His-370, and Asp-384 and probably renders Wat-10 more reactive, enabling a nucleophilic attack. **(B)** tetrahedral intermediate is stabilized by hydrogen bonds of the resulting hydroxyl groups with Nδ of His-382 as well as Asp-266, Glu-324, and zinc, respectively. **(C)** reformation of a carbonyl group with the peptide moiety as leaving group. His-382 can accept a hydrogen atom from the tetrahedral intermediate, whereas the peptide is poised to accept a hydrogen from Glu-324. **(D)** product release.

The complex structure reveals a dense interaction network of the four amino acids of the stem peptide with AmiA-cat, although some hydrogen bonds are water-mediated. Of all the amino acids, D-iGln forms the majority of hydrogen bonds and contributes strongly towards binding and orientation of the ligand, while L-Ala D-Ala and L-Lys only make one hydrophobic interaction each. The active site is formed by the three amino acid residues; H265, H370, and D384, which coordinate the zinc ion, as well as a catalytic E324 (Fig. 5). A structurally conserved water molecule, "*w10*", is present in both apo and ligand structures and in good position to attack the scissile bond. This catalytic water makes it possible to infer a plausible mechanism in which E324 and D266 bind the hydrogens and the zinc ion contacts one free electron pair of *w10*. Well

oriented, the remaining lone pair of *w10* attacks the lactyl carbon, introducing a tetrahedral intermediate. This tetrahedral intermediate is stabilized by H382 providing a proton for the resulting oxanion. Re-formation of a carbonyl leads to the release of cleaved carbohydrate backbone and peptide stem.

The entire mechanism of PGN engagement is, however, more complex. To further enhance our understanding, we examined surface properties of AmiA-cat and the conservation of residues among related amidases as well as the upper and lower ends of the binding site. Mapping the conserved residues onto the molecular surface and examination of the electrostatic surface potential of the upper part of the binding site gave further insights where neighboring sugar moieties may bind. Similarly, examining the properties of Ami-cat at the lower end of the binding site hints the binding of the pentaglycine bridge which correlates with the biological assay results that the enzyme discriminates PGN based on the presence of the pentaglycine bridge.

AmiA and GlcA are required for proper septum formation and cell separation

Deletion of each of the AmiA and GlcA separately as well as altogether brings about interesting phenotypes. Comparative fluorescent and scanning electron microscopic (SEM) analysis showed that cell separation is significantly affected. This is manifested in increased cell cluster formation in all the mutants (Fig. 6, 7). Deletion of the whole *atl* shows a substantially higher cluster formation suggesting that the coordinated action of both enzymes to be crucial for proper cell separation. A comparative view on the surface of the WT and mutant cell surfaces reveals that, all the mutants show a more “rough” surface of most likely unprocessed “old” peptidoglycan, which is more pronounced in the *atl* mutant (Fig. 7A).

Transmission electron microscopic (TEM) imaging of each of the mutants further revealed that, lack of amidase results most likely in a weak peptidoglycan layer that cannot withstand osmotic pressure differences between the inner and outer cellular milieu. This is presumably due to over expression and over activity of other hydrolases that weaken the PGN or that improper crosslinking is taking place that costs rigidity deficits of the wall structure. Even more interesting is the phenotype of the *glcA* deletion mutant which shows improper septum formation. Some of the cells show asymmetric

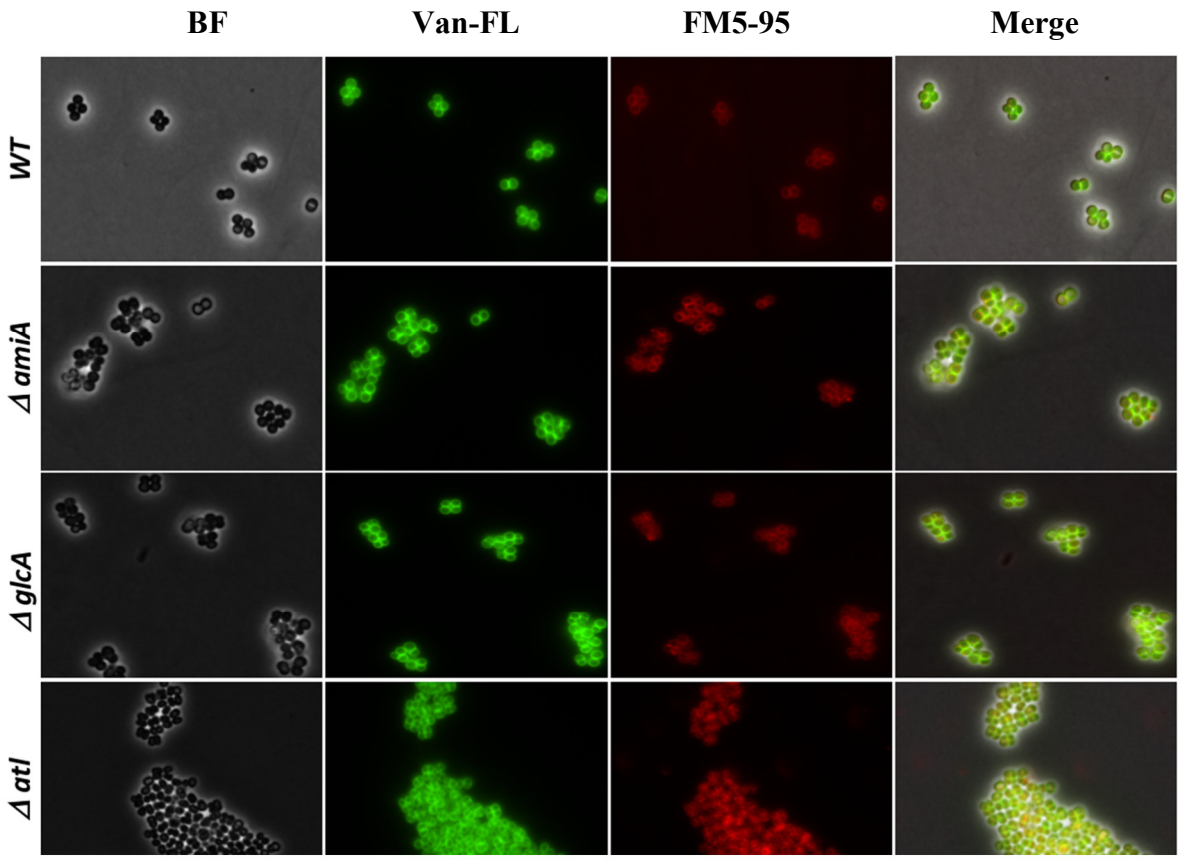

Figure 6. Fluorescence microscopic images SA113 and its mutants. WT and deletion mutants *ΔamiA*, *ΔglcA* as well as *Δatl* were grown to mid-exponential phase and labelled with BODIPY™ FL Vancomycin (green) and cell wall staining FM5-95 (red). Images reveal impaired cell separation and different degree of aggregation. Deletion of the whole Atl leads to formation of much larger cell clusters.

septa leading to “kidney like” structures while others have multiple septa formed next to each other in parallel instead of the regular perpendicular septum formation (Fig. 7B). This irregular septum formation might be due to the separate activity of AmiA, since it does not require the presence of or pre-digestion with the GlcA. What is interesting is that though the function of AmiA is still intact, it seems that it is not determinant in properly localizing the next septation point. If it plays any role, then at least it needs the coordinated action with the GlcA to localize the septation point properly. This complete disarray of coordination in proper septum formation gives a preliminary evidence that the GlcA might have additional functions not only in the proper septum formation but also in coordination of a cell division complex.

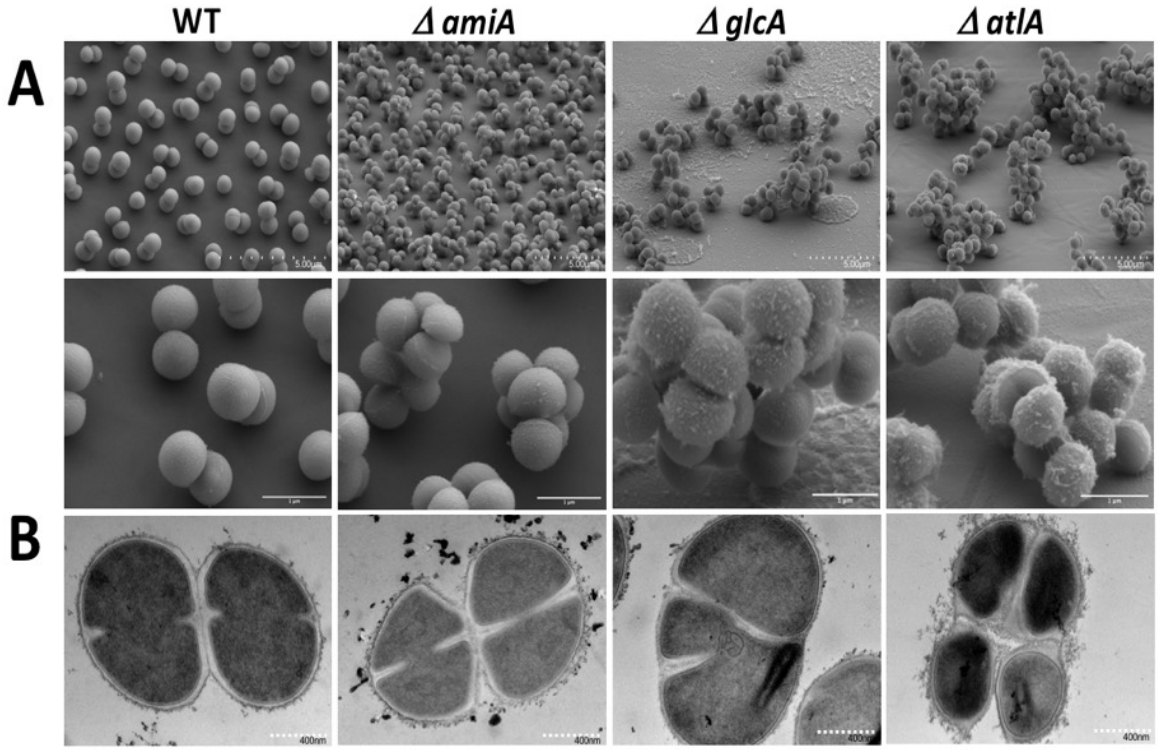

Figure 7. *S. aureus* major autolysin (atl) amidase and N-acetylglucosaminidase are important factors for proper cell separation. A**)** Scanning electron microscopic (SEM) pictures of the WT and deletion mutants of the amidase only (ΔamiA), the N-acetylglucoseaminidase only (ΔglcA) as well as both the *amiA* and *glcA* (Δatl) showing impaired cell separation and different degree of aggregation. Deletion of the whole Atl leads to formation of much larger cell clusters. B) Transmission electron microscopic (TEM) images of exponential grown SA113 and its mutants. In Δ*amiA* cells, the old CW is rougher than in the WT and particles are released consisting presumably of unprocessed PG. In Δ*glcA,* proper septum formation is disrupted asymmetric septa formation is now clearly visible. In Δ*atl,* even separated cells are still connected by thread-like structures forming unseparated cell clusters.

Deletion of AmiA and GlcA, results in lowered peptidoglycan crosslinking

Comparative analysis of the peptidoglycan layers of each mutant with The WT was carried out by isolation and subsequent digestion of the peptidoglycan with the muramidase mutanolysin. Equal amounts of peptidoglycan from the WT and mutants were digested and the released muropeptides were resolved with RP-HPLC. Comparison of the peak area units of the whole chromatogram with peak areas of individual fragments revealed significant differences in the degree of crosslinking. The total composition of the PG fragments was largely the same in the WT and its Δ*atl* mutant. However, in the Δ*atl* mutant, the short PG fragments (mono- to pentamer) were increased 1.5 to 2-fold, while the longer PG fragments (≥ octamer) were about 2-fold

lesser compared to the WT and plasmid complemented mutant values (Fig. 8). Although to a lower proportion compared to the Atl mutant, loss of each of the enzymes AmiA and GlcA results in a lower degree of PGN crosslinking as well. These results clearly show that Atl plays a very important role not only in cell separation, but also in coordination of proper cell division and peptidoglycan synthesis.

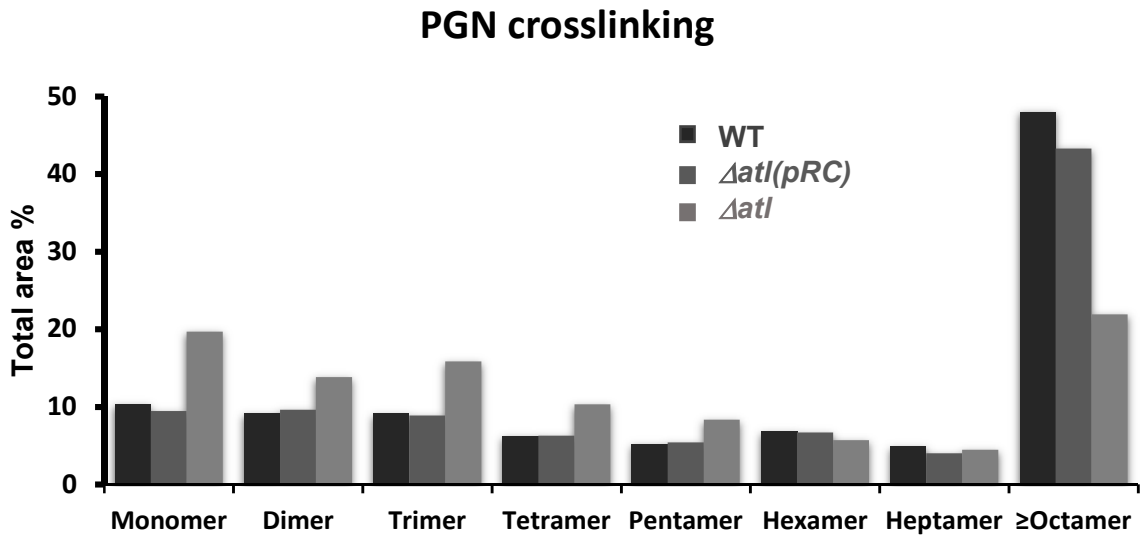

Figure 8. Distribution of muropeptide fragments and cross-linking pattern of SA113 WT, SA113△atl and SA113△atl (pRC14) strains digested with mutanolysin. Deletion of the Atl leads to a significantly lower degree of crosslinking of the peptidoglycan mesh. This is readily visible in the lower amount of the higher-order cross linked portion while showing higher proportion of the lower-order cross linked fragments of solubilized muropeptide fragments from monomers to heptamers in the mutant strain.

Deletion of AmiA and GlcA, show increased oxacillin tolerance

In previous studies with Bacillus and Staphylococcus, it has been shown that mutants with reduced autolysin activity show increased tolerance towards antibiotics active on the cell wall. It has been assumed that antibiotics that inhibit the biosynthesis of a structurally functional cell wall ultimately lead to cell death, since the autolysins on the cell surface hydrolyze more peptidoglycan than the cell can rebuild. The consequence is that the cell wall becomes too weak to maintain the turgor pressure in the cell, which leads to leakage and lysis of the cells [57, 58]. To verify this observation and evaluate the role of AmiA and GlcA as well as Atl, each of the strains were inoculated from an overnight culture to an OD of 0.1 and incubated for two hours.

From each culture, a serial dilution of 10^{-2} to 10^{-8} was prepared and 5µl aliquots were spotted on TSA plates containing 0.1 µg/ml oxacillin. The results clearly confirm that loss of activity of each of the enzymes leads to reduced oxacillin efficacy and increased tolerance. We see that the Δ*atl*, Δ*amiA* und Δ*glcA* mutants were 10,000 - to 100,000-times more tolerant to oxacillin than the parent strain (Fig. 9). This result is in agreement with earlier observations that hydrolytic enzymes on the cell surface are required to augment the wall damage initiated by oxacillin and other β-lactam antibiotics to produce a bactericidal effect [58].

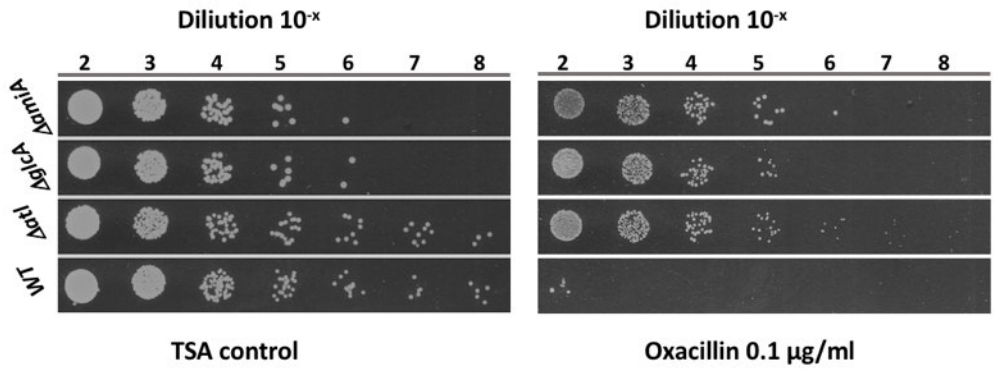

Figure 9. Antibiotic susceptibility profile of SA113 WT, SA113DamiA, SA113DglcA and SA113Datl. Deletion of Atl, AmiA and GlcA results in reduced oxacillin susceptibility. Each of the strains were inoculated from an overnight culture to an OD of 0.1 and incubated for two hours. From each culture a serial dilution of 10^{-2} to 10^{-8} was prepared and 5µl aliquots were spotted on TSA plates containing 0.1 µg/ml oxacillin.

The AmiA repeat domains R1ab and R2ab hinder cell separation and foster aggregate formation

The Atl amidase, AmiA is composed of the catalytic Ami domain and repeats R1ab and R2ab. Crystal structure elucidation reveals that each repeat folds into two half-open beta-barrels. Small-angle X-ray scattering of the mature amidase reveals the presence of flexible linkers (L1 and L2) separating the Ami, R1ab, and R2ab units. The linkers act as a hinge region allowing a high flexibility and fidelity of the amidase domain [2]. In order for proper cell separation to take place, the repeat regions target AmiA and GlcA to the septum in two ways: The repeats a) are repelled by the wall teichoic acid (WTA) which is mainly present in the mature cell wall [43], and b) bind to the lipoteichoic acid (LTA) which is localized in the septum [2]. In this way they direct AmiA and GclA to the septum, where their active sites can optimally carry out the final step of cell division by resolving the PG-interlinked daughter cells. All data suggest that the repeats direct the catalytic amidase domain to the septum, where it can optimally

perform the final step of cell division [59]. Based on these evidences, we question whether the external addition of purified R1ab-R2ab repeats interferes with cell separation. If the repeats are localized in the septum, they can sterically hinder the attachment of Atl, which should lead to restricted cell separation and increased aggregation. We therefore, recombinantly produced and purified the repeat domains R1-R2 together and added them to an early exponentially growing cultures of OD 0.1 of the corresponding WT and mutant strains. After 2h of cultivation, microscopic analysis of the WT, Δ*amiA* and Δ*glcA* cultures show massive increase in cell

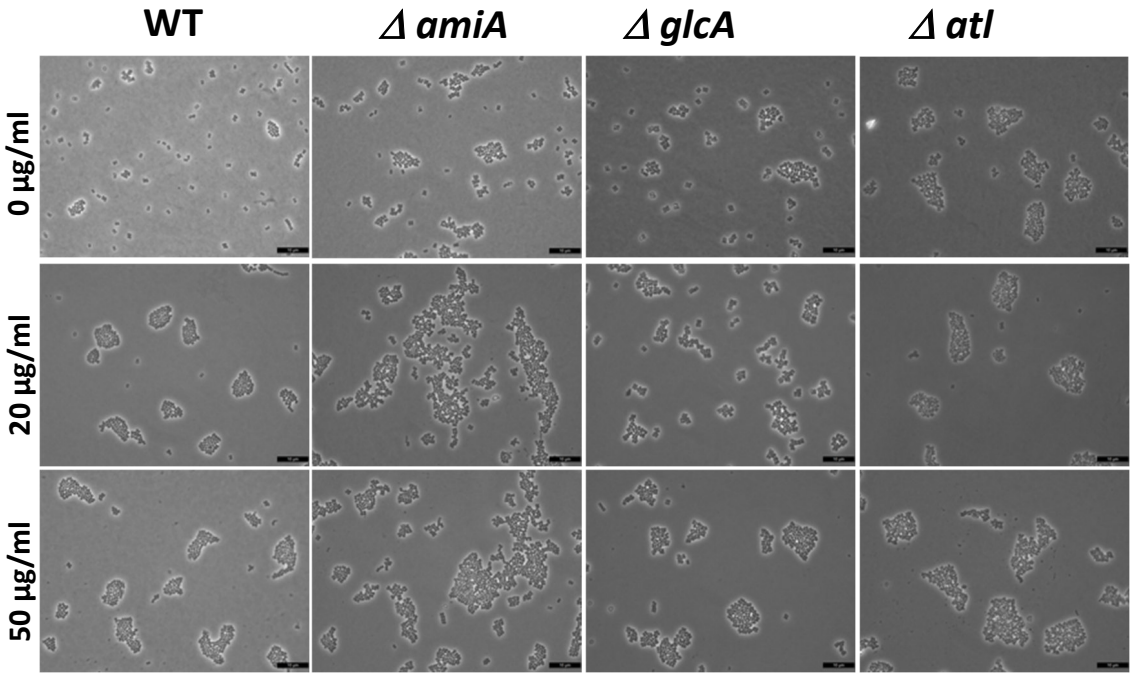

Figure 10. Atl amidase repeat domains $AM_{R1,2}$ hinder cell separation and foster aggregate formation. The amidase repeat domains $AM_{R1,2}$ are purified and added to TSB medium inoculated with each of the WT and mutants to an OD of 0.1. After two hours of incubation at 37 °C under shaking, samples were observed under the microscope. All the cultures show increased aggregation except the *atl* deletion mutant which any way has built large cell clumps.

aggregation (Fig. 10). Understandably, the Δ*atl* culture that has already formed large cell clusters, showed hardly any change after the repeats were added. This observation cements the findings of previous works that the repeats are binding domains that localize the enzymes to the septum by binding to LTA and peptidoglycan that are not yet covered by wall teichoic acids. Addition of excess purified repeat domains leads to excess binding to the septum, thereby blocking the action of Atl and hence leading to a phenotype of an Atl mutant strain, namely aggregation.

AmiA degrades staphylococcal peptidoglycan specifically and releases peptides of varying lengths

The cell wall degrading activity of the amidase domain of the staphylococcal major autolysin, Atl, was described in several previous works. Oshida et al. described the activity of the amidase using zymogram analysis using heat inactivated staphylococcal whole cells as amidase- and *M. luteus* cells as N-acetylglucosaminidase substrates without showing any structural evidence [36]. Later Lutzner et al. developed a novel

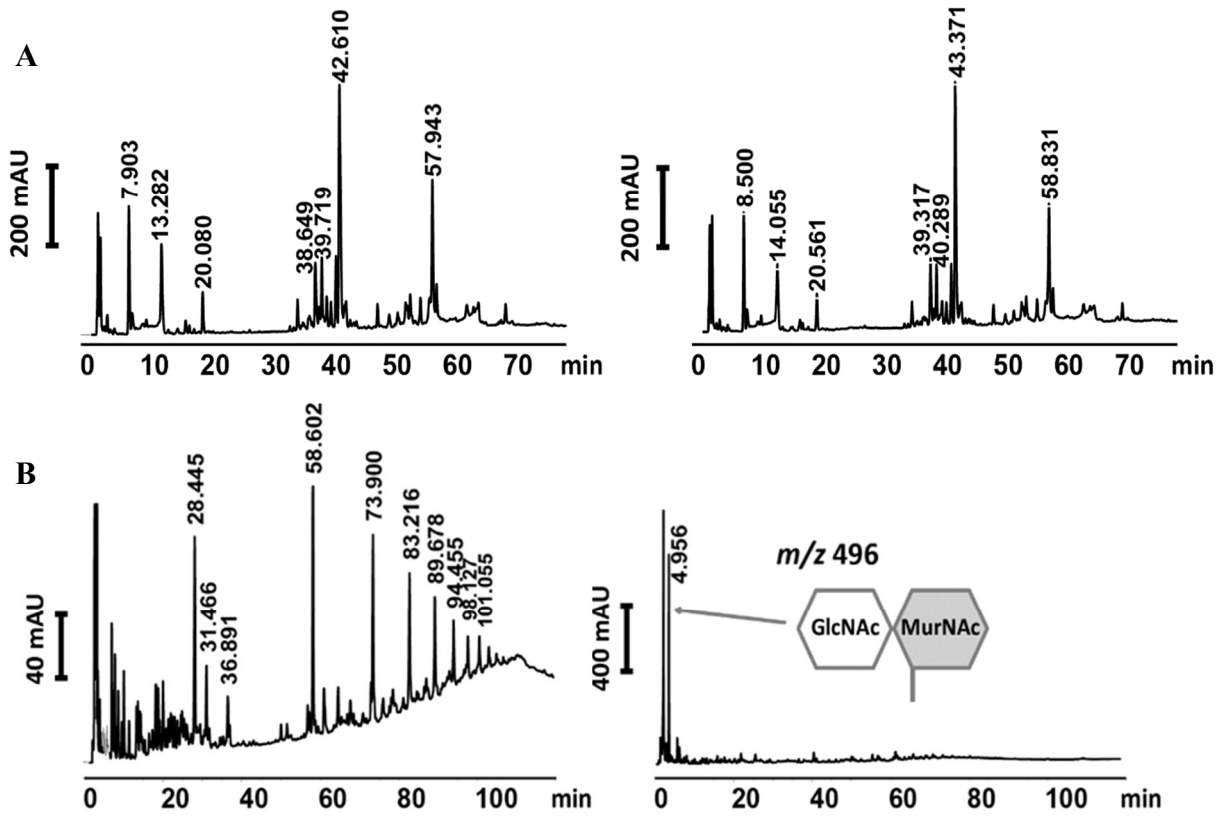

Figure 11. Muramidase (mutanolysin) and amidase digestion pattern of staphylococcal PG. (A) RP-HPLC analysis of soluble PG released after digestion with mutanolysin showing the characteristic peak pattern of monomeric up to heptameric PG fragments ending in a hump of unresolved polymeric fraction as described previously [1]. (B) HPLC analysis of soluble PG fragments released after digestion with AmiA shows a distinctly different peak pattern.

fluorescent substrate for *S. epidermidis* Atl amidase AmiE. But this substrate has no similarity with the natural peptidoglycan since it neither has glycan components nor is the peptide sequence the same as the natural substrate [60]. Biswas et al. have used PGN to show the mass difference extracted from an HPLC-MS analysis after a lysostaphin and amidase double digestion [42]. But surprisingly, none of these and other studies made so far have used the natural substrate, purified staphylococcal whole peptidoglycan and shown the specific activity of the Atl-amidase. As there are

enzymes with diverse hydrolytic activities even on a single substrate, for example LytN shows both amidase and peptidase activities when tested on staphylococcus peptidoglycan [33], it is necessary and important to verify the activity spectrum of Atl-amidase on its natural environment and substrate. Therefore, after getting more insight through the crystal structure studies, we incubated purified *S. aureus* and *B. subtilis* peptidoglycan first with the muramidase Mutanolysin for 16 hours followed by Atl-amidase to verify its specificity. As expected, Atl-amidase did not digest *B. subtilis* PGN

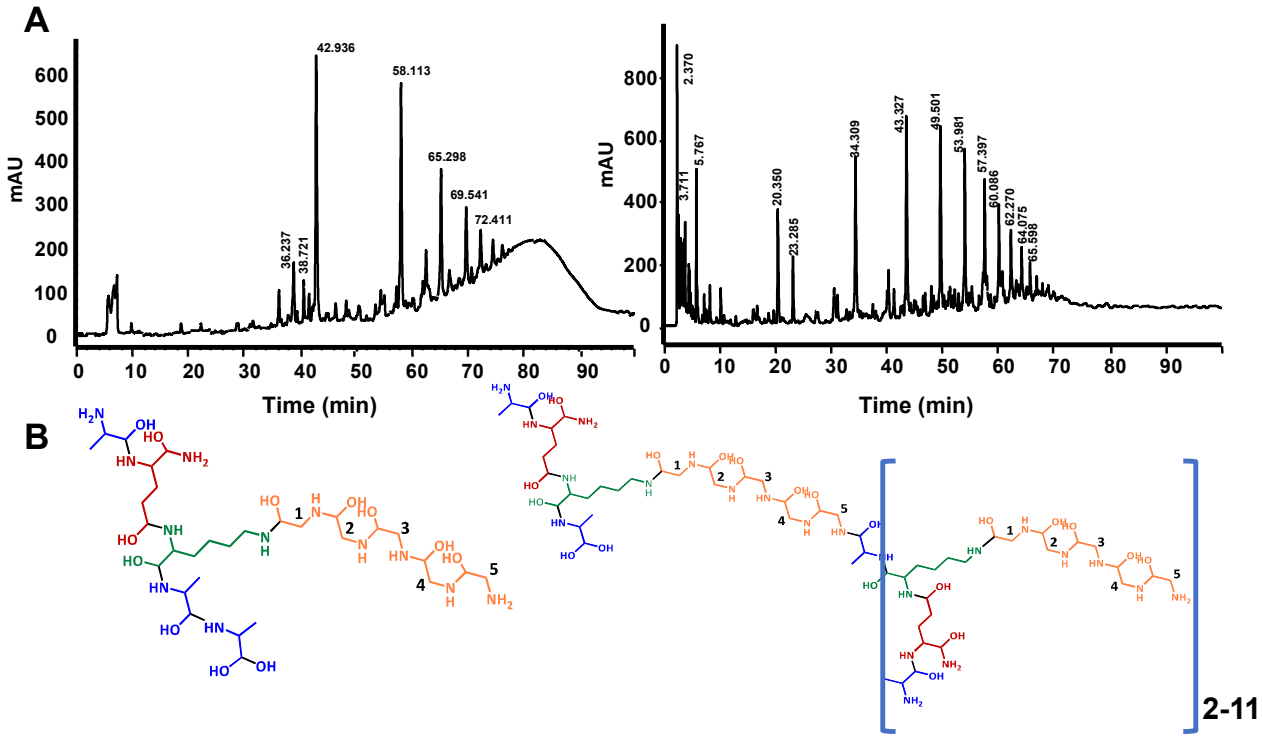

Figure 12. HPLC profile of Mutanolysin and AmiA solubilized staphylococcal PG. (**A**) showing peaks of released muropeptides and peptides by mutanolysin and AmiA hydrolysis of PGN (**B**) Molecular structures of the released peptides, uncrosslinked and with single bridge crosslink (monomer and dimer) representing the first two peaks. Each further peak depicts the peptide elongated by one cross linkage unit shown in brackets up to an extension of 12-15mer length.

(Fig. 11A) while it degraded the *S. aureus* PGN (Fig. 11B). These results confirm our observations on the crystal structure and substrate docking studies that, polymeric peptidoglycan with its pentaglycine bridge is the natural substrate of Atl-amidase. To further verify the specific activity mechanism of the Atl-amidase, we compared the digestion pattern of *S. aureus* PGN with Mutanolysin and Atl- amidase (Fig. 12A). As expected, HPLC chromatogram of the solubilized products from both digestions showed distinctly different peak patterns. While the peak patterns of the Mutanolysin digestion products are already well characterized, analysis of the solubilized products

by HPLC-MS confirmed amidase activity by the release of PGN peptides of increasing lengths (Fig. 12B). The masses of the major peaks revealed that, the amidase effectively cleaved between the N-acetylmuramic acid and the L-Ala of the stem peptide releasing cross linked peptides of increasing lengths, each time by a mass value that exactly matches the mass of the next crosslinking peptide fragment (Table 1). The peptides were resolved so well according to their length, that it was even possible to enumerate the peaks according to the number of the pentaglycine bridges contained.

Table 1. Amino acid composition and mass analysis of AmiA released peptide fragments of *S. aureus* peptidoglycan

Peptide	m/z calc.	m/z Obs.
AQK$(G)_5$AA	772.818	773,440
AQK$(G)_5$ [AQ $(G)_5$KA]AA	1456,542	1456,819
AQK$(G)_5$ [AQ $(G)_5$KA]$_2$AA	2140,266	2140,299
AQK$(G)_5$ [AQ $(G)_5$KA]$_3$AA	2823,990	2823,861
AQK$(G)_5$ [AQ $(G)_5$KA]$_4$AA	3507,714	3507,236
AQK$(G)_5$ [AQ $(G)_5$KA]$_5$AA	4190,062	4190,753
AQK$(G)_5$ [AQ $(G)_5$KA]$_6$AA	4874,400	4874,270
AQK$(G)_5$ [AQ $(G)_5$KA]$_7$AA	5557,735	5557,631
AQK$(G)_5$ [AQ $(G)_5$KA]$_8$AA	6241,070	6241,171
AQK$(G)_5$ [AQ $(G)_5$KA]$_9$AA	6924,405	6924,679
AQK$(G)_5$ [AQ $(G)_5$KA]$_{10}$AA	7608,744	7609,011
AQK$(G)_5$ [AQ $(G)_5$KA]$_{11}$AA	8291,075	8290,972
AQK$(G)_5$ [AQ $(G)_5$KA]$_{12}$AA	8975,414	8975,952

GlcA requires uncrosslinked glycan strand to render its activity

In the same way as the determination of the Atl-amidase activity in previous works of Oshida et al. [36], activity of the Atl-N-acetylglucosaminidase was determined by zymogram analysis using heat inactivated *M. luteus* cells, since GlcA showed hardly

any cell wall activity in *S. aureus*. But there was no explanation as to why an enzyme expressed, secreted and processed by *S. aureus* does not show any activity on its cell wall. To verify its activity, *S. aureus* peptidoglycan was isolated and digested with purified GlcA and AmiA. The solubilized digestion products were then further analyzed by HPLC. The results verify that, while the amidase digested peptidoglycan showed solubilized fragments (Fig. 13A), no fragment peaks were observed in the HPLC chromatogram of the GlcA digestion (Fig. 13B). This is in line with previous zymogram analysis results where GlcA showed hardly any cell wall activity in *S. aureus*.

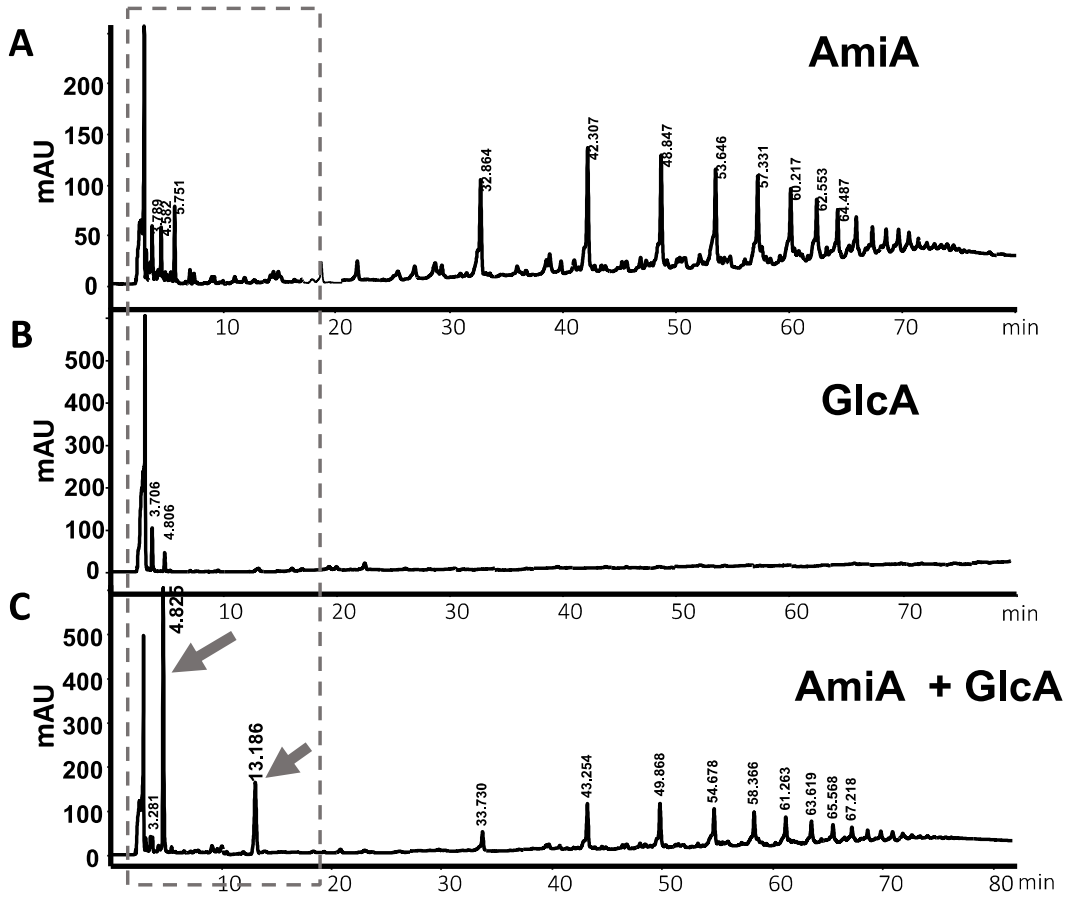

Figure 13. RP-HPLC profile of soluble fragments obtained after hydrolysis of PGN*. (**A**) with AmiA, (**B**) with GlcA, (**C**) with GlcA after prior digestion with AmiA; AmiA was heat-inactivated at 95 °C for 3 min before digestion with GlcA. After the double digestion, two distinct peaks at RT 4.8 and 13.1 min appear as main products, indicated by red arrows. * please note the different scales in A = 250, B = 600 and C = 600 mAU.

We therefore postulated that the N-acetylglucosaminidase activity might be dependent on amidase activity or both enzymes work in coordination as they are expressed together. We therefore used an amidase pre-digested PGN as a substrate and digested it further with GlcA overnight. After this double digestion, two additional main peaks appeared at RT 4.8 and 13.1 min in the HPLC chromatogram while the peaks

specific to amidase remain unaltered (Fig. 13C). MS analysis of the peaks revealed that the peak at RT 4.8 min corresponds to MurNAc-GlcNAc disaccharide and that of RT 13.1 min corresponds to its *O*-acetylated form (Fig. 14A,B). This shows that unsubstituted glycan chain is the natural substrate of GlcA while *O*-acetylation of MurNAc does not affect its activity.

GlcA is not an *endo*- but an *exo*-β-N-acetylglucosaminidase

Since we observed only MurNAc-GlcNAc disaccharides as products of N-acetylglucosaminidase digestion, the next logical and equally important question is if GlcA is an *endo*-β-1,4-N-acetylglucosaminidase as described heretofore or if it is rather an *exo*-acting enzyme. To answer this question, GlcA digestion and product formation on a previously Atl-amidase digested peptidoglycan was monitored over a period of 0

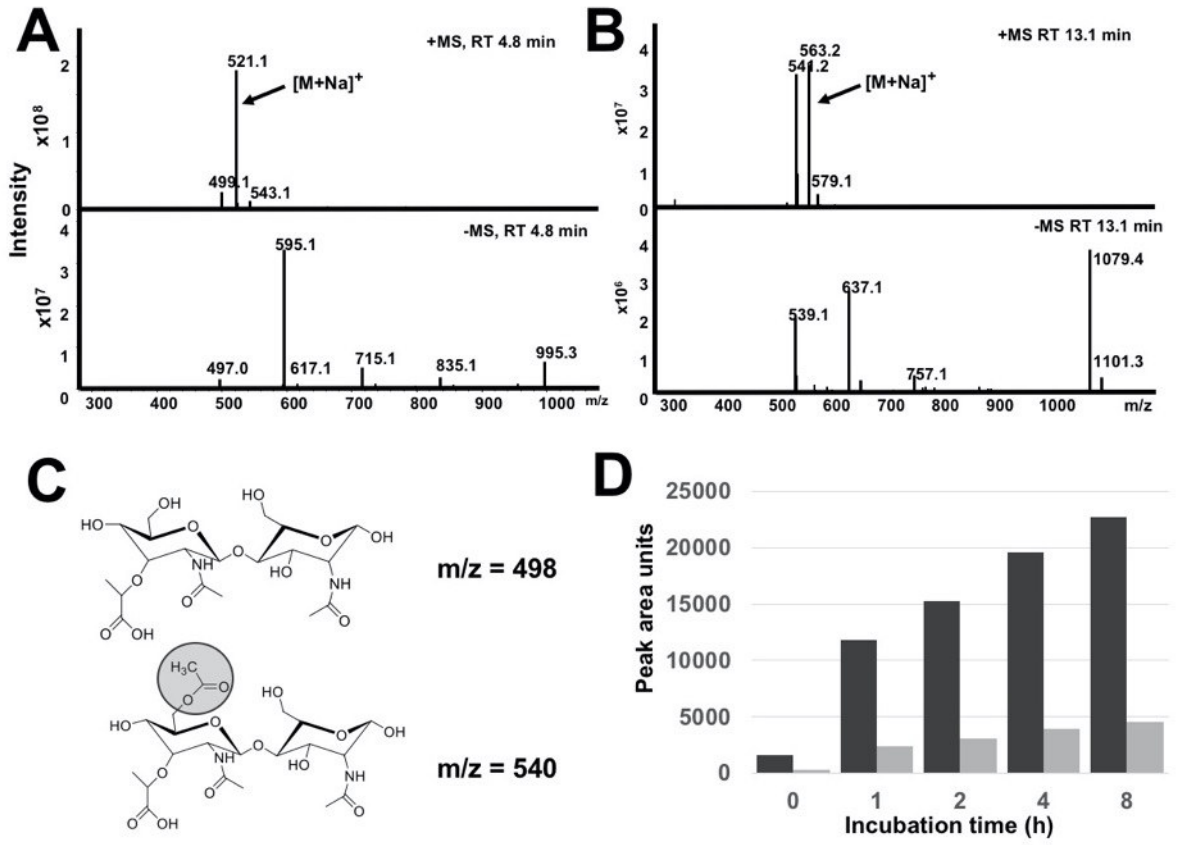

Figure 14. Mass spectrometric and time lapse profile of the GlcA digestion disaccharide products, MurNac-GlcNac. The mass of the two distinct HPLC peaks at Rt 4.8 min (**A**) and 13.1 min (**B**) shown in Fig. 13C was determined. (**C**) The mass of m/z = 498 corresponds to MurNAc-GlcNAc and of m/z = 540 to *O*-acetylated MurNAc-GlcNAc. (**D**) Time course of MurNAc-GlcNAc release by AmiA and GlcA digestion measured by RP-HPLC. Black bar represents MurNAc-GlcNAc and grey bar *O*-acetylated MurNAc-GlcNAc.

to 8 hours by HPLC analysis. If the Atl N-acetylglucosaminidase is an *endo*-enzyme, as described in the literature, glycan products of different sizes should be detected in at least some of the timepoints. If it is an *exo*-enzyme, only disaccharide products with increasing concentrations over time should be found. Indeed, HPLC analysis of the samples at different time points revealed that only the MurNAc-GlcNAc-disaccharide peaks appeared increasing with time (Fig. 14D). There was no other glycan chain of any length detected other than the disaccharides. These results clearly show two important facts. First; GlcA requires the prior removal of attached peptides to the glycan backbone for it to render its activity and second; GlcA is **not an *endo*- but an *exo*-**acting enzyme chewing down the glycan ends up to the point where the stem peptide is intact.

Concluding remarks

The major autolysin of staphylococcus, Atl, in general, and of *S. epidermidis*, AtlE in particular, has been studied extensively in its structural arrangement; its genetic organization and regulation; its function in cell division and separation; its role in biofilm formation; its role in host cell adhesion and invasion as well as its activity on peptidoglycan. Although several studies have focused on these different functional and structural aspects of Atl, little is known about the interplay of its domains AmiA and GlcA during cell division and separation.

With this study, we provide a highly resolved complex structure of the catalytic amidase domain of *S. aureus* Atl, AmiA-cat. We resolved its specific molecular ligand interaction mechanism that significantly broadens our knowledge on how Staphylococci process their peptidoglycan. Although structures of other cell wall lytic enzymes have been determined before [61-64], this is the second structural elucidation of a bacterial amidase at all. It is also the first of any bacterial amidase resolution in which both the PGN component and the water molecule that carries out the nucleophilic attack on the carbonyl carbon of the scissile bond are present, as well as it is the first peptidoglycan amidase complex structure of an important human pathogen.

In order to understand the role played by each enzyme domains, we generated *S. aureus atl* mutants carrying deletions of the *amiA* (Δ*amiA-R1-R2*) and *glcA* (Δ*R3-glcA*) domains as well as the entire *atl* (Δ*atl*) gene and compared the resulting morphological changes. Through electron microscopic studies, we were able to show that each of these enzymes play a significant role in cell aggregation, proper septum formation and cell separation. Notably, loss of GlcA activity results in aberrant septum formation manifested by deformed and in part "kidney" like cell clusters. Despite a lowered peptidoglycan crosslinking, we observed that the Δ*atl*, Δ*amiA* und Δ*glcA* mutants were 10,000 - to 100,000-times more tolerant to oxacillin than the parent strain. This result elaborates not only the importance of this study in understanding the role of Atl domains in cell division and separation, but also that hydrolytic enzymes on the cell surface are required to augment the wall damage initiated by oxacillin and other β-lactam antibiotics to produce a bactericidal effect.

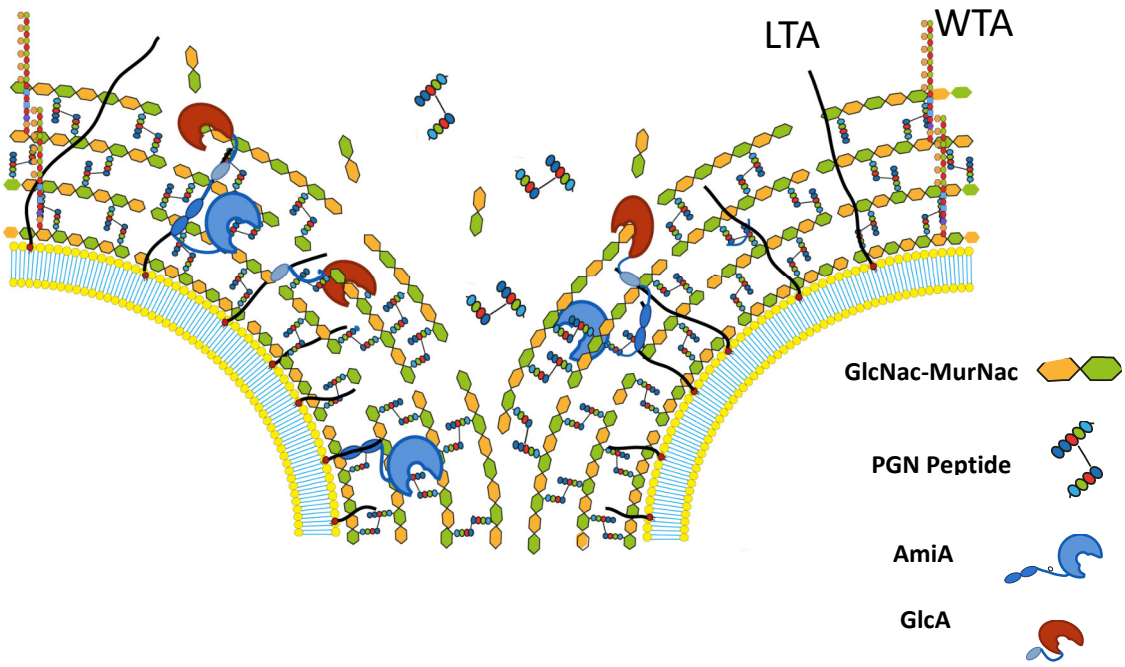

Figure 15. Illustration of the concerted action of AmiA and GlcA at the septum during cell separation in *Staphylococcus aureus*. At the septum, where the wall teichoic acids are not yet attached, both the amidase (AmiA) and glucoseamonidase (GlcA) attach to the peptidoglycan with their repeat domains. While the AmiA cuts the peptides off the glycan backbone, the GlcA follows chewing down the GlcNAc-MurNAc polysacchride and releasing disaccharides.

In all studies made hitherto, AmiA activity has been investigated mainly with synthetic substrates or in zymograms but not exclusively with its natural substrate, the staphylococcal peptidoglycan. This work shows for the first time, the activity of both

AmiA and GlcA on their natural substrate, the staphylococcal peptidoglycan. Both the AmiA-R1-R2 and the R3-GlcA were cloned and purified. Comparative peptidoglycan digestion with the purified AmiA revealed that, AmiA is specific to its host staphylococcal peptidoglycan. In addition, digestion products of AmiA, the cross-peptides, were resolved using HPLC separation methods. Structural compositions were determined by HPLC-MS analysis and the results confirmed the hitherto showed amidase activity that it cuts between the MurNAc of the glycan backbone and L-Ala of the stem peptide of its substrate peptidoglycan. It was possible to resolve crosslinked peptide products up to a length of 20-mer for the first time. Each peak showed additional mass value that corresponds to a tetrapeptide-pentaglycine fragment (monomer) which is exactly the fragment of the next crosslinking. Moreover, we revealed the mechanism by which GlcA digests peptidoglycan thereby answering the recurring question why it does not digest *S. aureus* whole peptidoglycan in zymograms. We identified that the naked glycan backbone is the natural GlcA substrate and it in turn is a product of prior digestion of peptidoglycan by AmiA. This implies that the cutting (resolution) of PGN occurs in a defined order, in which AmiA first hydrolyses the crosspeptides, and only then can GlcA chew back the naked glycan strand until the next peptide crosslinking position. Equally significant and novel are analysis results in this work which disproved the hitherto conclusion that the staphylococcal N-acetylglucosaminidase, GlcA, is an endo-β-1,4-N-acetylglucosaminidase. Identifying the right substrate and digestion products revealed that GlcA is not an *endo*- but an *exo*-β-N-acetylglucosaminidase that cuts back the glycan backbone from its end releasing only GlcNAc-MurNAc disaccharide product.

Taking all together, this study shows, for the first time, a complete functional picture of the *S. aureus* major autolysin, Atl, from its crystal structure to its ligand interaction and activity mechanisms. Moreover, it reveals the specific enzymatic activity mechanism and coordination in digesting the septal peptidoglycan during cell separation as well as the specific role of the amidase and glucosaminidase component domains in cell division and separation processes.

Chapter II

Adaptive and non-adaptive responses of the *S. carnosus femB* mutant in its structure, antimicrobial susceptibility and excretion of cytoplasmic proteins

Introduction

Peptidoglycan biosynthesis is one of the preferred targets for antibiotics, as this macromolecule is unique to eubacteria and inhibition of its production is generally bactericidal. The most widely used class of antibiotics that target the cell wall are β-lactams and their derivatives. Their introduction into therapy has, however, invariably been followed by the development and spread of resistance in the target bacteria. Gram-positive bacteria have developed two main strategies against β-lactams: drug inactivation by β-lactamases and intrinsic resistance mediated by modified, low-affinity variants of the target enzymes, the penicillin-binding proteins (PBPs). However, the effectiveness of these low-affinity PBPs in peptidoglycan synthesis depends on correctly synthesized peptidoglycan precursors in order to reach high-level β-lactam resistance. Specifically, the pentaglycyl interpeptide structure, which is characteristic of the peptidoglycan of *S. aureus* has a great impact on the level of β-lactam resistance that is achieved. In methicillin resistant *S. aureus* (MRSA) strains, the major determinant of methicillin resistance is the acquired *mecA* gene, which encodes for PBP2A, an enzyme insensitive to β-lactam acylation [65].

High-level β-lactam resistance is also dependent on several additional elements, which were initially identified by transposon mutagenesis and termed *fem* (factor essential for methicillin resistance) or *aux* (auxiliary) genes. Around 30 *fem/aux* determinants have been identified so far and most are housekeeping genes, involved in a variety of cellular processes [66, 67]. Among them are three closely related factors - *fmhB* and the co-transcribed *femA* and *femB* genes that encode the FemX, FemA and FemB

proteins, respectively. the FemABX family proteins are non-ribosomal peptidyl transferases, which use glycyl-tRNA as a glycine donor to sequentially transfer the five glycine residues to the stem peptide of the PG precursor lipid II during the inner membrane stages of PGN synthesis. The process takes place with strict substrate specificity in which FemX adds the first glycine whereas FemA adds the second and third glycines, while FemB adds the fourth and fifth glycines. Although structurally and functionally related, these factors cannot substitute for one another [18, 20].

The FemX, encoded by *fmhB* was shown to be essential [68]. However, mutants from transposon inactivation or deletion of *femA and femB* grew poorly but were viable. These mutants with shortened interpeptide bridge show not only impaired growth but also display massive reduction in cell wall crosslinking, aberrant septum formation, and hypersusceptibility to antibiotics including all β-lactams [69, 70]. For instance, methicillin resistance is completely abolished upon inactivation of *femA* in a methicillin-resistant *S. aureus* strain. These results lead the Fem-proteins to be regarded as potential targets for novel antibacterial agents, which could restore β-lactam susceptibility in MRSA [71].

Similar to the peptidoglycan, the cytoplasmic membrane is one of the dynamic structures of a bacterial cell. One of its main functions is the selective passage of larger molecules like proteins, that are usually above the size of 100 Da, by distinct protein secretion systems. The two major secretion pathways that are usually referred to the "classical secretion systems" are the SEC and Twin-Arginine (TAT) pathways. They rely on a distinct signal peptide motif at the N-terminus of the substrate to select and carry out their function. In many organisms where the classical secretion systems are not involved in the excretion of cytosolic proteins, the "nonclassical protein secretion" takes place. They are the holin-antiholin systems, the ABC transporters and the ESAT-6 secretion system that translocate proteins independent of any signal sequence. In *S. aureus*, over 20 typical cytosolic proteins are excreted, starting already in the exponential phase and it appears to be more pronounced in clinical isolates than in the non-pathogenic staphylococcal species [72, 73].

However, in bacteria as well as in eukaryotes, typical cytoplasmic proteins that do not possess any signal sequence and not transported by the non-classical pathways, are

found in the supernatant. Various *S. aureus* mutants have been analyzed with respect to the release of cytoplasmic proteins. For example, we have shown in a previous study that, in the major autolysin, Atl, deletion mutant, cytosolic proteins were hardly found in the supernatant, but were entrapped within the huge cell clusters of the mutant [70]. In the wall teichoic acid deficient tagO mutant, with its increased autolysis activity, excretion of cytosolic proteins was increased compared to the WT, confirming the importance of peptidoglycan integrity and autolysis in the excretion and/or release of cytosolic proteins [72].

Aim of the study

In our previous study using the *atl* deletion mutant, we have observed that peptidoglycan integrity and autolysin activity are factors that play important roles in excretion of cytoplasmic proteins.

The factors essential for the expression of methicillin resistance (fem), encode the FemABX peptidyl transferases involved in non-ribosomal pentaglycine interpeptide bridge biosynthesis. While femX is essential, Tn inactivation of *femA* and *femB* lead to viable mutants that grew poorly. Both mutants showed reduced peptidoglycan (PGN) cross linking, reduced whole-cell autolysis and increased sensitivity to β-lactam antibiotics. They also show aberrant placement of cross walls, and stunted cell separation showing key functions of the pentaglycine interpeptide bridge.

We therefore aim to investigate the role of *femB* deletion on the morphology and physiology of the cell, integrity of its peptidoglycan as well as susceptibility towards antibiotics and cell wall hydrolytic enzyme Lysostaphin. Lowering of lysostaphin susceptibility is aimed with the intention of using *S. carnosus* as an expression platform for cell wall hydrolytic enzymes that target the pentapeptide bridge structure.

Moreover, we aim to find out the role of FemB, and consequently, the effect of peptidoglycan structural alteration in the pentaglycine bridge on the excretion of cytoplasmic proteins as was observed with the deletion of the staphylococcal major autolysin Atl.

Results and discussion

Under this section, results of the following publications are summarized and discussed.

1. **Nega M**, Dube L, Kull M, Ziebandt AK, Ebner P, Albrecht D, Krismer B, Rosenstein R, Hecker M & Götz F (2015) Secretome analysis revealed adaptive and non-adaptive responses of the *Staphylococcus carnosus* femB mutant. *Proteomics* **15**: 1268-1279.

2. Ebner P, Prax M, **Nega M**, Koch I, Dube L, Yu W, Rinker J, Popella P, Flötenmeyer M & Götz F (2015) Excretion of cytoplasmic proteins (ECP) in *Staphylococcus aureus*. *Mol Microbiol* **97**: 775-789.

3. Ebner P, Rinker J, Nguyen MT, Popella P, **Nega M**, Luqman A, Schittek B, Di Marco M, Stevanovic S & Götz F (2016) Excreted Cytoplasmic Proteins Contribute to Pathogenicity in *Staphylococcus aureus*. *Infect Immun* **84**: 1672-1681.

The effect of *femB* deletion on growth, methicillin susceptibility and lysostaphin tolerance

The *femAB* operon and the pentaglycine crossbridges are unique features of staphylococci which makes both the FemAB proteins and the pentaglycine structure interesting targets for staphylococcus specific drug design. In this work we investigated if depletion of the FemB protein is lethal and determine the phenotypic defects associated with lack of its expression in *S. carnosus* which is generally regarded as safe (GRAS) strain. We used the *S. carnosus* strain background with the assumption that a viable strain with a good growth could be used as an expression platform for cell wall hydrolytic enzymes that target the pentapeptide bridge structure such as lysostaphin.

We constructed a *femB* deletion mutant in *S. carnosus* TM300, in which the femAB operon is orthologous to that of *S. aureus,* by replacing *femB* with an erythromycin cassette, *ermB*. The femB mutant was complemented with the plasmid pPSHG5femB,

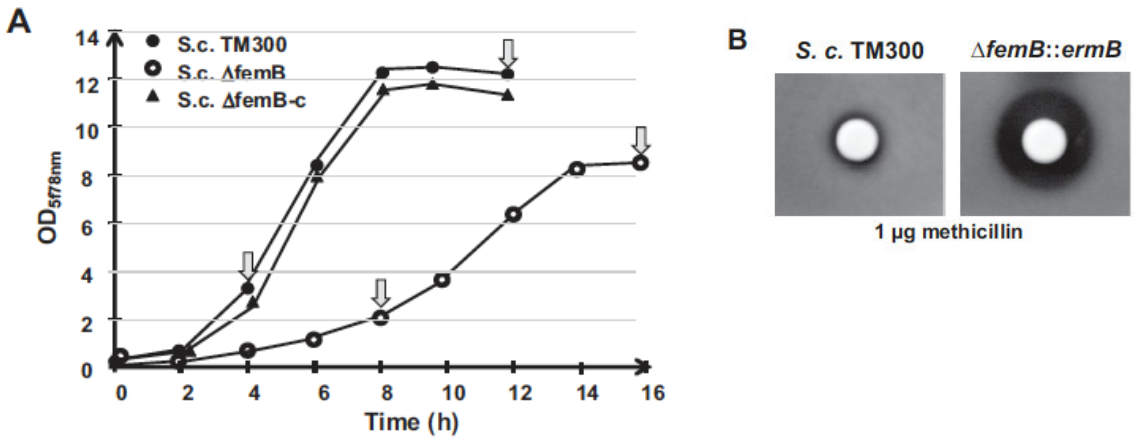

Figure 1. Comparative phenotypic features of *S. carnosus*, its femB mutant, and the complementary mutant. (A) Growth was severely affected in the femB mutant; arrow indicates sampling time for protein analysis. (B) Agar diffusion assay showing femB mutant methicillin susceptibility. S.c. TM300: wild type; ΔfemB: femB deletion mutant; ΔfemB-c: mutant complemented with pPSHG5femB

which was constructed by cloning femB under the control of a galactose-inducible promoter. The deletion mutant has a shortened glycine interpeptide bridge in the murein structure which is a stress factor that leads to metabolic adjustments to be made. Therefore, the mutant growth was severely affected with a growth rate lowered by more than half the WT values. This growth deficiency could be restored successfully by the plasmid complemented mutant (Fig.1A). The mutant also showed a much higher sensitivity towards methicillin compared to the WT (Fig. 1B) while showing high resistance to lysostaphin. Since lysostaphin targets exclusively the pentapeptide

bridge, this alteration of the target peptide leads to a more than 3000-fold increase in MIC values from 0.01µg/mL in the WT to 32 µg/mL in the *femB* deletion mutant strain.

The role of FemB on cell physiology and cell separation

Microscopic analyses showed that cells of the femB mutant form cell clusters indicating a defect in daughter cell separation. Peptidoglycan staining with fluorescent Vancomycin (Van-FL) revealed a massive accumulation of fluorescence intensity in the septum region of the femB mutant suggesting that the degree of cross-linking of

A

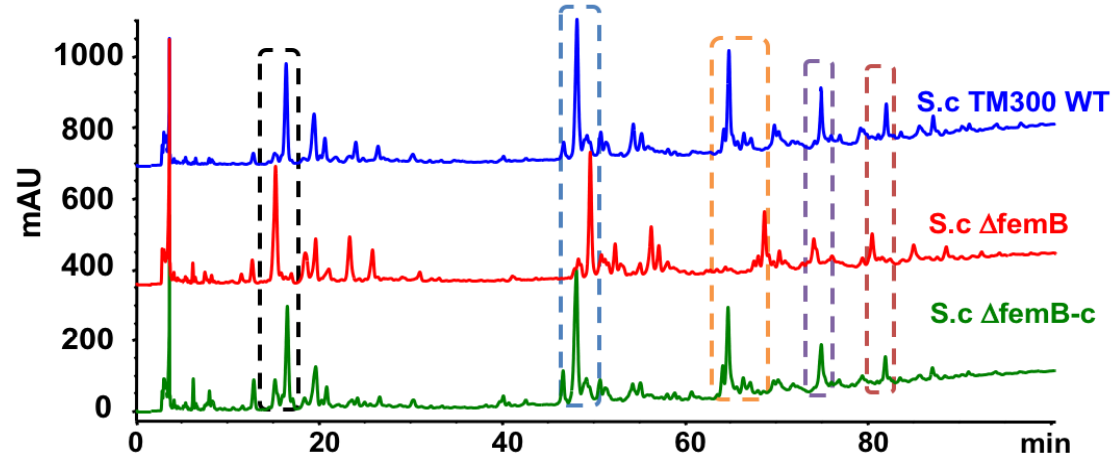

B

	1-mer (%)	2-mer (%)	3-mer (%)	4-mer (%)	5-mer (%)
S. c. TM300	22	33	22	16	8
S. c. Δ*femB*	33	31	15	12	10
S. c. Δ*femB* comp.	21	36	22	15	6

Figure 2. Peptidoglycan composition is altered in the S. carnosusfemB strain. **(A)** HPLC analysis of mutanolysin digested PGN of the wild-type strain of S. carnosus TM300, the mutant S.cfemB, and the complemented mutant. **(B)** Eluted UV-absorbing peaks were integrated, and the corresponding muropeptides highlighted by the dotted area in (A) were quantified as a percentage of the total area of identified peaks. Dotted areas represent monomers to pentamers (left to right).

the PGN network was considerably decreased. In order to confirm and measure the degree of crosslinking, peptidoglycan was isolated from the WT, mutant and the complemented mutant and digested with the muramidase mutanolysin, that degrades peptidoglycan by hydrolyzing the MurNac-GlcNac glycosidic bond of the glycan backbone. Comparison of the amount of each of the solubilized peptidoglycan

fragments showed that the mutant contained more of the un-crosslinked and lower crosslinked fragments and less of the fragments with higher crosslinking. The monomeric fragments were roughly 50% more abundant in the mutant compared to the WT, and the tri- and tetramer fragments were less in comparative abundance.

As with vancomycin, fluorescence intensity with FM 464, a cell impermeant membrane stain, was increased in the septum region of the femB mutant, indicating increased penetration of the dye through the cell wall to the membrane site, which correlates with the lower peptidoglycan crosslinking observed. Ultimately, DNA staining with DAPI revealed enlarged nucleoid in the mutant, which could have resulted from decreased chromosomal condensation. In all microscopic image analyses, the femB mutant cells were enlarged with an average cell diameter 132% higher than the WT or the complemented mutant.

Deletion of *femB* and its effect in excretion of cytoplasmic proteins

A very surprising effect of the *femB* deletion was the drastic increase of secreted proteins. We have analyzed and compared the amount of both the cytoplasmic and secreted proteins in the exponential and stationary phases. Our first observation was

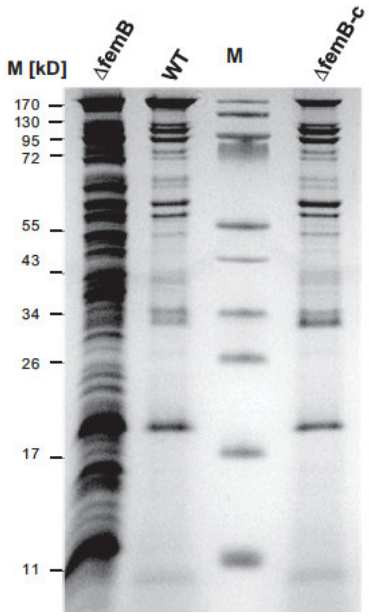

Figure 3. Comparative phenotypic features of S. carnosus, its femB mutant, and the complementary mutant: SDS-PAGE of culture supernatant proteins; cells were cultivated for 13 h in the presence of 0.25% galactose. WT: wild type; S.c. TM300; ΔfemB: femB deletion mutant; ΔfemB-c: mutant complemented with pPSHG5femB; M: marker proteins.

a massive release of proteins in the supernatant which was readily visible on SDS-PAGE analysis (Fig. 2), while the cytosolic protein content remained more or less the same. We compared the secreted protein amount in the supernatant quantitatively using five different *femB* mutant isolates in the exponential and stationary growth phases. The results revealed that the protein content in the *femB* mutant was always roughly 5 to 6 times higher than in the WT. Therefore, comparative secretome analysis was performed to determine the qualitative protein abundance in the supernatant of the *femB* deletion mutant using 2D-PAGE and mass spectroscopic analysis. Due to the growth rate difference (Fig. 1A), protein samples were taken at the exponential growth phase after 4 h (for the WT) and 8 h (for the *femB* mutant), as well as after 12 h (for the WT) and 16 h (for the *femB* mutant) for the stationary growth phase. Protein spots of each of three 2D gels of the WTand the *femB* mutant were analyzed by mass spectroscopy and 82 different proteins could be identified and quantified. Using the Delta2D software (DECODON) for better visualization, thirty six selected protein spots showing the most significant differences in intensity between the WTand *femB* mutant were identified and characterized.

Proteins showing increased abundance in the secretome of the *femB* mutant belong mainly to cytosolic proteins followed by cell wall/membrane anchored proteins and extracellular proteins. From the 30 proteins analyzed that are more abundant in the *femB* mutant, four proteins belonged to signal peptide-dependent transported proteins. These enzymes are involved in murein turnover and daughter cell separation, and their increased production in the *femB* mutant is most likely a compensatory response to partially resolve the cell wall interlinked cell clusters.

Out of the 20 cytosolic proteins identified, eleven proteins belonged to enzymes of the central metabolic pathways whereas four were enzymes involved in protein folding and oxidative stress situations. The rest represent 50S ribosomal proteins such as RplC, RplE, RplF, and RplJ.

To verify this secretome analysis data, four cytosolic proteins: fructose-bisphosphate aldolase (FabA), glyceraldehyde-3-phosphate dehydrogenase (GapA), enolase (Eno), and NADH-dehydrogenase (Ndh-2) were chosen and analyzed. Each protein was detected using specific antibodies in the cytoplasm, cell wall and supernatant fractions

at different time points among the WT, mutant and complemented mutant strains. The results show no marked difference in protein amounts in the cytosolic fractions. There was however, a clear difference in the cell wall fraction and culture supernatant showing a significant increase in the *femB* mutant confirming that the cytosolic target proteins were abundantly exported. Transcriptome analysis showed that transcription of genes encoding cell wall lytic enzymes was up-regulated in the *femB* mutant, while that of cytosolic target genes was unchanged.

Spatial and temporal pattern of excretion of cytoplasmic proteins

Having observed that, excretion of cytoplasmic proteins is not due to cell lysis but a common physiological feature in bacteria and eukaryotes, and that cell stress situations such as in the *femB* mutant lead to increased excretion; the next logical question is to find out the spatial and temporal pattern of this excretion mechanism. These investigations were carried out using the pathogenic *S. aureus* instead of *S. carnosus.* Two glycolytic model proteins which we already analyzed in the experiments with the *S. carnosus femB* mutant; fructose-bisphosphate aldolase (FabA) and enolase (Eno), were chosen and their relative abundance in the supernatant was measured using western blot analysis. The IgG binding protein, Sbi, which is secreted via the sec-pathway was used as a control. The results show that both FabA and Eno were secreted during the exponential growth phase. FabA showed a steady increase until 8 hours with a slight decrease afterwards whereas Eno showed its strongest excretion after 4 hours with a steady decrease afterwards until 10 hours.

In order to find out the location of this excretion, a cell wall back binding approach was followed. Both proteins were fused to the cell wall binding domain LysM. These fusion proteins were then detected on the cell surface using protein specific primary antibodies followed by fluorescent labelled secondary antibodies. In this case, the not excreted Ndh2 was used as a control. The results show that fluorescent signals were only visible at the cross walls and septum regions. There was no signal on single or non-dividing cells. This results were further confirmed using transmission electron microscopy with an immunogold-labelling of the three proteins. These results lead to the conclusion that excretion of cytoplasmic proteins occur during cell division across the septum region.

Excretion of cytoplasmic proteins and its role in *S. aureus* Pathogenicity

Similar to the “nonclassical protein export”, little is known about the role of these excreted proteins in staphylococcal pathogenicity. We therefore selected two of the typical cytoplasmic proteins, aldolase (FbaA) and glyceraldehyde-3-phosphate dehydrogenase (GAPDH), which we already found out as to whether, how and where they are excreted, to investigate their impact on staphylococcal pathogenicity.

The first question was if there is any correlation between pathogenicity of a strain and the amount of excreted proteins. Indeed, comparative analysis shows a correlation between pathogenicity and amount of excreted protein. The more virulent the strain, the more abundant excreted proteins are in the supernatant. To find out how FbaA and GAPDH specifically contribute to virulence, binding studies to different host matrix proteins was carried out. The results show that both proteins bind to plasminogen, vitronectin and fibrinogen. They also increase adherence of JE2 to HaCaT and HEK293 cells by a factor of 1.5 to 1.8, whereas invasion was rather decreased in the presence of these proteins.

Investigation of cytotoxicity with cell proliferation (MTT) assay in MonoMac6 cells and keratinocyte cell line HaCaT cells showed cytotoxicity in a dose dependent manner. FbaA showed comparatively high cytotoxicity to both MM6 and HaCaT cells, while GAPDH was cytotoxic only to MM6 cells.

Since exogenously applied FbaA and GAPDH contribute to host cell adherence and are cytotoxic to host cells, a *Galleria mellonella* infection model was used to compare the virulence of JE2 with and without exogenously applied proteins to investigate their effects *in vivo*. Larvae infected with JE2 together with FbaA and GAPDH were significantly more rapidly killed than those without and the control group injected with PBS and proteins only. The results clearly showed that GAPDH and FbaA enhance virulence of *S. aureus* USA300 JE2 in a *Galleria mellonella* infection model.

Concluding remarks

Understanding Peptidoglycan biosynthesis is crucial in finding ways of combating antibiotic resistance, since peptidoglycan is one of the preferred targets for antibiotic treatment. One of the crucial steps in staphylococcal peptidoglycan biosynthesis is the addition of the five glycine residues to the stem peptide of the PG precursor lipid II by the non-ribosomal peptidyl transferases FemA, FemB and FemX using glycyl-tRNA as a glycine donor. In this study we have examined the effects of deletion of the *femB* and the consequent alteration of the cell wall structure of *S. carnosus* and its effect on the morphology, physiology and antibiotic susceptibility of the organism. We have found out that shortening of the interpeptide bridge from five to three glycine residues poses a life-threatening problem for the organism leading to expanded cells, retarded growth, reduced peptidoglycan crosslinking, high susceptibility to cell wall antibiotics and surprisingly high secretion and release of proteins into the culture supernatant.

We further investigated the excretion pattern of cytoplasmic proteins in the pathogenic *S. aureus*. We were able to show that the main excretion of cytoplasmic proteins takes place at the septum mainly during the exponential growth phase. Furthermore, we investigated the role of these excreted proteins during infection. The excreted “moonlighting proteins” FbaA and GAPDH are surface exposed by interacting with Atl and lead to increased adherence of *S. aureus* USA300 JE2 in keratinocytes and monocytes. We showed that these proteins bind to both vitronectin and fibrinogen as well as plasminogen of host cells. This binding property to certain extracellular host matrix proteins and their ability of back binding to staphylococcal surface via Atl as well as the weak interaction with PGN explains their role in adherence. Summing up these evidences, excretion of cytoplasmic proteins are important factors in staphylococcal pathogenicity.

References

1. de Jonge BL, Chang YS, Gage D, Tomasz A: **Peptidoglycan composition in heterogeneous Tn551 mutants of a methicillin-resistant *Staphylococcus aureus* strain**. *J Biol Chem* 1992, **267**(16):11255-11259.
2. Zoll S, Schlag M, Shkumatov AV, Rautenberg M, Svergun DI, Götz F, Stehle T: **Ligand-binding properties and conformational dynamics of autolysin repeat domains in staphylococcal cell wall recognition**. *J Bacteriol* 2012, **194**(15):3789-3802.
3. Boneca IG, Huang ZH, Gage DA, Tomasz A: **Characterization of *Staphylococcus aureus* cell wall glycan strands, evidence for a new beta-N-acetylglucosaminidase activity**. *J Biol Chem* 2000, **275**(14):9910-9918.
4. Snowden MA, Perkins HR, Wyke AW, Hayes MV, Ward JB: **Cross-linking and O-acetylation of newly synthesized peptidoglycan in *Staphylococcus aureus* H**. *J Gen Microbiol* 1989, **135**(11):3015-3022.
5. Silhavy TJ, Kahne D, Walker S: **The bacterial cell envelope**. *Cold Spring Harb Perspect Biol* 2010, **2**(5):a000414.
6. Pucci MJ, Thanassi JA, Ho HT, Falk PJ, Dougherty TJ: ***Staphylococcus haemolyticus* contains two D-glutamic acid biosynthetic activities, a glutamate racemase and a D-amino acid transaminase**. *J Bacteriol* 1995, **177**(2):336-342.
7. Tipper DJ, Katz W, Strominger JL, Ghuysen JM: **Substituents on the alpha-carboxyl group of D-glutamic acid in the peptidoglycan of several bacterial cell walls**. *Biochemistry* 1967, **6**(3):921-929.
8. Komatsuzawa H, Fujiwara T, Nishi H, Yamada S, Ohara M, McCallum N, Berger-Bachi B, Sugai M: **The gate controlling cell wall synthesis in *Staphylococcus aureus***. *Mol Microbiol* 2004, **53**(4):1221-1231.
9. Benson TE, Marquardt JL, Marquardt AC, Etzkorn FA, Walsh CT: **Overexpression, purification, and mechanistic study of UDP-N-acetylenolpyruvylglucosamine reductase**. *Biochemistry* 1993, **32**(8):2024-2030.
10. Bouhss A, Mengin-Lecreulx D, Blanot D, van Heijenoort J, Parquet C: **Invariant amino acids in the Mur peptide synthetases of bacterial peptidoglycan synthesis and their modification by site-directed mutagenesis in the UDP-MurNAc:L-alanine ligase from *Escherichia coli***. *Biochemistry* 1997, **36**(39):11556-11563.
11. Patin D, Boniface A, Kovac A, Herve M, Dementin S, Barreteau H, Mengin-Lecreulx D, Blanot D: **Purification and biochemical characterization of Mur ligases from *Staphylococcus aureus***. *Biochimie* 2010, **92**(12):1793-1800.
12. Bouhss A, Crouvoisier M, Blanot D, Mengin-Lecreulx D: **Purification and characterization of the bacterial MraY translocase catalyzing the first membrane step of peptidoglycan biosynthesis**. *J Biol Chem* 2004, **279**(29):29974-29980.
13. Chung BC, Zhao J, Gillespie RA, Kwon DY, Guan Z, Hong J, Zhou P, Lee SY: **Crystal structure of MraY, an essential membrane enzyme for bacterial cell wall synthesis**. *Science* 2013, **341**(6149):1012-1016.
14. Pless DD, Neuhaus FC: **Initial membrane reaction in peptidoglycan synthesis. Lipid dependence of phospho-n-acetylmuramyl-pentapeptide translocase (exchange reaction)**. *J Biol Chem* 1973, **248**(5):1568-1576.
15. Hu Y, Helm JS, Chen L, Ye XY, Walker S: **Ramoplanin inhibits bacterial transglycosylases by binding as a dimer to lipid II**. *J Am Chem Soc* 2003, **125**(29):8736-8737.

16. Mengin-Lecreulx D, Texier L, Rousseau M, van Heijenoort J: **The murG gene of *Escherichia coli* codes for the UDP-N-acetylglucosamine: N-acetylmuramyl-(pentapeptide) pyrophosphoryl-undecaprenol N-acetylglucosamine transferase involved in the membrane steps of peptidoglycan synthesis**. *J Bacteriol* 1991, **173**(15):4625-4636.
17. Berger-Bachi B, Tschierske M: **Role of fem factors in methicillin resistance**. *Drug Resist Updat* 1998, **1**(5):325-335.
18. Ehlert K, Schroder W, Labischinski H: **Specificities of FemA and FemB for different glycine residues: FemB cannot substitute for FemA in staphylococcal peptidoglycan pentaglycine side chain formation**. *J Bacteriol* 1997, **179**(23):7573-7576.
19. Henze U, Sidow T, Wecke J, Labischinski H, Berger-Bachi B: **Influence of femB on methicillin resistance and peptidoglycan metabolism in *Staphylococcus aureus***. *J Bacteriol* 1993, **175**(6):1612-1620.
20. Schneider T, Senn MM, Berger-Bachi B, Tossi A, Sahl HG, Wiedemann I: **In vitro assembly of a complete, pentaglycine interpeptide bridge containing cell wall precursor (lipid II-Gly5) of *Staphylococcus aureus***. *Mol Microbiol* 2004, **53**(2):675-685.
21. Figueiredo TA, Sobral RG, Ludovice AM, Almeida JM, Bui NK, Vollmer W, de Lencastre H, Tomasz A: **Identification of genetic determinants and enzymes involved with the amidation of glutamic acid residues in the peptidoglycan of *Staphylococcus aureus***. *Plos Pathog* 2012, **8**(1):e1002508.
22. Munch D, Roemer T, Lee SH, Engeser M, Sahl HG, Schneider T: **Identification and *in vitro* analysis of the GatD/MurT enzyme-complex catalyzing lipid II amidation in *Staphylococcus aureus***. *Plos Pathog* 2012, **8**(1):e1002509.
23. Ruiz N: **Bioinformatics identification of MurJ (MviN) as the peptidoglycan lipid II flippase in *Escherichia coli***. *Proc Natl Acad Sci U S A* 2008, **105**(40):15553-15557.
24. Ruiz N: ***Streptococcus pyogenes* YtgP (Spy_0390) complements *Escherichia coli* strains depleted of the putative peptidoglycan flippase MurJ**. *Antimicrob Agents Chemother* 2009, **53**(8):3604-3605.
25. Sham LT, Butler EK, Lebar MD, Kahne D, Bernhardt TG, Ruiz N: **Bacterial cell wall. MurJ is the flippase of lipid-linked precursors for peptidoglycan biogenesis**. *Science* 2014, **345**(6193):220-222.
26. Navratna V, Nadig S, Sood V, Prasad K, Arakere G, Gopal B: **Molecular basis for the role of *Staphylococcus aureus* penicillin binding protein 4 in antimicrobial resistance**. *J Bacteriol* 2010, **192**(1):134-144.
27. Vollmer W, Joris B, Charlier P, Foster S: **Bacterial peptidoglycan (murein) hydrolases**. *FEMS Microbiol Rev* 2008, **32**(2):259-286.
28. Yamada S, Sugai M, Komatsuzawa H, Nakashima S, Oshida T, Matsumoto A, Suginaka H: **An autolysin ring associated with cell separation of *Staphylococcus aureus***. *J Bacteriol* 1996, **178**(6):1565-1571.
29. Chan YG, Frankel MB, Missiakas D, Schneewind O: **SagB Glucosaminidase Is a Determinant of *Staphylococcus aureus* Glycan Chain Length, Antibiotic Susceptibility, and Protein Secretion**. *J Bacteriol* 2016, **198**(7):1123-1136.
30. Wheeler R, Turner RD, Bailey RG, Salamaga B, Mesnage S, Mohamad SA, Hayhurst EJ, Horsburgh M, Hobbs JK, Foster SJ: **Bacterial Cell Enlargement Requires Control of Cell Wall Stiffness Mediated by Peptidoglycan Hydrolases**. *MBio* 2015, **6**(4):e00660.
31. Stapleton MR, Horsburgh MJ, Hayhurst EJ, Wright L, Jonsson IM, Tarkowski A, Kokai-Kun JF, Mond JJ, Foster SJ: **Characterization of IsaA and SceD, two putative**

lytic transglycosylases of *Staphylococcus aureus*. *J Bacteriol* 2007, **189**(20):7316-7325.

32. Kajimura J, Fujiwara T, Yamada S, Suzawa Y, Nishida T, Oyamada Y, Hayashi I, Yamagishi J, Komatsuzawa H, Sugai M: **Identification and molecular characterization of an N-acetylmuramyl-L-alanine amidase Sle1 involved in cell separation of *Staphylococcus aureus***. *Mol Microbiol* 2005, **58**(4):1087-1101.
33. Frankel MB, Hendrickx AP, Missiakas DM, Schneewind O: **LytN, a murein hydrolase in the cross-wall compartment of *Staphylococcus aureus*, is involved in proper bacterial growth and envelope assembly**. *J Biol Chem* 2011, **286**(37):32593-32605.
34. Ramadurai L, Lockwood KJ, Nadakavukaren MJ, Jayaswal RK: **Characterization of a chromosomally encoded glycylglycine endopeptidase of *Staphylococcus aureus***. *Microbiology* 1999, **145 (Pt 4)**:801-808.
35. Thumm G, Götz F: **Studies on prolysostaphin processing and characterization of the lysostaphin immunity factor (Lif) of *Staphylococcus simulans* biovar *staphylolyticus***. *Mol Microbiol* 1997, **23**(6):1251-1265.
36. Oshida T, Sugai M, Komatsuzawa H, Hong YM, Suginaka H, Tomasz A: **A *Staphylococcus aureus* autolysin that has an N-acetylmuramoyl-L-alanine amidase domain and an endo-beta-N-acetylglucosaminidase domain: cloning, sequence analysis, and characterization**. *Proc Natl Acad Sci U S A* 1995, **92**(1):285-289.
37. Heilmann C, Hussain M, Peters G, Götz F: **Evidence for autolysin-mediated primary attachment of *Staphylococcus epidermidis* to a polystyrene surface**. *Mol Microbiol* 1997, **24**(5):1013-1024.
38. Albrecht T, Raue S, Rosenstein R, Nieselt K, Götz F: **Phylogeny of the staphylococcal major autolysin and its use in genus and species typing**. *J Bacteriol* 2012, **194**(10):2630-2636.
39. Sugai M, Komatsuzawa H, Akiyama T, Hong YM, Oshida T, Miyake Y, Yamaguchi T, Suginaka H: **Identification of endo-beta-N-acetylglucosaminidase and N-acetylmuramyl-L-alanine amidase as cluster-dispersing enzymes in *Staphylococcus aureus***. *J Bacteriol* 1995, **177**(6):1491-1496.
40. Demleitner G, Götz F: **Evidence for importance of the *Staphylococcus hyicus* lipase pro-peptide in lipase secretion, stability and activity**. *FEMS Microbiol Lett* 1994, **121**(2):189-197.
41. Rosenstein R, Götz F: **Staphylococcal lipases: biochemical and molecular characterization**. *Biochimie* 2000, **82**(11):1005-1014.
42. Biswas R, Voggu L, Simon UK, Hentschel P, Thumm G, Götz F: **Activity of the major staphylococcal autolysin Atl**. *FEMS Microbiol Lett* 2006, **259**(2):260-268.
43. Schlag M, Biswas R, Krismer B, Kohler T, Zoll S, Yu W, Schwarz H, Peschel A, Götz F: **Role of staphylococcal wall teichoic acid in targeting the major autolysin Atl**. *Mol Microbiol* 2010, **75**(4):864-873.
44. Baba T, Schneewind O: **Instruments of microbial warfare: bacteriocin synthesis, toxicity and immunity**. *Trends Microbiol* 1998, **6**(2):66-71.
45. Borisova M, Gaupp R, Duckworth A, Schneider A, Dalugge D, Muhleck M, Deubel D, Unsleber S, Yu W, Muth G *et al*: **Peptidoglycan Recycling in Gram-Positive Bacteria Is Crucial for Survival in Stationary Phase**. *MBio* 2016, **7**(5).
46. Kluj RM, Ebner P, Adamek M, Ziemert N, Mayer C, Borisova M: **Recovery of the Peptidoglycan Turnover Product Released by the Autolysin Atl in *Staphylococcus aureus* Involves the Phosphotransferase System Transporter MurP and the Novel 6-phospho-N-acetylmuramidase MupG**. *Front Microbiol* 2018, **9**:2725.
47. Charles A. Janeway J, Medzhitov R: **Innate Immune Recognition**. *Annual Review of Immunology* 2002, **20**(1):197-216.

48. Ozinsky A, Underhill DM, Fontenot JD, Hajjar AM, Smith KD, Wilson CB, Schroeder L, Aderem A: **The repertoire for pattern recognition of pathogens by the innate immune system is defined by cooperation between toll-like receptors**. *Proc Natl Acad Sci U S A* 2000, **97**(25):13766-13771.
49. Takeuchi O, Hoshino K, Kawai T, Sanjo H, Takada H, Ogawa T, Takeda K, Akira S: **Differential roles of TLR2 and TLR4 in recognition of gram-negative and gram-positive bacterial cell wall components**. *Immunity* 1999, **11**(4):443-451.
50. Yoshimura A, Lien E, Ingalls RR, Tuomanen E, Dziarski R, Golenbock D: **Cutting edge: recognition of Gram-positive bacterial cell wall components by the innate immune system occurs via Toll-like receptor 2**. *J Immunol* 1999, **163**(1):1-5.
51. Travassos LH, Girardin SE, Philpott DJ, Blanot D, Nahori MA, Werts C, Boneca IG: **Toll-like receptor 2-dependent bacterial sensing does not occur via peptidoglycan recognition**. *EMBO Rep* 2004, **5**(10):1000-1006.
52. Volz T, Nega M, Buschmann J, Kaesler S, Guenova E, Peschel A, Rocken M, Götz F, Biedermann T: **Natural *Staphylococcus aureus*-derived peptidoglycan fragments activate NOD2 and act as potent costimulators of the innate immune system exclusively in the presence of TLR signals**. *FASEB J* 2010, **24**(10):4089-4102.
53. Chamaillard M, Hashimoto M, Horie Y, Masumoto J, Qiu S, Saab L, Ogura Y, Kawasaki A, Fukase K, Kusumoto S *et al*: **An essential role for NOD1 in host recognition of bacterial peptidoglycan containing diaminopimelic acid**. *Nat Immunol* 2003, **4**(7):702-707.
54. Girardin SE, Boneca IG, Viala J, Chamaillard M, Labigne A, Thomas G, Philpott DJ, Sansonetti PJ: **Nod2 is a general sensor of peptidoglycan through muramyl dipeptide (MDP) detection**. *J Biol Chem* 2003, **278**(11):8869-8872.
55. Hasegawa M, Yang K, Hashimoto M, Park JH, Kim YG, Fujimoto Y, Nunez G, Fukase K, Inohara N: **Differential release and distribution of Nod1 and Nod2 immunostimulatory molecules among bacterial species and environments**. *J Biol Chem* 2006, **281**(39):29054-29063.
56. Nigro G, Fazio LL, Martino MC, Rossi G, Tattoli I, Liparoti V, De Castro C, Molinaro A, Philpott DJ, Bernardini ML: **Muramylpeptide shedding modulates cell sensing of *Shigella flexneri***. *Cell Microbiol* 2008, **10**(3):682-695.
57. Rogers HJ, Forsberg CW: **Role of autolysins in the killing of bacteria by some bactericidal antibiotics**. *J Bacteriol* 1971, **108**(3):1235-1243.
58. Best GK, Best NH, Koval AV: **Evidence for participation of autolysins in bactericidal action of oxacillin on *Staphylococcus aureus***. *Antimicrob Agents Chemother* 1974, **6**(6):825-830.
59. Götz F, Heilmann C, Stehle T: **Functional and structural analysis of the major amidase (Atl) in Staphylococcus**. *Int J Med Microbiol* 2014, **304**(2):156-163.
60. Lutzner N, Patzold B, Zoll S, Stehle T, Kalbacher H: **Development of a novel fluorescent substrate for Autolysin E, a bacterial type II amidase**. *Biochem Biophys Res Commun* 2009, **380**(3):554-558.
61. Hermoso JA, Monterroso B, Albert A, Galan B, Ahrazem O, Garcia P, Martinez-Ripoll M, Garcia JL, Menendez M: **Structural basis for selective recognition of pneumococcal cell wall by modular endolysin from phage Cp-1**. *Structure* 2003, **11**(10):1239-1249.
62. Low LY, Yang C, Perego M, Osterman A, Liddington RC: **Structure and lytic activity of a *Bacillus anthracis* prophage endolysin**. *J Biol Chem* 2005, **280**(42):35433-35439.
63. Monterroso B, Lopez-Zumel C, Garcia JL, Saiz JL, Garcia P, Campillo NE, Menendez M: **Unravelling the structure of the pneumococcal autolytic lysozyme**. *Biochem J* 2005, **391**(Pt 1):41-49.

64. Zoll S, Patzold B, Schlag M, Götz F, Kalbacher H, Stehle T: **Structural basis of cell wall cleavage by a staphylococcal autolysin**. *Plos Pathog* 2010, **6**(3):e1000807.
65. Hartman BJ, Tomasz A: **Low-affinity penicillin-binding protein associated with beta-lactam resistance in *Staphylococcus aureus***. *J Bacteriol* 1984, **158**(2):513-516.
66. Berger-Bachi B: **Insertional inactivation of staphylococcal methicillin resistance by Tn551**. *J Bacteriol* 1983, **154**(1):479-487.
67. De Lencastre H, Wu SW, Pinho MG, Ludovice AM, Filipe S, Gardete S, Sobral R, Gill S, Chung M, Tomasz A: **Antibiotic resistance as a stress response: complete sequencing of a large number of chromosomal loci in *Staphylococcus aureus* strain COL that impact on the expression of resistance to methicillin**. *Microb Drug Resist* 1999, **5**(3):163-175.
68. Tschierske M, Mori C, Rohrer S, Ehlert K, Shaw KJ, Berger-Bachi B: **Identification of three additional femAB-like open reading frames in *Staphylococcus aureus***. *FEMS Microbiol Lett* 1999, **171**(2):97-102.
69. Maidhof H, Reinicke B, Blumel P, Berger-Bachi B, Labischinski H: **femA, which encodes a factor essential for expression of methicillin resistance, affects glycine content of peptidoglycan in methicillin-resistant and methicillin-susceptible *Staphylococcus aureus* strains**. *J Bacteriol* 1991, **173**(11):3507-3513.
70. Stranden AM, Ehlert K, Labischinski H, Berger-Bachi B: **Cell wall monoglycine cross-bridges and methicillin hypersusceptibility in a femAB null mutant of methicillin-resistant *Staphylococcus aureus***. *J Bacteriol* 1997, **179**(1):9-16.
71. Ling B, Berger-Bachi B: **Increased overall antibiotic susceptibility in *Staphylococcus aureus* femAB null mutants**. *Antimicrob Agents Chemother* 1998, **42**(4):936-938.
72. Pasztor L, Ziebandt AK, Nega M, Schlag M, Haase S, Franz-Wachtel M, Madlung J, Nordheim A, Heinrichs DE, Götz F: **Staphylococcal major autolysin (Atl) is involved in excretion of cytoplasmic proteins**. *J Biol Chem* 2010, **285**(47):36794-36803.
73. Ziebandt AK, Weber H, Rudolph J, Schmid R, Hoper D, Engelmann S, Hecker M: **Extracellular proteins of *Staphylococcus aureus* and the role of SarA and sigma B**. *Proteomics* 2001, **1**(4):480-493.

Acknowledgements

This work would not have been possible without the special support of my mentor and supervisor Prof. Dr. Friedrich Götz. Fritz, I thank you very much not only for the support but also for the extensive personal and professional guidance and the scientific freedom you gave me in the lab to pursue my ideas in doing research. I also thank you for the full trust you bestow upon me in the long years of working together. I would also like to thank Prof. Dr. Andreas Peschel not only for long years of working together but also for reviewing and evaluating this thesis as my second supervisor.

I take this chance to thank everyone, former and current members, of the department of Microbial Genetics for their support in the day to day lab life and at times outside the lab. I also would like to specially thank my longtime colleagues and friends Andreas Kulik for the support in MS analyses, Bernhard Krismer for the valuable discussions and manuscript review and for their friendship over the years. Thank you Katja Schlatterer for helping in cell culture handling and all the members of the research group of Prof. A. Peschel in the department of Infection Biology for their helpfulness and always welcoming environment.

My thank goes to members of the “neighbour” lab especially Dhana, Nadine, Laura, Cruz, Philipp and Peter as well as all others not only for helping me in using the microscopy facility but also the nice discussions that were not limited to science. I thank you for lending me your ears not only in the hey days but also low hours of my PhD research time.

Nobody has been more important to me in the pursuit of this goal than the members of my family. I would like to thank my parents and my siblings, whose love and encouragement are always with me in whatever I pursue. Most importantly, I wish to thank my loving and supportive wife, Fikirte, and my two wonderful children who are actually my best friends, Eyob and Kaleb, for their encouragement, unwavering support and patience all the time providing me unending inspiration.

Appendix

THE JOURNAL OF BIOLOGICAL CHEMISTRY VOL. 289, NO. 16, pp. 11083–11094, April 18, 2014

Structure-Function Analysis of *Staphylococcus aureus* Amidase Reveals the Determinants of Peptidoglycan Recognition and Cleavage*

Received for publication, February 10, 2014, and in revised form, February 26, 2014 Published, JBC Papers in Press, March 5, 2014, DOI 10.1074/jbc.M114.557306

Felix Michael Büttner[‡1], **Sebastian Zoll**[‡1], **Mulugeta Nega**[§], **Friedrich Götz**[§], **and Thilo Stehle**[‡¶2]

From the [‡]*Interfaculty Institute of Biochemistry, University of Tübingen, Hoppe-Seyler-Strasse 4, 72076 Tübingen, Germany, the* [§]*Microbial Genetics, Interfaculty Institute of Microbiology and Infection Medicine, University of Tübingen, Auf der Morgenstelle 28, 72076 Tübingen, Germany, and the* [¶]*Department of Pediatrics, Vanderbilt University School of Medicine, Nashville, Tennessee 37232*

Background: Autolysins ensure the plasticity of bacterial cell walls, and deletion leads to impaired cell clusters.
Results: High resolution structures of *Staphylococcus aureus* amidase AmiA shed light on peptidoglycan binding and cleavage.
Conclusion: AmiA distinguishes peptidoglycan mostly by the peptide, and cleavage is facilitated by a zinc-activated water molecule.
Significance: These structures will inform strategies to develop new therapeutics against MRSA.

The bifunctional major autolysin AtlA of *Staphylococcus aureus* cleaves the bacterium's peptidoglycan network (PGN) at two distinct sites during cell division. Deletion of the enzyme results in large cell clusters with disordered division patterns, indicating that AtlA could be a promising target for the development of new antibiotics. One of the two functions of AtlA is performed by the *N*-acetylmuramyl-L-alanine amidase AmiA, which cleaves the bond between the carbohydrate and the peptide moieties of PGN. To establish the structural requirements of PGN recognition and the enzymatic mechanism of cleavage, we solved the crystal structure of the catalytic domain of AmiA (AmiA-cat) in complex with a peptidoglycan-derived ligand at 1.55 Å resolution. The peptide stem is clearly visible in the structure, forming extensive contacts with protein residues by docking into an elongated groove. Less well defined electron density and the analysis of surface features indicate likely positions of the carbohydrate backbone and the pentaglycine bridge. Substrate specificity analysis supports the importance of the pentaglycine bridge for fitting into the binding cleft of AmiA-cat. PGN of *S. aureus* with L-lysine tethered with D-alanine via a pentaglycine bridge is completely hydrolyzed, whereas PGN of *Bacillus subtilis* with *meso*-diaminopimelic acid directly tethered with D-alanine is not hydrolyzed. An active site mutant, H370A, of AmiA-cat was completely inactive, providing further support for the proposed catalytic mechanism of AmiA. The structure reported here is not only the first of any bacterial amidase in which both the PGN component and the water molecule that carries out the nucleophilic attack on the carbonyl carbon of the scissile bond are present; it is also the first peptidoglycan amidase complex structure of an important human pathogen.

Gram-positive, spherical staphylococci arrange in clusters and colonize the skin or mucous membranes, causing severe infections in infants, the elderly, transplantation patients, and people suffering from immunocompromising diseases, such as AIDS. Staphylococci are among the main causes of hospital-acquired infections (1). *Staphylococcus aureus* and *Staphylococcus epidermidis* are the most abundant human pathogens of the *Staphylococcus* genus. Both species form a biofilm that protects them from the human immune system (2) and antibiotics as well as contributing to persistent infections (3). In the case of *S. epidermidis*, this multilayered polysaccharide matrix (4) is responsible for infections of patients with implants, such as intravasal catheters, prostheses, or pacemakers (2, 5). This may require implant replacement and cause severe complications for the affected patients (6). The biofilm of *S. aureus* primarily serves as protection but also contributes to its pathogenicity (7). *S. aureus* is responsible for a large number of life-threatening infections that can result in diseases, such as endocarditis, meningitis, pneumonia, septicaemia, and toxic shock syndrome (8).

Resistance against *S. aureus* is on the rise, posing a serious threat to human health. There is therefore an urgent need for the development of new antibiotics to control emerging methicillin-resistant and vancomycin-resistant *S. aureus* strains (MRSA[3] and VRSA, respectively). Worldwide numbers are not available, but with about 132,000 cases in Germany per year (9), hospital-acquired MRSA currently accounts for ~20% of all staphylococcus infections (10), whereas in the early 1990s, the MRSA fraction was only ~1% (11). In high risk areas, such as

* This work was supported by the Collaborative Research Center TRR34.
The atomic coordinates and structure factors (codes 4KNK and 4KNL) have been deposited in the Protein Data Bank (http://wwpdb.org/).
[1] Both authors contributed equally to this work.
[2] To whom correspondence should be addressed: Interfaculty Institute of Biochemistry, University of Tübingen, Hoppe-Seyler-Strasse 4, 72076 Tübingen, Germany. Tel.: 49-7071-29-73043; Fax: 49-7071-29-5565; E-mail: thilo.stehle@uni-tuebingen.de.

[3] The abbreviations used are: MRSA and VRSA, methicillin-resistant and vancomycin-resistant *S. aureus*, respectively; AtlA, bifunctional major autolysin of *S. aureus*; AmiA, amidase of *S. aureus*; AmiE, amidase of *S. epidermidis*; AmiA-cat and AmiE-cat, catalytic domain of AmiA and AmiE, respectively; AmiD, amidase of *E. coli*; NAGase, glucosaminidase of *S. aureus*; PGN, peptidoglycan network; MtetP, muramyl tetrapeptide (MurNAc-L-Ala-D-iGln-L-Lys(NHAc)-D-Ala-NH_2); MTP, muramyl tripeptide (L-Ala-D-iGlu-L-Lys); anhydro-MTP, 1,6-anhydro-MTP; MurNAc, *N*-acetylmuramic acid; D-iGln, D-isoglutamine; D-iGlu, D-isoglutamic acid; Wat, water; *meso*-DAP, *meso*-diaminopimelic acid; NAc, *N*-acetyl.

intensive care units, the MRSA infection rate increases up to 37% (12), causing 5,000 deaths and leading to additional costs of ~380 million € (9) per year in Germany alone. In the United States, annual *S. aureus* infections have reached 475,000, 275,000 of which are MRSA-related, with $1–10 billion in extra expenses for the health care system and ~11,000 to ~19,000 deaths (13, 14). Targeting staphylococcal enzymes, critical for survival and growth of the bacterium, represents an attractive strategy for the development of new antibiotics.

Several hydrolytic enzymes ensure the plasticity of the staphylococcal cell wall by processing the complex PGN network. One of these, the major autolysin AtlA, is composed of two enzymes with hydrolytic activity (an amidase (AmiA) and a glucosaminidase (NAGase)) that cleave PGN at different locations (15). In the precursor AtlA protein, the two catalytic functions (cat) are each linked to targeting repeats (R1–R3) and also connected to a propeptide and a signal peptide (Fig. 1*A*). Posttranslational processing generates active AmiA and NAGase, which both localize at the septal region (16), where they process staphylococcal PGN during cell growth and division. *S. aureus* AtlA deletion mutants show a severely impaired phenotype that is unable to proliferate, forming large cell clusters instead (17). These findings demonstrate the essential function of AtlA in the *S. aureus* life cycle and also highlight a therapeutic potential for specific inhibition of AtlA.

The staphylococcal Atl domain organization is highly conserved in all of the species, with the amidase being the most conserved domain. It has been shown that the Atl-based phylogenetic tree correlates well with the corresponding 16 S rRNA- and core genome-based tree and represents a useful tool for staphylococcal genus and species typing (18).

The catalytic domain of AmiA (referred to here as AmiA-cat) is a zinc-dependent amidase that cleaves the amide bond between the peptide stem and carbohydrate backbone of PGN (16, 19, 20). The previously proposed mechanism for hydrolysis of the lactyl-alanine bond was based on *in silico* docking studies of the homologous catalytic domain AmiE from *S. epidermidis* (19). Further data from structures of a homologous protein originate from *Escherichia coli* (21). Consequently, detailed structural information on amidase-PGN interaction in Gram-positive bacteria is limited to date.

To determine the specificity of recognition and the mechanism of catalysis of AmiA-cat, we determined crystal structures of the enzyme in the absence (Fig. 1*B*) and presence (Fig. 2*A*) of the muramyltetrapeptide MurNAc-L-Ala-D-iGln-L-Lys-NHAc-D-Ala-NH_2 (MtetP), a ligand that includes the previously characterized minimal ligand for the *S. epidermidis* amidase (muramyltripeptide) (19). Both structures were solved to high resolution, and they unambiguously establish the specificity of interaction as well as the reaction mechanism used by this essential cell wall enzyme. Our results form an excellent basis for the design of new antibiotic lead structures.

EXPERIMENTAL PROCEDURES

Molecular Biology—The cDNA coding for AmiA-cat (residues 199–421) was cloned into a pGEX-4–3T vector for expression. The expressed protein contains an N-terminal GST tag fused to AmiA-cat with a six-amino acid thrombin-cleavable linker. Active site mutants were created using site-directed mutagenesis as described in the QuikChange® protocol (22).

Protein Expression and Purification—Proteins were expressed in *E. coli* BL21 (DE3). After induction, cultures were incubated for 72 h at 20 °C. Harvested cells were then resuspended in buffer (150 mM NaCl, 50 mM Tris, pH 8.0) supplemented with PMSF and Roche Applied Science Complete protease inhibitor mix. Filtered cell lysate was loaded onto a 5-ml GSTrap FF column (GE Healthcare). 100 units of thrombin were added for on-column overnight cleavage at 20 °C and release of the fusion protein. Size exclusion chromatography removed the remaining small impurities and aggregates from the protein. Purity was confirmed by SDS-PAGE and MALDI-MS.

Protein Crystallization—AmiA-cat crystals belong to space group C2 and contain two protomers in the asymmetric unit, giving rise to a solvent content of 41.2%. Crystals were grown using the hanging drop vapor diffusion method at 20 °C. 1 μl of protein solution (11 mg/ml) was mixed with 1 μl of a well solution containing 0.1 M MES/imidazole buffer at pH 6.5 and a mix of sodium formate, ammonium acetate, sodium citrate, racemic sodium/potassium tartrate, and sodium oxamate at concentrations of 0.02 M each as well as 12.5% (w/v) PEG 1000, 12.5% (w/v) PEG 3350, and 12.5% (w/v) 2-methyl-2,4-pentanediol (Molecular Dimensions). Microseeding improved crystal quantity and quality. In order to obtain catalytically inactive enzyme, the AmiA-cat crystals were first incubated for 72 h in well solution supplemented with 20 mM EDTA to remove the active site zinc ion. For complex formation, crystals were next soaked for 60 h in well solution containing 20 mM EDTA and 20 mM MtetP. Crystals yielding a complex belong to space group $P2_1$ with four protomers in the asymmetric unit and similar solvent content. All crystals could be directly flash-frozen in liquid nitrogen because the well solutions contained sufficient cryoprotectant.

X-ray Diffraction—All data were collected at 100 K on PILATUS detectors using synchrotron radiation at beamlines X06DA and X06SA of the Swiss Light Source in Villigen, Switzerland.

Structure Determination—Indexing, integrating, and scaling were done with the XDS software package (23). Molecular replacement for all AmiA-cat structures was performed with PHASER (24, 25). Initial phases for AmiA-cat were determined with an AmiE search model (Protein Data Bank accession code 3LAT, 81% identity). The refined AmiA-cat structure was then used to solve the ligand structure by molecular replacement. Model building, refinement, and validation were performed with Coot (26, 27), the CCP4 suite (28–31), Phenix (32), and the MolProbity Web page (33). The coordinate and parameter files for MtetP were obtained from the PRODRG2 server (34). Simulated annealing (Phenix) was performed to remove model bias for the ligand structure, especially in the active site. The ligand was then added manually and modeled according to difference or simulated annealing omit density maps in Coot. The final structures contain almost all of the 223 residues, with the exception of 13–15 poorly ordered N-terminal and 1–4 C-terminal amino acids. Figures were generated with PyMOL (35), and electrostatic potentials were calculated with PBD2PQR and APBS 2.1 (36), implemented in PyMOL.

Purification of Peptidoglycan—PGN was isolated from *S. aureus* SA113 (37) or *Bacillus subtilis* ATCC 6051 using the method of de Jonge *et al.* (38) with some modifications. Briefly, cells were grown to $A_{578\ nm}$ of 0.6 and harvested by centrifugation at 3,000 × *g* for 30 min, boiled with 5% SDS for 30 min, and broken with glass beads. Insoluble PGN was harvested by centrifugation at 30,000 × *g* for 30 min and washed several times with lukewarm water to remove SDS. Broken cell walls were suspended in 100 mM Tris-HCl, pH 7.2, treated with 10 μg/ml DNase (Sigma) and 50 μg/ml RNase (Sigma) for 2 h, and subsequently treated with 100 μg/ml trypsin for 16 h at 37 °C. To remove wall teichoic acid, the PGN preparations were incubated with 48% hydrofluoric acid for 24 h at 4 °C while stirring. PGN was harvested by centrifugation at 30,000 × *g* for 30 min and washed several times with water until complete removal of hydrofluoric acid. The final PGN product was lyophilized.

Preparation and HPLC/MS Analysis of PGN—Purified PGN (5 mg) was resuspended in 1 ml of 25 mM sodium phosphate buffer (pH 6.8) and digested with mutanolysin for 16 h at 37 °C. The enzyme reaction was stopped by boiling the sample for 5 min at 95 °C, and insoluble contaminants were removed by centrifugation. 50 μl of AmiA-cat, AmiA-H370A, or AmiA gel filtration buffer as a negative control were added to 100 μl of mutanolysin-digested PGN and incubated overnight at 37 °C while stirring. HPLC separation of digestion products was carried out on a reversed-phase column (Poroshell 120 EC-C18 4.6 × 150 mm, 2.7 μm; Agilent Technologies, Waldbronn, Germany) fitted with a poroshell EC-C18, 4.6-mm guard column using an Agilent 1200 system operating ChemStation software.

HPLC was performed using a linear 150-min gradient from 100% HPLC-buffer A (100 mM sodium phosphate, pH 2.2, and 5% methanol) to 100% HPLC-buffer B (100 mM sodium phosphate, pH 2.8, and 30% methanol) with a column temperature of 52 °C. Detection was made at 205 nm. Samples were prepared by mixing 100 μl of the product with an equal volume of 0.5 M sodium borate buffer (pH 8.0) containing freshly dissolved sodium borohydride (10 mg/ml) and reduced for 30 min at room temperature. The reaction was stopped, and excess borohydride was deactivated by lowering the pH to <3 using 20% phosphoric acid. 100 μl of the prepared sample was injected.

LC/MS analysis of these samples was performed with an Agilent HPLC-electrospray ionization-MS system (LC/MSD Ultra Trap System XCT 6330), using a gradient of A (H_2O with 0.1% formic acid) and B (0.06% formic acid in acetonitrile) as follows: 0–10% B:A over 25 min, 10% B to 27 min, and 100% B to 30 min at 0.4 ml min^{-1} at 40 °C on a Nucleosil 100 C18 3 μm column (100 × 2-mm inner diameter) with a precolumn (10 × 2-mm inner diameter, Dr. Maisch, Ammerbuch, Germany). Detection of *m*/*z* values consistent with AmiA-cat digestion products was conducted using Agilent Data Analysis for 6300 Series Ion Trap LC/MS 6.1 version 3.4 software (Bruker-Daltonik GmbH).

RESULTS

Overall Structures of Unliganded and MtetP-bound AmiA-cat—The structures of unliganded and liganded AmiA-cat were determined at high resolution (1.12 and 1.55 Å, respectively, Table 1), allowing us to analyze their salient features with confidence. The proteins adopt a globular, mixed α/β fold that is highly similar to that of the previously reported unliganded AmiE-cat structure (19). Essential features of this fold are seven α-helices that surround a central six-stranded β-sheet (Fig. 1*B*). The rear of the β-sheet is shielded by two long α-helices, whereas its front is solvent-accessible and forms the bottom of a recessed groove. In the case of unliganded AmiA-cat, one end of this groove accommodates a zinc ion that is required for catalysis. Residues His-265, His-370, and Asp-384 directly coordinate the zinc ion (Fig. 1*B*), and nearby residues Glu-324 and His-382 are positioned to participate in catalysis. To produce a complex with MtetP, the zinc ion was first removed by treatment of the AmiA-cat crystals with EDTA, followed by extensive soaking with MtetP (see "Experimental Procedures"). Ligand binding was confirmed by a simulated annealing omit density map that displays unbiased electron density for MtetP over the entire tetrapeptide and as far as the *N*-acetylmuramic acid (MurNAc) moiety of the ligand. The tetrapeptide portion of MtetP is well defined by electron density (Fig. 2*B*), showing that this part of the ligand binds in an extended conformation to the recessed groove. The lactate moiety of MurNAc linking the peptide to the carbohydrate as well as the cyclic MurNAc moiety are less well ordered, suggesting higher mobility due to fewer defined interactions. These differences in mobility are reflected in the *B*-factor distribution of the ligand (Fig. 2*B*). The MtetP-bound AmiA-cat crystals contain four molecules in their asymmetric unit, only two of which contain fully occupied ligand binding sites. The flexible, cyclic MurNAc moiety presented sufficient electron density for model building in both copies. The binding sites of the remaining two molecules are less accessible due to smaller solvent channels. As a result, they contain electron density features that suggest only partially bound ligand.

With the exception of the active site region, unliganded and liganded AmiA-cat exhibit no structural differences. The two structures can be superimposed with a root mean square deviation of 0.2 Å (DaliLite pairwise (39)) onto each other, demonstrating that ligand binding does not induce larger structural changes.

Interactions of AmiA-cat with MtetP—Inspection of the structure of AmiA-cat in complex with MtetP reveals a sophisticated interaction network that significantly extends knowledge derived from earlier *in silico* docking (19). The tetrapeptide backbone of MtetP is anchored into the binding groove along its entire length via several direct or water-mediated hydrogen bonds to protein residues (Fig. 3). In addition, all four amino acid side chains of MtetP (L-Ala, D-iGln, L-Lys-NHAc, and D-Ala-NH_2) are also involved in individual contacts with the protein, accounting for specificity. These interactions are detailed in Fig. 3 and summarized below.

The methyl side chain of the first amino acid of MtetP, L-Ala, inserts into a small hydrophobic pocket formed by residues Ala-288 and Val-290 (Fig. 3, *A* and *C*). The methyl group of L-Ala is also only 4.4 Å away from the Cα carbon of the conserved Gly-311. Lack of a side chain at position 311 contributes to specificity because even a medium sized side chains would lead to clashes with the L-Ala group.

The short amide side chain of D-isoglutamine (D-iGln), which is a key determinant of ligand binding (20), projects into a shal-

High Resolution Complex Structure of S. aureus Amidase AmiA

TABLE 1

Data collection and refinement statistics for AmiA-cat (Protein Data Bank code 4KNK) and liganded AmiA-cat (Protein Data Bank code 4KNL)

Values for the highest resolution bin are given in parentheses.

Parameters	AmiA-cat	Liganded AmiA-cat
Beamline	X06DA (PX III)	X06SA (PX I)
Space group	C2	$P2_1$
Cell dimensions (Å)	$a = 96.9, b = 81.7, c = 68.7$ $\alpha = \gamma = 90°. \beta = 128.8°$	$a = 67.7, b = 82.8, c = 77.6$ $\alpha = \gamma = 90°. \beta = 95.9°$
Wavelength (Å)	1.00000	1.00605
Detector	Pilatus 2M	Pilatus 6M
Resolution (Å)	50-1.12 (1.15-1.12)	50.0-1.55 (1.59-1.55)
Measured reflections	885,445 (14,326)	442,448 (27,121)
Unique reflections	146,370 (6,937)	122,742 (8,927)
R_{meas} (%)	4.7% (60.3%)	6.5% (82.3%)
Completeness (%)	92.6% (59.7%)	99.5% (98.1%)
Redundancy	6.0 (2.0)	3.6 (3.0)
$I/\sigma(I)$	21.1 (1.8)	13.9 (1.7)
CC1/2 (%)	100 (71.7)	99.9 (69.7)
Resolution (Å)	40.9-1.12	48.2-1.55
R_{work}/R_{free}	12.09/13.89	17.12/19.81
No. of atoms	3,894	7,321
Protein	3,318	6,531
Water	535	630
MtetP		102
Zn^{2+}	2	
Others	39	58
B-Factors (Å²)		
Wilson	13.7	24.5
Mean	16.9 (7.9–41.8)	25.9 (11.9–69.9)
Protein	15.1 (7.9–38.8)	25.3 (11.9–69.9)
Water	27.9 (9.0–41.8)	33.1 (14.8–55.9)
MtetP		36.7 (18.0–61.5)
Zn^{2+}	12.5 (12.2–12.8)	
Others	27.8 (11.0–38.7)	37.0 (18.8–53.0)
Root mean square deviations		
Bond length (Å)	0.009	0.012
Bond angles (degrees)	1.389	1.380
Ramachandran plot		
Most favorable (%)	97.4	97.6
Allowed (%)	2.6	2.4
Disallowed (%)	0.0	0.0

low pocket and forms direct hydrogen bonds with the hydroxyl group of Thr-380 and Nϵ of His-370, as well as two water-mediated hydrogen bonds to Asp-381 (Fig. 3, *B* and *C*). The side chain of His-382 seals the pocket on one side, whereas Thr-380 is located at the other end.

The side chain of the third amino acid, L-Lys, is acetylated (L-Lys-NHAc) in MtetP to approximate the physiologic state of this residue in PGN, where it is linked to additional glycine residues (see Fig. 7*A*). Specificity of recognition derives primarily from hydrophobic interactions between the aliphatic side chain of L-Lys-NHAc and the side chain of Trp-310. The entire lysine side chain lies parallel to the large indole ring of Trp-310, with distances below 4 Å (Fig. 3*B*). In addition, a water molecule (Wat-7) bridges the carbonyl oxygen of D-Ala and Nϵ of L-Lys-NHAc, thus helping to fix the orientation of the lysine side chain. Similarly, the peptide oxygen of Lys-NHAc forms a water-mediated (Wat-1) hydrogen bond with Asn-317.

The fourth residue, D-Ala-NH_2, is engaged in backbone hydrogen bond formation, but its side chain is at least partially exposed to solvent. The terminal amide group of D-Ala-NH_2 participates in a network of water-mediated hydrogen bonds that help to fix its orientation with respect to the protein and the preceding L-Lys-NHAc side chain (Fig. 3, *B* and *C*). These interactions would still be possible in the context of either a pentaglycine bridge or a free carboxyl terminus.

The carbohydrate moiety of MtetP engages in fewer interactions with AmiA-cat than the peptide moiety, resulting in its higher flexibility. The *N*-acetyl oxygen of MurNAc forms an intramolecular hydrogen bond with the L-Ala nitrogen and via Wat-4 water-mediated contacts to AmiA-cat. The NAc-methyl group inserts in the hydrophobic portion (Ala-288, Val-290, and Phe-293) of the otherwise hydrophilic binding pocket (Fig. 3, *A* and *C*). Only Thr-267, Asn-269, and Glu-277 directly bond with MurNAc. Interestingly, the anomeric carbon is in α-configuration instead of β-configuration.

Active Site—The bound zinc ion in the unliganded structure marks the center of the active site of the enzyme (Fig. 1*B*). The ion is coordinated by the side chains of His-265, His-370, and Asp-384, with a water (Wat-10) completing its almost perfect tetrahedral coordination sphere. Although the zinc had to be removed to prepare the complex with MtetP, its position can be reliably inferred from superposition. Inspection of the unliganded and liganded structures shows two water molecules (Wat-9 and Wat-10) in each case, at most shifted by 1 Å. Wat-9 is located next to the position of the zinc ion, as well as Wat-10. Coordination of Wat-9 involves His-370, Asp-384, and Wat-10 (Fig. 3*A*). A fourth hydrogen bond is formed between Wat-9 and the carbonyl group of the scissile amide bond between L-Ala and the lactate of MurNAc in the ligand (Fig. 3, *A* and *C*). The high mobility or partial occupancy of Wat-9, indicated by a high *B*-factor, make a vital role unlikely. However, it may support stabilization of intermediate states during catalysis. The scissile bond is positioned directly adjacent to Wat-10, suggesting that the reaction mechanism proceeds by a Wat-10-medi-

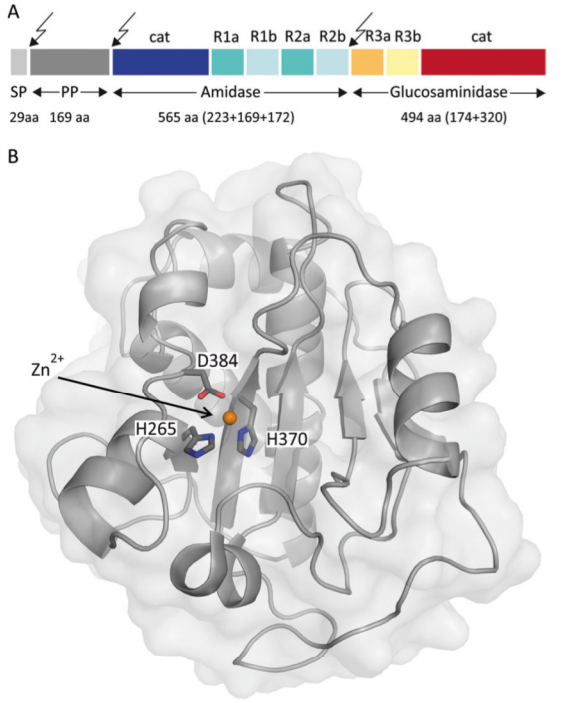

FIGURE 1. **Prepro-AtlA holoenzyme and structure of AmiA-cat.** *A*, domain arrangement of AtlA with sites of post-translational cleavage indicated by *arrows*. *SP*, signal peptide; *PP*, propeptide; *cat*, catalytic domain; *R*, repeat domain. This figure was adapted and modified from Ref. 19. *B*, mixed α/β fold of unliganded AmiA-cat in a schematic representation with a *transparent surface*. The zinc ion (*orange*) and its coordinating residues (*dark gray*) are highlighted.

ated nucleophilic attack. Two residues, Asp-266 and Glu-324, lie next to Wat-10 and probably serve to enhance its nucleophilicity, thus favoring an attack on the lactyl amide bond. The carbonyl atom of the scissile amide bond of MtetP is hydrogen-bonded to His-382, which helps to orient the lactic acid moiety in the active site. We note that the His-382 side chain has different orientations in the unliganded and liganded AmiA-cat structures.

Putative Reaction Mechanism—The architecture of the active site and the observed interactions between protein and substrate are very much consistent with a reaction mechanism in which Wat-10 attacks the scissile bond. This water is hydrogen-bonded to the Asp-266 carbonyl and Glu-324 carboxyl groups, which would lead to both hydrogens of Wat-10 facing toward these residues and the free electron pairs of the Wat-10 oxygen facing toward zinc and the bond connecting the lactyl and peptide moieties (Fig. 4*A*). The likely role of the zinc ion is to polarize the oxygen of Wat-10, rendering it more reactive. The remaining free electron pair of the Wat-10 oxygen would then be able to perform a nucleophilic attack on the scissile bond of MtetP. His-382 could provide a proton for stabilization of the resulting oxyanion, whereas Glu-324 could accept a hydrogen from Wat-10 (Fig. 4*B*). Stabilization of the tetrahedral intermediate would involve the zinc ion and Nδ of His-382, which could each interact with one of the resulting hydroxyl groups as well as the side chains of Asp-266 and Glu-324. In the next step, the tetrahedral intermediate again forms a carbonyl group but with the peptide moiety as the leaving group rather than the previously attacking water molecule, leading to the separation of the carbohydrate and peptide moieties of PGN (Fig. 4*C*). At the same time, the N terminus of the new peptide is poised to accept a hydrogen from Glu-324, whereas His-382 can accept a hydrogen atom from the tetrahedral intermediate. Finally, the cleavage products are released from the active site (Fig. 4*D*).

Implications for PGN Binding and Cleavage—The MtetP compound is a substrate for AmiA-cat, which cleaves large PGN structures in its physiologic setting. It is possible and indeed likely that additional contacts between PGN components and AmiA-cat exist and that the interactions between PGN and AmiA-cat are somewhat more complex than depicted here. Nevertheless, analysis of surface properties provides at least some clues as to how AmiA-cat would engage components of PGN that extend beyond the muramyltetrapeptide (*i.e.* the MurNAc-GlcNAc glycan polymer and the pentaglycine bridge) (Fig. 5*A*).

A number of residues largely conserved among bacterial amidases (Fig. 5, *B* and *C*) define the spacious carbohydrate binding pocket. Thr-267 and Glu-277 together with Met-281 and Phe-293 form the bottom of the pocket, whereas Tyr-280 on one side and Ala-268, Asn-269, and Ser-273 on the other side enclose the carbohydrate and form the lateral edges. Analysis of the complex shows that MurNAc does not engage in many specific contacts on its own. Based on chemical and geometric restraints, we therefore modeled a plausible conformation of GlcNAc-MurNAc-GlcNAc in the carbohydrate pocket (Fig. 5*A*), which is concurrent with a previously proposed three-dimensional structure of PGN (40) and nicely follows the carbohydrate groove. Steric constraints lead to a minor shift of MurNAc out of the binding pocket in the presence of β-1,4-linked GlcNAc molecules. Hydrogen bonds formed with O1 of MurNAc fall away in this model, whereas hydrophobic interactions and hydrogen bonds of the NAc moiety remain. Nevertheless, only the oxygen atoms O6 of preceding and succeeding GlcNAc may each form additional hydrogen bonds (preceding GlcNAc with His-382 or Wat-5 and succeeding GlcNAc with Gly-276, Glu-277, and Wat-66; data not shown). Physiologically, weaker interactions with MurNAc and the glycan strand make sense because the enzyme achieves its specificity through engagement of the tetrapeptide stem and must dissociate from the PGN after cleavage has occurred.

Investigation of the electrostatic surface of AmiA-cat gives two plausible orientations in terms of uncharged contact area for the pentaglycine bridge linked to L-Lys in PGN (Fig. 5*A*), although Cϵ and Nϵ would not superimpose with the complex. In both cases, glycines would be able to loosely interact with conserved (Fig. 5*B*) and uncharged AmiA-cat surface residues. Previous data showed that the presence or absence of the glycine bridge has little effect on catalysis (19, 20), indicating that interactions of the glycines with AmiA-cat contribute little binding energy. Nonetheless, the pentaglycine bridge is most likely important for specificity.

Substrate Specificity—In order to relate the structural data to functional experiments, we investigated wild-type AmiA-cat and an active site mutant AmiA-H370A for its ability to digest

High Resolution Complex Structure of S. aureus Amidase AmiA

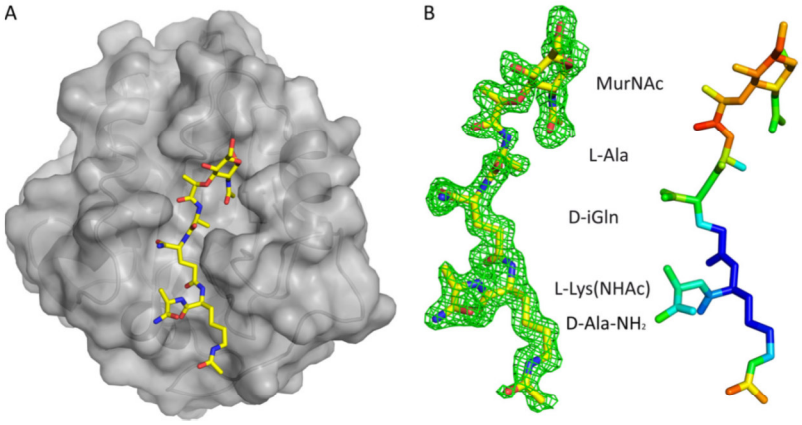

FIGURE 2. **AmiA-cat in complex with MtetP.** *A*, AmiA-cat (*semitransparent gray surface*) bound MtetP (*yellow sticks*) in the active site. *B*, the *close-up* on MtetP surrounded by omit density illustrates that the ligand is well defined. Still, the *B*-factor distribution of MtetP displays the elevated flexibility of its MurNAc moiety. The difference omit map is shown at a σ level of 2.0, and the *color scale* for *B*-factors ranges from *blue* (20 Å^2) to *red* (50 Å^2).

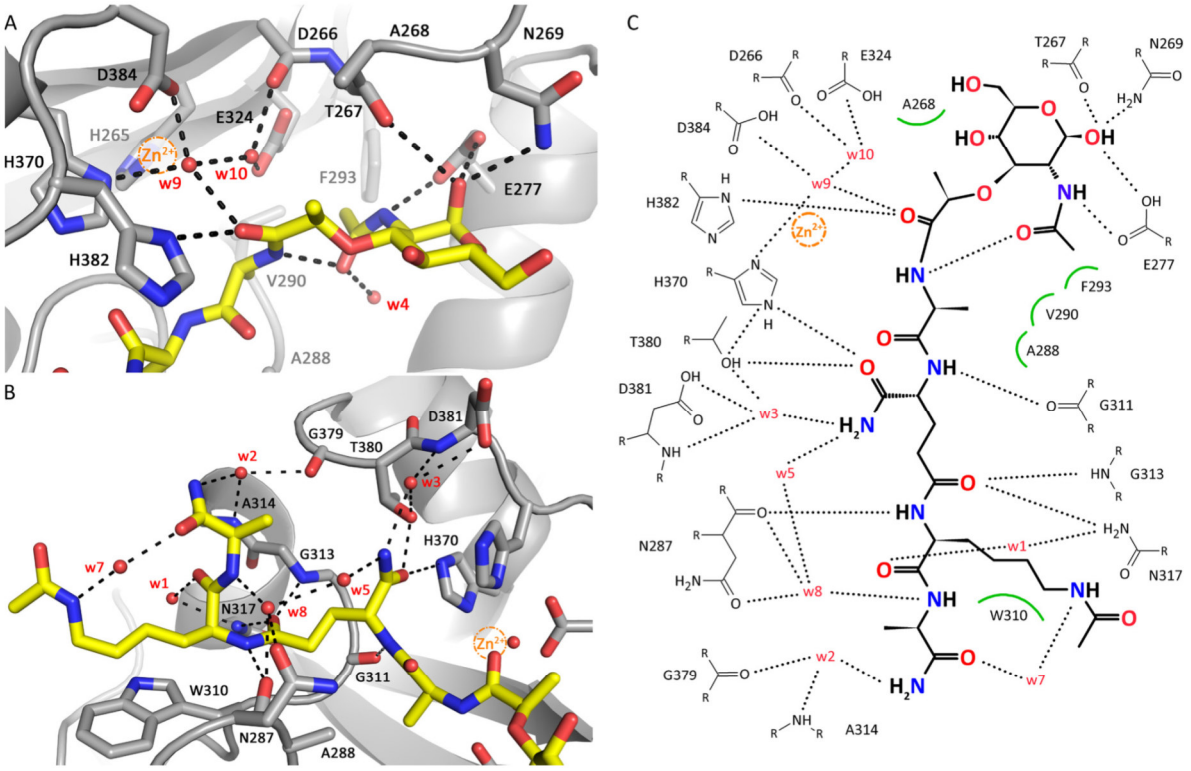

FIGURE 3. **Interactions between AmiA-cat and MtetP.** *A*, interactions of AmiA-cat with the MurNAc moiety and L-Ala of MtetP at the active site. The zinc ion from the native structure (*orange sphere*) is superimposed on the AmiA-cat complex (*gray*) with MtetP (*yellow*). *B*, *close-up* of the interactions of the peptide moiety of MtetP with AmiA. *C*, ChemSketch (57) plot of interactions between MtetP and AmiA-cat. Van-der-Waals interactions are depicted as *green arcs*, and hydrogen bonds are shown as *black dashed lines*. Coordination of Wat-9 involves His-370, Asp-384, and Wat-10 and a hydrogen bond with the carbonyl oxygen of the scissile amide bond in the ligand, which itself is positioned by interaction with His-382. Wat-10 lies next to Asp-266, Glu-324, Wat-9, and the carbonyl carbon of the scissile bond. MurNAc forms an intramolecular and four further hydrogen bonds with Glu-277, Thr-267, and Asn-269. Hydrophobic interactions of the methyl groups involve Ala-268 and Phe-293, respectively. L-Ala inserts into a small hydrophobic pocket formed by residues Ala-288 and Val-290. The amide side chain of D-iGln forms direct hydrogen bonds with Thr-380 and His-370 as well as two water-mediated hydrogen bonds to Asp-381. The carbonyl oxygen bonds with Gly-313 and Asn-317. L-Lys is stabilized by interactions with Asn-287 as well as Asn-317, whereas the acetylated side chain engages in hydrophobic interactions with Trp-310. A water (Wat-7 (*w7*)) bridges Nϵ of L-Lys-NHAc and the carbonyl oxygen of D-Ala, which engages additional water-mediated interactions with AmiA-cat residues Asn-287, Ala-314, and Gly-379.

PGN from *S. aureus* as well as *B. subtilis*. Both PGN structures were first predigested with mutanolysin, which cleaves the glycosidic bond between GlcNAc and MurNAc, to facilitate the digestion. AmiA-cat completely hydrolyzed *S. aureus* PGN, whereas the AmiA-H370A mutant was inactive (Fig. 6, *A*–*C*). Analysis by HPLC shows that the main product generated by

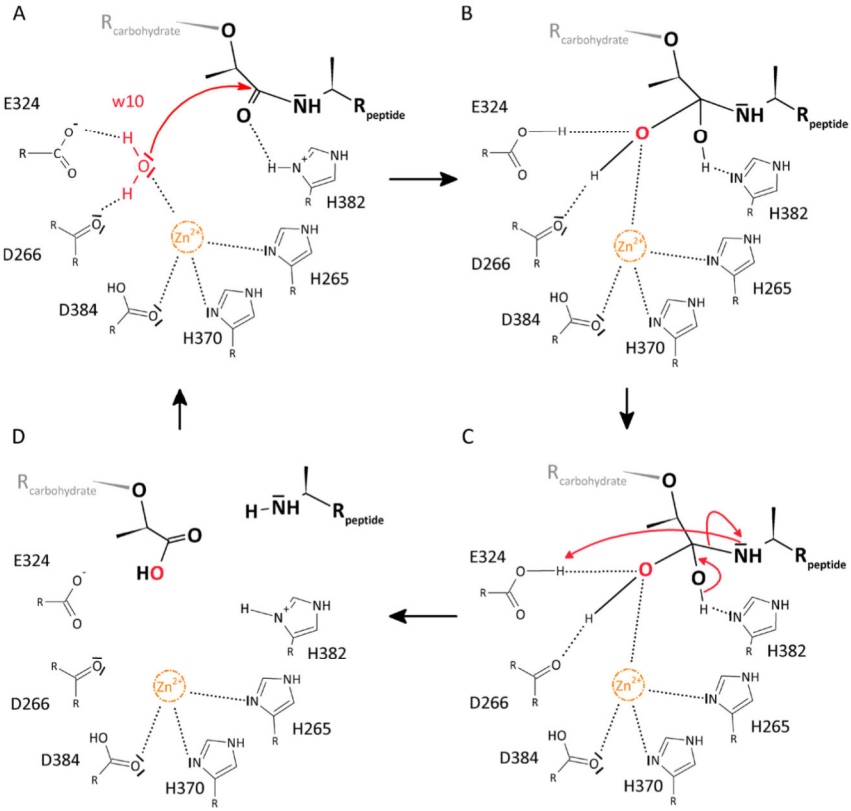

FIGURE 4. **Proposed reaction mechanism of AmiA.** *A*, Wat-10 (*w10*) is hydrogen-bonded to Asp-266 and Glu-324, and its free electron pairs face toward the scissile bond. Zn^{2+} is complexed by His-265, His-370, and Asp-384 and probably renders Wat-10 more reactive, enabling a nucleophilic attack. *B*, tetrahedral intermediate is stabilized by hydrogen bonds of the resulting hydroxyl groups with Nδ of His-382 as well as Asp-266, Glu-324, and zinc, respectively. *C*, reformation of a carbonyl group with the peptide moiety as leaving group. His-382 can accept a hydrogen atom from the tetrahedral intermediate, whereas the peptide is poised to accept a hydrogen from Glu-324. *D*, product release.

AmiA-cat is the disaccharide GlcNAc-MurNAc, with a mass of *m/z* 496 (Fig. 6, *B* and *F*). Interestingly, the intensity of the GlcNAc-MurNAc peak (Fig. 6*B*) represents the sum of the PGN oligomers seen in Fig. 6*A*, indicating that >95% of the PGN substrate was digested.

In contrast to *S. aureus*, *B. subtilis* PGN could not be hydrolyzed by AmiA-cat (Fig. 6, *D* and *E*). The major differences in PGN structure of *S. aureus* and *B. subtilis* are illustrated in Fig. 7. *B. subtilis* incorporates D-isoglutamic acid into the peptide linking the glycan chains (Fig. 7*B*), whereas *S. aureus* converts this amino acid to D-iGln (Fig. 7*A*). It is, however, unlikely that this difference is solely responsible for the inability of AmiA-cat to cleave *B. subtilis* PGN because the homologous AmiE enzyme still hydrolyzed synthetic substrates composed of MurNAc-L-Ala-D-iGlu-L-Lys, albeit with lower efficiency (20). We consider it more likely that two other alterations in the PGN structures are responsible for the observed difference in activity. The *B. subtilis* PGN carries a *meso*-diaminopimelic acid (*meso*-DAP), which has an amidated ϵ-carboxylate and a free α-carboxylate and also features a directly cross-linked peptide stem (Fig. 7*B*), without the pentaglycine bridge found in the *S. aureus* PGN. These two major differences probably prevent a proper fit of the *B. subtilis* PGN structure into the binding cleft of AmiA-cat.

DISCUSSION

We have determined high resolution structures of the catalytic region of the *S. aureus* amidase AmiA in its unliganded form and in complex with a compound that includes MurNAc and the tetrapeptide L-Ala-D-iGln-L-Lys-D-Ala. To crystallize the wild-type enzyme in complex with ligand while avoiding cleavage, it proved critical to first remove the catalytic zinc ion through extensive incubation with EDTA and then soak crystals with ligand, whose high concentrations reflect the environment in PGN. Analysis of the two structures provides insights into the parameters that govern specificity as well as the catalytic mechanism.

AmiA-cat folds into a compact structure with a long, exposed ligand binding groove that appears ideally suited to access its specific cleavage sites within the dense, highly cross-linked PGN structure. In addition to the catalytically active AmiA-cat domain, the mature enzyme also contains four repeat domains (Fig. 1*A*). Analysis of the highly homologous *S. epidermidis* amidase has shown that these repeats probably anchor the protein to lipoteichoic acid protruding from the staphylococcal cell wall (41). Importantly, the repeats are flexibly linked to the catalytically active domain, allowing cleavage to proceed efficiently (41). The position of the bound MtetP ligand sheds light

High Resolution Complex Structure of S. aureus Amidase AmiA

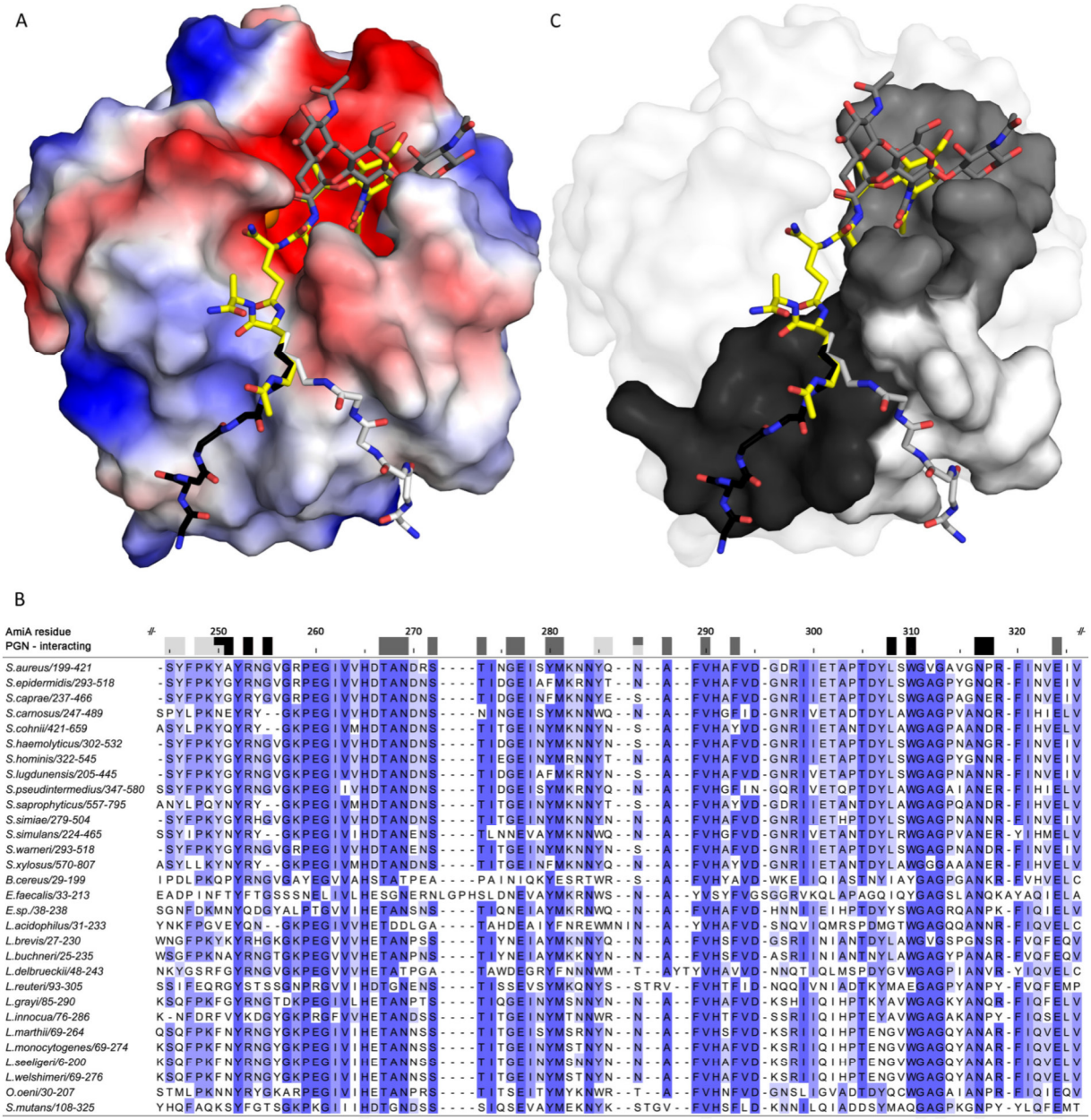

FIGURE 5. **AmiA-cat binding to PGN.** *A*, electrostatic surface of AmiA-cat with MtetP (*yellow*), zinc (*orange*), and modeled PGN components (*dark gray*, *black*, and *light gray*). Uncharged (*white surface area*), positively charged (*blue areas*), and negatively charged residues (*red surface*) are shown. The spacious hydrophilic pocket harboring the zinc ion and active site also accommodates MurNAc. Adjacent GlcNAc rings (*dark gray sticks*) shift MurNAc slightly when modeled as a polymer. The lower peptide moiety of MtetP binds in the mostly uncharged region of the binding cleft. Two conformations for the pentaglycine bridge (*black* and *light gray sticks*, respectively) linked to L-Lys of MtetP were modeled according to uncharged surface area and possible hydrogen bonds. *B*, a multisequence alignment of bacterial amidases with identical residues *colored* by conservation from *light* to *dark blue*. Residues forming the carbohydrate binding pocket, marked by *dark gray boxes*, are highly conserved among all compared amidases. Surface-exposed amino acids near the two pentaglycine bridges are marked in *black* and *light gray* for the respective conformation models. Conservation, especially among staphylococci is high for both. Alignment was calculated using Clustal Omega (58), and the output was created using Jalview (59). *C*, conserved residues mapped on the AmiA-cat surface according to the *color scheme* used in *A* and *B*.

on the interaction of amidases with more complex, branched PGN fragments. Thus, the structure of liganded AmiA-cat allows us to visualize how the enzyme acts in a physiologic setting. In addition to the groove that accommodates the tetrapeptide of MtetP, AmiA-cat contains surface features that probably allow for binding of MurNAc-GlcNAc polymers at one end and a pentaglycine bridge at the other end of the groove. The peptide composition of PGN in staphylococci is

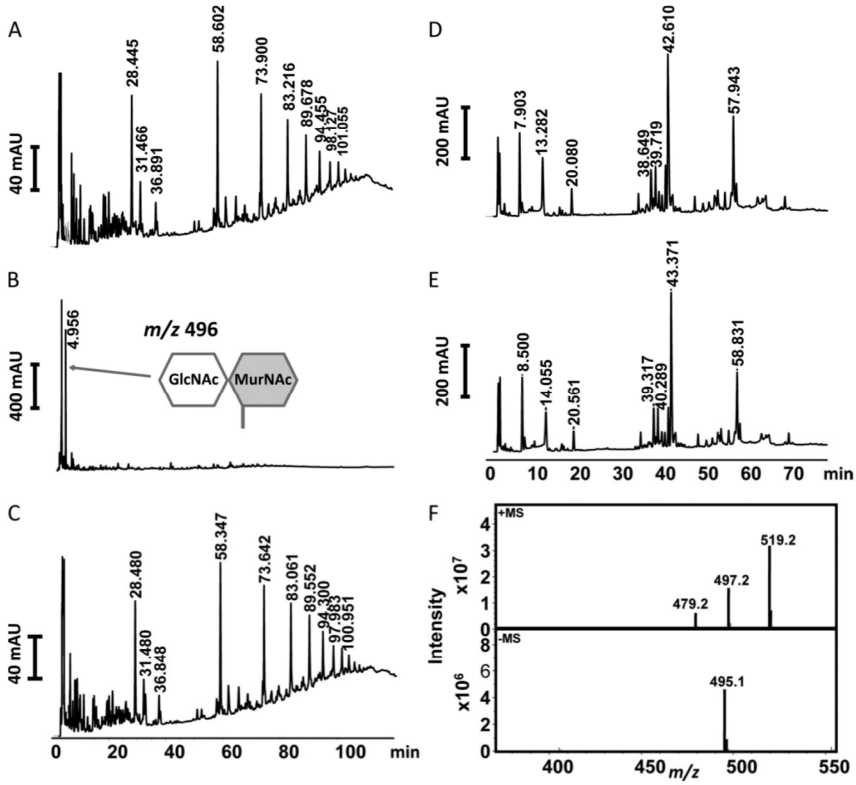

FIGURE 6. **RP-HPLC profile of mutanolysin-digested PGN fragments after incubation with enzyme.** *A*, *S. aureus* PGN fragments incubated with elution buffer of AmiA-cat as control. Three peaks around 28 min contain monomer species of one peptide stem with carbohydrates, peaks at 58 min comprise species with two peptide stems, peaks at 73 min cover fragments with three peptide stems, and continuing accordingly. *B*, *S. aureus* PGN fragments incubated with AmiA-cat result in completely digested polymers with GlcNAc-MurNAc fragments remaining. *C*, *S. aureus* PGN fragments incubated with active site mutant AmiA-H370A show no catalytic activity. *D*, *B. subtilis* PGN fragments incubated with elution buffer of AmiA-cat result in a pattern similar to *A* but with specific retention times for *B. subtilis*. *E*, *B. subtilis* PGN fragments incubated with AmiA-cat exhibit no activity of the staphylococcal amidase for *B. subtilis* PGN. *F*, mass analysis of the major product shown in *B*, which corresponds to the disaccharide GlcNAc-MurNAc (*m/z* 496).

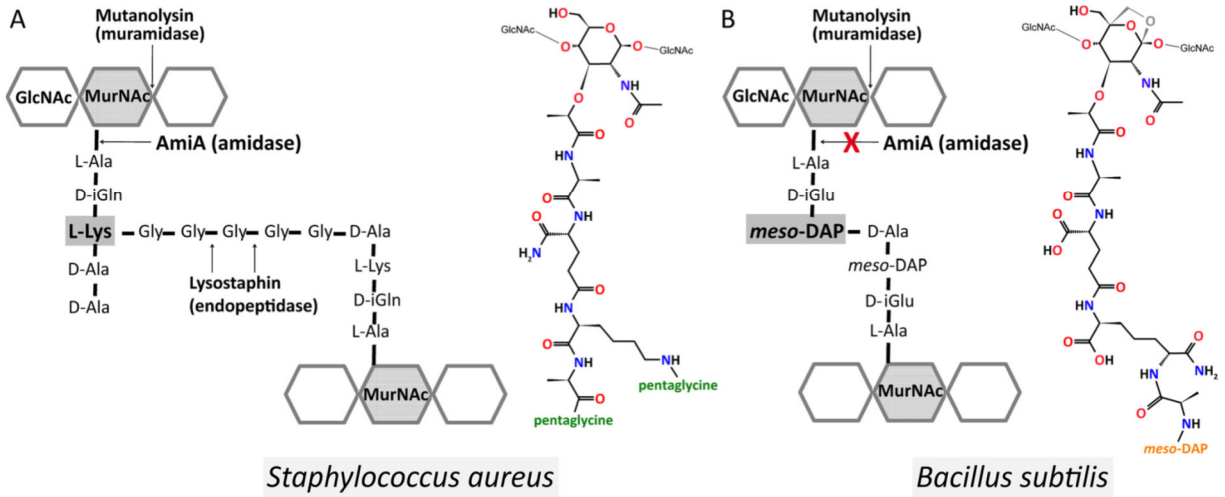

FIGURE 7. **Schematic and molecular illustration of the PGN structures.** *A*, in *S. aureus*, the PGN subunit is composed of D-isoglutamine and L-lysine and is cross-linked via a pentaglycine bridge (43). It comprises C-terminally either D-Ala-D-Ala or D-Ala-pentaglycine. *B*, *B. subtilis* PGN from vegetative cells (53, 55), however, contains D-isoglutamic acid and amidated *meso*-DAP and lacks a D-alanine at the *meso*-DAP α-carboxyl group, and it is directly cross-linked with D-alanine of the next subunit. In addition, *B. subtilis* PGN has 1,6-anhydro-MurNAc, shown in *gray*, at its terminus instead of a reducing MurNAc.

well conserved, typically using a pentaglycine bridge that connects D-Ala of one peptide stem with the Nϵ from L-Lys of another stem (42–44). Variations in *S. aureus* and among subspecies exist (43, 44) but are rare. Also, they concentrate on the variation of the pentaglycine bridge in terms of length and composition. The number of glycines may vary from four to six, or one glycine may be substituted by a serine or an alanine (43, 44). Although structures of several bacterial amidases have been determined (19, 45–52), the amidase AmiD from *E. coli* is the only catalytically active amidase for which structural data of an uncleaved ligand-enzyme complex have been available prior to this work (21).

The PGN of *E. coli* and *B. subtilis* is highly similar (42) and belongs to the type of variation A1γ (43). It differs in amino acid composition (D-iGln and L-Lys are substituted with D-iGlu and *meso*-DAP, respectively) as well as direct cross-linkage of amino acids 3 and 4 (no interpeptide bridge) from the PGN of *S. aureus* (42), which has a PGN of the A3α type of variation (43). Additionally, *E. coli* and *B. subtilis* PGN has anhydro-MurNAc at the terminus of the carbohydrate backbone (42, 53), whereas PGN of *S. aureus* always presents reducing MurNAc (54). Further differences within the *E. coli* and the *B. subtilis* A1γ type of variation include deviations in the presence or absence of an unlinked, terminal D-Ala and amidation of *meso*-DAP carboxyl groups (53, 55).

The inability to digest *B. subtilis* PGN presumably is a cumulative effect because D-iGlu instead of D-iGln is tolerated (20), and a *meso*-DAP, which is amidated at its second carboxyl group, itself is flexible enough to be accommodated at the lysine binding site of AmiA-cat. In addition, Asn-317 could partially compensate for a negative charge resulting from the absent, unlinked, terminal D-Ala of *B. subtilis* PGN. However, the direct cross-linkage is most likely to cause a clash with AmiA-cat due to a high rigidity and bulky side chain compared with a pentaglycine bridge. Since each of these differences is likely tolerated on its own, we suggest that the combined differences account for substrate specificity.

Although the *E. coli* enzyme AmiD and AmiA both belong to the amidase 2 family and are zinc-dependent, the two enzymes share a sequence identity of only 21%, have different substrates, and exhibit large structural differences (Fig. 8), including differences in the active site shown by a 2.0-Å root mean square deviation of α-carbon atoms (Dali server (56)). For example, the proton donor in AmiD is a lysine instead of a histidine residue (His-382 in AmiA). His-370 and Thr-380 that stabilize D-iGln in AmiA are replaced by a histidine and an arginine, which are better suited to bond with D-iGlu from A1γ-PGN variants. The free carboxylate of *meso*-DAP or D-Ala could be stabilized by another arginine of AmiD. Interestingly, this is not the case in the two available complex structures of AmiD (cocrystallized with tripeptide L-Ala-D-iGlu-L-Lys (MTP) and soaked with anhydro-MurNAc-L-Ala-D-iGlu-L-Lys (anhydro-MTP)) due to crystal contacts. Also, lysine was used as the third amino acid of the peptide stem instead of *meso*-DAP. Because anhydro-MurNAc does not occur in *S. aureus* PGN and the carbohydrate binding pocket of AmiD is smaller than in AmiA, one can draw only limited conclusions for binding and catalysis of staphylococcal PGN from these structures. Moreover, the

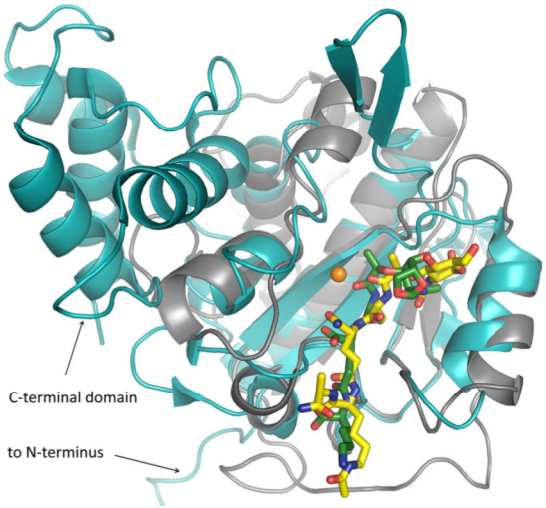

FIGURE 8. **Comparison of the AmiA-cat complex (*gray schematic*) with AmiD from *E. coli* (*cyan schematic*; Protein Data Bank code 3D2Y).** Superimposition of the two bacterial amidases reveals a similar fold solely around the binding and active site. AmiD deviates by a 2.0-Å root mean square deviation (DaliLite pairwise) from the AmiA-cat main chain, amino acids in the active and binding sites differ, and AmiD contains additional motifs at its N and C termini. Ligand positioning of anhydro-MTP (*green sticks*) to AmiD is comparable with the AmiA-cat complex with MtetP (*yellow sticks*). However, anhydro-MTP has an overall shift in relation to MtetP, and interactions of enzyme with ligand are unalike. Additionally, the MurNAc moiety, including the scissile bond, lies in the direct vicinity of the zinc binding residues and is in the anhydro form, which does not occur in staphylococci. Zn^{2+} from the unliganded AmiA-cat structure in *orange* was superimposed.

AmiD complex structure of anhydro-MTP lacks space for both the zinc ion and a water molecule in the active site, which could be activated by the zinc ion and attack the scissile bond. Thus, the structure of AmiA-cat from *S. aureus* presented here provides new information both about how the ligand is contacted and also about how catalysis is performed.

The presented results also significantly extend prior knowledge obtained from *in silico* molecular docking of a tripeptide into the highly homologous amidase structure of *S. epidermidis*, AmiE-cat (19). Although the overall model and the orientation of the ligand agree with our structure, the ligand used for docking AmiE-cat lacked the C-terminal D-Ala and the acetyl group at the L-Lys side chain. The latter resulted in a non-physiologic positive charge due to the protonated Nϵ of the lysine. Although some of the predicted hydrogen bonds and hydrophobic interactions could be validated by our complex structure, the majority of interactions identified in this work were not projected. Furthermore, the docking model did not take the nucleophilic water in the active site into account, causing the substrate to locate closer to the zinc ion. Additionally, a non-physiological zinc ion caused the backbone to shift at residue 63 (Ala-268 in AmiA-cat), making the carbohydrate binding pocket smaller.

Inspection of the liganded AmiA-cat structure directly suggests strategies for inhibition. A competitive inhibitor of AmiA should contain the tetrapeptide stem of MtetP because all four residues make strong interactions with the enzyme. D-Ala, however, contributes least and could therefore be omitted or replaced. The main contact maintained by L-Lys is the hydro-

phobic interaction with Trp-310. L-Ala and especially D-iGln are conserved in staphylococcal PGN and should be part of a lead structure. Changes in these residues are not tolerated by the enzyme (19) and would therefore not lead to a competitive compound. A reasonable approach would be the introduction of an noncleavable, peptide-mimicking group at the position of the L-Ala-lactyl peptide bond. Suitable bioisosteres are hydroxyethylene or dihydroxyethylene that imitate the tetragonal transition state. Modification of the carbohydrate (*e.g.* at C1 to form a salt bridge with Glu-277) would also increase affinity for AmiA-cat. On the other hand, it may be advantageous to exchange the sugar moiety and end the lead structure with a non-cleavable lactate analog linked to a cyclic compound because carbohydrate synthesis is expensive.

In conclusion, we have solved the complex structure of AmiA-cat with its ligand, the PGN component MtetP, at high resolution. Inspection of the interactions observed in the complex leads to a plausible model for catalysis and allows us to predict the binding locations of the adjacent GlcNAc molecules and the pentaglycine bridge. We show that the crystallized enzyme is active and that it possesses a narrow specificity that enables it to digest PGN structures from *S. aureus* but not from *B. subtilis*. The complex structure offers plausible explanations for these differences in catalytic activity. Our work moreover provides new data on the mechanism of the crucial amidase reaction that may help in the development of therapeutics against MRSA.

Acknowledgments—We thank the team at the Swiss Light Source (Villigen, Switzerland) for beamtime and support. We also acknowledge Andreas Maurer from the Kalbacher laboratory (Tübingen) for the MALDI analysis.

REFERENCES

1. Baron, S. (1996) in *Medical Microbiology* (Baron, S., ed) 4th Ed., Chapter 12, University of Texas, Galveston, TX
2. O'Gara, J. P., and Humphreys, H. (2001) *Staphylococcus epidermidis* biofilms: importance and implications. *J. Med. Microbiol.* **50,** 582–587
3. Götz, F. (2002) Staphylococcus and biofilms. *Mol. Microbiol.* **43,** 1367–1378
4. Heilmann, C., Schweitzer, O., Gerke, C., Vanittanakom, N., Mack, D., and Götz, F. (1996) Molecular basis of intercellular adhesion in the biofilm-forming *Staphylococcus epidermidis*. *Mol. Microbiol.* **20,** 1083–1091
5. Götz, F. G. P. (2000) in *Infections Associated with Indwelling Medical Devices* (Waldvogel, F. A., and Bisno, A. L., eds) pp. 55–88, American Society for Microbiology Press, Washington, D. C.
6. Hall-Stoodley, L., Costerton, J. W., and Stoodley, P. (2004) Bacterial biofilms: from the natural environment to infectious diseases. *Nat. Rev. Microbiol.* **2,** 95–108
7. Archer, N. K., Mazaitis, M. J., Costerton, J. W., Leid, J. G., Powers, M. E., and Shirtliff, M. E. (2011) *Staphylococcus aureus* biofilms: properties, regulation, and roles in human disease. *Virulence* **2,** 445–459
8. Lowy, F. D. (1998) *Staphylococcus aureus* infections. *N. Engl. J. Med.* **339,** 520–532
9. Köck, R., Becker, K., Cookson, B., van Gemert-Pijnen, J. E., Harbarth, S., Kluytmans, J., Mielke, M., Peters, G., Skov, R. L., Struelens, M. J., Tacconelli, E., Navarro Torné, A., Witte, W., and Friedrich, A. W. (2010) Methicillin-resistant *Staphylococcus aureus* (MRSA): burden of disease and control challenges in Europe. *Euro Surveill.* **15,** 19688
10. European Antimicrobial Resistance Surveillance System (2009) *EARSS Annual Report 2008*, pp. 55–58, European Centre for Disease Prevention and Control, Bilthoven, The Netherlands
11. Kresken, M., Hafner, D., Schmitz, F.-J., and Wichelhaus, T. A. (2009) Resistenzsituation bei klinisch wichtigen Infektionserregern gegenüber Antibiotika in Deutschland und im mitteleuropäischen Raum. Bericht über die Ergebnisse einer multizentrischen Studie der Arbeitsgemeinschaft Empfindlichkeitsprüfungen & Resistenz der Paul-Ehrlich-Gesellschaft für Chemotherapie e.V. aus dem Jahre 2007, p. 9, Antiinfectives Intelligence, Rheinbach, Germany
12. Kohlenberg, A., Schwab, F., Geffers, C., Behnke, M., Rüden, H., and Gastmeier, P. (2008) Time-trends for Gram-negative and multidrug-resistant Gram-positive bacteria associated with nosocomial infections in German intensive care units between 2000 and 2005. *Clin. Microbiol. Infect.* **14,** 93–96
13. Klein, E., Smith, D. L., and Laxminarayan, R. (2007) Hospitalizations and deaths caused by methicillin-resistant *Staphylococcus aureus*, United States, 1999–2005. *Emerg. Infect. Dis.* **13,** 1840–1846
14. Zeller, J. L., Burke, A. E., and Glass, R. M. (2007) JAMA patient page. MRSA infections. *JAMA* **298,** 1826
15. Biswas, R., Voggu, L., Simon, U. K., Hentschel, P., Thumm, G., and Götz, F. (2006) Activity of the major staphylococcal autolysin Atl. *FEMS Microbiol. Lett.* **259,** 260–268
16. Schlag, M., Biswas, R., Krismer, B., Kohler, T., Zoll, S., Yu, W., Schwarz, H., Peschel, A., and Götz, F. (2010) Role of staphylococcal wall teichoic acid in targeting the major autolysin Atl. *Mol. Microbiol.* **75,** 864–873
17. Heilmann, C., Hussain, M., Peters, G., and Götz, F. (1997) Evidence for autolysin-mediated primary attachment of *Staphylococcus epidermidis* to a polystyrene surface. *Mol. Microbiol.* **24,** 1013–1024
18. Albrecht, T., Raue, S., Rosenstein, R., Nieselt, K., and Götz, F. (2012) Phylogeny of the staphylococcal major autolysin and its use in genus and species typing. *J. Bacteriol.* **194,** 2630–2636
19. Zoll, S., Pätzold, B., Schlag, M., Götz, F., Kalbacher, H., and Stehle, T. (2010) Structural basis of cell wall cleavage by a staphylococcal autolysin. *PLoS Pathog.* **6,** e1000807
20. Lützner, N., Pätzold, B., Zoll, S., Stehle, T., and Kalbacher, H. (2009) Development of a novel fluorescent substrate for Autolysin E, a bacterial type II amidase. *Biochem. Biophys. Res. Commun.* **380,** 554–558
21. Kerff, F., Petrella, S., Mercier, F., Sauvage, E., Herman, R., Pennartz, A., Zervosen, A., Luxen, A., Frère, J. M., Joris, B., and Charlier, P. (2010) Specific structural features of the *N*-acetylmuramoyl-L-alanine amidase AmiD from *Escherichia coli* and mechanistic implications for enzymes of this family. *J. Mol. Biol.* **397,** 249–259
22. Stratagene (2006) QuikChange® Site-Directed Mutagenesis Kit: Instruction Manual, Stratagene, La Jolla, CA
23. Kabsch, W. (2010) *XDS*. *Acta Crystallogr. D Biol. Crystallogr.* **66,** 125–132
24. McCoy, A. J., Grosse-Kunstleve, R. W., Adams, P. D., Winn, M. D., Storoni, L. C., and Read, R. J. (2007) Phaser crystallographic software. *J. Appl. Crystallogr.* **40,** 658–674
25. McCoy, A. J. (2007) Solving structures of protein complexes by molecular replacement with Phaser. *Acta Crystallogr. D Biol. Crystallogr.* **63,** 32–41
26. Emsley, P., and Cowtan, K. (2004) Coot: model-building tools for molecular graphics. *Acta Crystallogr. D Biol. Crystallogr.* **60,** 2126–2132
27. Emsley, P., Lohkamp, B., Scott, W. G., and Cowtan, K. (2010) Features and development of Coot. *Acta Crystallogr. D Biol. Crystallogr.* **66,** 486–501
28. Winn, M. D., Ballard, C. C., Cowtan, K. D., Dodson, E. J., Emsley, P., Evans, P. R., Keegan, R. M., Krissinel, E. B., Leslie, A. G., McCoy, A., McNicholas, S. J., Murshudov, G. N., Pannu, N. S., Potterton, E. A., Powell, H. R., Read, R. J., Vagin, A., and Wilson, K. S. (2011) Overview of the CCP4 suite and current developments. *Acta Crystallogr. D Biol. Crystallogr.* **67,** 235–242
29. Potterton, E., Briggs, P., Turkenburg, M., and Dodson, E. (2003) A graphical user interface to the CCP4 program suite. *Acta Crystallogr. D Biol. Crystallogr.* **59,** 1131–1137
30. Matthews, B. W. (1968) Solvent content of protein crystals. *J. Mol. Biol.* **33,** 491–497
31. Kantardjieff, K. A., and Rupp, B. (2003) Matthews coefficient probabilities: improved estimates for unit cell contents of proteins, DNA, and protein-nucleic acid complex crystals. *Protein Sci.* **12,** 1865–1871
32. Adams, P. D., Afonine, P. V., Bunkóczi, G., Chen, V. B., Davis, I. W., Echols, N., Headd, J. J., Hung, L. W., Kapral, G. J., Grosse-Kunstleve, R. W., Mc-

High Resolution Complex Structure of S. aureus Amidase AmiA

Coy, A. J., Moriarty, N. W., Oeffner, R., Read, R. J., Richardson, D. C., Richardson, J. S., Terwilliger, T. C., and Zwart, P. H. (2010) PHENIX: a comprehensive Python-based system for macromolecular structure solution. *Acta Crystallogr. D Biol. Crystallogr.* **66,** 213–221

33. Chen, V. B., Arendall, W. B., 3rd, Headd, J. J., Keedy, D. A., Immormino, R. M., Kapral, G. J., Murray, L. W., Richardson, J. S., and Richardson, D. C. (2010) MolProbity: all-atom structure validation for macromolecular crystallography. *Acta Crystallogr. D Biol. Crystallogr.* **66,** 12–21
34. Schüttelkopf, A. W., and van Aalten, D. M. (2004) PRODRG: a tool for high-throughput crystallography of protein-ligand complexes. *Acta Crystallogr. D Biol. Crystallogr.* **60,** 1355–1363
35. DeLano, W. L. (2012) *The PyMOL Molecular Graphics System*, version 1.5.0.4, Schrödinger, LLC, New York
36. Baker, N. A., Sept, D., Joseph, S., Holst, M. J., and McCammon, J. A. (2001) Electrostatics of nanosystems: application to microtubules and the ribosome. *Proc. Natl. Acad. Sci. U.S.A.* **98,** 10037–10041
37. Iordanescu, S., and Surdeanu, M. (1976) Two restriction and modification systems in *Staphylococcus aureus* NCTC8325. *J. Gen. Microbiol.* **96,** 277–281
38. de Jonge, B. L., Chang, Y. S., Gage, D., and Tomasz, A. (1992) Peptidoglycan composition in heterogeneous Tn551 mutants of a methicillin-resistant *Staphylococcus aureus* strain. *J. Biol. Chem.* **267,** 11255–11259
39. Hasegawa, H., and Holm, L. (2009) Advances and pitfalls of protein structural alignment. *Curr. Opin. Struct. Biol.* **19,** 341–348
40. Meroueh, S. O., Bencze, K. Z., Hesek, D., Lee, M., Fisher, J. F., Stemmler, T. L., and Mobashery, S. (2006) Three-dimensional structure of the bacterial cell wall peptidoglycan. *Proc. Natl. Acad. Sci. U.S.A.* **103,** 4404–4409
41. Zoll, S., Schlag, M., Shkumatov, A. V., Rautenberg, M., Svergun, D. I., Götz, F., and Stehle, T. (2012) Ligand-binding properties and conformational dynamics of autolysin repeat domains in staphylococcal cell wall recognition. *J. Bacteriol.* **194,** 3789–3802
42. Vollmer, W., Joris, B., Charlier, P., and Foster, S. (2008) Bacterial peptidoglycan (murein) hydrolases. *FEMS Microbiol. Rev.* **32,** 259–286
43. Schleifer, K. H., and Kandler, O. (1972) Peptidoglycan types of bacterial cell walls and their taxonomic implications. *Bacteriol. Rev.* **36,** 407–477
44. de Jonge, B. L., Chang, Y. S., Gage, D., and Tomasz, A. (1992) Peptidoglycan composition of a highly methicillin-resistant *Staphylococcus aureus* strain. The role of penicillin binding protein 2A. *J. Biol. Chem.* **267,** 11248–11254
45. Low, L. Y., Yang, C., Perego, M., Osterman, A., and Liddington, R. (2011) Role of net charge on catalytic domain and influence of cell wall binding domain on bactericidal activity, specificity, and host range of phage lysins. *J. Biol. Chem.* **286,** 34391–34403
46. Yang, D. C., Tan, K., Joachimiak, A., and Bernhardt, T. G. (2012) A conformational switch controls cell wall-remodelling enzymes required for bacterial cell division. *Mol. Microbiol.* **85,** 768–781
47. Cheng, X., Zhang, X., Pflugrath, J. W., and Studier, F. W. (1994) The structure of bacteriophage T7 lysozyme, a zinc amidase and an inhibitor of T7 RNA polymerase. *Proc. Natl. Acad. Sci. U.S.A.* **91,** 4034–4038
48. Low, L. Y., Yang, C., Perego, M., Osterman, A., and Liddington, R. C. (2005) Structure and lytic activity of a *Bacillus anthracis* prophage endolysin. *J. Biol. Chem.* **280,** 35433–35439
49. Liepinsh, E., Généreux, C., Dehareng, D., Joris, B., and Otting, G. (2003) NMR structure of *Citrobacter freundii* AmpD, comparison with bacteriophage T7 lysozyme and homology with PGRP domains. *J. Mol. Biol.* **327,** 833–842
50. Martínez-Caballero, S., Lee, M., Artola-Recolons, C., Carrasco-López, C., Hesek, D., Spink, E., Lastochkin, E., Zhang, W., Hellman, L. M., Boggess, B., Mobashery, S., and Hermoso, J. A. (2013) Reaction products and the x-ray structure of AmpDh2, a virulence determinant of *Pseudomonas aeruginosa*. *J. Am. Chem. Soc.* **135,** 10318–10321
51. Carrasco-López, C., Rojas-Altuve, A., Zhang, W., Hesek, D., Lee, M., Barbe, S., André, I., Ferrer, P., Silva-Martin, N., Castro, G. R., Martínez-Ripoll, M., Mobashery, S., and Hermoso, J. A. (2011) Crystal structures of bacterial peptidoglycan amidase AmpD and an unprecedented activation mechanism. *J. Biol. Chem.* **286,** 31714–31722
52. Prigozhin, D. M., Mavrici, D., Huizar, J. P., Vansell, H. J., and Alber, T. (2013) Structural and biochemical analyses of *Mycobacterium tuberculosis* *N*-acetylmuramyl-L-alanine amidase Rv3717 point to a role in peptidoglycan fragment recycling. *J. Biol. Chem.* **288,** 31549–31555
53. Warth, A. D., and Strominger, J. L. (1971) Structure of the peptidoglycan from vegetative cell walls of *Bacillus subtilis*. *Biochemistry* **10,** 4349–4358
54. Boneca, I. G., Huang, Z. H., Gage, D. A., and Tomasz, A. (2000) Characterization of *Staphylococcus aureus* cell wall glycan strands, evidence for a new β-*N*-acetylglucosaminidase activity. *J. Biol. Chem.* **275,** 9910–9918
55. Atrih, A., Bacher, G., Allmaier, G., Williamson, M. P., and Foster, S. J. (1999) Analysis of peptidoglycan structure from vegetative cells of *Bacillus subtilis* 168 and role of PBP 5 in peptidoglycan maturation. *J. Bacteriol.* **181,** 3956–3966
56. Holm, L., and Rosenström, P. (2010) Dali server: conservation mapping in 3D. *Nucleic Acids Res.* **38,** W545–W549
57. Advanced Chemistry Development, Inc. (2012) *ACD/ChemSketch Freeware*, version 10.00, Advanced Chemistry Development, Inc., Toronto, Canada
58. Sievers, F., Wilm, A., Dineen, D., Gibson, T. J., Karplus, K., Li, W., Lopez, R., McWilliam, H., Remmert, M., Söding, J., Thompson, J. D., and Higgins, D. G. (2011) Fast, scalable generation of high-quality protein multiple sequence alignments using Clustal Omega. *Mol. Syst. Biol.* **7,** 539
59. Waterhouse, A. M., Procter, J. B., Martin, D. M., Clamp, M., and Barton, G. J. (2009) Jalview Version 2: a multiple sequence alignment editor and analysis workbench. *Bioinformatics* **25,** 1189–1191

COMMUNICATIONS BIOLOGY

ARTICLE

https://doi.org/10.1038/s42003-020-01405-2 OPEN

New insights in the coordinated amidase and glucosaminidase activity of the major autolysin (Atl) in *Staphylococcus aureus*

Mulugeta Nega[1], Paula Maria Tribelli[1,2], Katharina Hipp[3], Mark Stahl[4] & Friedrich Götz[1✉]

After bacterial cell division, the daughter cells are still covalently interlinked by the peptidoglycan network which is resolved by specific hydrolases (autolysins) to release the daughter cells. In staphylococci, the major autolysin (Atl) with its two domain enzymes, N-acetylmuramyl-L-alanine amidase (AmiA) and β-N-acetylglucosaminidase (GlcA), resolves the peptidoglycan to release the daughter cells. Internal deletions in each of the enzyme domains revealed defined morphological alterations such as cell cluster formation in Δ*amiA*, Δ*glcA* and Δ*atl*, and asymmetric cell division in the Δ*glcA*. A most important finding was that GlcA activity requires the prior removal of the stem peptide by AmiA for its activity thus the naked glycan strand is its substrate. Furthermore, GlcA is not an *endo*-β-N-acetylglucosaminidase but an *exo*-enzyme that cuts the glycan backbone to disaccharides independent of its *O*-acetylation modification. Our results shed new light into the sequential peptidoglycan hydrolysis by AmiA and GlcA during cell division in staphylococci.

[1] Microbial Genetics, Interfaculty Institute of Microbiology and Infection Medicine Tübingen (IMIT), University of Tübingen, Auf der Morgenstelle 28, D-72076 Tübingen, Germany. [2] Departamento de Química Biológica FCEyN-UBA, Buenos Aires, Argentina. [3] Max Planck Institute for Developmental Biology, Max-Planck-Ring 5, D-72076 Tübingen, Germany. [4] Zentrum für Molekularbiologie der Pflanzen (ZMBP), University of Tübingen, Auf der Morgenstelle 32, D-72076 Tübingen, Germany. ✉email: friedrich.goetz@uni-tuebingen.de

CW biosynthesis and degradation during bacterial cell division is a balanced process. The CW remodeling and also cell separation is carried out by bacterial hydrolases. To maintain cell integrity and to avoid cell lysis, each cell wall hydrolase has a specific target in PG processing: (i) the amidase cleaves the amide bond between N-acetylmuramic acid and the L-alanine residue of the stem peptide, (ii) glucosaminidase catalyzes the hydrolysis of the glycosidic linkages, whereas (iii) peptidase cleaves amide bonds between amino acids within the PG chain[1]. Most bacteria produce a whole range of different PG hydrolases that perform different tasks such as nicking of PG to incorporate new monomers, remodeling and turnover of PG during growth, cell division, and cell separation[2]. In staphylococci, the last step in cell division is the separation of the two interlinked daughter cells by cell wall (CW) hydrolases. The separation of daughter cells is mainly catalyzed by the so-called "major autolysin", Atl. This is a secreted bifunctional multidomain enzyme typical for the genera *Staphylococcus* and *Macrococcus*[3]. Atl of both *S. aureus* and *S. epidermidis* is processed into two bacteriolytic active domains, the ≈62 kDa N-acetylmuramyl-L-alanine amidase (AmiA) and the ≈51 kDa endo-beta-N-acetylglucosaminidase (GlcA)[4–6]. The 51 kDa GlcA from *S. aureus* was described as an endo-beta-N-acetylglucosaminidase[7]. Deletion of the entire *atl* gene in *S. epidermidis* led to huge cell cluster formation indicating that daughter cell separation was severely affected and the supernatants lacked five prominent proteins[4]. This defect could largely be complemented by *atl* or *amiA* alone. Interestingly, to compensate for the loss of *atl*, staphylococci induce another 35 kDa autolysin (*aaa*) with a cysteine, histidine-dependent amidohydrolase/peptidase (CHAP) domain[8,9]. Atl proteins mediate attachment of staphylococcal cells to polymer surfaces and enhance biofilm formation[4,10,11].

Atl is proteolytically processed to the two enzymes AmiA and GlcA[4,5,12]. This processing occurs in such a way that each of the enzymes is supplied with repeat domains generating AmiA-R1ab/R2ab and R3ab-GlcA (Fig. 1a). The repeat regions target AmiA and GlcA to the septum in two ways: (a) the repeats are repelled by the wall teichoic acid (WTA), which is mainly present in the mature CW[13], and (b) the repeats bind to the lipoteichoic acid (LTA), which is localized in the septum[14]. In this way, the repeats direct AmiA and GclA to the septum, where they can optimally carry out the final step of cell division by resolving the PG-interlinked daughter cells.

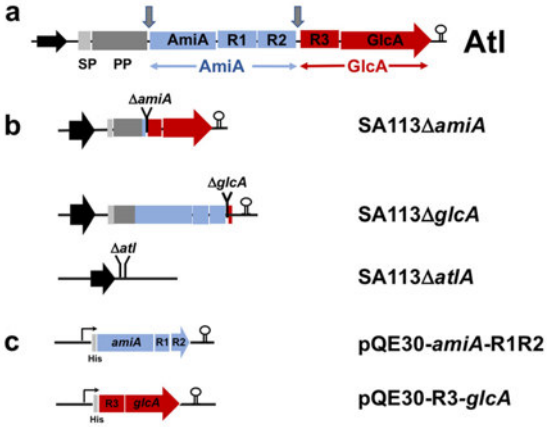

Fig. 1 Organization of the domain structure of the *S. aureus* major autolysin (Atl) and construction of mutants and expression vectors. a Atl is organized as a multidomain protein starting with the signal peptide (SP), which is followed by the propeptide (PP), the amidase (AmiA-R1R2), and the glucosaminidase (R3-GlcA) domains. A certain proportion of Atl is post-translocationally processed as indicated by arrows. The repeats, connected by a linker, represent LTA-binding domains that target the enzymes to the septum. **b** Deletion constructs of the *amiA* (Δ*amiA*) and *glcA* (Δ*glcA*) domains and the entire *atl* (Δ*atl*) gene. **c** *amiA* and *glcA* expression constructs in pQE30 fitted with an N-terminal His-tag.

To obtain more insight into the amidase, the structure of the soluble 214 aa catalytic domain of amidase from *S. epidermidis* (AmiE) and *S. aureus* (AmiA) were determined[15,16]. Both amidases adopt an almost identical globular fold, with several alpha-helices surrounding a central beta-sheet. In the active site, an essential zinc ion is buried which stabilizes the transition state during catalysis. The minimal substrates for AmiE and AmiA is the muramyltripeptide which must contain a di-amino acid lysine. AmiE and AmiA reveal a striking and unexpected homology to the family of the mammalian PG recognition proteins (PGRPs), some of which also possess amidase activity[16].

The Atl amidase is composed of the catalytic Ami domain and repeats R1ab and R2ab. These three modules are separated by two linkers, L1 and L2[14,17]. The two repeats (R1ab and R2ab) target the Ami to the septum where LTA serves as a receptor. The crystal structure of R2ab reveals that each repeat folds into two half-open beta-barrel; and small-angle X-ray scattering of the mature amidase reveals the presence of flexible linkers (L1 and L2) separating the Ami, R1ab, and R2ab units. The linkers act as a hinge region allowing high flexibility and fidelity of the amidase domain. All data suggest that the repeats direct the catalytic amidase domain to the septum, where it can optimally perform the final step of cell division[14]. The functional and structural analysis of the major autolysin (Atl) in *Staphylococcus* has been reviewed by Götz et al.[18].

Although several studies have focused on the functional and the structural analysis of Atl, little is known about the interplay of AmiA and GlcA during cell division and separation. Here, we compared morphological changes of *S. aureus atl* mutants carrying deletions of the *amiA* (Δ*amiA-R1-R2*), *glcA* (Δ*R3-glcA*) domains and the entire *atl* (Δ*atl*). In the past, AmiA activity has been investigated mainly with synthetic substrates or in zymograms, here we demonstrate its activity with its natural substrate PG. Moreover, we demonstrate that the glucosaminidase GlcA is not an endo- but an exo-beta-N-acetylglucosaminidase which is only active with the naked glycan strand after AmiA has cleaved off the crosspeptides. This implies that the cutting (resolution) of PG occurs in a defined order, in which AmiA first hydrolyzes the crosspeptides, and only then can GlcA dissect the glycan strand to disaccharides units.

Results

Morphological characterization of *S. aureus amiA*, *glcA*, and *atl* mutants by scanning and transmission electron microscopy (SEM and TEM). The staphylococcal major autolysin, Atl, is a multidomain protein composed of the signal peptide (SP), the propeptide (PP), the catalytic domain (cat) of the amidase AmiA followed by the repeat domains R1 and R2, and the glucosaminidase domain (GlcA) which is preceded by the R3 repeat domain (Fig. 1a). To compare the morphological consequences of each enzyme, we constructed internal deletion mutants in the *S. aureus* SA113 strain. In SA113Δ*amiA*, the *amiA* domain together with the repeats R1 and R2 were deleted. In SA113Δ*glcA* the R3 and *glcA*, whereas in Δ*atl* the entire *atl* gene was deleted (Fig. 1b).

Comparative scanning electron microscopic (SEM) analysis of SA113 and the mutants Δ*amiA*, Δ*glcA* and Δ*atl* grew to mid-exponential phase revealed that in all mutants, the cell separation was affected as manifested by increased cell cluster formation, indicating that both, AmiA and GlcA contribute to cell separation

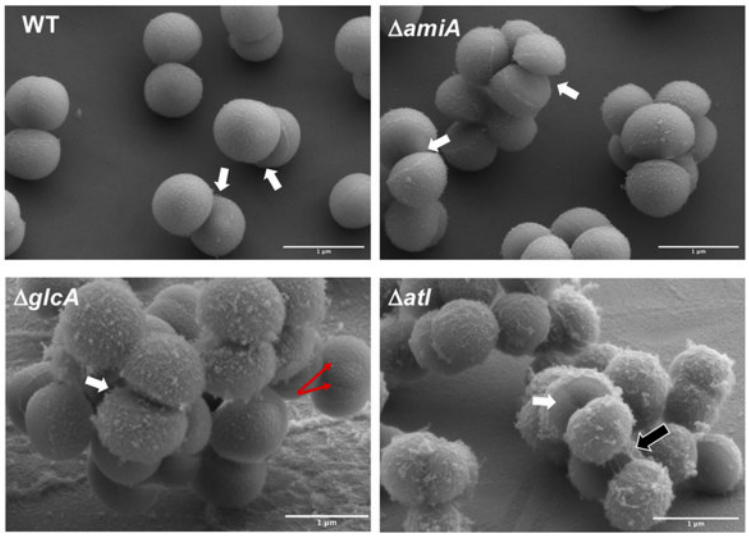

Fig. 2 Comparative SEM images of exponential grown SA113 and its mutants. WT cells have smooth old CW with well-separated daughter cells. Some cell pairs are already broken open by a mechanical crack popping apart the daughter cells (white arrows). In Δ*amiA*, cells are noticeably more clumped with the popped cells while the old CW is rougher than in the WT. In Δ*glcA*, the roughness of the old CW was further intensified with pockmarked elevations, and in some cells, asymmetric septa were formed (red arrows). Finally, Δ*atl* showed the highest clumped phenotype, with lots of separate cells that are still connected by thread-like PG structures (black arrow); the rough surface of the old CW is full with pockmarked elevations which represent accumulations of unprocessed PG. Popped cells (white arrows) are seen in all mutants; red arrows, indicate asymmetric septa; black arrow, indicates thread-like PG structures by which the neighboring cells are still connected. Scale bars 1 µm.

(Fig. 2). In both WT and the mutants, popped daughter cells were seen that were mechanically cracked apart as described by Zhou et al.[19]. Popped daughter cells were seen in all mutants indicating that this part of cell division is not affected in the mutants. In Δ*amiA*, cells are more clumped and the old CW is rougher than in the WT. In Δ*glcA* the roughness of the old CW was further intensified with pockmarked elevations and one can see that in some cells, asymmetric septa were formed (red arrows). Finally, Δ*atl* showed the highest clumping phenotype and most rough cell surface; there were lots of separate cells that are still connected by thread-like PG structures (Fig. 2). This difference in cell cluster formation in the mutants was further confirmed by forward scatter flow cytometric measurements of WT SA113, Δ*amiA*, Δ*glcA*, and Δ*atl* cells grown to mid-exponential phase. The results clearly show that the mean cluster size increases in the order WT < Δ*amiA* < Δ*glcA* < Δ*atl* confirming the previous microscopic observations (Supplementary Fig. 4).

In order to confirm our hypothesis that the thread-like structures are filaments of unprocessed "old" PG, we digested heat-inactivated mutant Δ*atl* cells that were grown to mid-exponential phase with purified AmiA and GlcA. A comparison of the digested and undigested samples with SEM analysis showed that the clumping phenotype of the undigested sample is completely abolished and cells were separated. More importantly, the rough surface becomes smooth confirming that the "old" PG was processed by the externally added enzymes (Fig. 3).

Through cross-sectional analysis of dividing cells using TEM, it has become more precisely visible which deformations occur during cell division (Fig. 4). In the WT strain, the cells are dividing into three alternating perpendicular planes, with sister cells remaining attached to each other after division and the resulting point of attachment was usually not exactly at the point corresponding to the center of the previous septal disk as described already by Tzagoloff and Novick 1977[20]. In Δ*amiA*, some thread-like structures were released, most likely sheared-off CW residues; otherwise the division planes looked normal like in the WT. In Δ*glcA*, however, there was a high proportion of cells where the division plane was asymmetric giving rise to "kidney" like cell arrays. Apparently, the perpendicular sequence of the cell division plane was disturbed (Fig. 4 and Supplementary Fig. 1). In Δ*atl* such asymmetric septa formations were not seen; however, the clumping phenotype is extreme, and even separated cells are still connected by thread-like PG structures. The different morphological features of the mutants indicate that AmiA and GlcA are important determinants of cell division and separation with distinct functions.

Deletion of *atl* results in decreased PG cross-linking. For the analysis of PG cross-linking, PG isolated from the SA113, its Δ*atl* mutant and complemented mutant Δ*atl*(pRC14) were resuspended with buffer, adjusted to OD 3.0 and digested with mutanolysin. The released muropeptides were resolved with RP-HPLC, and area units of each fragment were compared relative to the area units of the whole chromatogram (Fig. 5a). The total composition of the PG fragments was largely the same in SA113 and its Δ*atl* mutant. However, in the Δ*atl* mutant, the short PG fragments (mono- to pentamer) were increased 1.5 to twofold, while the longer PG fragments (≥octamer) were about twofold decreased (Fig. 5a, b). The shift from polymeric to oligomeric PG fragments in the Δ*atl* mutant was also confirmed by the decrease of the hump at later elution times (>100 min). These results show that in the Δ*atl* mutant, not only cell separation but also PG cross-linking was impaired. To see which enzyme contributes most to PG cross-linking, we also analyzed Δ*amiA* and Δ*glcA* mutants. In both mutants, PG cross-linking was decreased as well but not as low as in the Δ*atl* mutant suggesting that both the AmiA and GlcA contribute to PG cross-linking (Supplementary Fig. 3).

Digestion of PG by AmiA caused the release of cross-linked peptides of varying length. As a control, we digested purified *S.*

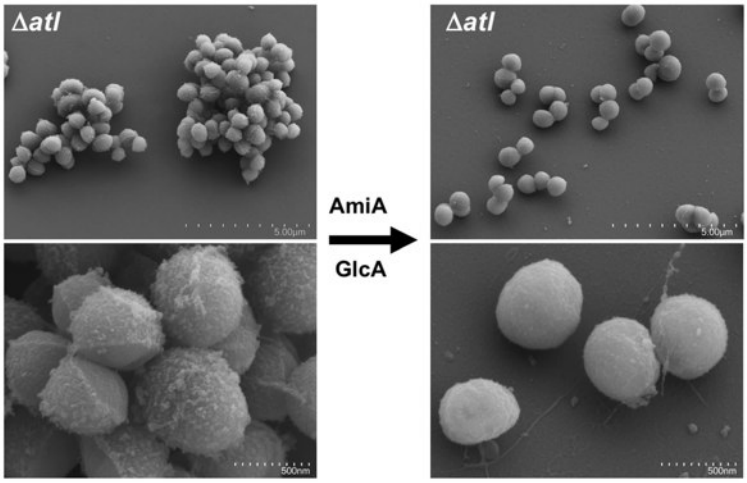

Fig. 3 Scanning electron microscopic (SEM) analysis of enzyme digested SA113Δ*atl* cells. Cells grown to mid-exponential phase were centrifuged and resuspended in 50 mM phosphate buffer pH 7.0 and heat-inactivated at 65 °C for 30 min. A portion of it was digested with purified AmiA and GlcA. SEM analysis of both the digested and undigested cells shows smoothening of the surface and removal of old PG from the surface. The images at the bottom are magnifications (scale bar 500 nm) of the same upper sample image (scale bar 5 µm) showing details of surface smoothness and separation.

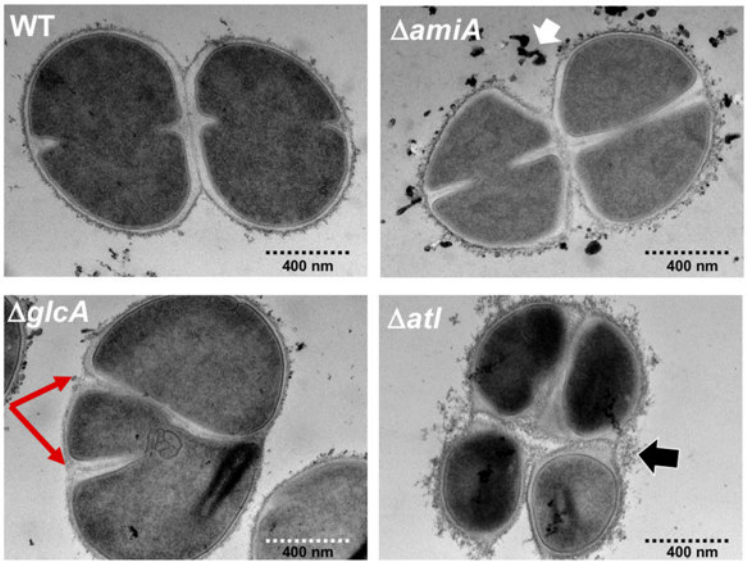

Fig. 4 Transmission electron microscopic (TEM) images of exponential grown SA113 and its mutants. Through cross-sectional analysis of dividing cells using TEM, it is more precisely visible which deformations occur during cell division. In Δ*amiA* cells, the old CW is rougher than in the WT but division symmetry is unaffected. In Δ*glcA*, the asymmetric septa formation is now clearly visible than in the SEM images (red arrows). In Δ*atl*, even separated cells are still connected by thread-like PG structures (black arrow). Scale bars 400 nm.

aureus 113 PG with the muramidase mutanolysin and separated the solubilized digestion products by RP-HPLC. As described previously[21], we obtained the typical peak pattern from monomeric up to heptameric PG fragments followed by a hump of the unresolved polymeric fraction (Fig. 6a). AmiA digestion was carried out in the same way as with mutanolysin. AmiA (AmiA-R1-R2) was isolated from *E. coli* M15 (pQE30Ω*amiA-R1-R2*) (Fig. 1c) and purified via its N-terminal His_6-tag. After the digestion of PG with AmiA, the solubilized PG fragments were analyzed by RP-HPLC. We could resolve between 15 and 20 peaks (Fig. 6b). Mass spectrometric (MS) analysis of the major peaks revealed that the amidase effectively cleaved between the N-acetylmuramic acid and the L-Ala of the stem peptide, thus releasing cross-linked peptides of varying lengths, from mono- up to >12-mer (Fig. 7a and Supplementary Table 2). Each peak showed a mass value that corresponds to a tetrapeptide-pentaglycine fragment (peptide monomer) that is exactly the fragment of the next cross-linking (Fig. 7b).

GlcA requires the prior removal of stem peptide by amidase for its activity. Like AmiA, the glucosaminidase, GlcA, was isolated from *E. coli* M15 (pQE30Ω*R3-glcA*) (Fig. 1c) and purified via its N-terminal His_6-tag. While AmiA digested PG shows the typical

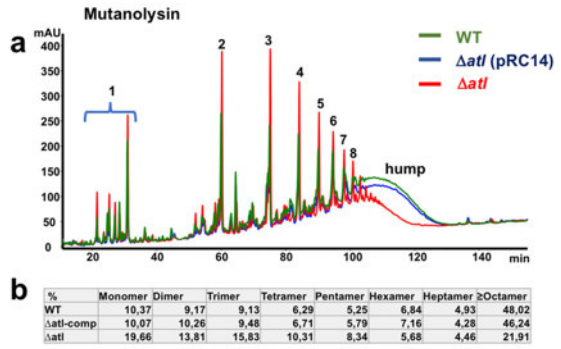

%	Monomer	Dimer	Trimer	Tetramer	Pentamer	Hexamer	Heptamer	≥Octamer
WT	10,37	9,17	9,13	6,29	5,25	6,84	4,93	48,02
Δatl-comp	10,07	10,26	9,48	6,71	5,79	7,16	4,28	46,24
Δatl	19,66	13,81	15,83	10,31	8,34	5,68	4,46	21,91

Fig. 5 RP-HPLC profiles of solubilized muropeptides of mutanolysin digested PG. a Muropeptide profile of WT, Δ*atl* and the plasmid complemented Δ*atl* (pRC14) strains. The peaks 1–8, up to a retention time (RT) of ~100 min, represent soluble monomeric to octameric muropeptide fragments. The peak areas of the smaller fragments (peaks 1–5) is much higher in the Δ*atl* mutant than in the WT, indicating that in Δ*atl*, PG cross-linking is decreased. Higher-order cross-linked polymeric muropeptides (RT > 100 min) are characterized by a hump of the unresolved polymeric fraction. **b** Percent distribution of muropeptide fragments of the WT, plasmid complemented Δ*atl*, and Δ*atl* mutant. The figure is representative of three independent experiments.

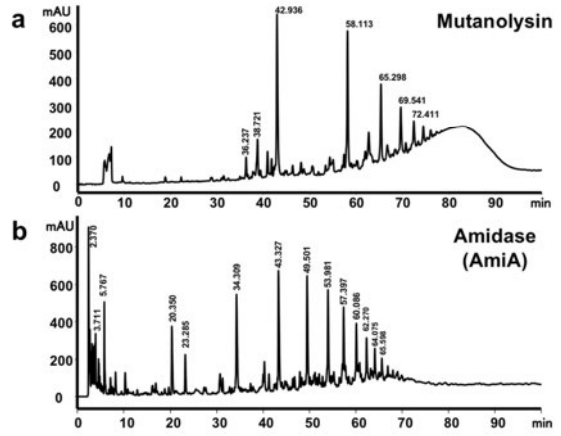

Fig. 6 Muramidase (mutanolysin) and amidase (AmiA) digestion pattern of staphylococcal PG. a RP-HPLC analysis of soluble PG of *S. aureus* SA113 released after digestion with mutanolysin showing the characteristic peak pattern of monomeric up to heptameric PG fragments ending in a hump of an unresolved polymeric fraction as described previously[21]. **b** HPLC analysis of soluble PG fragments released after digestion with AmiA shows a distinctly different peak pattern.

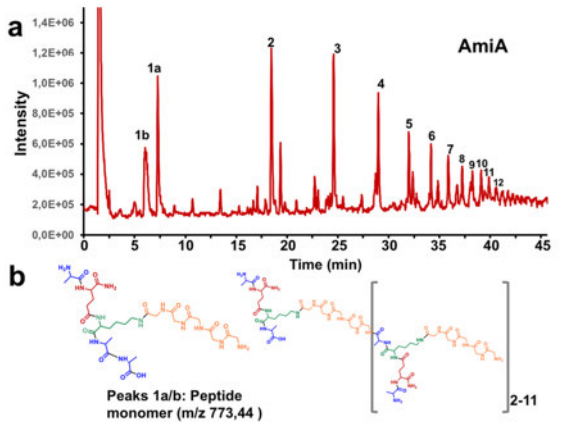

Fig. 7 HPLC/MS profile of AmiA solubilized staphylococcal PG. a showing peaks (1–12) of the peptides released by AmiA hydrolysis of PG between MurNAc of the glycan backbone and L-Ala of the stem peptide in increasing length. The mass of each numbered peak corresponds to the number of crosspeptides composed of the stem peptide and the pentaglycine bridge (monomer). **b** Structural representation of the peptide peaks 1a/b (peptide monomer) and the extension of the monomeric structure up to its 12-mer shown in square brackets.

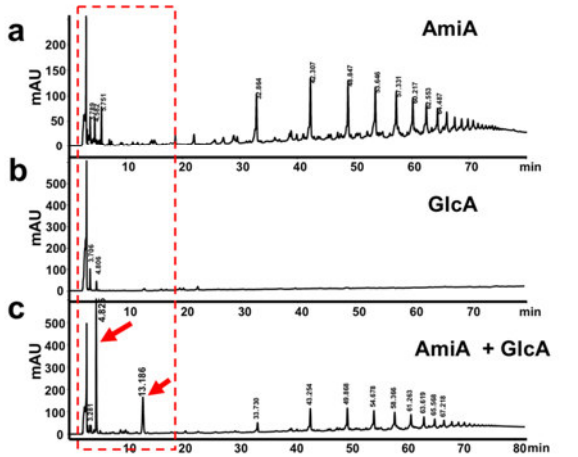

Fig. 8 RP-HPLC profile of soluble fragments obtained after hydrolysis of PG*. a with AmiA, **b** with GlcA, **c** with GlcA after prior digestion with AmiA; AmiA was heat-inactivated at 95 °C for 3 min before digestion with GlcA. After the double digestion, two distinct peaks at RT 4.8 and 13.1 min appear as main products, indicated by red arrows. *Please note the different scales in **a** = 250, **b** = 600, and **c** = 600 mAU. All samples are heat-inactivated at 95 °C for 3 min before analysis.

soluble PG fragments (Fig. 8a), no soluble PG fragments were observed with GlcA (Fig. 8b), suggesting that GlcA cannot cleave PG. Therefore, we assumed that GlcA is active only if PG is predigested with AmiA. To verify this assumption, we predigested PG with AmiA for 16 h, inactivated the AmiA by heating to 95 °C for five minutes, followed by digestion with GlcA for a further 16 h. Now two main peaks appeared at RT 4.8 and 13.1 min, while the peaks specific to AmiA remain unaltered (Fig. 8c). The masses of the peaks at RT 4.8 and 13.1 min were m/z 498 and m/z 540 (reduced form) (Fig. 9a, b), indicating that the peak at RT 4.8 corresponds to MurNac-GlcNac disaccharides and the one at RT 13.1 to *O*-acylated MurNac-GlcNac (Fig. 9c). This result shows that GlcA is only active with an unsubstituted glycan chain that is free of peptide subunits. It also shows that *O*-acetylation of MurNAc does not affect GlcA activity.

GlcA is not an endo- but an exo-β-N-acetylglucosaminidase. Since GlcA treatment of the AmiA-predigested PG only resulted in disaccharide products, we assumed that GlcA is not an endo- but must be an exo-β-N-acetylglucosaminidase. If GlcA is an endoenzyme, as described in the literature[5,22], we should see glycan products of different sizes in the course of time. We, therefore, digested AmiA predigested PG with GlcA and followed the product formation over a period of 0 to 8 h. If GlcA is an

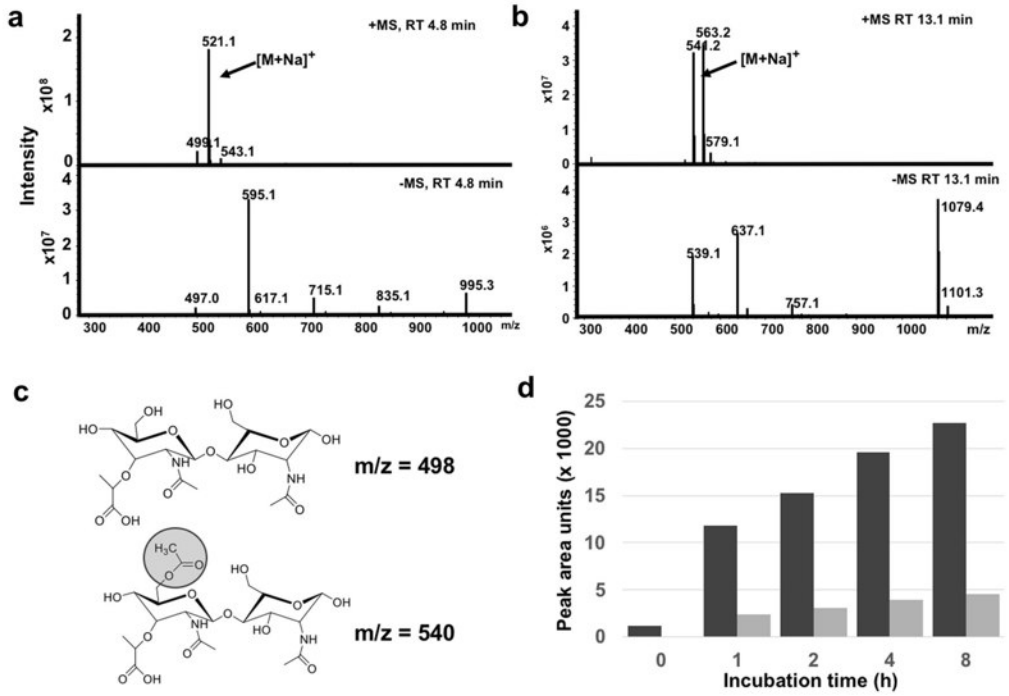

Fig. 9 Mass spectrometric and time-lapse profile of the GlcA digestion disaccharide products, MurNac-GlcNac. The mass of the two distinct HPLC peaks at Rt 4.8 min (**a**) and 13.1 min (**b**) shown in Fig. 7c was determined. **c** The mass of m/z = 498 corresponds to MurNAc-GlcNAc and of m/z = 540 to *O*-acetylated MurNAc-GlcNAc. **d** Time course of MurNAc-GlcNAc release by AmiA and GlcA digestion measured by RP-HPLC. The black bar represents MurNAc-GlcNAc and the gray bar *O*-acetylated MurNAc-GlcNAc. The figure is representative of three independent experiments.

exoenzyme, we should only see disaccharide products with increasing concentrations over time. Indeed, HPLC analysis of the samples at different time points showed that only MurNAc-GlcNAc disaccharide peaks appeared that increased with time (Fig. 9d). This result clearly shows that first, the substrate of GlcA is the naked glycan strand devoid of cross-linking peptides, and second, GlcA is an exo-β-N-acetylglucosaminidase that acts on the outer tip of the glycan chain releasing only MurNAc-GlcNAc-disaccharides.

Discussion

In staphylococci, separation of the daughter cells is mainly catalyzed by the so-called "major autolysin", Atl. This bifunctional multidomain protein consists of the two murein hydrolase domains, the amidase (AmiA) and glucosaminidase (GlcA) with their adjoining repeats. The cell morphological changes of mutants in which the entire *atl* gene is deleted have been described in *S. aureus* and *S. epidermidis*[4,23]. The *atl* mutant formed huge cell clusters and in SEM images the daughter cells were largely unseparated. To learn more about the function of the AmiA and GlcA, Bose et al.[10] investigated internal *amiA* or *glcA* deletions in *S. aureus*. The growth rate of the mutant was not impaired compared to the WT, however, both showed a clumping phenotype and both enzymes are essential for biofilm formation.

Atl forms a ring structure on the cell surface at the septal region for the next cell division site[24]. This peripheral ring consists of a large belt of PG in the division plane[25]. The resolution of this ring occurs within milliseconds ("popping"), and the separating cells split open asymmetrically leaving the daughters connected by a hinge[19,26]. By SEM, we observed, both in WT and the mutants, the peripheral ring as well as cracked daughter cells with the typical features of a smooth and flat septal wall and a rough outer wall (Fig. 2). This might suggest that cell division is not principally affected in the Δ*amiA* and the Δ*glcA* mutants. However, when we examined dividing cells with TEM, we see significantly more differences between the Δ*amiA* and the Δ*glcA* mutants. The main difference is that, in 25–35% of the Δ*glcA* mutant cells, the division is asymmetric with a non-separated, kidney-shaped cell cluster; the asymmetric septum formation is indicated by red arrows (Fig. 4 and Supplementary Figs. 1 and 2). The dark spots seen in Δ*amiA* (white arrow) represent artifacts during sample preparation and imaging. In the Δ*glcA* mutant, the crosspeptides are hydrolyzed by the AmiA to generate naked glycan strands. The question is how (if) these unprocessed glycan strands cause this irregular septum formation. Wheeler et al. showed that particularly the lack of glucosaminidases Atl, SagA, ScaH, and SagB cause an increased surface stiffness and increased glycan chain length[27,28]. We assume that the asymmetric septum formation in the Δ*glcA* mutant is caused by the long unprocessed glycan strands, causing an increase in surface stiffness and a decrease in cell elasticity. Long unprocessed glycan strands and the resulting increased stiffness could affect the orthogonal septa formation for the next cell division thus causing the asymmetrical cell division. Digestion and processing of the septum can progress since AmiA does not need the presence and activity of GlcA. This result shows that GlcA is crucial for the generation of alternating perpendicular planes and thus for the symmetry of cell division. *S. aureus* cells divide into three alternating perpendicular planes, with sister cells remaining attached to each other after division[20]. With *glcA*, we have identified a gene/enzyme which contributes to a symmetrical cell division.

In the Δ*atl* mutant, some part of the PG will be resolved because there are several minor amidases like the Aaa that are upregulated[4,8,9]. Moreover, in the Δ*atl* mutant, a number of secondary PG hydrolases (Aaa, SsaA, Aly, SA2437, SA2097, SA0620, SA2353, SA2332, SA0710, SA2100, LytH, IsaA, LytM, SceD) were increased in the secretome and the corresponding genes were transcriptionally upregulated, suggesting a compensatory mechanism for the *atl* mutation[29]. Such back-up PG hydrolases might rescue the deleterious effect in cell separation in Δ*atl*.

The structure of AmiA is resolved[15]. Its activity is described as a N-acetylmuramyl-L-alanine amidase, which cleaves the bond between the lactyl group of MurNAc and the peptide subunit of PG in several previous works. Oshida et al. and others described the activity of the amidase with zymogram analysis using heat-inactivated staphylococcal whole cells as amidase substrates and *Micrococcus luteus* as glucosaminidase substrates without showing any structural evidence[4–6]. Later Lutzner et al. developed a novel fluorescent substrate for *S. epidermidis* Atl amidase AmiE. But this substrate has no similarity with the natural PG since it neither has glycan components nor is the peptide sequence the same as the natural substrate[30]. Biswas et al. have used PG to show the mass difference extracted from an HPLC-MS analysis after a lysostaphin and amidase double digestion[23]. But surprisingly, none of these and other studies performed so far, have used the natural substrate, purified staphylococcal whole PG, and shown the specific activity of the Atl amidase. As there are enzymes with diverse hydrolytic activities, for example, LytN shows both amidase and peptidase activities when tested on staphylococcus PG[31], it is necessary and important to verify the activity spectrum of Atl amidase on its natural substrate. Furthermore, the crystal structure of the catalytic domain of AmiA in complex with a PG-derived ligand shows that the pentaglycine bridge is important for fitting into the binding cleft of AmiA[15]. The binding groove of the AmiA structure also explains why only the Lys-type PG of *S. aureus* can be hydrolyzed and not the meso-diaminopimelic acid (meso-DAP) type PG of *B. subtilis*. By treatment of PG with AmiA, more than 12 peaks could be resolved that correlated perfectly with the mass of mono- to >12-mer crosspeptides (Fig. 8a). This result shows the activity of AmiA with its natural substrate the staphylococcal PG. We also can demonstrate that it does not have additional PG-peptidase activity as seen for example with the amidase LytN[31]. The number of resolved peaks suggests that the glycan strands can be longer than 12 disaccharide units, with a predominant length of three and ten disaccharides. These results correlate well with earlier studies by Boneca et al.[32].

One of the most important part of this study was the finding that the glucosaminidase GlcA is not an endo- but an exo-β-N-acetylglucosaminidase. How it came about to denote the *S. aureus* glucosaminidase as an endo-β-N-acetylglucosaminidase is in retrospect not completely comprehensible[22,33]. Later, the characterization of the 51 kDa GlcA from *S. aureus* as an *endo*-beta-N-acetylglucosaminidase lacks clear experimental evidence as well[7], indicating that, in none of these reports an *endo*-activity has been really demonstrated. The crystal structures of *S. aureus* N-acetylglucosaminidase of the major autolysin (Atl) alone and in complex with fragments of PG revealed that N-acetylglucosaminidase of *S. aureus* and the muramidase (lysozyme) approach the substrate at alternate glycosidic bond positions[34]. The catalytic analysis revealed that reduced (MurNAc-GlcNAc)$_2$ as a substrate was cleaved to the disaccharides MurNAc-GlucNAc and MurNAc-GlcNAc^{red}, indicating that the staphylococcal GlcA is an *N*-acetylglucosaminidase; whereas the products MurNAc^{red} and GlcNAc-MurNAc-GlcNAc^{red} would have indicated a muramidase activity[34]. But, by using (MurNAc-GlcNAc)$_2$ as a substrate, it is not possible to distinguish between an endo- or exo-GlcA. It is difficult to distinguish if the disaccharide products are MurNAc-GlcNAc, GlcNAc-MurNAc, or a mixture of both. We think that the reducing end of the glycan strand is MurNAc since Lipid II is incorporated as GlcNAc-MurNAc[35].

GlcA cannot hydrolyze cross-linked PG. While AmiA digests PG to the variably long crosspeptides (Figs. 7a and 8a), GlcA did not produce any digestion products (Fig. 8b), indicating that cross-linked PG cannot be cleaved by GlcA. This explains why in zymogram the 52 kDa GlcA showed almost no bacteriolytic activity with *S. aureus* but with *Micrococcus luteus* cells[4]. This discrepancy was explained by the fact that *M. luteus* PG is less cross-linked than that of *S. aureus*[18]. In order to verify if cross-linked PG is not a substrate for GlcA, we double digested PG with AmiA and GlcA (Fig. 8c). While the amount of crosspeptides remains unaltered, two new predominant peaks appeared which turned out to be *O*-acylated and none-*O*-acylated MurNAc-GlcNAc disaccharides (Fig. 9a–c). This result confirms that GlcA is only active if the cross-linked peptides were previously removed by AmiA, confirming that the naked glycan strand is the substrate for GlcA. Similarly, the fact that we see only the two disaccharide peaks reveals that GlcA is an *exo*-N-acetylglucosaminidase. Had it been an endoenzyme, one would have expected intermediary oligosaccharides of different sizes. But this was observed at no time point. We only saw increasing peak areas for non-*O*-acylated (≈80%) and *O*-acylated (≈20%) MurNAc-GlcNAc peaks (Fig. 9d). PG *O*-acetylation is not only found in *S. aureus* but also in other pathogenic staphylococcal species Bera et al.[36] and contributes to increased pathogenicity by immune evasion[37]. Our results reveal that the GlcA activity is not hindered by *O*-acetylation of the glycan backbone in contrast to the muramidase lysozyme, as previously described[38].

Here, we unraveled three major differences between the muramidase lysozyme and GlcA. (i) Lysozyme hydrolyzes cross-linked PG, (ii) it represents an endoenzyme, and (iii) its binding to PG is markedly decreased by PG *O*-acetylation. On the other hand, GlcA cannot cleave cross-linked PG, rather it affords a 'naked' glycan strand; it is an exoenzyme and its activity is not inhibited by *O*-acetylation of MurNAc.

With this study, we show PG processing by Atl occurs in a defined order as illustrated in the model (Fig. 10). At first, the N-

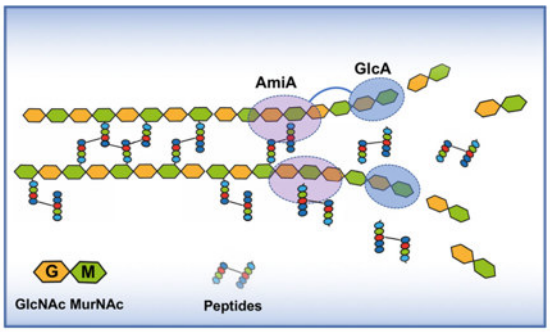

Fig. 10 Model of staphylococcal PG processing by Atl. PG processing by Atl occurs in a defined order. Upper strand: in the unprocessed Atl, AmiA and GlcA are linked together. AmiA slides along one strand of the PG and cuts off the crosspeptides exposing an unmodified "naked" glycan strand which is now substrate for GlcA. The exo-β-N-acetylglucosaminidase GlcA chops down the glycan strand into GlcNAc-MurNAc disaccharide units. Lower strand: proteolytically processed individual AmiA and GlcA act separately and are most likely involved in processing loose ends thus contributing to "smoothen" the CW.

acetylmuramyl-L-alanine amidase (AmiA) comes into play by hydrolyzing the crosspeptides leaving a naked glycan strand behind. This glycan strand is chopped down to GlcNAc-MurNAc disaccharides by the exo-β-N-acetylglucosaminidase (GlcA) following AmiA. In the unprocessed Atl, the two enzymes are combined in one protein in exactly the right catalytic order, AmiA-GlcA. This makes sense as AmiA must first free PG from crosspeptides before GlcA can be active. In both *S. aureus* and *S. epidermidis*, Atl is proteolytically processed to individual AmiA and GlcA enzymes. This also makes sense in so far as during the PG processing loose ends will be created that can be chopped down more easily by the individual enzymes thus contributing to "smoothen" the CW. Here, we have decoded the actual activity of glucosaminidase (GlcA) and show that the separation of the daughter cells takes place through a precisely coordinated interaction of AmiA and GlcA.

Methods

Bacterial strains, media, and growth conditions. For all experiments *S. aureus* SA113, which is a NCTC 8325 derivative[39], its Δ*atl* deletion mutant SA113Δ*atl::spc* and the complemented mutant SA113Δ*atl::spc* (pRC14) were used[23,40]. Staphylococci were cultivated in tryptic soy broth (TSB), and *E. coli* DC10B in basic medium (BM) (1% soy peptone, 0.5% yeast extract, 0.5% NaCl, 0.1% glucose, and 0.1% K_2HPO_4, pH 7.2) at 37 °C and shaking at 150 rpm. When appropriate, the medium was supplemented with 10 µg/mL chloramphenicol for *Staphylococcus* strains and 100 µg/mL ampicillin for *E. coli* strains.

Generation of markerless Δ*amiA* and Δ*glcA* deletion mutants in *S. aureus* SA113. For the construction of the markerless *amiA* mutant, ~1000 bp fragment upstream of the catalytic domain of *amiA* and an ~1200 bp fragment downstream of its second repeat domain (R2) was amplified with primers Ami_Up Fwd/Rev and Ami_Down Fwd/Rev. Similarly, the markerless *glcA* mutant was generated by amplifying fragments of similar size upstream of the glucosaminidase repeat domain (R3) and downstream of its catalytic domain from SA113 genomic DNA using primers Glc_Up Fwd/Rev and Glc_Down Fwd/Rev (see supplementary Table 1 for a complete list of primers). Shuttle vector pBASE6[41] was linearized with EcoRV and the three fragments per construct were ligated by Gibson assembly[42]. Chemically competent *E. coli* DC10B cells, which lack dcm methylation and therefore allow direct plasmid transfer into *S. aureus*[43], were transformed with pBASE6-amiA_del and pBASE6-glcA_del plasmids, and successful transformants were selected and grown on LB agar plates supplemented with 100 µg/ml ampicillin. Electrocompetent SA113 cells were transformed by electroporation as described[44] with 2–4 µg of plasmid DNA (1 mm cuvette, 23 kV/cm), which was isolated and verified by the transformed *E. coli* DC10B cells. After electroporation, a prewarmed BM medium was added and the cells were further incubated for 2 h at 37 °C, which finally were plated on BM agar supplemented with 10 µg/ml chloramphenicol. The temperature-sensitive vector pBASE6 allows anhydrotetracycline-inducible expression of *secY* antisense RNA for counter-selection against the plasmid[41]. The deletion of both genes *amiA* and *glcA* was further conducted as described previously[41,45]. The correct sequence of the obtained plasmid constructs was verified by colony PCR and subsequent sequencing using the primers pBASE6_Fwd/Rev. Successful markerless deletion mutants were verified by PCR analysis and sequencing using primers AmiA_KO Fwd/Rev and GlcA_KO Fwd/Rev for *amiA* and *glcA* deletion, respectively.

Cloning and expression of *S. aureus* amidase AmiA and glucosaminidase GlcA. *amiA* with its two repeat regions *amiA-R1-R2* and *glcA* with its repeat domain *R3-glcA*[14,15] were cloned and expressed with an N-terminal His_6-tag in *E. coli* M15 using the IPTG inducible plasmid pQE30[23,46]. Cells were cultivated in 2xYT to OD_{578nm} 0.5 at 37 °C, and then induced with 1 mM IPTG for 4 h at 20 °C. The cells were harvested by centrifugation and washed twice in PBS containing cOmplete protease inhibitor cocktail (Roche). The obtained cell pellets were then lysed using a French press. The crude extract was centrifuged (15 min, 5000 × *g* at 4 °C) and AmiA and GlcA enzymes were then purified using Ni-NTA superflow affinity chromatography (Qiagen) as described by the manufacturer. The imidazole elution fraction was further purified on a Superdex 75 size-exclusion chromatography column using 20 mM pH 7.5 sodium phosphate buffer containing 150 mM NaCl.

Preparation of peptidoglycan (PG). PG was isolated using the method developed by de Jonge et al.[21] with slight modification. Briefly, cells were grown until reaching an $OD_{578\,nm}$ of 0.8 and harvested by centrifugation at 3000 × *g* for 30 min, washed twice with ice-cold 0.9% NaCl, boiled with 5% sodium dodecyl sulfate (SDS) for 30 min, washed and broken using 106 µM glass beads (Sigma) and FastPrep FP120 cell milling apparatus (Bio 101, La Jolla, Calif.). Insoluble polymeric PG was harvested by centrifugation at 30,000 × *g* for 20 min and washed several times with lukewarm water to remove the SDS. Broken CWs were suspended in 100 mM Tris-HCl, pH 7.2, 20 µg/ml $MgCl_2$ and treated with 10 µg/ml DNase and 50 µg/ml RNase for 2 h at 37 °C. The broken cells were again centrifuged, resuspended with 2 M urea, and incubated for 1 h at room temperature. The broken cells were washed repeatedly with water to remove the urea and resuspended with 100 mM Tris/HCl, pH 7.2, and subsequently digested with 100 µg/ml trypsin for 16 h at 37 °C with the addition of 20 mM $CaCl_2$. To remove wall teichoic acid, the PG preparations were incubated on a magnetic stirrer with 48% hydrofluoric acid (HF) for 48 h at 4 °C. PG was harvested by centrifugation at 30,000 × *g* for 30 min and washed several times with water until the complete removal of HF. Washed PG was finally lyophilized and stored.

HPLC analysis of muramidase, amidase, and glucosaminidase digested PG. PG was analyzed basically as described previously[21] with some minor modifications. Purified PG was dissolved in 25 mM pH 6.8 sodium phosphate buffer and digested with the corresponding enzyme or enzyme combination for 16 h or the defined time. The resulting muropeptides or other corresponding products were reduced with sodium borohydride and separated by RP-HPLC using a Poroshell 120 EC-C18 (Agilent Technologies, Waldbronn, Germany) column (2.7-µm particle size, 150 × 4.6 mm, 120-Å pore size) and a linear gradient from 5% to 30% MeOH in 100 mM sodium phosphate buffer pH 2.2 at a flow rate of 0.6 ml/min. Peaks were detected at 205 nm.

Mass spectrometric (MS) analysis and identification of AmiA and GlcA-digested PG fragments. For the analysis of digested PG samples, an Acquity UPLC/Synapt G2 LC/MS system from Waters (Manchester) was used. A sample volume of 7 µl was injected onto a Waters Acquity C18 CSH 2.1 × 100 mm, 1.7-µm column, operated at a flow rate of 176 µl/min and a temperature of 52 °C. A 50 min gradient from 99% A (Water, 0.1% TFA) to 10% B (Methanol, 0.1% TFA) was used to separate the analytes, followed by a 48-min gradient from 10 to 15% B. The mass spectrometer was operated in ESI positive mode with a scan range from 50 to 2000 at a scan rate of 0.5 s/scan. Data were analyzed with Waters MassLynx software.

Scanning (SEM) and transmission electron microscopy (TEM). For SEM cells were fixed in 2.5% glutaraldehyde/4% formaldehyde in PBS for 2 h at room temperature and mounted on poly-L-lysine-coated coverslips. Cells were post-fixed with 1% osmium tetroxide for 45 min on ice. Subsequently, samples were dehydrated in a graded ethanol series followed by critical point drying (Polaron) with CO_2. Finally, the cells were sputter-coated with a 3-nm thick layer of platinum (CCU-010, Safematic) and examined with a field emission scanning electron microscope (Regulus 8230, Hitachi High Technologies) at an accelerating voltage of 5 kV. For TEM, cells were high-pressure frozen (HPF Compact 03, Engineering Office M. Wohlwend GmbH) in capillaries, freeze-substituted (AFS2, Leica Microsystems) with 2% OsO_4 and 0.4% uranyl acetate in acetone as substitution medium and embedded in Epon. Ultrathin sections were stained with uranyl acetate and lead citrate and analyzed with a Tecnai Spirit (Thermo Fisher Scientific) operated at 120 kV.

Flow cytometric cell cluster analysis. Cells were inoculated from an overnight culture to OD 0.1 and grown to mid-exponential phase. Samples were taken from each flask and diluted 1:100 in PBS and size distribution was analyzed using a forward scatter (FSC-A) measurement on a BD FACS Fortessa. Data were analyzed using FlowJo software.

Reporting summary. Further information on experimental design is available in the Nature Research Reporting Summary linked to this paper.

Data availability

The authors declare that the main data supporting the findings of this study are available within the article and its Supplementary Information files. Extra data are available from the corresponding author upon request.

Received: 20 March 2020; Accepted: 15 October 2020;
Published online: 20 November 2020

References

1. Vermassen, A. et al. Cell wall hydrolases in bacteria: insight on the diversity of cell wall amidases, glycosidases and peptidases toward peptidoglycan. *Front. Microbiol.* **10**, 331 (2019).
2. Vollmer, W., Joris, B., Charlier, P. & Foster, S. Bacterial peptidoglycan (murein) hydrolases. *FEMS Microbiol. Rev.* **32**, 259–286 (2008).

3. Albrecht, T., Raue, S., Rosenstein, R., Nieselt, K. & Götz, F. Phylogeny of the staphylococcal major autolysin and its use in genus and species typing. *J. Bacteriol.* **194**, 2630–2636 (2012).
4. Heilmann, C., Hussain, M., Peters, G. & Götz, F. Evidence for autolysin-mediated primary attachment of *Staphylococcus epidermidis* to a polystyrene surface. *Mol. Microbiol.* **24**, 1013–1024 (1997).
5. Oshida, T. et al. A *Staphylococcus aureus* autolysin that has an N-acetylmuramoyl-L-alanine amidase domain and an endo-beta-N-acetylglucosaminidase domain: cloning, sequence analysis, and characterization. *Proc. Natl Acad. Sci. USA* **92**, 285–289 (1995).
6. Sugai, M. et al. Identification of endo-beta-N-acetylglucosaminidase and N-acetylmuramyl-L-alanine amidase as cluster-dispersing enzymes in *Staphylococcus aureus*. *J. Bacteriol.* **177**, 1491–1496 (1995).
7. Sugai, M. et al. Purification of a 51 kDa endo-beta-N-acetylglucosaminidase from *Staphylococcus aureus*. *Fems Microbiol. Lett.* **52**, 267–272 (1989).
8. Hirschhausen, N., Schlesier, T., Peters, G. & Heilmann, C. Characterization of the modular design of the autolysin/adhesin Aaa from *Staphylococcus aureus*. *PLoS ONE* **7**, e40353 (2012).
9. Heilmann, C., Hartleib, J., Hussain, M. S. & Peters, G. The multifunctional *Staphylococcus aureus* autolysin aaa mediates adherence to immobilized fibrinogen and fibronectin. *Infect. Immun.* **73**, 4793–4802 (2005).
10. Bose, J. L., Lehman, M. K., Fey, P. D. & Bayles, K. W. Contribution of the *Staphylococcus aureus* Atl AM and GL murein hydrolase activities in cell division, autolysis, and biofilm formation. *PLoS ONE* **7**, e42244 (2012).
11. Porayath, C. et al. Autolysin mediated adherence of *Staphylococcus aureus* with fibronectin, gelatin and heparin. *Int. J. Biol. Macromol.* **110**, 179–184 (2018).
12. Sugai, M., Akiyama, T., Komatsuzawa, H., Miyake, Y. & Suginaka, H. Characterization of sodium dodecyl sulfate-stable *Staphylococcus aureus* bacteriolytic enzymes by polyacrylamide gel electrophoresis. *J. Bacteriol.* **172**, 6494–6498 (1990).
13. Schlag, M. et al. Role of staphylococcal wall teichoic acid in targeting the major autolysin Atl. *Mol. Microbiol.* **75**, 864–873 (2010).
14. Zoll, S. et al. Ligand-binding properties and conformational dynamics of autolysin repeat domains in staphylococcal cell wall recognition. *J. Bacteriol.* **194**, 3789–3802 (2012).
15. Büttner, F. M., Zoll, S., Nega, M., Götz, F. & Stehle, T. Structure-function analysis of *Staphylococcus aureus* amidase reveals the determinants of peptidoglycan recognition and cleavage. *J. Biol. Chem.* **289**, 11083–11094 (2014).
16. Zoll, S. et al. Structural basis of cell wall cleavage by a staphylococcal autolysin. *PLoS Pathog.* **6**, e1000807 (2010).
17. Marino, M., Banerjee, M., Jonquieres, R., Cossart, P. & Ghosh, P. GW domains of the *Listeria monocytogenes* invasion protein InlB are SH3-like and mediate binding to host ligands. *EMBO J.* **21**, 5623–5634 (2002).
18. Götz, F., Heilmann, C. & Stehle, T. Functional and structural analysis of the major amidase (Atl) in *Staphylococcus. Int. J. Med. Microbiol* **304**, 156–163 (2014).
19. Zhou, X. et al. Bacterial division. Mechanical crack propagation drives millisecond daughter cell separation in *Staphylococcus aureus*. *Science* **348**, 574–578 (2015).
20. Tzagoloff, H. & Novick, R. Geometry of cell division in *Staphylococcus aureus*. *J. Bacteriol.* **129**, 343–350 (1977).
21. de Jonge, B. L., Chang, Y. S., Gage, D. & Tomasz, A. Peptidoglycan composition in heterogeneous Tn551 mutants of a methicillin-resistant *Staphylococcus aureus* strain. *J. Biol. Chem.* **267**, 11255–11259 (1992).
22. Wadstrom, T. Bacteriolytic enzymes from *Staphylococcus aureus*. Properties of the endo-beta-N-acetylglucosaminidase. *Biochem. J.* **120**, 745–752 (1970).
23. Biswas, R. et al. Activity of the major staphylococcal autolysin Atl. *Fems Microbiol Lett.* **259**, 260–268 (2006).
24. Yamada, S. et al. An autolysin ring associated with cell separation of *Staphylococcus aureus*. *J. Bacteriol.* **178**, 1565–1571 (1996).
25. Turner, R. D. et al. Peptidoglycan architecture can specify division planes in *Staphylococcus aureus*. *Nat. Commun.* **1**, 26 (2010).
26. Bailey, R. G. et al. The interplay between cell wall mechanical properties and the cell cycle in *Staphylococcus aureus*. *Biophys. J.* **107**, 2538–2545 (2014).
27. Chan, Y. G., Frankel, M. B., Missiakas, D. & Schneewind, O. SagB glucosaminidase is a determinant of *Staphylococcus aureus* glycan chain length, antibiotic susceptibility, and protein secretion. *J. Bacteriol.* **198**, 1123–1136 (2016).
28. Wheeler, R. et al. Bacterial cell enlargement requires control of cell wall stiffness mediated by peptidoglycan hydrolases. *mBio* **6**, e00660 (2015).
29. Pasztor, L. et al. Staphylococcal major autolysin (Atl) is involved in excretion of cytoplasmic proteins. *J. Biol. Chem.* **285**, 36794–36803 (2010).
30. Lützner, N., Patzold, B., Zoll, S., Stehle, T. & Kalbacher, H. Development of a novel fluorescent substrate for autolysin E, a bacterial type II amidase. *Biochem. Biophys. Res. Commun.* **380**, 554–558 (2009).
31. Frankel, M. B., Hendrickx, A. P., Missiakas, D. M. & Schneewind, O. LytN, a murein hydrolase in the cross-wall compartment of *Staphylococcus aureus*, is involved in proper bacterial growth and envelope assembly. *J. Biol. Chem.* **286**, 32593–32605 (2011).
32. Boneca, I. G., Huang, Z. H., Gage, D. A. & Tomasz, A. Characterization of *Staphylococcus aureus* cell wall glycan strands, evidence for a new beta-N-acetylglucosaminidase activity. *J. Biol. Chem.* **275**, 9910–9918 (2000).
33. Tipper, D. J. Mechanism of autolysis of isolated cell walls of Staphylococcus aureus. *J. Bacteriol.* **97**, 837–847 (1969).
34. Mihelic, M. et al. The mechanism behind the selection of two different cleavage sites in NAG-NAM polymers. *IUCrJ* **4**, 185–198 (2017).
35. Terrak, M. et al. The catalytic, glycosyl transferase and acyl transferase modules of the cell wall peptidoglycan-polymerizing penicillin-binding protein 1b of *Escherichia coli*. *Mol. Microbiol.* **34**, 350–364 (1999).
36. Bera, A., Biswas, R., Herbert, S. & Götz, F. The presence of peptidoglycan O-acetyltransferase in various staphylococcal species correlates with lysozyme resistance and pathogenicity. *Infect. Immun.* **74**, 4598–4604 (2006).
37. Shimada, T. et al. *Staphylococcus aureus* evades lysozyme-based peptidoglycan digestion that links phagocytosis, inflammasome activation, and IL-1beta secretion. *Cell Host Microbe* **7**, 38–49 (2010).
38. Bera, A., Herbert, S., Jakob, A., Vollmer, W. & Götz, F. Why are pathogenic staphylococci so lysozyme resistant? The peptidoglycan O-acetyltransferase OatA is the major determinant for lysozyme resistance of *Staphylococcus aureus*. *Mol. Microbiol.* **55**, 778–787 (2005).
39. Iordanescu, S. & Surdeanu, M. Two restriction and modification systems in *Staphylococcus aureus* NCTC8325. *J. Gen. Microbiol* **96**, 277–281 (1976).
40. Herbert, S. et al. Repair of global regulators in *Staphylococcus aureus* 8325 and comparative analysis with other clinical isolates. *Infect. Immun.* **78**, 2877–2889 (2010).
41. Geiger, T. et al. The stringent response of *Staphylococcus aureus* and its impact on survival after phagocytosis through the induction of intracellular PSMs expression. *PLoS Pathogens* **8**, e1003016 (2012).
42. Gibson, D. G. et al. Enzymatic assembly of DNA molecules up to several hundred kilobases. *Nat. Methods* **6**, 343–345 (2009).
43. Monk, I. R., Shah, I. M., Xu, M., Tan, M. W. & Foster, T. J. Transforming the untransformable: application of direct transformation to manipulate genetically *Staphylococcus aureus* and *Staphylococcus epidermidis*. *mBio* **3**, https://doi.org/10.1128/mBio.00277-11 (2012).
44. Löfblom, J., Kronqvist, N., Uhlen, M., Stahl, S. & Wernerus, H. Optimization of electroporation-mediated transformation: *Staphylococcus carnosus* as model organism. *J. Appl. Microbiol.* **102**, 736–747 (2007).
45. Bae, T. & Schneewind, O. Allelic replacement in *Staphylococcus aureus* with inducible counter-selection. *Plasmid* **55**, 58–63 (2006).
46. Hirschhausen, N. et al. A novel staphylococcal internalization mechanism involves the major autolysin Atl and heat shock cognate protein Hsc70 as host cell receptor. *Cell Microbiol.* **12**, 1746–1764 (2010).

Acknowledgements

This work was supported by the Deutsche Forschungsgemeinschaft (DFG) TRR 261, as well as by DFG, Germany´s Excellence Strategy—EXC 2124—390838134 "Controlling Microbes to Fight Infections". We acknowledge support by the Open Access Publishing Fund of the University of Tübingen.

Author contributions

F.G. and M.N. designed the study. M.N., P.M.T., and F.G. designed the experiments. M. N. performed most of the experiments. M.S. performed MS analysis. K.H. performed EM analysis. P.M.T. contributed to manuscript writing and proofreading. F.G. and M.N. wrote the paper.

Funding

Open Access funding enabled and organized by Projekt DEAL.

Competing interests

The authors declare no competing interests.

Additional information

Supplementary information is available for this paper at https://doi.org/10.1038/s42003-020-01405-2.

Correspondence and requests for materials should be addressed to F.Göt.

Reprints and permission information is available at http://www.nature.com/reprints

Publisher's note Springer Nature remains neutral with regard to jurisdictional claims in published maps and institutional affiliations.

1268 DOI 10.1002/pmic.201400343 *Proteomics* 2015, *15*, 1268–1279

RESEARCH ARTICLE

Secretome analysis revealed adaptive and non-adaptive responses of the *Staphylococcus carnosus femB* mutant

Mulugeta Nega[1], Linda Dube[1]*, Melanie Kull[1], Anne-Kathrin Ziebandt[1], Patrick Ebner[1], Dirk Albrecht[2], Bernhard Krismer[3], Ralf Rosenstein[1], Michael Hecker[2] and Friedrich Götz[1]*

[1] Microbial Genetics, Interfaculty Institute of Microbiology and Infection Medicine, University of Tübingen, Tübingen, Germany
[2] Institute for Microbiology, University of Greifswald, Greifswald, Germany
[3] Cellular and Molecular Microbiology Division, Medical Microbiology and Hygiene Institute, University of Tübingen, Tübingen, Germany

FemABX peptidyl transferases are involved in non-ribosomal pentaglycine interpeptide bridge biosynthesis. Here, we characterized the phenotype of a *Staphylococcus carnosus femB* deletion mutant, which was affected in growth and showed pleiotropic effects such as enhanced methicillin sensitivity, lysostaphin resistance, cell clustering, and decreased peptidoglycan cross-linking. However, comparative secretome analysis revealed a most striking difference in the massive secretion or release of proteins into the culture supernatant in the *femB* mutant than the wild type. The secreted proteins can be categorized into typical cytosolic proteins and various murein hydrolases. As the transcription of the murein hydrolase genes was up-regulated in the mutant, they most likely represent an adaption response to the life threatening mutation. Even though the transcription of the cytosolic protein genes was unaltered, their high abundance in the supernatant of the mutant is most likely due to membrane leakage triggered by the weakened murein sacculus and enhanced autolysins.

Received: July 22, 2014
Revised: October 6, 2014
Accepted: November 25, 2014

Keywords:
Cytosolic proteins / FemB / Microbiology / Peptidoglycan / Secretome / *Staphylococcus carnosus*

Additional supporting information may be found in the online version of this article at the publisher's web-site

1 Introduction

In many organisms where the classical secretion systems are not involved in the excretion of cytosolic proteins, the "non-classical protein secretion" takes place. Proteins undergoing this secretion show no simple sequence motifs except that they are more disordered in structure than those remaining in the cytoplasm [1]. In *Staphylococcus aureus*, over 20 typical cytosolic proteins are excreted, starting already in the exponential phase and it appears to be more pronounced in clinical isolates than in the non-pathogenic staphylococcal species [2, 3]. Various *S. aureus* mutants have been analyzed with respect to the release of cytoplasmic proteins. For example, in the *atl* (major autolysin) mutant, cytosolic proteins were hardly found in the supernatant, but were entrapped within the huge cell clusters of this mutant [2]. In the wall teichoic acid deficient *tagO* mutant, with its increased autolysis activity, excretion of cytosolic proteins was increased compared to the wt, confirming the importance of autolysis in excreting cytosolic proteins.

Correspondence: Professor. Friedrich Götz, Microbial Genetics, University Tübingen, Auf der Morgenstelle 28, 72076 Tübingen, Germany
E-mail: friedrich.goetz@uni-tuebingen.de
Fax: +49-7071-295937

Abbreviations: **BM**, basic medium; **CHAP**, cysteine- and histidine-dependent amidohydrolase/peptidase; **CY**, cytosolic fraction; **LTA**, lipoteichoic acid; **LtaS**, lipoteichoic acid synthase; **MW**, molecular weight; **PGN**, peptidoglycan; **PFL**, pyruvate formate lyase; **wt**, wild type

*These authors contributed equally to this work.

Proteomics 2015, *15*, 1268–1279

Here, we investigated a *femB* deletion mutant of *Staphylococcus carnosus*, which has a shortened glycine interpeptide bridge in the murein structure. The factors essential for the expression of methicillin resistance (fem), encode the FemABX peptidyl transferases involved in non-ribosomal pentaglycine interpeptide bridge biosynthesis [4,5]. While femX is essential, *Tn* mutants, but no deletion mutants, could be generated in *S. aureus*. Both mutants showed a reduced peptidoglycan (PGN) cross linking and glycine content, decreased lysostaphin susceptibility, reduced whole-cell autolysis, increased sensitivity to β-lactam antibiotics [6], an aberrant placement of cross walls, and stunted cell separation [7] showing key functions of the pentaglycine interpeptide bridge.

We could construct a *femB* deletion mutant in *S. carnosus* in which the *femAB* operon is orthologous to that of *S. aureus* [8]. The most striking phenotype of the femB mutant was the massive release of proteins into the culture supernatant. The excreted proteins could be classified into two groups: those secreted via the canonical Sec pathway, and those representing typical cytosolic proteins lacking a signal sequence. The results suggest that the release of cytosolic proteins is due to the altered PGN structure, which makes the cell envelope leaky enough for the release of cytosolic proteins.

2 Materials and methods

2.1 Bacterial strains, growth conditions, and oligonucleotide primers

S. carnosus strains TM300 [9, 10], its deletion mutant Δ*femB::ermB*, the complementary mutant Δ*femB::ermB* (pPSHG5femB), *Escherichia coli* strain DH5α [11], and *Micrococcus luteus* DSM 20030^T [12, 13] were cultivated at 37°C and shaken in basic medium (BM; 1% soy peptone, 0.5% yeast extract, 0.5% NaCl, 0.1% glucose, and 0.1% K_2HPO_4; pH 7.4). When appropriate, BM was supplemented with 10 μg/mL chloramphenicol, 2.5 μg/mL erythromycin, or 100 μg/mL ampicillin. Oligonucleotide primers used for cloning and Northern blot analysis are listed in Supporting Information Table 1.

2.2 Preparation of extracellular proteins for preparative 2DE

Cells were harvested at a comparable time point of the growth phase (Fig. 1 and Supporting Information Table 2) by centrifugation at 9000 × *g* for 15 min at 4°C. Extracellular proteins in the culture supernatant were precipitated with 10% trichloroacetic acid overnight at 4°C, subsequently pelleted by centrifugation at 9000 × *g* for 40 min at 4°C, and washed eight times with ethanol. The protein pellet was dried and resuspended in an appropriate volume of rehydration buffer consisting of 8 M urea, 2 M thiourea, 4% w/v CHAPS, 1% DTT,

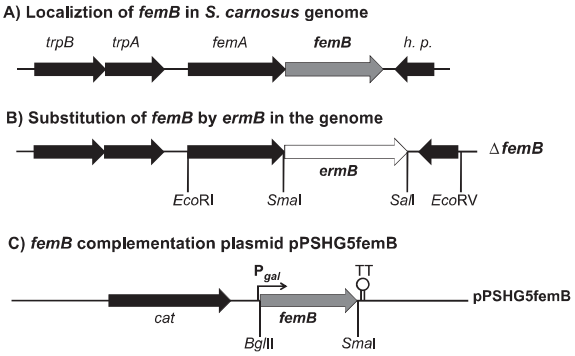

Figure 1. Construction of the *femB* deletion mutant and complementation. (A) Location of the *fem* operon in the chromosome of *S. carnosus* and (B) the *femB* deletion mutant (Δ*femB::ermB*). (C) Complementation plasmid pPSHG5femB. *cat*: chloramphenicol resistance gene; *ermB*: erythromycin resistance gene; *trpA, trpB*: tryptophan synthetase alpha and beta chain; *h.p.*: hypothetical protein.

and 0.7% pharmalyte, pH 3–10 and centrifuged at 16 000 × *g* for 15 min at room temperature. The protein concentration was determined using Bradford assay according to the manufacturer's instructions (Bio-Rad Laboratories, München, Germany). For 2D PAGE, 500 μg of secreted proteins was applied.

2.3 Preparation of cytosolic proteins for preparative 2DE

Cells of 40 mL cultures were harvested at two time points (Fig. 1 and Supporting Information Table 2) and centrifuged for 15 min at 9000 × *g* at 4°C. The pellets were then resuspended in 1 mL ice-cold TE buffer (10 mM Tris and 1 mM EDTA; pH 7.5) and disrupted by homogenization using glass beads and TissueLyser (Qiagen) twice for 30 s at 30 Hz. To remove cell fragments and insoluble proteins, the cleared lysate was centrifuged for 20 min at 20 000 × *g* at 4°C. The protein concentration was determined using Bradford assay. For 2D PAGE, 500 μg was used and mixed with rehydration buffer to a final concentration containing 8 M urea, 2 M thiourea, 4% w/v CHAPS, 1% DTT, and 0.7% pharmalyte (pH 3–10).

2.4 2D-PAGE and computational analysis

Protein patterns of the *S. carnosus* wt and the *femB* mutant were compared visually and quantitatively with Delta2D software (DECODON) after 2D PAGE was performed as described in earlier studies [14, 15]. For each condition, three independent experiments were performed. Only statistically reproducible differences were included in the results. For identified proteins, several analyses were performed. The theoretical localization of proteins was predicted with PSORT (http://www.psort.org/psortb/), the prediction of N-terminal

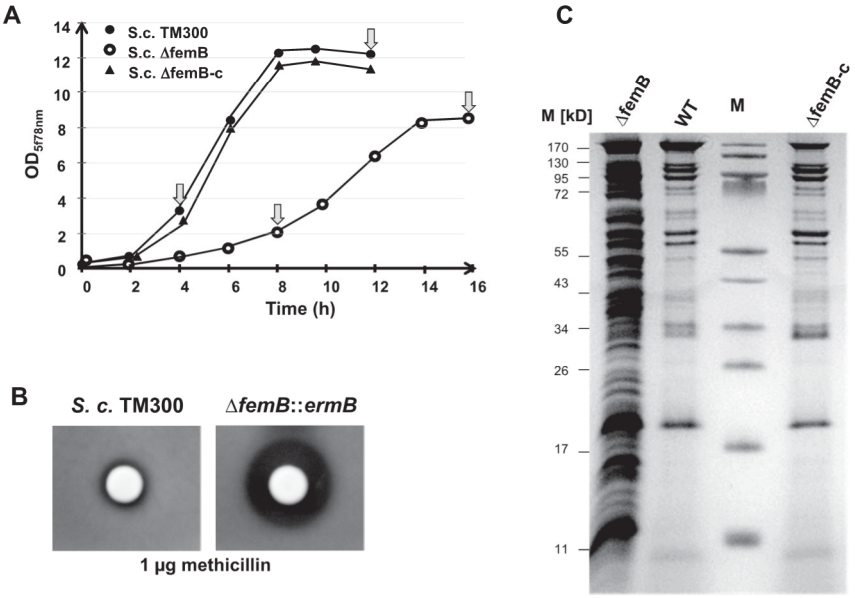

Figure 2. Comparative phenotypic features of *S. carnosus*, its *femB* mutant, and the complementary mutant. (A) Growth was severely affected in the *femB* mutant; arrow indicates sampling time for analysis. (B) Agar diffusion assay showing *femB* mutant methicillin susceptibility. (C) SDS-PAGE of culture supernatant proteins; cells were cultivated for 13 h in the presence of 0.25% galactose. wt: wild type; S.c. TM300; ΔfemB: femB deletion mutant; ΔfemB-c: mutant complemented with *pPSHG5femB;* M: marker proteins.

signal sequences was performed with SignalP version 3.0 (http://www.cbs.dtu.dk/services/SignalP/), and the non-classical secretion of proteins was predicted with SecretomP version 2.0 (http://www.cbs.dtu.dk/services/SecretomeP/). The theoretical molecular weight (MW) and p*I* for mature proteins without any signal sequence were calculated using the p*I*/MW tool (http://www.expasy.org/tools/pi_tool.html).

2.5 Supporting information

Construction of the *S. carnosus femB* deletion mutant, construction of *femB* expression plasmid, antimicrobial susceptibility testing, purification and analysis of PGN, analysis of proteins in the supernatant, analysis of membrane and cytosolic fractions by SDS-PAGE, Western blot analysis, fluorescence microscopy, RNA isolation and northern blot analysis, and protein identification by MS are described as Supporting Information.

3 Results

3.1 Construction and characterization of the *femB* deletion mutant in *S. carnosus* TM300

FemB (Sca_1020) of *S. carnosus* TM300 revealed 82% identity and 92% similarity to FemB (SAOUHSC_01374) of *S. aureus* NCTC 8325 and the *femAB* genes are organized in an operon downstream of the tryptophan synthase genes (*trpBA*) (Fig. 1A). In *S. carnosus* TM300, the deletion mutant was created by replacing *femB* with an erythromycin cassette (*ermB*) [16]. The *femB* mutant was complemented with the plasmid pPSHG5femB, which was constructed by cloning *femB* under the control of a galactose-inducible promoter (Fig. 1B). Growth deficiency of the *femB* mutant could be complemented by pPSHG5femB (Fig. 1C and Fig. 2A). It also showed an increased susceptibility to methicillin (Fig. 2B) but high resistance to lysostaphin, with a more than 3000-fold increase in the MIC values from 0.01 to 32 µg/mL. This is in agreement with lysostaphin's cleavage preference for the pentaglycine interpeptide bridge [17].

Phase and fluorescence microscopic analyses showed that cells of the *femB* mutant are clustered (Fig. 3) suggesting a defect in daughter cell separation. Vancomycin staining (Van-FL) revealed a massive accumulation of fluorescence intensity in the *femB* mutant in the septum region suggesting that the degree of cross-linking of the PGN network was considerably decreased. As with vancomycin, fluorescence intensity with FM 4–64, a cell impermeant membrane stain, was increased in the septum region of the *femB* mutant, indicating increased penetration of the dye through the cell wall to the membrane site (Fig. 3). Ultimately, DNA-staining with DAPI revealed enlarged DNA areas (nucleoid) in the mutant, which could have resulted from decreased chromosomal condensation (Fig. 3). In all microscopic images, the *femB* mutant cells were enlarged, the average cell diameter was 132% increased compared to the wt; while the complementary mutant ΔfemB (PSHG5femB) closely resembles the wt (Fig. 3). Comparative HPLC analysis of PGN isolated from the wt, Δ*femB*, and the complementary mutant showed that the mutant contained roughly 50% more of monomeric fragments than the wt, and less tri- and tetramer fragments (Fig. 4), which indicates a decreased level of PGN crosslinking.

Proteomics 2015, *15*, 1268–1279

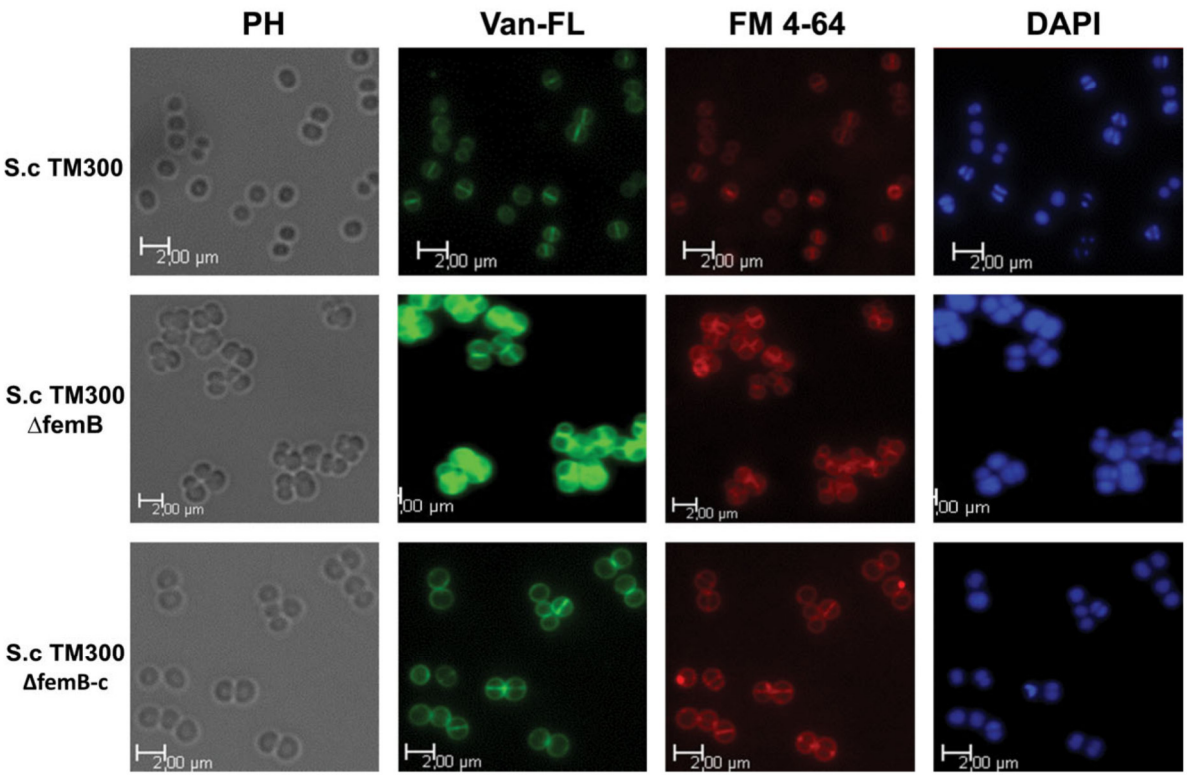

Figure 3. Microscopic analysis of *S. carnosus* and its *femB* mutant. *S.c.* TM300Δ*femB* forms large cell clusters. Cell wall staining with vancomycin shows intensive fluorescence particularly in the septum and membrane staining (FM 4–64) revealed intensified florescence. The DAPI stained nucleoid shows significant enlargement, whereas the wt (upper row) and the complementary mutant (lower row) looked roughly similar.

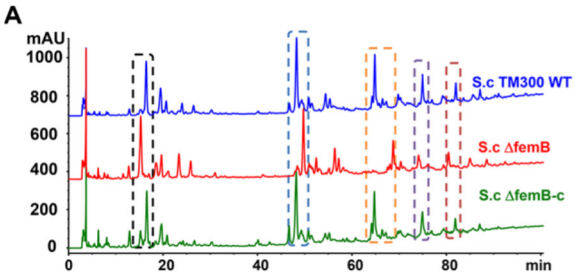

B

	1-mer (%)	2-mer (%)	3-mer (%)	4-mer (%)	5-mer (%)
S. c. TM300	22	33	22	16	8
S. c. Δ*femB*	33	31	15	12	10
S. c. Δ*femB* comp.	21	36	22	15	6

Figure 4. Peptidoglycan composition is altered in the *S. carnosus*Δ*femB* strain. (A) HPLC analysis of mutanolysin-digested PGN of the wild-type strain of *S. carnosus* TM300, the mutant *S.c*Δ*femB*, and the complemented mutant. (B) Eluted UV-absorbing peaks were integrated, and the corresponding muropeptides highlighted by the dotted area in (A) were quantified as a percentage of the total area of identified peaks. Dotted areas represent monomers to pentamers (left to right).

3.2 The *femB* mutant is characterized by the high abundance of secreted proteins

Another eye-catching phenotype of the *femB* mutant was the drastic increase of secreted proteins (Fig. 2C). Quantitative analysis of these proteins in the exponential and stationary growth phases revealed that the protein content in the *femB* mutant was always roughly 5 to 6 times higher than in the wt, while the cytosolic protein content remained more or less the same (Table 1 and Supporting Information Fig. 1). Comparative secretome analysis was performed to determine protein abundance in the supernatant of the *femB* mutant. Due to the growth rate difference (Fig. 2A), protein samples for 2D-PAGE were taken at the exponential growth phase after 4 h (wt) and 8 h (*femB* mutant), as well as after 12 h (wt) and 16 h (*femB* mutant) for the stationary growth phase (Fig. 2A and Supporting Information Fig. 2). Protein spots of each of three 2D gels of the wt and the *femB* mutant were analyzed by mass spectroscopy and 82 different proteins could be identified and quantified (Supporting Information Table 2).

Though the overall protein pattern was similar, the *femB* mutant showed a much higher protein quantity in most of the spots. Protein amounts were therefore compared using

Table 1. Protein content in supernatant and cytosol of wt and *femB* mutant

Strains	Harvest- time	OD_{578} [a)]	Protein amount (μg/mL cell culture)	
			Supernatant [a)]	Cytosol [a)]
Exponential growth phase				
S. c. WT	4 h	4.5	0.87	22.60
S. c. Δ*femB*	8 h	3.3	5.74	22.28
Stationary growth phase				
S. c. WT	12 h	12.1	2.20	29.40
S. c. Δ*femB*	16 h	9.23	10.31	25.48

a) Indicates the mean values of the three measurements.

the Delta2D software (DECODON) for better visualization (Fig. 5). Proteins in the wt were designated green and in the *femB* mutant red. Equal amount of proteins would then result in yellow spots. Thirty six selected protein spots showing the most significant differences in intensity between the wt and *femB* mutant were identified and characterized (Tables 2 and 3).

3.3 Few proteins show increased abundance in the wt secretome compared to the *femB* mutant

Only seven proteins were less abundant in the mutant secretome (Fig. 5). Four of them belonged to signal peptide-dependent transported proteins: SceB, Sca0421, Sca2221, and Sca2250 (Table 2). SceB showed 60% identity with Staphylococcal secretory antigen A (SsaA) of *Staphylococcus epidermidis* and *S. aureus*. SsaA is described in *S. epidermidis* as a highly antigenic protein [18]. The proteins Sca2250 and Sca0421 revealed no significant similarity to known proteins. Interestingly, the polyglycerol phosphate synthase LtaS (lipoteichoic acid synthase), a lipoteichoic acid biosynthesis enzyme, was also less abundant in the mutant. LtaS and its homologs in other Gram-positive bacteria were predicted to be polytopic membrane proteins with a large enzymatic domain located on the extracellular side of the bacterial membrane. According to this topological prediction, a cleaved fragment of the LtaS protein containing the complete enzymatic sul-

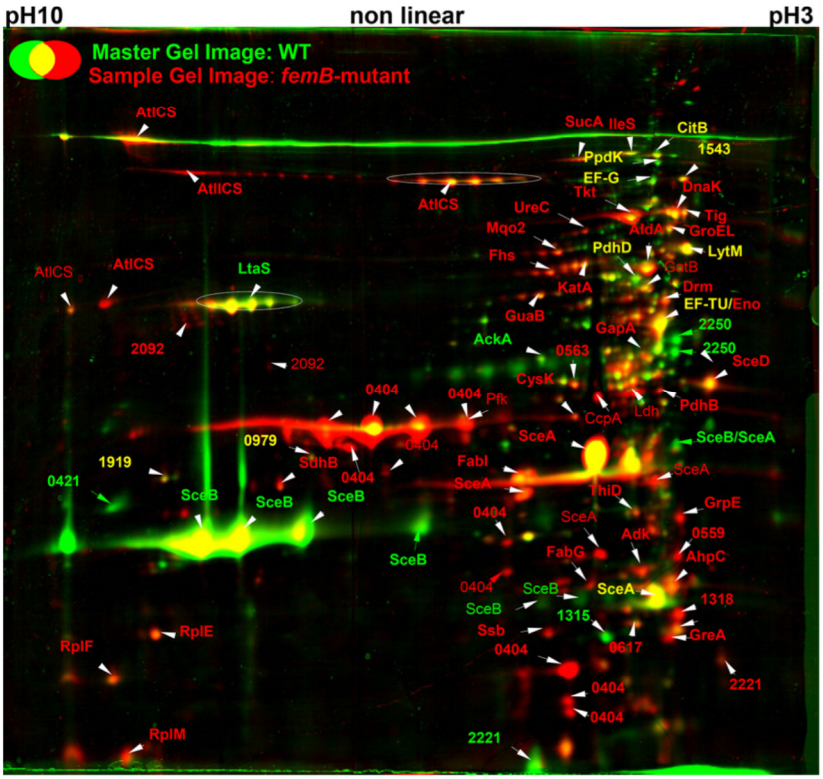

Figure 5. Differential 2D-PAGE of secretomes of *S. carnosus* wt and its *femB* mutant after 12 and 16 h incubation, respectively. Proteins (500 μg) of the culture supernatant were separated by 2D-PAGE and stained with colloidal coomassie silver blue and compared using the Delta2D image analysis software. The secretome of the WT (green) and *femB* mutant (red) were overlaid using Delta2D software. Dominant spots retain their colors and equally distributed ones showed yellow color. Protein spots were identified by MALDI-TOF MS.

Table 2. Proteins less abundant in the secretome of the *femB* mutant

Protein[a),b)]	Function	*S. carnosus* TM300 gene ID	*S. aureus* N315 homolog gene ID	*S. aureus* COL homolog gene ID	Ratio *femB* mutant/wild type[c)]	Signal sequence[d)]	MW (kDa)[f)]	p*I*[f)]
Extracellular proteins								
SceB[1]	SceB precursor	Sca_1790	SA2093 *ssaA*	SACOL2291	−8.0	+	25.3	7.9
SceB[2]	SceB precursor	Sca_1790	SA2093 *ssaA*	SACOL2291	−5.3	+	25.3	7.9
SceB[3]	SceB precursor	Sca_1790	SA2093 *ssaA*	SACOL2291	−2.8	+	25.3	7.9
Sca0421	Hypothetical protein	Sca_0421	–	–	−6.2	+	34.5	9.7
Sca2250	Hypothetical protein	Sca_2250	–	–	−9.2	+	37.2	4.5
Membrane localization								
LtaS[1]	Polyglycerol phosphate synthase LtaS	Sca_0366	SA0674	SACOL0778	−4.2	–	74.3	9.0
LtaS[2]	Polyglycerol phosphate synthase LtaS	Sca_0366	SA0674	SACOL0778	−3.5	–	74.3	9.0
LtaS[3]	Polyglycerol phosphate synthase LtaS	Sca_0366	SA0674	SACOL0778	−2.6	–	74.3	9.0
Cytosolic proteins								
AckA	Acetate kinase homolog	Sca_1316	SA1533	–	−5.8	–	43.6	5.5
Sca1315	Hypothetical protein	Sca_1315	SA1532	SACOL1759	−2.2	–	18.8	5.2

a) Subcellular localization was predicted using PSORTb.
b) Several identified spots of one protein were numbered.
c) Volume ratios in the range of 1 to ∞ indicate an increase of the volume of the respective protein spot and volume ratios in the range −1 to −∞ indicate a decrease of the volume of the respective protein spot. Only volume ratios ≥ 2 and ≤ −2 were defined as significant changes between the different strains.
d) Typical signal sequence was predicted using SignalP.
e) Non-classical secretion was predicted using SecretomeP.
f) Theoretical molecular weight (MW) and p*I* were calculated for mature proteins without signal sequence using MW/p*I* tools.
Superscripts 1–3 refer to differently processed protein spots.

fatase domain was detected in the supernatant and cell wall-associated fractions in *S. aureus* [3,19]. Recently, the structure of the extracellular LtaS protein was determined and found to contain the complete enzymatic sulfatase [20]. Two typical cytosolic proteins, the acetate kinase homolog (AckA) and a hypothetical protein (Sca1315), were also found to be less abundant in the mutant secretome than in the wt (Table 2).

3.4 Proteins showing increased abundance in the secretome of the *femB* mutant belong to three categories

3.4.1 Murein hydrolases

From the 30 proteins analyzed that are more abundant in the *femB* mutant (Table 3), four proteins belonged to signal peptide-dependent transported proteins: AtlCS, the major autolysin; SceA, which resembled SceD and IsaA of *S. aureus*; Sca0404, a LysM family protein; and Sca2221, a hypothetical protein. All of these enzymes are involved in murein turnover and daughter cell separation, and their increased production in the *femB* mutant is most likely a compensatory response to partially resolve the cell-wall interlinked cell clusters. AtlCS, the major autolysin, organized similarly to its homologs in *S. aureus* (AtlA) and *S. epidermidis* (AtlE) [21–23], is produced as a bifunctional precursor protein and functions primarily to hydrolyze the murein in the septum of the daughter cells catalyzing cell separation. The occurrence of multiple protein spots (Fig. 5 and Table 3) is most likely due to their processing in defined substructures of the precursor protein [22]. SceA belongs to the early and highly expressed exoproteins in *S. carnosus* [24], and its similarity to SceD (32%) and immunodominant antigen IsaA (37%) of *S. aureus* and *S. epidermidis* suggests that it is a cell wall hydrolase. IsaA and SceD are two putative lytic transglycosylases of *S. aureus* with autolytic activity. The inactivation of *sceD* resulted in impaired cell separation, as indicated by cell clumping [25]. Sca0404 belongs to the LysM family of proteins and is similar in size to autolysins Aae and Aaa [26,27] that contain repetitive sequences in their N-terminal portion that represent the PGN-binding domain (LysM) and a C-terminally located cysteine- and histidine-dependent amidohydrolase/peptidase (CHAP) domain with bacteriolytic activity in many proteins [28]. Lastly, Sca2221 is a small (17 kDa) protein, which shows no conspicuous similarity.

3.4.2 Cytosolic proteins

The vast majority of increased protein spots in the *femB* mutant were typical cytosolic proteins (Table 3). We identified 20 highly salient proteins, some of which represent typical enzymes of central metabolic pathways, such as FabG, FabI, GuaB, PdhB, OdhA, ThiD, Tkt, TpiA, UreC, Sca0081 (putative intracellular protease/amidase), Sca0563 (NADH-

Table 3. Proteins more abundant in the secretome of the *S. carnosus femB* mutant

Protein[a),b)]	Function	*S. carnosus* TM300 gene ID	*S. aureus* N315 homolog gene ID	*S. aureus* COL homolog gene ID	Ratio *femB* mutant/wild type[c)]	Signal sequence[d)]	Non-classical secretion[e)]	MW (kDa)[f)]	p[f)]
Extracellular proteins									
AtlCS[2]	Major autolysin precursor	Sca_0659	SA0905 *atlA*	SACOL1062	9.8	+	–	133.1	9.2
AtlCS[3]	Major autolysin precursor	Sca_0659	SA0905 *atlA*	SACOL1062	8.8	+	–	133.1	9.2
AtlCS[4]	Major autolysin precursor	Sca_0659	SA0905 *atlA*	SACOL1062	8.8	+	–	133.1	9.2
AtlCS[5]	Major autolysin precursor	Sca_0659	SA0905 *atlA*	SACOL1062	8.6	+	–	133.1	9.2
AtlCS[6]	Major autolysin precursor	Sca_0659	SA0905 *atlA*	SACOL1062	6.8	+	–	133.1	9.2
AtlCS[7]	Major autolysin precursor	Sca_0659	SA0905 *atlA*	SACOL1062	6	+	–	133.1	9.2
AtlCS[10]	Major autolysin precursor	Sca_0659	SA0905 *atlA*	SACOL1062	2.2	+	–	133.1	9.2
AtlCS[11]	Major autolysin precursor	Sca_0659	SA0905 *atlA*	SACOL1062	2.1	+	–	133.1	9.2
SceA	SceA precursor	Sca_1598	SA1898 *sceD* SA2356 *isaA*	SACOL2088 SACOL22584	3.6	+	–	22.2	5.2
SceA[1]	SceA precursor	Sca_1598	SA1898 *sceD* SA2356 *isaA*	SACOL2088 SACOL22584	3.3	+	–	22.2	5.2
SceA[2]	SceA precursor	Sca_1598	SA1898 *sceD* SA2356 *isaA*	SACOL2088 SACOL22584	3.4	+	–	22.2	5.2
Sca0404	LysM family protein	Sca_0404	–	–	6.8	+	–	32.4	6.1
Sca0404[1]	LysM family protein	Sca_0404	–	–	17.8	+	–	32.4	6.1
Sca0404[2]	LysM family protein	Sca_0404	–	–	12.3	+	–	32.4	6.1
Sca0404[3]	LysM family protein	Sca_0404	–	–	4.1	+	–	32.4	6.1
Sca0404[4]	LysM family protein	Sca_0404	–	–	6.9	+	–	32.4	6.1
Sca0404[5]	LysM family protein	Sca_0404	–	–	6.1	+	–	32.4	6.1
Sca0404[6]	LysM family protein	Sca_0404	–	–	4.1	+	–	32.4	6.1
Sca0404[7]	LysM family protein	Sca_0404	–	–	4.9	+	–	32.4	6.1
Sca0404[8]	LysM family protein	Sca_0404	–	–	6.5	+	–	32.4	6.1
Sca0404[9]	LysM family protein	Sca_0404	–	–	4.5	+	–	32.4	6.1
Sca0404[10]	LysM family protein	Sca_0404	–	–	3.3	+	–	32.4	6.1
Sca2221	Hypothetical protein	Sca_2221	–	–	2.8	+	–	17.1	5.1
Cell wall anchored proteins									
Sca2092	Hypothetical protein	Sca_2092	–	–	2.7	+	–	48.1	7.9
Sca2092	Hypothetical protein	Sca_2092	–	–	13.66	+	–	48.1	7.9
Membrane proteins									
Fhs	Formate-tetrahydrofolate ligase homolog	Sca_1337	SA1553 *fhs*	SACOL1782	3.6	–	–	59.9	5.4
Fhs[1]	Formate-tetrahydrofolate ligase homolog	Sca_1337	SA1553 *fhs*	SACOL1782	5	–	–	59.9	5.4
GlpD	Aerobic glycerol-3-phosphate dehydrogenase homolog	Sca_0950	SA1142 *glpD*	SACOL1321	4.2	–	+	62.7	5.8
Lqo2	Putative lactate:quinone oxidoreductase	Sca_2266	SA2400 *mqo2*	SACOL2623	3.0	–	–	55.5	5.4
Lqo2[1]	Putative lactate:quinone oxidoreductase	Sca_2266	SA2400 *mqo2*	SACOL2623	4.0	–	–	55.5	5.4
SdhB	Succinate dehydrogenase iron-sulfur protein subunit homolog	Sca_0767	SA0996 *sdhB*	SACOL1160	6.3	–	–	30.8	6.5
Cytosolic proteins									
FabG	3-oxoacyl-(acyl-carrier protein) reductase	Sca_0854	SA1074 *fabG*	SACOL1245	3.1	–	–	26.1	5.2
FabI	Putative trans-2-enoyl-ACP reductase	Sca_0612	SA0869 *fabI*	SACOL1016	7.0		–	28.0	5.5
GapA	Glyceraldehyde-3-phosphate dehydrogenase	Sca_0424	SA0727 *gap*	SACOL1016	3.8	–	+	36.3	4.7

Table 3. Continued

Protein[a),b)]	Function	S. *carnosus* TM300 gene ID	S. *aureus* N315 homolog gene ID	S. *aureus* COL homolog gene ID	Ratio *femB* mutant/wild type[c)]	Signal sequence[d)]	Non-classical secretion[e)]	MW (kDa)[f)]	p*I*[f)]
GrpE	Putative GrpE protein (HSP-70 cofactor)	Sca_1203	Sa1410 *grpE*	SACOL1638	2.3	–	+	23.0	4.3
GuaB	Putative inositol-monophosphate dehydrogenase	Sca_0049	SA0375 *guaB*	SACOL0460	2.2	–	–	52.8	5.5
KatA	Catalase	Sca_2336	SA1170 *katA*	SACOL0866	2.1	–	–	57.2	5.3
KatA[1]	Catalase	Sca_2336	SA1170 *katA*	SACOL0866	2.9	–	–	57.2	5.3
PdhB	Pyruvate dehydrogenase E1 component beta subunit homolog	Sca_0720	SA0944 *pdhB*	SACOL1103	10	–	–	35.2	4.6
RplC	50S ribosomal protein L3 homolog	Sca_1735	SA2047 *rplC*	SACOL_2239	2.2	–	+	23.7	9.6
RplE	50S ribosomal protein P5 homolog	Sca_1723	SA2035 *rplE*	SACOL2227	5.1	–	–	20.2	9.0
RplF	Probable 50S ribosomal protein L6	Sca_1720	SA2033 *rplF*	SACOL2224	3.5	–	+	19.6	9.5
RplJ	50S ribosomal protein L10 homolog	Sca_0195	SA0497 *rplJ*	SACOL0585	2.4	–	–	17.8	5.1
OdhA	Putatative 2-oxoglutarate dehydrogenase E1 component	Sca_1058	SA1245 *kgd*	SACOL1449	2.7	–	+	105.6	5.3
Tig	Trigger factor homolog	Sca_1281	SA1499 *tig*	SACOL1722	2.2	–	–	49.5	4.3
ThiD	Putative phosphomethylpyrimidine kinase	Sca_1595	SA1896 *thiD*	SACOL2085	2.1	–	–	29.8	5.3
Tkt	Putative transketolase	Sca_0983	SA1177 *tkt*	SACOL1377	3	–	–	72.8	5.0
TpiA	Triosephosphate isomerase homolog	Sca_0426	SA0729 *tpi*	SACOL0840	4.7	–	–	27.5	4.8
UreC	UreC urease alpha subunit homolog	Sca_1782	SA2084 *ureC*	SACOL2282	3.9	–	–	62.4	5.3
Sca0081	Putative intracellular protease/amidase	Sca_0081	–	–	6.8	–	–	25.7	6.7
Sca0559	Putative peptidyl-prolyl cis-trans isomerase	Sca_0559	SA0815	SACOL0957	2.1	–	–	21.8	4.4
Sca0563	NADH-dependent flavin oxidoreductase	Sca_0563	SA0817	SACOL0392	2.2	–	–	42.3	5.3
Sca1991	Pyruvate oxidase	Sca_1991	SA2327	SACOL0893	3.8	–	–	63.6	6.1

a) Subcellular localization was predicted using PSORTb.
b) Several identified spots of one protein were numbered.
c) Volume ratios in the range of 1 to ∞ indicate an increase of the volume of the respective protein spot and volume ratios in the range −1 to −∞ indicate a decrease of the volume of the respective protein spot. Only volume ratios ≥ 2 and ≤ −2 were defined as significant changes between the different strains.
d) Typical signal sequence was predicted using SignalP.
e) Non-classical secretion was predicted using SecretomeP.
f) Theoretical molecular weight (MW) and p*I* were calculated for mature proteins without signal sequence using MW/p*I* tools.
Superscripts refer to differently processed protein spots.

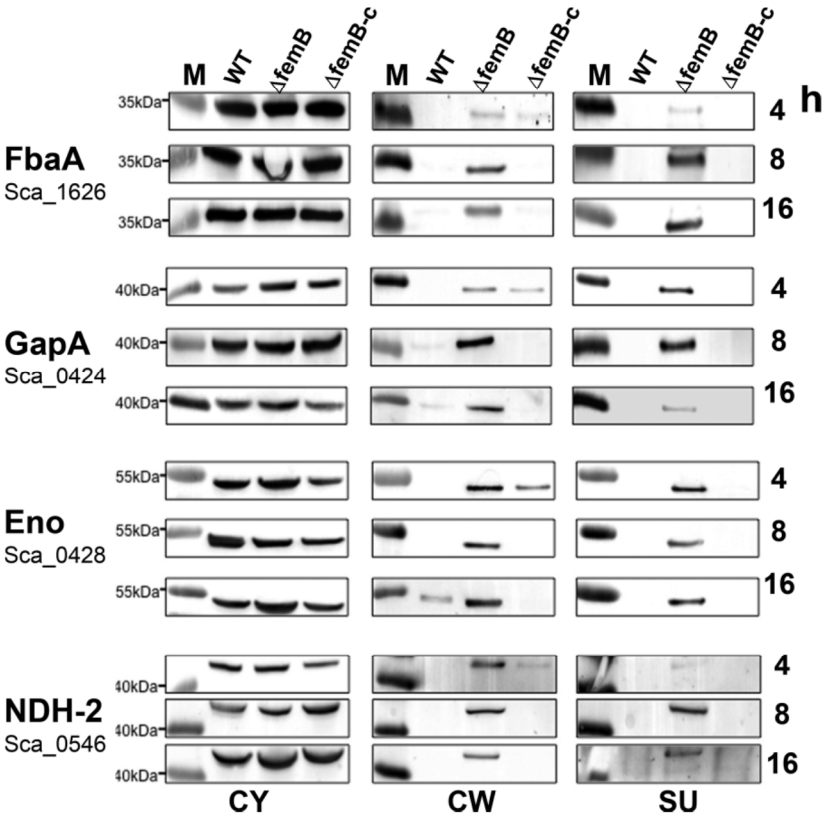

Figure 6. Localization of cytoplasmic marker proteins of *S. carnosus* wt, its *femB* mutant and the complementary mutant (femB-c) in the cytosole, cell wall, and supernatant by Western blot after 4, 8, and 16 h cultivation. The proteins fructose-bisphosphate aldolase (FabA), glyceraldehyde-3-phosphate dehydrogenase (GapA), enolase (Eno), and NADH-dehydrogenase (NDH-2) were each detected using specific antibodies. M: prestained molecular weight marker.

dependent flavin oxidoreductase), and Sca1991 (pyruvate oxidase). Others are involved in protein folding and oxidative stress situations—GrpE, Tig, Sca0559 (putative peptidyl-prolyl cis-trans isomerase), and KatA, while still others represent 50S ribosomal proteins such as RplC, RplE, RplF, and RplJ.

3.4.3 Membrane-associated enzymes

Four membrane-associated enzymes increased in the culture supernatant: formate-tetrahydrofolate ligase (Fhs), Lqo, GlpD, and SdhB (Table 3). Fhs transfers formyl groups to 10-formyl-tetrahydrofolate (formyl-THF). In anaerobic conditions, PFL (pyruvate formate lyase) is important as a formate donor [29]. GlpD (aerobic glycerol-3-phosphate dehydrogenase) is membrane-associated in *S. aureus* and strongly activated by detergents. In the *femB* mutant Lqo (earlier named Mqo2) was enhanced; it is required for the reassimilation of L-lactate during NO·-stress. Lqo is also critical to respiratory growth in L-lactate as a sole carbon source [30]. Finally, SdhB is part of the succinate dehydrogenase complex (Sdh) consisting of three subunits: a membrane-bound cytochrome b-558 (SdhC), a flavoprotein containing an FAD-binding site (SdhA), and an iron-sulfur protein with a binding region signature of the 4Fe-4S-type (SdhB) [31]. Sdh is part of the TCA cycle, which plays a central role in oxidative growth, and catalyzes the oxidation of succinate to fumarate by donating $FADH_2$ for oxidative phosphorylation.

3.4.4 Localization analysis of four typical cytoplasmic proteins

To verify the data of secretome analysis, we purified four typical *S. aureus*- specific cytosolic proteins, raised rabbit antibodies, and determined the presence of the target proteins in the cytosolic fraction, the cell wall fraction, and the culture supernatant by Western blotting (Fig. 6). The antibodies cross-reacted with the highly conserved *S. carnosus* counterparts. The cytosolic proteins investigated were glyceraldehyde-3-phosphate dehydrogenase (GapA), enolase (Eno), fructose-1,6-bisphosphat-aldolase (FbaA), and NADH dehydrogenase (NDH-2). In the cytosolic fraction (CY), there was no marked difference in protein amounts between the wt, the *femB* mutant, and the complemented *femB* mutant. There was, however, a clear difference in the cell wall fraction (CW) and culture supernatant (SU) showing a significant increase in the *femB* mutant confirming that the cytosolic target proteins were abundantly exported.

Proteomics 2015, *15*, 1268–1279

3.4.5 Transcription of genes encoding cell-wall lytic enzymes was up-regulated in the *femB* mutant, while that of cytosolic target genes was unchanged

Northern blot analysis of a selected set of genes encoding secreted and cytosolic proteins was performed to examine a possible correlation with the increased protein secretion. RNA was isolated from the wt, its *femB* mutant, and the complemented mutant in the exponential growth phase. The transcripts for the *sceA*, *sceB*, *sceD*, *atlCS*, and *sca*_0404 genes are clearly increased in the *femB* mutant, which correlates well with the increased amount of protein in the supernatant of the *femB* mutant (Supporting Information Table 3). Only SceB was an exception, as it was more abundant in the wt secretome. However, the transcription level of genes encoding the cytosolic proteins AhpC, GapA, KatA, Eno, and Tkt was essentially unchanged in the wt and the mutant, though these proteins were more abundant in the secretome of the mutant (Supporting Information Table 3).

4 Discussion

Here, we showed that the alteration of the cell wall structure in the *femB* mutant of *S. carnosus* had an enormous impact on morphology and physiology: expanded cells, retarded growth, high susceptibility to cell wall antibiotics, decrease of PGN crosslinking or unusually high secretion, and release of proteins into the culture supernatant. These pleiotropic effects suggest that the shortening of the interpeptide bridge from five to three glycine residues poses a life-threatening problem for the cells. The comparative analysis of secreted proteins in wt and *femB* mutant revealed that some proteins were less but the vast majority was more abundant in the mutant. The question is which of the differently expressed proteins in the secretome of the mutant is a response to adaptation or represents collateral damage.

It is very likely that the various Sec-dependent enzymes overexpressed in the *femB* mutant represent an adaptation response as the transcription of the corresponding genes is increased in the mutant. AtlCS, SceA, and Sca0404 represent murein hydrolyses. AtlCS belongs to the major staphylococcal autolysins Atl [21]. In staphylococci, Atl is crucial for daughter cell separation [32]. The other two secondary murein hydrolases, which were over-represented in the secretome of the *femB* mutant, were SceA and Sca0404. SceA is homologous to SceD and IsaA which represent two putative lytic transglycosylases in *S. aureus* [25] and Sca0404 belongs to the LysM family of proteins that represents a PGN-binding domain [33]. Because of the four- to nine-fold overexpression of the murein hydrolases AtlCS, SceA, and Sca0404 we assume that they represent a compensation reaction to accommodate the altered PGN structure in order to partially allow cell wall growth and daughter cell separation.

Proteins with a decreased prevalence in the secretome of the *femB* mutant were SceB, LtaS, AckA, and Sca1315. Particularly SceB and LtaS are interesting as their decreased production might also be part of the survival strategy of the *femB* mutant. SceB belongs to the prominently secreted exoproteins in *S. carnosus*; it is homologous to the *S. epidermidis* SsaA [18], which contains a cysteine- and histidine-dependent amidohydrolases and peptidases (CHAP) domain, which functions in some proteins as a L-muramoyl-L-alanine amidase or a D-alanyl-glycyl endopeptidase within the PGN [34, 35]. Particularly, the D-alanyl-glycyl endopeptidase activity could be fatal in the *femB* mutant, as it would further decrease the degree of PGN cross-linking thus aggravating the already weakened murein network. Surprisingly, the membrane-associated LtaS was also decreased in the secretome of the *femB* mutant. Lipoteichoic acid (LTA), an important cell wall component of Gram-positive bacteria, is membrane-anchored via its lipid moiety. LtaS is required for LTA backbone synthesis and it has been shown recently that the enzyme accumulates at the cell division site [36]. Therefore, its presence in the secretome of the wt was not surprising, but its decreased presence in the secretome of the *femB* mutant was. In principle, we expected an increased LtaS expression in the *femB* mutant, as LTA synthesis is required for bacterial growth and cell division [37] and a decreased LtaS might worsen the growth defect of the *femB* mutant. Recently, it has been shown that LTA serves as a receptor for the Atl-repeats at the cross wall [38]. If the LTA content were decreased in the *femB* mutant, then back-binding of AtlCS to the cross wall would be affected; therefore the up-regulation of AtlCS as a compensation reaction would make sense.

However, the vast majority of proteins overrepresented in the secretome of the *femB* mutant represent typical cytosolic proteins (Table 3). With a few examples—FbaA, GapA, Eno, and Ndh-2—we showed in Western blots that these proteins are highly increased in the cell-wall fraction and the supernatant of the *femB* mutant (Fig. 6). Interestingly, their quantity in the cytosolic fraction was essentially similar to that of the wt and the complemented mutant, which suggests that the level of gene expression should not differ much in the wt and mutant. Indeed, transcription analysis revealed no significant difference in the tested *ahpC*, *gapA*, *katA*, *eno*, and *tkt* genes (Supporting Information Table 3). Release of typical cytosolic proteins into the culture supernatant, also referred to as "non-classical protein excretion," has been observed in many Gram-positive and Gram-negative bacteria such as staphylococci, streptococci, *Bacillus subtilis*, *Listeria monocytogenes*, or *E. coli*. In particular, glycolytic enzymes, chaperones, translation factors, or enzymes involved in detoxification of ROS were found in the supernatants by secretome analysis [39–44].

As there is no indication for an increased gene expression for the corresponding proteins, we don't think that they contribute much to the survival strategy of the *femB* mutant. We assume that the increased release of these proteins can be

ascribed to a collateral damage of the altered cell wall structure and the increased autolysis activity.

We appreciate the expert technical help of Regine Stemmler. This work was funded by the German Research Foundation: SFB766 and TR-SFB34.

The authors have declared no conflict of interest.

5 References

[1] Bendtsen, J. D., Kiemer, L., Fausboll, A., Brunak, S., Non-classical protein secretion in bacteria. *BMC Microbiol.* 2005, *5*, 58.

[2] Pasztor, L., Ziebandt, A. K., Nega, M., Schlag, M. et al., Staphylococcal major autolysin (atl) is involved in excretion of cytoplasmic proteins. *J. Biol. Chem.* 2010, *285*, 36794–36803.

[3] Ziebandt, A. K., Weber, H., Rudolph, J., Schmid, R. et al., Extracellular proteins of *Staphylococcus aureus* and the role of SarA and sigma B. *Proteomics* 2001, *1*, 480–493.

[4] Berger-Bächi, B., Genetic basis of methicillin resistance in *Staphylococcus aureus*. *Cell Mol. Life Sci.* 1999, *56*, 764–770.

[5] Rohrer, S., Maki, H., Berger-Bächi, B., What makes resistance to methicillin heterogeneous? *J. Med. Microbiol.* 2003, *52*, 605–607.

[6] Maidhof, H., Reinicke, B., Blumel, P., Berger-Bächi, B. et al., *femA*, which encodes a factor essential for expression of methicillin resistance, affects glycine content of peptidoglycan in methicillin-resistant and methicillin-susceptible *Staphylococcus aureus* strains. *J. Bacteriol.* 1991, *173*, 3507–3513.

[7] Henze, U., Sidow, T., Wecke, J., Labischinski, H. et al., Influence of *femB* on methicillin resistance and peptidoglycan metabolism in *Staphylococcus aureus*. *J. Bacteriol.* 1993, *175*, 1612–1620.

[8] Rosenstein, R., Nerz, C., Biswas, L., Resch, A. et al., Genome analysis of the meat starter culture bacterium *Staphylococcus carnosus* TM300. *Appl. Environ. Microbiol.* 2009, *75*, 811–822.

[9] Schleifer, K. H., Fischer, U., Description of a new species of the genus *Staphylococcus*: *Staphylococcus carnosus*. *Int. J. Syst. Bacteriol.* 1982, *32*, 153–156.

[10] Götz, F., Staphylococcus carnosus: a new host organism for gene cloning and protein production. *Soc. Appl. Bacteriol. Symp. Ser.* 1990, *19*, 49S–53S.

[11] Hanahan, D., Studies on transformation of *Escherichia coli* with plasmids. *J. Mol. Biol.* 1983, *166*, 557–580.

[12] Schleifer, K. H., Kloos, W. E., Moore, A., Taxonomic status of *Micrococcus luteus* (Schroeter 1872) Cohn 1872: correlation between peptidoglycan type and genetic compatibility. *Int. J. Syst. Bacteriol.* 1972, *22*, 224–227.

[13] Wieser, M., Denner, E. B., Kampfer, P., Schumann, P. et al., Emended descriptions of the genus *Micrococcus*, *Micrococcus luteus* (Cohn 1872) and *Micrococcus lylae* (Kloos et al. 1974). *Int. J. Syst. Evol. Microbiol.* 2002, *52*, 629–637.

[14] Eymann, C., Dreisbach, A., Albrecht, D., Bernhardt, J. et al., A comprehensive proteome map of growing *Bacillus subtilis* cells. *Proteomics* 2004, *4*, 2849–2876.

[15] Bernhardt, J., Büttner, K., Scharf, C., Hecker, M., Dual channel imaging of two-dimensional electropherograms in *Bacillus subtilis*. *Electrophoresis* 1999, *20*, 2225–2240.

[16] Brückner, R., Gene replacement in *Staphylococcus carnosus* and *Staphylococcus xylosus*. *FEMS Microbiol. Lett.* 1997, *151*, 1–8.

[17] Thumm, G., Götz, F., Studies on prolysostaphin processing and characterization of the lysostaphin immunity factor (Lif) of *Staphylococcus simulans* biovar *staphylolyticus*. *Mol. Microbiol.* 1997, *23*, 1251–1265.

[18] Lang, S., Livesley, M. A., Lambert, P. A., Littler, W. A. et al., Identification of a novel antigen from *Staphylococcus epidermidis*. *FEMS Immunol. Med. Microbiol.* 2000, *29*, 213–220.

[19] Gatlin, C. L., Pieper, R., Huang, S. T., Mongodin, E. et al., Proteomic profiling of cell envelope-associated proteins from *Staphylococcus aureus*. *Proteomics* 2006, *6*, 1530–1549.

[20] Lu, D., Wormann, M. E., Zhang, X., Schneewind, O. et al., Structure-based mechanism of lipoteichoic acid synthesis by *Staphylococcus aureus* LtaS. *Proc. Natl. Acad. Sci. USA* 2009, *106*, 1584–1589.

[21] Albrecht, T., Raue, S., Rosenstein, R., Nieselt, K. et al., Phylogeny of the staphylococcal major autolysin and its use in genus and species typing. *J. Bacteriol.* 2012, *194*, 2630–2636.

[22] Heilmann, C., Hussain, M., Peters, G., Götz, F., Evidence for autolysin-mediated primary attachment of *Staphylococcus epidermidis* to a polystyrene surface. *Mol. Microbiol.* 1997, *24*, 1013–1024.

[23] Oshida, T., Sugai, M., Komatsuzawa, H., Hong, Y. M. et al., A *Staphylococcus aureus* autolysin that has an N-acetylmuramoyl-L-alanine amidase domain and an endo-beta-N-acetylglucosaminidase domain: cloning, sequence analysis, and characterization. *Proc. Natl. Acad. Sci. USA* 1995, *92*, 285–289.

[24] Montenbruck, I. P., Eberhard-Karls-Universität, Thesis 128 Tübingen 1992.

[25] Stapleton, M. R., Horsburgh, M. J., Hayhurst, E. J., Wright, L. et al., Characterization of IsaA and SceD, two putative lytic transglycosylases of *Staphylococcus aureus*. *J. Bacteriol.* 2007, *189*, 7316–7325.

[26] Heilmann, C., Thumm, G., Chhatwal, G. S., Hartleib, J. et al., Identification and characterization of a novel autolysin (Aae) with adhesive properties from *Staphylococcus epidermidis*. *Microbiology* 2003, *149*, 2769–2778.

[27] Heilmann, C., Hartleib, J., Hussain, M. S., Peters, G., The multifunctional *Staphylococcus aureus* autolysin Aaa mediates adherence to immobilized fibrinogen and fibronectin. *Infect. Immunity* 2005, *73*, 4793–4802.

[28] Hirschhausen, N., Schlesier, T., Peters, G., Heilmann, C., Characterization of the modular design of the autolysin/adhesin Aaa from *Staphylococcus aureus*. *Plos One* 2012, *7*, e40353.

[29] Leibig, M., Liebeke, M., Mader, D., Lalk, M. et al., Pyruvate formate lyase acts as a formate supplier for metabolic

processes during anaerobiosis in *Staphylococcus aureus*. *J. Bacteriol.* 2011, *193*, 952–962.

[30] Fuller, J. R., Vitko, N. P., Perkowski, E. F., Scott, E. et al., Identification of a lactate-quinone oxidoreductase in *Staphylococcus aureus* that is essential for virulence. *Front Cell Infect. Microbiol.* 2011, *1*, 19.

[31] Hederstedt, L., Rutberg, L., Succinate dehydrogenase–a comparative review. *Microbiol. Rev.* 1981, *45*, 542–555.

[32] Götz, F., Heilmann, C., Stehle, T., Functional and structural analysis of the major amidase (Atl) in *Staphylococcus*. *Int. J. Med. Microbiol.* 2014, *304*, 156–163.

[33] Frankel, M. B., Schneewind, O., Determinants of murein hydrolase targeting to cross-wall of *Staphylococcus aureus* peptidoglycan. *J. Biol. Chem.* 2012, *287*, 10460–10471.

[34] Bateman, A., Rawlings, N. D., The CHAP domain: a large family of amidases including GSP amidase and peptidoglycan hydrolases. *Trends Biochem. Sci.* 2003, *28*, 234–237.

[35] Rigden, D. J., Jedrzejas, M. J., Galperin, M. Y., Amidase domains from bacterial and phage autolysins define a family of gamma-D,L-glutamate-specific amidohydrolases. *Trends Biochem. Sci.* 2003, *28*, 230–234.

[36] Reichmann, N. T., Picarra Cassona, C., Monteiro, J. M., Bottomley, A. L. et al., Differential localization of LTA synthesis proteins and their interaction with the cell division machinery in Staphylococcus aureus. *Mol. Microbiol.* 2014, *92*, 273–286.

[37] Gründling, A., Schneewind, O., Synthesis of glycerol phosphate lipoteichoic acid in *Staphylococcus aureus*. *Proc. Natl. Acad. Sci. USA* 2007, *104*, 8478–8483.

[38] Zoll, S., Schlag, M., Shkumatov, A. V., Rautenberg, M. et al., Ligand-binding properties and conformational dynamics of autolysin repeat domains in staphylococcal cell wall recognition. *J. Bacteriol.* 2012, *194*, 3789–3802.

[39] Sibbald, M. J., Ziebandt, A. K., Engelmann, S., Hecker, M. et al., Mapping the pathways to staphylococcal pathogenesis by comparative secretomics. *Microbiol. Mol. Biol. Rev.* 2006, *70*, 755–788.

[40] Tjalsma, H., Antelmann, H., Jongbloed, J. D., Braun, P. G. et al., Proteomics of protein secretion by *Bacillus subtilis*: separating the "secrets" of the secretome. *Microbiol. Mol. Biol. Rev.* 2004, *68*, 207–233.

[41] Ziebandt, A. K., Becher, D., Ohlsen, K., Hacker, J. et al., The influence of *agr* and *sigmaB* in growth phase dependent regulation of virulence factors in *Staphylococcus aureus*. *Proteomics* 2004, *4*, 3034–3047.

[42] Li, M., Rosenshine, I., Tung, S. L., Wang, X. H. et al., Comparative proteomic analysis of extracellular proteins of enterohemorrhagic and enteropathogenic *Escherichia coli* strains and their ihf and ler mutants. *Appl. Environ. Microbiol.* 2004, *70*, 5274–5282.

[43] Trost, M., Wehmhoner, D., Karst, U., Dieterich, G. et al., Comparative proteome analysis of secretory proteins from pathogenic and nonpathogenic Listeria species. *Proteomics* 2005, *5*, 1544–1557.

[44] Xia, X. X., Han, M. J., Lee, S. Y., Yoo, J. S., Comparison of the extracellular proteomes of *Escherichia coli* B and K-12 strains during high cell density cultivation. *Proteomics* 2008, *8*, 2089–2103.

Molecular Microbiology (2015) 97(4), 775–789

doi:10.1111/mmi.13065
First published online 19 June 2015

Excretion of cytoplasmic proteins (ECP) in *Staphylococcus aureus*

Patrick Ebner,[1] Marcel Prax,[1] Mulugeta Nega,[1] Iris Koch,[2] Linda Dube,[1] Wenqi Yu,[1] Janina Rinker,[1] Peter Popella,[1] Matthias Flötenmeyer[2] and Friedrich Götz[1]*

[1]*Microbial Genetics, Interfaculty Institute of Microbiology and Infection Medicine (IMIT), University of Tübingen, Auf der Morgenstelle 28, 72076 Tübingen, Germany.*
[2]*Max Planck Institute for Developmental Biology, Spemannstr. 35, 72076 Tübingen, Germany.*

Summary

Excretion of cytoplasmic proteins (ECP) is a common physiological feature in bacteria and eukaryotes. However, how these proteins without a typical signal peptide are excreted in bacteria is poorly understood. We studied the excretion pattern of cytoplasmic proteins using two glycolytic model enzymes, aldolase and enolase, and show that their excretion takes place mainly during the exponential growth phase in *Staphylococcus aureus* very similar to that of Sbi, an IgG-binding protein, which is secreted via the Sec-pathway. The amount of excreted enolase is substantial and is comparable with that of Sbi. For localization of the exit site, we fused aldolase and enolase with the peptidoglycan-binding motif, LysM, to trap the enzymes at the cell wall. With both immune fluorescence labeling and immunogold localization on electron microscopic thin sections aldolase and enolase were found apart from the cytoplasmic area particularly in the cross wall and at the septal cleft of dividing cells, whereas the non-excreted Ndh2, a soluble NADH:quinone oxidoreductase, is only seen attached to the inner side of the cytoplasmic membrane. The selectivity, the timing and the localization suggest that ECP is not a result of unspecific cell lysis but is mediated by an as yet unknown mechanism.

Introduction

The cytoplasmic membrane (CM) is the most dynamic structure of bacterial cells. Its main function is the formation of a selective permeability barrier that regulates the passage of substances into and out of the cell. It allows the undirected transition of water and uncharged molecules up to molecular weight of about 200 Daltons but does not allow the passage of larger molecules or any charged substances, except, by means of special transport systems (Rothfield and Finkelstein, 1968).

Normally, proteins that are translocated across the CM are distinguished by appropriate signal peptides and are translocated by defined transport systems like the Sec- or TAT-translocation pathway (Bogsch *et al.*, 1998; Berks *et al.*, 2005; Driessen and Nouwen, 2008). However, there are typical cytoplasmic proteins (CPs) described, lacking a signal sequence and are still found extracellularly. One of the first reports on a typical CP found on the bacterial cell surface came from Vincent Fischetti's group. Glyceraldehyde-3-phosphate dehydrogenase (GAPDH) was found in large amounts on the cell surface of pathogenic streptococcal species as well as in the supernatant of several bacteria, fungi and even protozoans (Pancholi and Fischetti, 1993). Interestingly, this GAPDH functions also as an Adenosine diphosphate (ADP)-ribosylating enzyme, a reaction that is stimulated by nitric oxide. In group B streptococci, GAPDH acts as an inducer of apoptosis of murine macrophages (Oliveira *et al.*, 2012). In enterohemorrhagic and enteropathogenic *Escherichia coli*, GAPDH was exposed on the surface where it binds to human plasminogen and fibrinogen, suggesting a role in pathogenesis (Egea *et al.*, 2007).

There are a number of other CPs excreted, such as α-enolase (Pancholi and Fischetti, 1998), glucose-6-phosphate isomerase (Hughes *et al.*, 2002), glutamine synthetase (Suvorov *et al.*, 1997), ornithine carbamoyltransferase (Hughes *et al.*, 2002), fibrinogen-binding protein A of *Listeria monocytogenes* (Dramsi *et al.*, 2004) or Fbp54 of *Streptococcus pyogenes* (Courtney *et al.*, 1996). All these proteins do not contain a traditional signal peptide and appear to be typical 'moonlighting' proteins with different intra- and extracellular activities.

The term 'moonlighting' protein refers to a single protein that has multiple functions. For example, the mammalian thymidine phosphorylase catalyzes the intracellular dephosphorylation of thymidine but acts outside as a platelet-derived endothelial cell growth factor, which stimu-

Accepted 19 May, 2015. *For correspondence. E-mail friedrich.goetz@uni-tuebingen.de; Tel. (+49) 7071 2974635; Fax (+49) 7071 295937.

lates endothelial cell growth and chemotaxis (Jeffery, 1999). Most moonlighting proteins represent evolutionarily conserved (ancient) enzymes. The glycolytic enzymes GAPDH and enolase as well as the cell stress proteins chaperonin 60, Hsp70 and prolyl cis-trans isomerase, are among the most common of the bacterial moonlighting proteins. They play a role in bacterial virulence, as they are involved in adhesion and modulation of cell signaling processes. An overview of bacterial moonlighting proteins and their role in virulence is presented by Henderson and Martin (2013).

With the advent of secretome studies, it turned out that approximately 25% of the secretome in *Bacillus subtilis* or *Staphylococcus aureus* were typical CPs (Li *et al.*, 2004; Tjalsma *et al.*, 2004; Ziebandt *et al.*, 2004; Sibbald *et al.*, 2006; 2010; Xia *et al.*, 2008; Kusch and Engelmann, 2014). In particular, glycolytic enzymes, chaperones, translation factors or enzymes involved in detoxification of reactive oxygen species were found in the supernatants by secretome analysis. Recently, it has been shown that in *S. aureus*, only a defined set of CPs were found in the secretome, whereas other highly expressed CPs such as Fhs, GuaB, SA0802 (Ndh-2), EF-TS, GlnA, PdhD and SucC were absent (Pasztor *et al.*, 2010). Two conclusions can be drawn from this observation: (i) there is no correlation between the quantity and the excretion level of CPs, and (ii) there must exist a specific selection procedure that decides which CPs are excreted.

In this context, an interesting observation has been made with the glycolytic enolase of *E. coli*. Like in other bacteria, the enolase from *E. coli* is also excreted. Its enzymatic reaction involves a transient covalent binding of the substrate 2-phosphoglycerate to the active site Lys341. Replacement of Lys341 with other amino acids not only prevented the automodification but also the export of enolase (Boel *et al.*, 2004). One of the enolase mutants (K341E) was almost as active as the wild-type enzyme and still was not exported, suggesting that the enolase export was correlated with the loss of modification and not the loss of glycolytic activity. Similar results have been obtained with the *B. subtilis* enolase, which contains a hydrophobic alpha-helical domain within the enzyme that contributes to its secretion together with the N-terminal region (Yang *et al.*, 2011; 2014). These examples are currently the strongest evidences that excretion of cytoplasmic proteins (ECP) is selective; this selectivity speaks against the indiscriminate excretion by cell lysis.

In bacteria, ECP is poorly understood. It is hotly debated whether the release of CPs is due to cell lysis or whether they are exported by a so far unknown transport mechanism (Wang *et al.*, 2013). This is exactly the question what we want to answer in the long term. Here we have selected two cytoplasmic model proteins involved in glycolysis, aldolase and enolase, and could demonstrate that the two enzymes were preferentially produced in the exponential growth phase in a bell-shape production profile, like Sec translocon secreted protein, and they were translocated across the CM at the septum region into the cross wall of dividing cells.

Results

Excretion of FbaA, Eno and secretion of Sbi takes place during the bacterial growth phase

In our studies, we used the glycolytic enzymes aldolase (FbaA) and enolase (Eno) as representatives for excreted CPs in *S. aureus* (Pasztor *et al.*, 2010). By studying the time course of their excretion, we should see whether their level was constant, permanently increasing or growth phase dependent. Therefore, we followed FbaA and Eno excretion during aerobic growth of SA113Δ*spa* (Fig. 1A) by immunoblot analysis (Fig. 1B). When examining the content of FbaA in the supernatant of a 2 ml cell culture over time, there was already a visible band seen after 4 h of growth whose intensity steadily increased up to 8 h. Afterwards, a slight decrease in intensity was observable toward 10 h followed by an increase toward 24 h again. With Eno, a similar trend was observed; the highest amount was reached at 4 and 5 h, then it declined until 10 h and increased again after 24 h. FbaA and Eno appeared to be produced preferentially in the exponential growth phase. In the Western blot, we can also follow the immunoglobulin-G (IgG) binding protein, Sbi (Zhang *et al.*, 1998), which is visible as a band slightly above Eno. Sbi has a typical signal peptide and is secreted via the Sec-pathway. When one plots the relative intensities of the bands in immunoblot (FbaA, Eno and Sbi) versus time, it appears that Eno even exceeds the amount of Sbi (Fig. 1C and D).

Interestingly, FbaA, Eno and the Sec-dependent Sbi show a similar production pattern: a rise in the early and mid-exponential phase, a decline toward the stationary phase and an accumulation toward 24 h. The only difference between FbaA and Eno is that the production of Eno is shifted to earlier growth phase compared with FbaA. However, essentially, the production course of the CPs shows a similar pattern as the Sec-dependent Sbi. It is clear now that ECP occurs mainly during growth. Our next challenge was to trace the localization of the exit site of ECP.

In vivo *localization of FbaA and Eno excretion*

So far it is not known where the CPs are translocated. To address this question, we tried to trace the excretion of

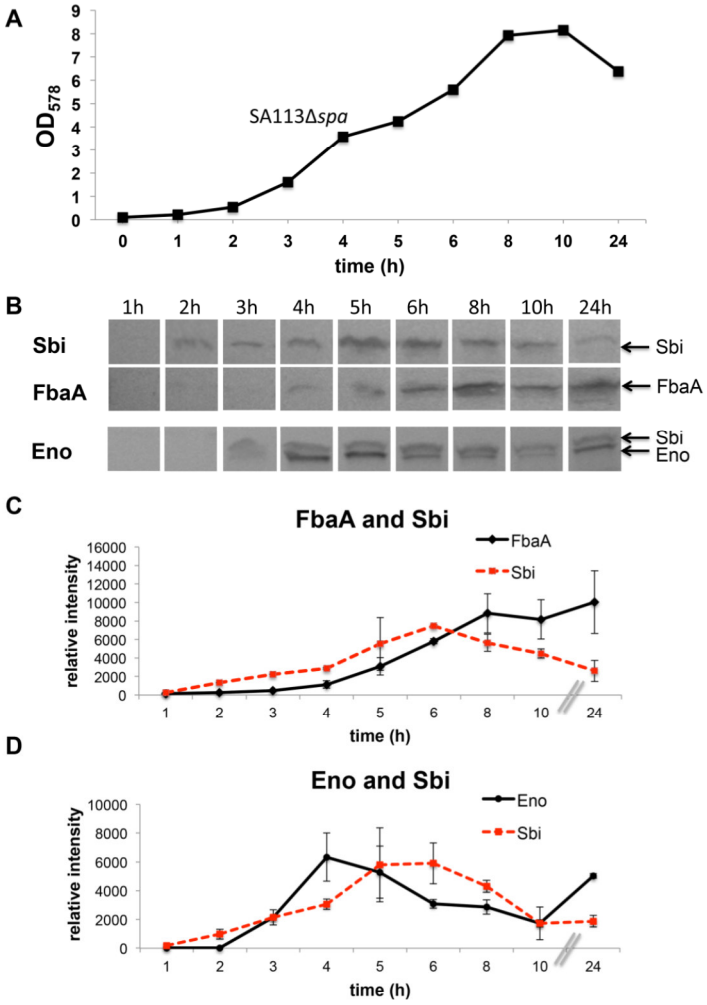

Fig. 1. Excretion of aldolase (FbaA), enolase (Eno) and the secretion of the IgG-binding protein (Sbi) during growth of SA113Δspa.
A. Growth curve of SA113Δ*spa* in BM medium.
B. Time course of the accumulated excretion of FbaA, Eno and Sbi during growth by Western blot analyses; concentrated proteins present in each of 2 ml supernatant were applied.
C. Relative intensities of the bands observed in Western blot (shown in B) were blotted against time: FbaA (solid lines) and Sbi (dashed lines).
D. Relative intensities of the bands observed in Western blot (shown in B) were blotted against time: Eno (solid lines) and Sbi (dashed lines). FbaA and Eno were identified with specific rabbit antibodies; Sbi, is detectable with any antibody as it is an IgG-binding protein. The theoretical masses of FbaA, Eno and Sbi are 31, 47 and 47 kDa, respectively; Sbi migrates at 50 kDa. All immunoblotting experiments were repeated $n = 3$ times; here we show one representative example.

FbaA and Eno in SA113Δ*spa* cells with specific antibodies. Monitoring of excreted aldolase and enolase was carried out with mid exponential cells, cultivated for 5 h where we see proper amounts of FbaA and Eno in the supernatant (Fig. 1B, C and D). For immuno labeling of excreted proteins, we used rabbit αFbaA and αEno antibodies and Cy3-labeled goat α-rabbit IgG as second antibody. However, fluorescence labeling of aldolase and enolase in the parent strain revealed no clear fluorescent signals or spots (Fig. S1A). Even increased expression by plasmid encoded enzymes in SA113Δ*spa* (pTtuf-*fbaA*) and SA113Δ*spa* (pTtuf-*eno*) clones (see constructs in Fig. 2A), fluorescence was hardly detectable (Fig. S1A). We assumed that the excreted FbaA and Eno diffused away from the exit site, thus becoming too diluted to allow a focused fluorescence labeling. We wondered how to prevent the protein's diffusion and to force their binding to the exit site. The LysM motif was the solution; it should retain LysM fusion proteins to the cell wall.

LysM-motif binds to staphylococcal peptidoglycan (PGN) fragments

The LysM motif is a widespread protein module, originally identified in enzymes that degrade bacterial cell walls, but it is also present in many other bacterial proteins (Bateman and Bycroft, 2000). Several of the LysM motifs containing proteins in *S. aureus* carry the LysM motif in tandem. We have chosen the CHAP-domain containing protein (SA0710) that contains only one LysM motif (Fig. 3A), which is apparently sufficient for cell wall targeting. The sequence of the 44 amino acid long LysM motif is underlined in Fig. 3B. To proof its ability to interact with staphylococcal PGN-fragments the 44 amino acid long LysM motif was N-terminal fused to mCherry that carries a C-terminal Strep-tag (Fig. 3C). The LysM-mCherry-strep protein was purified from SA113Δ*spa* (pTX-*lysM-mCh*) via streptavidin-affinity chromatography. Gel-shift experiments in native PAGE were carried out with PGN-

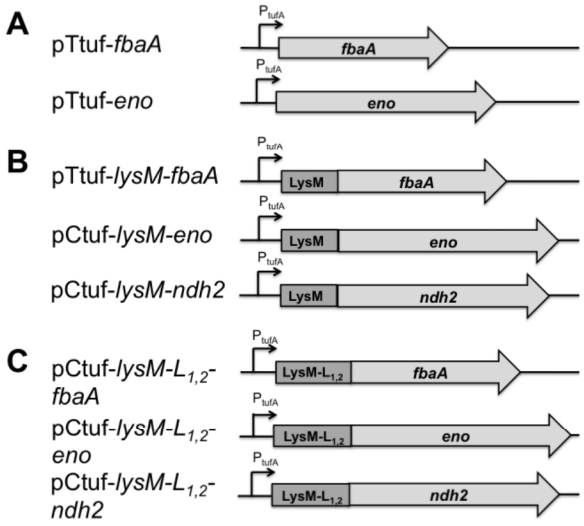

Fig. 2. Schematic representation of the constructs used for localization of excreted proteins. *fbaA*, aldolase; *eno*, enolase; *ndh2*, NADH:quinone oxidoreductase; *lysM*, motif for binding to PGN from *SA0710*; L_1, upstream flanking region of *lysM*; L_2, downstream flanking region of *lysM*; the parent plasmids were pTtuf and pCtufamp; *fbaA* and *eno* expression was under control of the constitutive promoter P_{tufA}.

fragments created by treatment with lysostaphin and partial mutanolysin digestion (Fig. 4A); undigested poly-PGN was too bulky. Surprisingly, LysM-mCherry was not binding to PGN fragments as no shift was observed. The reason could be that the motif was not sufficient for PGN binding. Therefore, we extended the motif by the flanking sequences L_1 and L_2 resulting in LysM-$L_{1,2}$ (80 aa) (Fig. 3B and D). This construct, LysM-$L_{1,2}$-mCherry, was now able to bind PGN (Fig. 4B). In native PAGE, the shift appeared as a protein smear due to the heterogeneously sized PGN substrates. PGN alone (control) was not stained by Coomassie blue (Fig. 4B).

ECP occurs at the septum of dividing cells

With the SA113Δ*spa* clones carrying the plasmids pCtuf-*lysM-fbaA/-eno/-ndh2*, pCtuf-*lysM-*$L_{1,2}$*-fbaA*/-eno/-*ndh2* fluorescence labeling of aldolase, enolase and Ndh2 was carried out (Fig. 5A and B). The clones expressing *lysM-fbaA/-eno* and clearly showed fluorescent signals along the septum and cross wall region with dot-like clusters particularly at the cleft of dividing cells (Fig. 5B). The accumulation at the septum region indicates that CPs were preferentially translocated at the septum site. As there was hardly any fluorescence visible in single cells (not shown), we assume that the translocation of the CPs occur preferentially during the cell division. Surprisingly, even in the pCtuf-*lysM-fbaA/-eno* clones that lack the $L_{1,2}$ linkers flanking the LysM motif, aldolase and enolase were targeted to the septum region, suggesting that the small 44 aa LysM motif alone is sufficient to fasten LysM-FbaA to the cell wall. However, the fluorescence intensity with $L_{1,2}$ linkers (LysM-$L_{1,2}$-FbaA or LysM-$L_{1,2}$-Eno clones) was much stronger. Weak fluorescence could also be detected on other positions of the cell envelope, which might represent remains from old septum or of new evolving septum sites. The clones expressing the non-excreted CP LysM-Ndh2 and LysM-$L_{1,2}$-Ndh2 did not show fluorescence at the cell envelope (Fig. 5A and B), thus representing an excellent (negative) control substantiating the FbaA and Eno localization results.

Staphylococcus aureus possesses 10 major secreted proteolytic enzymes including a metalloprotease [aureoly-

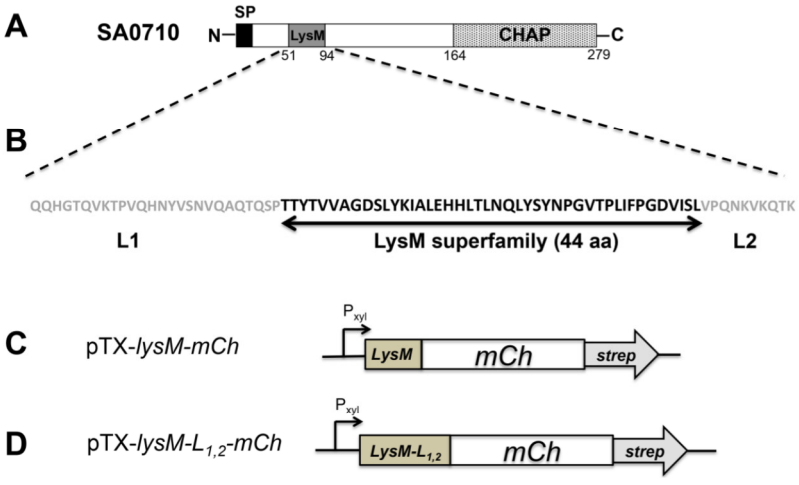

Fig. 3. Schematic representation of LysM motif of *SA0710* and *mCherry* constructs for gel-shift experiments.
A. *SA0710* from *S. aureus* SA113 consisting of SP (signal peptide), the LysM motif and the CHAP domain.
B. Amino acid (aa) sequence of the 44 aa long LysM core sequence underlined by arrow, and the flanking sequences L_1 and L_2.
C. and D. mCherry fusion constructs with LysM and LysM-$L_{1,2}$; both fusion proteins contained a C-terminal StrepTag II.

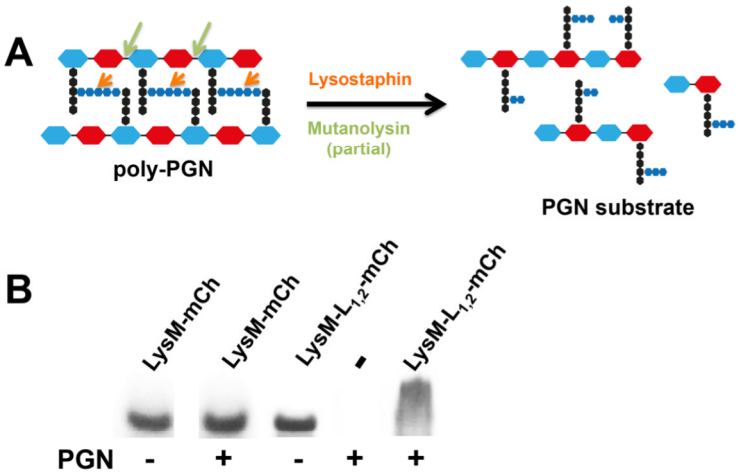

Fig. 4. Schematic representation of PGN substrate generation and gel shift assay with native PAGE.
A. PGN was isolated from SA113Δ*spa* and fragmented by fully lysostaphin digestion and partial mutanolysin digestion; these heterogeneous-sized PGN fragments were then used as substrate in the gel shift assay.
B. Streptavidin-affinity chromatography purified LysM-mCh as well as LysM-$L_{1,2}$-mCh were preincubation with or without PGN-substrate and applied to native PAGE; the gel was protein-stained with Coomassie blue: LysM-mCh was not shifted by PGN, only LysM-$L_{1,2}$-mCh was shifted in the presence of PGN; PGN alone was not stained by Coomassie blue.

sin (aur)], a V8 or SspA serine protease, two cysteine proteases [staphopain A (ScpA) and staphopain B (SspB)] and six serine-like proteases that are SspA homologues (SplABC-DEF) (Reed *et al.*, 2001; Shaw *et al.*, 2004). To largely rule out proteolytic degradation, the clones were also cultivated in the presence of cOmplete protease inhibitor cocktail (Roche). However, there was no difference in localization and excretion of FbaA and Eno compared with the absence of cOmplete. The addition of EDTA to inhibit of metalloproteases affected growth of *S. aureus* and could therefore not be used. In addition, we calculated the half-life and instability index of cytoplasmic target proteins by using the Expasy ProtParam tool (http://web.expasy.org/protparam/), which allows the computation of various physical and chemical parameters for a given protein (Wilkins *et al.*, 1999). Both the excreted proteins FbaA, Eno and GAPDH as well as the non-excreted proteins Ndh2, PdhD and GuaB were predicted as stable.

The LysM-$L_{1,2}$-fbaA/-eno expressing cells were enlarged compared with the parent strain. So was the average cell diameter of parent strains 0.93 µm (cell volume 0.43 µm^3) (Fig. 6), whereas the average diameter of the pCtuf-*lysM-L$_{1,2}$-fbaA/-eno* clones was 1.18 µm (cell volume 0.85 µm^3), showing that the cell volume of the pCtuf-*lysM-L$_{1,2}$-fbaA/-eno* clones was almost doubled. Besides the increased cell volume, the pCtuf-*lysM-L$_{1,2}$-fbaA* and -*eno* cells were also distinguished by forming tetrads (Fig. 5B). This effect was much less pronounced with only the LysM-fusions.

TEM thin sections and labeling of target proteins with immunogold

When we incubated as a control, the parent SA113Δ*spa* with the primary α-FbaA antibody and the immunogold labeled secondary antibody endogenous FbaA was only seen in the cytoplasm. In the absence of the primary antibody, no signal was seen largely ruling out an unspecific IgG-binding effect (Fig. S1C). However, thin sections of SA113Δ*spa* (pCtuf-*lysM-L$_{1,2}$-fbaA/-eno*) revealed signals in the cytoplasm as well as in the septum region and at the cleft of dividing cells (Fig. 7A and B), whereas cells expressing LysM-$L_{1,2}$-Ndh2 showed signals mainly at the inner side of the CM (Fig. 7B).

Ndh2 is attached to the inner side of the CM

Fusions of Ndh2 with mCherry revealed an accumulated fluorescence signal at the inner side of the CM, whereas the FbaA-mCh fusion showed fluorescence mainly in the cytoplasm (Fig. 8A). However, Ndh2 should be only loosely bound to the CM as it can easily be; furthermore, protein and membrane topology predictions did not reveal transmembrane domains. After disruption of cells containing the plasmids pCX-*fbaA-mCh*, the fluorescence was mainly found in the cytoplasmic fraction, whereas in cells with pCX-*ndh2-mCh*, the fluorescence remained largely in the cell debris (Fig. 8B).

Wall teichoic acid (WTA) has no apparent influence on targeting the LysM-L$_{1,2}$-fusion proteins

To address the question whether WTA had an influence on back binding of the LysM-$L_{1,2}$-fusion proteins to the cell wall, we transformed pTtuf-*lysM-fbaA* into the double mutant SA113Δ*spa*Δ*tagO*. The *tagO* mutant completely lacks WTA and has decreased surface hydrophilicity (Kohler *et al.*, 2009). The lack of WTA did not influence the localization of exit site; still, the LysM-$L_{1,2}$-FbaA/Eno fusion proteins only accumulated at the septum region in the same way as with the parent strain (Fig. S1B).

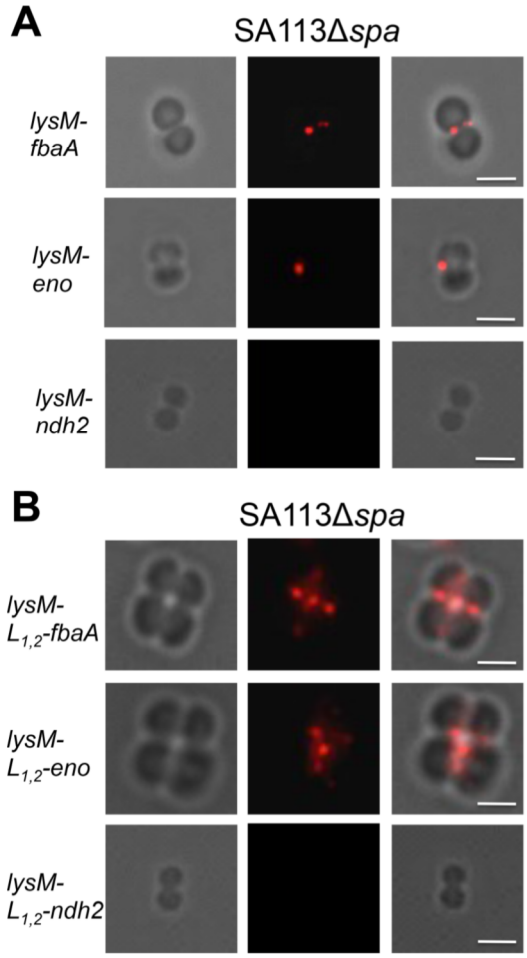

Fig. 5. Cellular localization of the excreted FbaA and Eno with and without N-terminal LysM-$L_{1,2}$ fusion by immunofluorescence.
A. SA113Δ*spa* (pCtuf-*lysM-fbaA*, pCtuf-*lysM-eno*, pCtuf-*lysM-ndh2*) with plasmid-encoded expression of LysM-FbaA; LysM-eno; LysM-ndh2;
B. SA113Δ*spa* (pCtuf-*lysM-*$L_{1,2}$*-fbaA*, pCtuf-*lysM-*$L_{1,2}$*-eno,* pCtuf-*lysM-*$L_{1,2}$*-ndh2*) with plasmid-encoded expression of LysM-$L_{1,2}$-FbaA; LysM-$L_{1,2}$-Eno, LysM-$L_{1,2}$-ndh2; only in the LysM–$L_{1,2}$ fusions of FbaA and Eno showed a clear accumulation of fluorescence was seen at the septum region. The presence of the LysM-$L_{1,2}$ caused a slightly increased cell size and tetrad formation.

Tetrad formation is due to blocking binding sites of cell wall lytic enzymes by LysM-$L_{1,2}$*-fusion proteins*

Both enlargement and tetrad formation is most likely due to the outcompeting of indigenous autolysins by our LysM-$L_{1,2}$-fusion proteins. Particularly, the tetrad formation in LysM-$L_{1,2}$-fbaA and -eno protein expressing clones is an indication of impaired cell separation after cell division. We assumed that excreted LysM-$L_{1,2}$ fusion proteins compete for the binding sites of endogenous autolysins involved in cell separation. Indeed, in an *in vitro* PGN degradation assay with mutanolysin, PGN hydrolysis was significantly reduced in the presence of LysM-$L_{1,2}$-mCh (Fig. 9).

Distribution of FbaA, Eno and Sbi in cytoplasm and supernatant of parent and clone strains

In immunoblot analyses, we compared the level of FbaA, Eno and Sbi in the cytoplasm and the supernatant of 4 h grown SA113Δ*spa* clones (Fig. 10A). In aldolase and enolase expressing plasmids, there was an expected progressive increase in protein size due to the fusion with LysM or LysM-$L_{1,2}$ respectively. This progressive increase was observed both in the cytoplasmic and supernatant fraction. Fortunately, Sec-translocated Sbi was also clearly visible. When comparing the abundance of the three proteins in the cytoplasm and supernatant, there is a clear distinction between aldolase and enolase on the one hand and Sbi on the other hand. Although aldolase and enolase showed high, Sbi showed only low abundance in the cytoplasm. Most likely this is due to the early capturing of Sbi by the Sec machinery. However, the amount of the three proteins does not differ significantly in the supernatant. Of course we have to consider that the plasmid encoded aldolase and enolase genes were overexpressed. On the other hand, the endogenous aldolase (30.8 kDa) and enolase (56.0 kDa) were also seen as clear bands in both the cytoplasmic fraction and the supernatant. If one compares the abundance of the three proteins in the supernatant, the amount of aldolase or enolase is quite comparable with that of Sbi; and this was a great surprise that two defined glycolytic enzymes were excreted at comparable level as a Sec-pathway secreted protein.

We wondered how much of the cytoplasmic aldolase was excreted. For this purpose, we compared the fluorescence intensity of FbaA-mCh in the cytoplasm with that of the supernatant over time (Fig. 10B). It turned out, that during exponential growth phase, approx. 2–3% of

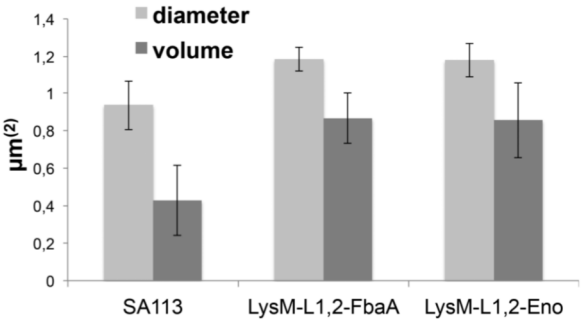

Fig. 6. Cell-size and cell-volume of SA113Δ*spa* and the LysM-$L_{1,2}$-FbaA/Eno expressing cells. Measurement of cell size and cell volume of SA113Δ*spa* and the LysM-$L_{1,2}$-FbaA/Eno expressing strains.

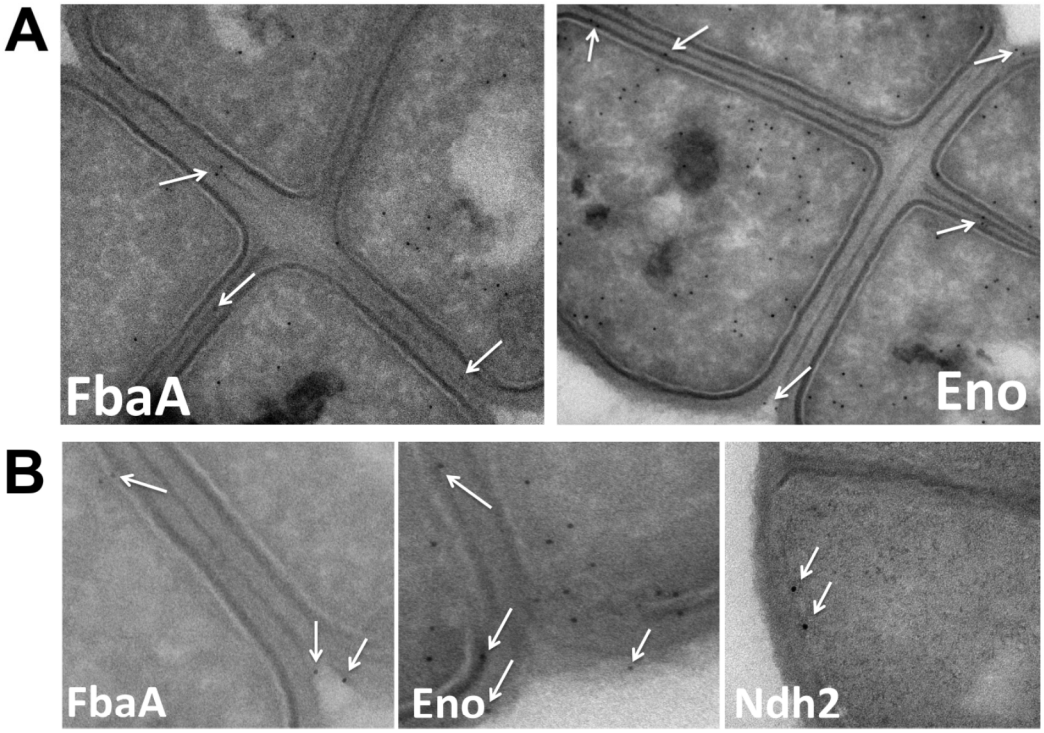

Fig. 7. Immunogold labeling of excreted FbaA, Eno and the non-excreted Ndh2 and detection by transmission electro microscopy (TEM).
A. Thin sections of SA113Δ*spa* (LysM-$L_{1,2}$-fbaA) and SA113Δ*spa* (LysM-$L_{1,2}$-eno) clones showing the center of cross wall sections of tetrad cells.
B. Thin sections of SA113Δ*spa* (LysM-$L_{1,2}$-fbaA), SA113Δ*spa* (LysM-$L_{1,2}$-eno) and SA113Δ*spa* (LysM-$L_{1,2}$-ndh2) clones showing the septal cleft of dividing cells. The 1st antibody was against the target protein, and the 2nd antibody was gold-labeled goat antibody against the 1st antibody. Arrows indicate the position of the target proteins.

FbaA-mCh was found in the supernatant, which increased up to 5% after 24 h.

Discussion

At first glance, ECP is a waste of resources and energy, unless the excreted proteins fulfill certain extracellular functions that are important for survival. One of the crucial questions was, how these CPs are excreted? Are they accidentally released by cell lysis, or rather by a defined export pathway? Does ECP play an important physiological role maybe during infection that we have overlooked so far? In this context, it is interesting that the immunization with certain excreted CPs protected mice from lethal *S. aureus* infection, suggesting that excreted CPs might play a crucial role in pathogenicity (Glowalla *et al.*, 2009). More recently, it has been shown that during biofilm formation, particularly in the stationary phase, various CPs were released and form a protein matrix that associates with the cell surface at low pH (Foulston *et al.*, 2014). This example also shows that ECP plays a role in structure and probably also in the antibiotic tolerance of biofilm-imbedded cells (Götz, 2002; Leibig *et al.*, 2011). For a better understanding of ECP, the aim of this work was to investigate the secretion patterns of selected CPs in more detail in the model organism *S. aureus*.

To better characterize the pattern of excretion, we have concentrated on two glycolytic model enzymes, FbaA and Eno, and followed their excretion progress in the course of aerobic growth. It turned out that FbaA and Eno were excreted during the growth phase in a bell-shape production profile that was strikingly similar to that of Sbi (Fig. 1B–D). If FbaA and Eno were excreted simply by cell lysis, one would have expected a monophasic gradual increase toward the stationary phase where cell lysis may start. The excretion during the exponential growth makes cell lysis unlikely as the main reason for ECP. In many bacteria cell, lysis occurs normally in the stationary growth phase as indicated by a decrease in OD and in colony-forming unit. However, during exponential growth phase, cell lysis should be the exception as it leads to cell death by disruption of membrane integrity and membrane potential. Many of the staining techniques used for the assessment of bacterial viability are based on monitoring membrane potential [Rhodamine 123 and DiBAC4(3)] or membrane integrity (SYTO 9/propidium iodide/GFP per-

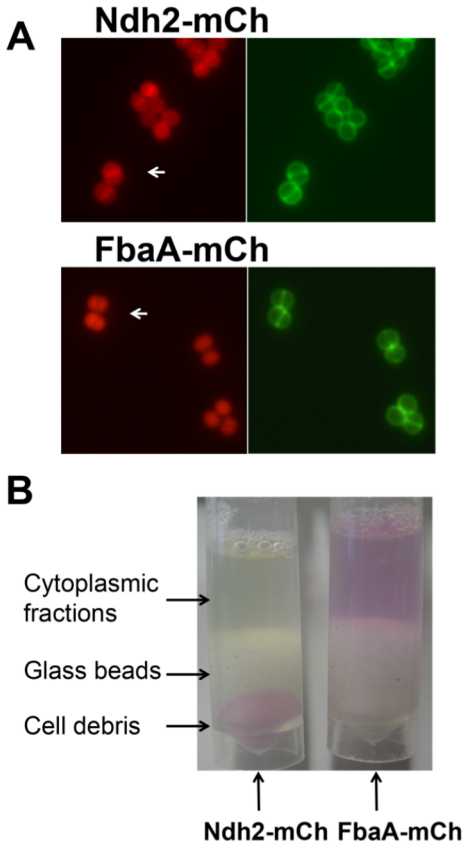

Fig. 8. Subcellular localization of Ndh2 and FbaA.
A. Subcellular localization of FbaA-mCh and Ndh2-mCh fusions in SA113Δ*spa* clones (left); BODIPY® FL vancomycin labeled clones for visualization of the septum.
B. Disrupted and pelleted SA113Δ*spa* clones expressing FbaA-mCh and Ndh2-mCh fusions.

sistence) (Jepras *et al.*, 1995; Banning *et al.*, 2002). In exponential growth, there is hardly cell lysis observed.

Sbi, the second IgG-binding protein in *S. aureus*, has a typical signal peptide and is secreted via the Sec-pathway (Zhang *et al.*, 1998). Part of Sbi appeared bound to the cell envelope by binding to lipoteichoic acid (LTA), but ≈ 50% is found in the culture supernatant (Smith *et al.*, 2012). We were also surprised by the relatively high amount of excreted Eno in the supernatant, which was comparable with that of Sbi. As a classically secreted protein, we had expected that the amount of Sbi is magnitudes higher than that of a certain CP. This shows that the excretion of FbaA and Eno is substantial and that they may exert an effect under certain environmental conditions such as after invasion of host cells and toward biofilm formation.

Such bell-shape expression profiles were also described in a proteome profiling study of *S. aureus* LPXTG surface proteins (Ythier *et al.*, 2012). Proteins such as Spa, FnbpA and ClfB showed a bell-shape expression profile when samples were taken during exponential growth (OD 0.2, 0.6, 1.8 and 2.2); there was also a declined production observed at higher OD values, like with FbaA, Eno and Sbi. The declined production could be due to decreased transcription; however, it could be also due to proteolytic degradation by cysteine protease (SspB), endopeptidase (SspA), staphopain (ScpA) or the metalloprotease aureolysin (Aur); aureolysin for example was shown to be responsible for cleavage of ClfB (McAleese *et al.*, 2001). To make sure whether proteolytic degradation could be responsible for the decline in FbaA, Eno and Sbi, we cultivated the cells in the presence of EDTA-free protease inhibitor cocktail. However, there was hardly a difference in the expression pattern; EDTA would inhibit growth of *S. aureus*. Both the excreted proteins FbaA, Eno and GAPDH as well as the non-excreted proteins Ndh2, PdhD and GuaB were predicted as stable using the Expasy ProtParam tool. This suggests that protein (in)stability is not a criterion that some CPs were detectable and others not in the culture supernatant. Therefore, the observed selectivity in ECP must have other reasons.

For the localization of FbaA and Eno, the fusion with LysM, a small PGN-binding motif, was crucial to prevent diffusion from the exit site. LysM is a widespread protein module in bacteria that targets proteins to PGN (Bateman and Bycroft, 2000; Heilmann *et al.*, 2005; Leo *et al.*, 2015). By translational fusion of LysM with FbaA and Eno, we could trap FbaA and Eno at the translocation site. With this new approach, we were able to identify FbaA and Eno translocation at the septum region of dividing cells (Fig. 5A and B). We were also able to confirm this results

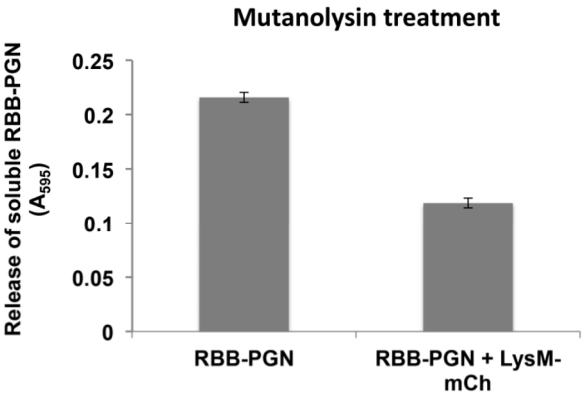

Fig. 9. Hydrolysis of RBB-labeled PGN by mutanolysin in the presence or absence of LysM-$L_{1,2}$-mCh. Mutanolysin activity was spectrophotometrically (A_{595}) determined by the release of soluble RBB-PGN fragments. In the presence of LysM-$L_{1,2}$-mCh, mutanolysin activity was decreased by almost 50%. RBB, Remazol Brilliant Blue; LysM-$L_{1,2}$-mCh, LysM motif was N-terminally fused to mCherry provided with a C-terminal Strep-tag II (Fig. 4C).

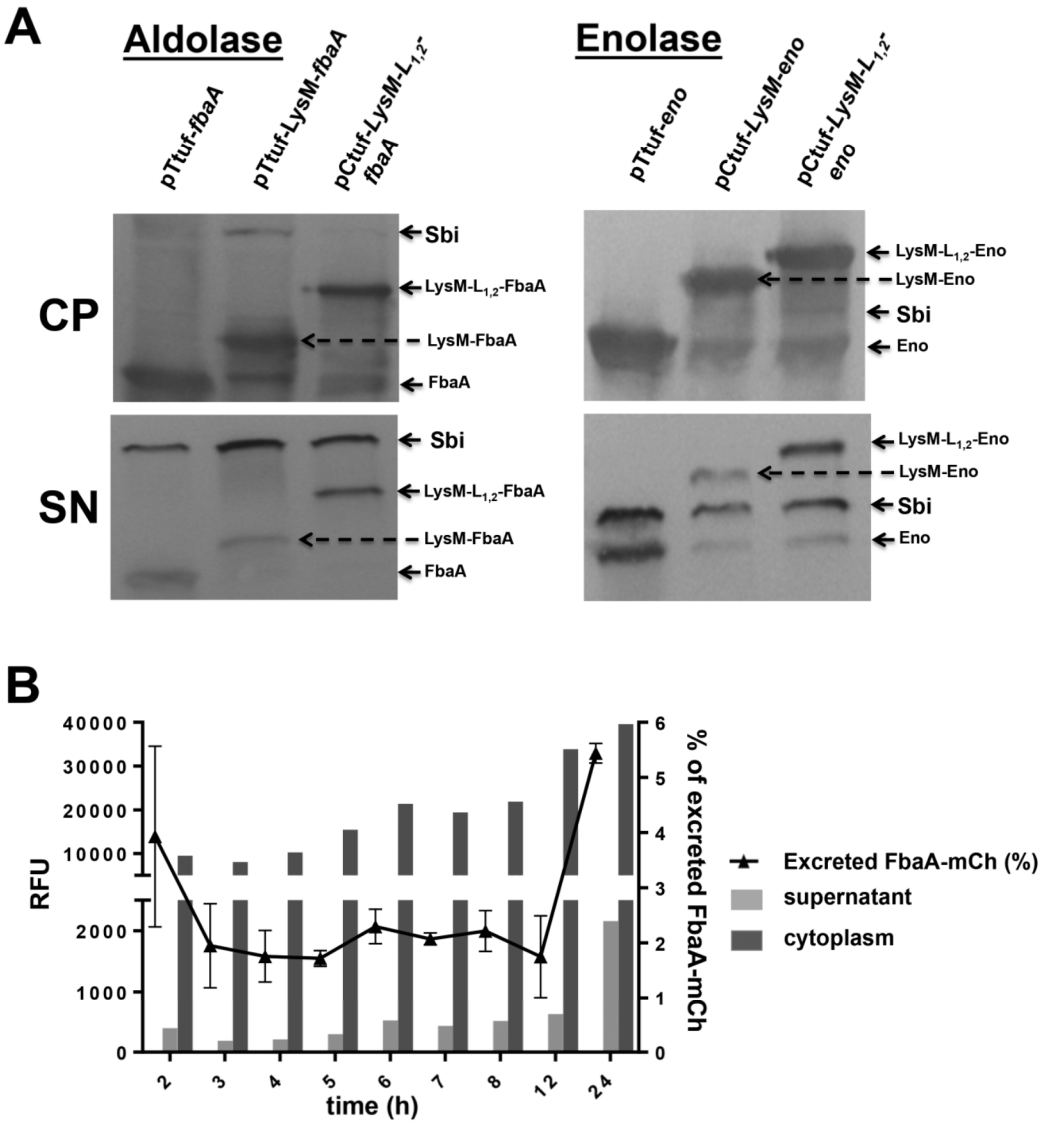

Fig. 10. Monitoring the expression of aldolase/enolase and corresponding LysM fusions by Western blot analysis and relative quantification of FbaA-mCh in the culture supernatant.
A. Aldolase (FbaA) and enolase (Eno) expression was determined in the cytoplasmic fraction (CM) and in the culture supernatant (SN) of parent strain SA113Δ*spa* as well as in the corresponding pTtuf-*eno/fbaA* and pCtuf-*lysM-eno/fbaA* pCtuf-*lysM-L*$_{1,2}$*-eno/fbaA* clones, cultivated for 5 h. Masses of the corresponding proteins: FbaA, 30.8 kDa; LysM-FbaA, 35.6 kDa; LysM-L$_{1,2}$-FbaA, 39.7 kDa; Eno, 47.12 kDa; LysM-Eno, 51.9 kDa; LysM-L$_{1,2}$-Eno, 56.0 kDa.
B. The relative amount of FbaA-mCh was followed over time (2, 3, 4, 5, 6, 7, 8, 12 and 24 h) by fluorescence measurement. The intracellular signal increased over time (dark gray), whereas the signal in the supernatant first decreased and subsequently increased (light gray). The relative amount of FbaA-mCh (black line) was stable at approximately 2%. After 24 h, the amount increased to 5.5%.

by transmission electron microscopy (TEM) (Fig. 7A and B). However, the signals in TEM immunogold are generally not so strong as the fluorescence signals (Schwarz and Humbel, 2014).

The interaction of LysM with PGN was significantly enhanced by the linker sequences, L$_{1,2}$ flanking LysM. This had some morphological consequences. In clones expressing LysM-L$_{1,2}$ FbaA/Eno fusions cells were not only enlarged but also formed more tetrads suggesting a defect in cell separation by impaired autolysin activity. For example, mutants of the major autolysin Atl or of the murein hydrolase LytN are affected in cell separation (Biswas *et al.*, 2006; Frankel *et al.*, 2011). LytN for example carries a LysM domain that might be in binding competition with LysM-L$_{1,2}$-fusions. We assumed that the tetrad formation by the LysM-L$_{1,2}$-fusions could be caused

by LysM's competing with autolysin-binding sites. Indeed, we were able to confirm this assumption by demonstrating that hydrolysis of RBB-labeled PGN by mutanolysin (endo-N-acetylmuramidase) was almost 50% inhibited in the presence of LysM-mCh fusion, suggesting that LysM-mCh displaced mutanolysin from the PGN binding and cleavage sites (Fig. 9).

We also wanted to know whether WTA had an influence on the localization of LysM-FbaA/Eno fusions. For example, the bifunctional autolysin Atl of *S. aureus* is processed to amidase-$R_{1,2}$ and R_3-glucosaminidase. These autolytic enzymes are targeted via the repeat domains (R) to the septal region of the cell where the repeat domains bind to LTA as receptor (Schlag *et al.*, 2010; Zoll *et al.*, 2012). Interestingly, WTA of the old cell wall prevented binding of the repeats, which was shown with the WTA-deficient mutant, Δ*tag*O, where the repeats were bound evenly distributed at the cell surface (Schlag *et al.*, 2010). However, when we expressed LysM-FbaA in the SA113Δ*spa*Δ*tagO*, double mutant LysM-FbaA was still targeted to the septum region, hence, WTA did not prevent LysM-FbaA/Eno targeting (Fig. S1B). The Δ*tag*O mutant has many phenotypic alterations compared with the parent strain (Weidenmaier *et al.*, 2004; Kohler *et al.*, 2009). However, one phenotype, which might play a role in ECP, is its increased autolysis activity and decreased PGN cross-linking. TEM analysis showed that the cell wall of the mutant became more translucent within 4 h, suggesting that cell wall integrity was affected (Schlag *et al.*, 2010). Because of the disintegrated cell wall structure and increased autolysis activity, one would have expected excretion of the LysM-FbaA/Eno fusions all over the cell envelope, but this is not the case. The fact that they are still largely excreted at the septum indicates that increased cell lysis has little impact on their targeting. We even want to go one step further by suggesting that cell lysis is not the driving force of ECP.

What could be the benefit of ECP for the cells? It is well documented that ECP plays a role in the cell cycle as well as in virulence (Götz *et al.*, 2015). For ECP in eukaryotes, the term '*moonlighting proteins*' has been coined (Jeffery, 1999). Moonlighting refers to a single protein that has multiple functions. For example, the mammalian thymidine phosphorylase catalyzes the intracellular dephosphorylation of thymidine but acts outside as a platelet-derived endothelial cell growth factor, which stimulates endothelial cell growth and chemotaxis (Jeffery, 1999). One possible benefit of ECP in eukaryotes could be that this export system is a way to clear unfolded proteins from the cytoplasm (Sloan *et al.*, 1994); a similar function might be also apply for bacteria, but there are no hard data yet. In pathogenic bacteria, various moonlighting proteins are involved in host cell adhesion and modulation of cell signaling, thus contributing to bacterial virulence (Henderson and Martin, 2013). For example, the *Neisseria meningitidis* aldolase is localized both in the cytoplasm and the outer membrane surface where it contributes to adhesion to human brain microvascular endothelial and HEp-2 cells (Tunio *et al.*, 2010). GAPDH in *S. pyogenes* binds to human proteins and stimulates B lymphocytes, in *E. coli* GAPDH induces an early IL-10 production, in *Streptococcus pneumoniae* excreted enolase binds to human complement inhibitor C4b-binding protein and contributes to complement evasion (Agarwal *et al.*, 2012) and finally, vaccination with certain cytosolic proteins protects mice from lethal *S. aureus* infection (Glowalla *et al.*, 2009). The role of ECP in virulence merits paying more attention to this topic.

Conclusion

The pattern of ECP during the exponential growth phase is strikingly similar to Sec machinery secreted proteins, raising the question whether FbaA and Eno are hitchhiking with some of the staphylococcal Sec pathways shown in Götz *et al.* (2015). The excretion of the model proteins FbaA and Eno during the exponential phase and their translocation at the septum compartment suggest that cell lysis is a too simple explanation for their excretion. We assume that FbaA and Eno are translocated across the CM by an as yet unknown mechanism. After translocation, they may accumulate in the cross wall of dividing daughter cells and are finally expelled into the environment after cell separation. So far it is not known for what purpose staphylococcal cells excreted these CPs. Possible explanations for this phenomenon could be the disposal of inactive and misfolded proteins, although there is no evidence yet; however, the potential role of ECP in virulence merits stronger attention. A model of the proposed excretion pathway of CPs is shown in Fig. 11.

Experimental procedures

Bacterial strains and growth conditions

All immunoblotting experiments were carried out with the marker-less *spa* (Protein A) deletion mutant, *S. aureus* SA113Δ*spa* and SA113Δ*spa*Δ*tagO*, to avoid IgG binding to Protein A (Schlag *et al.*, 2010). SA113 (ATCC 35556) is a derivative of RN1 (NCTC8325), *agr*, 11 bp deletion in *rbsU* (Iordanescu and Surdeanu, 1976; Herbert *et al.*, 2010). *E. coli* strain DC10B (Monk *et al.*, 2012) was used for cloning experiments. All strains were cultivated aerobically at 37°C under continuous shaking in basic medium (BM) composed of 1% soy peptone, 0.5% yeast extract, 0.5% NaCl, 0.1% glucose and 0.1% K_2HPO_4, pH 7.4. When appropriate, the medium was supplemented with either 10 μg ml^{-1} chloramphenicol or 25 μg ml^{-1} tetracycline for staphylococcal clones and 100 μg ml^{-1} ampicillin for *E. coli*. Strains and plasmid used in this study are indicated in Table 1.

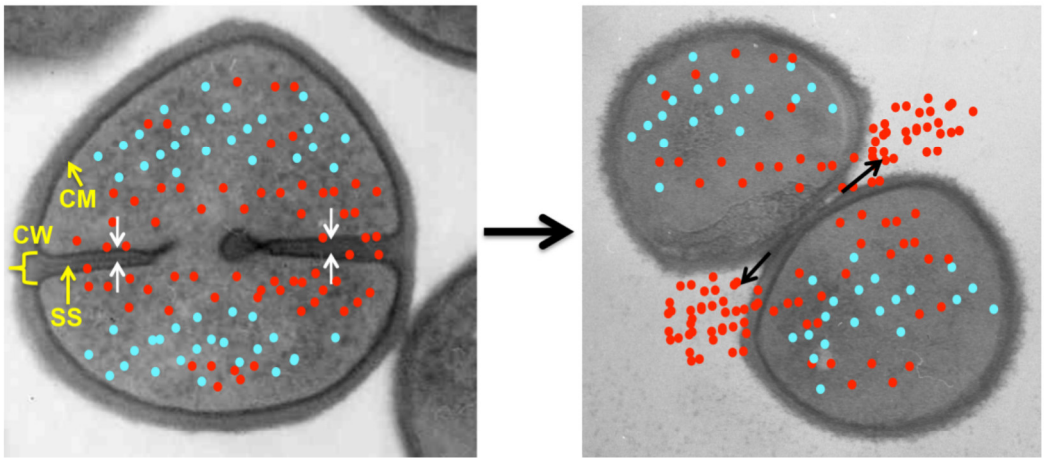

Fig. 11. Model for the localization of the translocation of cytoplasmic target proteins in *Staphylococcus aureus*.
A and B. The image is based on TEM thin sections of dividing and separating *S. aureus* cells in an earlier stage (Biswas *et al.*, 2006) (A) and a more progressed stage (unpublished) where daughter cells were almost separated (B). In the early stage of cell division, a septum is formed that gives rise to a septal space with the two cross walls. In the center of the cross wall is a thin electron-dense layer referred to as 'splitting system' (Giesbrecht *et al.*, 1998) along which autolysins cut the PGN interlinking the two daughter cells (Zoll *et al.*, 2012). We assume that CPs are translocated into the septal space where they may get transiently entrapped in the meshwork of the cross wall. With progression of cell separation, they are particularly clustered the cleft of dividing cells. When cell separation is almost completed (B), they are released into the environment. The red dots represent CPs that are excreted, and the blue dots those that are not excreted to illustrate the selection principle.

*Identification of Fba, Eno and Sbi in the culture supernatant of SA113Δ*spa *by immunoblot analyses*

SA113Δ*spa* was cultivated aerobically for 24 h in BM. At the indicated time points, 2 ml cell suspension was harvested by centrifugation at 17 000 × *g* for 5 min at 4°C (Fig. 1B). The culture supernatants were then mixed with 10 µl of Strata-Clean resin (Agilent, Waldbronn) and incubated under continuous shaking at room temperature (RT) for 15 min to enrich the proteins by binding to the resin. The resin was then pelleted by centrifugation at 17 000 × *g* and washed once with PBS. Samples were then resuspended in 20 µl 3 ×

Table 1. Strains and plasmids used in this study.

Strain or plasmid	Description	Source or reference
E. coli		
DC10B	F-mcrA Δ(mrr-hsdRMS-mcrBC) Φ8olacZΔM15 lacx74 recA1endA1 araD 139 Δ (ara leu)7697 galU galK rspL nup G λ-ΔSauUSI	Monk *et al.* (2012)
S. aureus		
SA113Δ*spa*	SA113Δ*spa* markerless deletion	Schlag *et al.* (2010)
SA113Δ*spa*Δ*tagO*	SA113Δ*spa*Δ*tag*O markerless deletion of *spa; tag*O::*erm*B	Schlag *et al.* (2010)
Plasmids		
pTtuf	Constitutive expression vector for staphylococci	This study
pTtuf-*fbaA*	Constitutive expression of *fbaA*	This study
pTtuf-*lysM-fbaA*	Constitutive expression of *lysM-fbaA*	This study
pTtuf-*eno*	Constitutive expression of *eno*	This study
pCtuf	Constitutive expression vector for staphylococci	Biswas *et al.* (2006)
pCtufamp	Shuttle vector for *E. coli* and staphylococci	This study
pCtufamp-*lysM-eno*	Constitutive expression of *lysM-eno*	This study
pCtufamp-*lysM-L$_{1,2}$-eno*	Constitutive expression of *lysM-L$_{1,2}$-eno*	This study
pCtufamp-*lysM-L$_{1,2}$-fbaA*	Constitutive expression of *lysM-L$_{1,2}$-fbaA*	This study
pCtufamp-*lysM-ndh2*	Constitutive expression of *lysM-ndh2*	This study
pCtufamp-*lysM-L$_{1,2}$-ndh2*	Constitutive expression of *lysM-L$_{1,2}$-ndh2*	This study
pCX-*fbaA-mCh*	Constitutive expression of *fbaA-mCh*	This study
pCX-*ndh2-mCh*	Constitutive expression of *ndh2-mCh*	This study
pTX30	Xylose inducible expression vector for staphylococci	Strauss *et al.* (1998)
pTX-*lysM-mCherry*	Xylose inducible expression of *lysM-mCherry*	This study
pTX-*lysM-L$_{1,2}$-mCherry*	Xylose inducible expression of *lysM-L$_{1,2}$-mCherry*	This study

Laemmli buffer, boiled for 7 min at 100°C and applied to a polyacrylamide gel. Subsequent to the gel electrophoresis, the gels were blotted with a Trans Blot (Bio-Rad, Munich) device, using a nitrocellulose membrane (Protran, GE, Frankfurt am Main). The membranes were then blocked overnight with RotiBlock blocking reagent (Roth, Karlsruhe). Incubation with primary α-FbaA and α-Eno rabbit-antibodies and secondary goat-anti-rabbit antibodies was performed for 60 min at RT. Detection was carried out using BCI/NBP (Sigma, Munich). At low OD values, the amount of detectable aldolase or enolase present in 2 ml supernatant might be very small. Therefore, we have in addition investigated the level of excreted proteins present in OD 2.0 by either increasing (1–3 h) or diluting (4–24 h) the volume of the harvested cell suspension (Fig. 1C). For example, when after 1 h the OD was ≈ 0.2, we have taken the supernatant of 10 ml cell culture.

*Expression of Fba, Eno and Sbi in the cytoplasm and culture supernatant of SA113Δ*spa *and corresponding clones by Western blot analyses*

SA113Δ*spa* and corresponding clones were cultivated aerobically for 5 h in BM. Cells of 5 ml cultures were harvested (Fig. 1) by centrifugation for 15 min at 9 000 × *g* at 4°C. The pellets were then resuspended in 1 ml PBS buffer and disrupted by homogenization using glass beads and Fast Prep 120 cell disruptor (Thermo Scientific, St. Leon-Roth) for four times for 30 s at full speed. To remove cell fragments and insoluble compartments, the lysate was centrifuged for 20 min at 20 000 × *g* at 4°C. Approximately 0.7 ml cytoplasm–PBS mixture was obtained, and 25 µl was applied to SDS-PAGE. The corresponding culture supernatants (5 ml) were mixed with 10 µl of StrataClean resin (Agilent, Waldbronn) and incubated under continuous shaking at RT for 15 min to enrich the proteins by binding to the resin, as described above. Western blot analyses were also performed as described above.

*Relative quantification of excreted FbaA-mCherry in the culture supernatant of SA113Δ*spa

SA113Δ*spa* and SA113Δ*spa* expressing *fbaA-mCh* were cultivated aerobically in BM. Samples were collected at 2, 3, 4, 5, 6, 7, 8, 12 and 24 h. The cultures were adjusted to $OD_{578} = 1$ for all samples and time points and spun down at 20 000 × *g* for 5 min. The supernatant was transferred to a new reaction tube. The obtained cell pellet was resuspended in the same volume of fresh BM. Relative fluorescence units of FbaA-mCherry were measured in the cytoplasm, by using whole cells and supernatant respectively. All values were blanked with SA113Δ*spa* cell suspension or the corresponding supernatant. Measurements were carried out in a black F-Bottom microtiter plate (Greiner, Frickenhausen) using a Tecan Infinite 200 (Tecan, Männedorf, Switzerland) plate reader with a constant gain of 115. The relative amount of excreted FbaA-mCherry was calculated using the cytoplasmic fluorescence units compared with the fluorescence measured in the supernatant.

Construction of the pTtuf-, pCtuf-pCtufamp- and pTX-expression vectors

The *tufA-lysM-fbaA* fusion was generated by gene synthesis (Geneart, Regensburg) and digested with *Pst*I and *Sac*I (Thermo Scientific, St. Leon-Roth) and ligated with the vector pTX30 (Strauss *et al.*, 1998) replacing the xylose inducible promoter, resulting in a constitutive pTtuf expression vector. To exchange the expressed genes, an upstream *Xho*I site and a downstream *Sac*I site was added. The *Shine Dalgarno* sequence 5′-AGGAGGT-3 was used for proper expression of the inserted genes. For the overexpression of *LysM-mCherry-strep* and *LysM-$L_{1,2}$-mCherry-strep*, pTX30 was digested with *Bam*HI and *Sac*I, the gene fusions *LysM-mCherry-strep* and *LysM-$L_{1,2}$-mCherry-strep* processed and amplified using primers containing the suitable restriction sites (Table S1). To simplify cloning into pCtuf (Biswas *et al.*, 2006), the *E. coli* origin of replication ColE1 and an ampicillin resistance gene were introduced into the vector, the new vector was named pCtufamp (this study), in order to be able to use *E. coli* as intermediary cloning host. The vector was linearized using *Pac*I and *Hind*III restriction endonucleases, and cloning was performed using Gibson Assembly (Gibson, 2009).

Purification of LysM-mCherry and LysM-$L_{1,2}$-mCherry

SA113Δspa containing the plasmids pTX-*lysM-mch* and pTX-*LysM-$L_{1,2}$-mCherry* were inoculated to an $OD_{578} \approx 0.1$ and grown for 2 h at 37°C to reach an $OD_{578} \approx 0.4$. Expression was induced by addition of 0.5% xylose. The cells were grown for 12 h at 30°C, harvested by centrifugation (7000 × *g* for 10 min) and washed twice in PBS (Biochrom). Pellets were resuspended in PBS, containing cOmplete protease inhibitor cocktail (Roche, Grenzach-Wyhlen) and broken down with glass beads (Roth, Karlsruhe) using FastPrep FP120 (Thermo Scientific, St. Leon-Roth), which then were centrifuged (17 000 × *g* for 5 min) to pellet the cell debris. The supernatant, containing the cytoplasmic fractions, was collected and mixed with pre-equilibrated StrepTactin Superflow resin (IBA, Goettingen) and incubated for 10 min at 4°C to allow the tagged protein to bind to the resin. The resin/protein mixture was then poured into an empty column and further treated as described by the manufacturer. Fractions were collected and analyzed by SDS-PAGE (Schagger and von Jagow, 1987).

Preparation of PGN

Polymeric PGN was isolated from SA113Δ*spa* according to de Jonge *et al.* (1992) with slight modifications. Briefly, cells were grown until $OD_{578nm} \approx 0.7$ and harvested by centrifugation at 3000 × *g* for 30 min, boiled with 5% SDS for 30 min and broken with glass beads. Insoluble polymeric PGN was harvested by centrifugation at 30 000 × *g* for 30 min and washed several times with lukewarm water to remove SDS. Broken cell walls were suspended in 100 mM Tris-HCl, pH 7.2, and treated first with 10 µg ml^{-1} DNase (Sigma, Munich) and 50 µg ml^{-1} RNase (Sigma, Munich) for 2 h and afterward with 100 µg ml^{-1} trypsin for 16 h at 37°C. After

enzyme deactivation and repeated washing with water, the PGN preparation was incubated with 48% hydrofluoric acid (HFA) for 48 h at 4°C to remove WTAs. PGN was harvested by centrifugation at 30 000 × *g* for 30 min and washed several times with water until complete removal of HFA.

Remazol Brilliant Blue PGN degradation assay with mutanolysin PGN labeling with RBB and mutanolysin protection assay

Isolated PGN was labeled with Remazol Brilliant Blue (RBB) (Sigma, Munich) as described by (Uehara *et al.*, 2010). PGN was incubated with 20 mM RBB in 0.25 M NaOH overnight at 37°C. The preparation was neutralized with HCl, and RBB-labeled PGN was pelleted by centrifugation (20 000 × *g*, 20 min at RT). The pellet was subsequently washed with water repeatedly until the supernatant remained clear. A measure of 0.5 ml of RBB-labeled PGN suspension was incubated at 37°C for 30 min with mutanolysin in PBS buffer (10 mM Na_2HPO_4, 2 mM KH_2PO_4, 137 mM NaCl and 2.7 mM KCl, pH 7.4) with and without the addition of LysM-$L_{1,2}$-mCh. The amount of released dye was measured by its absorption at 595 nm.

Native PAGE for PGN binding of LysM-mCherry and LysM-$L_{1,2}$-mCherry

Proteins were analyzed with SERVA*Gel*™ TG PRiME™ 12% Tris-Glycine Gels (Serva, Heidelberg). The protein samples were then mixed with an adequate amount of prepared PGN samples and incubated at RT for 10 min and subsequently mixed with 3 × native PAGE sample buffer and applied to the gel. Electrophoresis was performed by using a standard Tris/Glycine buffer system 0.25 mM Tris (Roth, Karlsruhe) and 0.192 M Glycine (Sigma, Munich) for 45 min at a constant 125 V for one gel. The gels were then stained with Coomassie blue staining solution for 20–30 min and afterward destained in destaining solution (10% ethanol 10% acetic acid in H_2O) for additional 30–60 min.

Localization of the excreted aldolase via immunofluorescence

For immunofluorescence microscopy, staphylococcal strains were grown aerobically until mid-exponential phase with appropriate antibiotic, then harvested by centrifugation, and washed twice with PBS. Cells were blocked with 3% BSA (Sigma, Munich) in PBS for 30 min at RT, followed by incubation with rabbit α-aldolase or α-enolase primary antibody (1:200) for 1 h at RT, washed twice with PBS and incubated with Cy3 (Sigma, Munich) conjugated goat α-rabbit IgG (1:1000) for 1 h at RT. Cells were then washed twice with 1 ml of PBS, and resuspended in 500 µl PBS. Cell suspensions (5 µl) were applied to poly-L-lysine coated glass slides (Sigma, Munich) and viewed with a Leica fluorescence microscope (Leica, Wetzlar, Germany).

Electron microscopy studies

Cells were cultivated for 5 h in BM, washed twice in PBS and subsequently fixed with 2% paraformaldehyde/0.05% glutaraldehyde in 0.1 M phosphate buffer pH 7.4, for 2 h at RT, washed two times in 0.1% glycine. Sample fixation and preparation by cryosectioning according to Tokuyasu (Tokuyasu, 1973). Briefly, the pellets were mixed with 10% warm gelatin and solidified on ice. This solid mixtures were cut into blocks of about 1 mm^3, cryoprotected in 2.3 M sucrose overnight at 4°C. The infiltrated blocks were frozen on cryosectioning stubs in liquid nitrogen. Thin sections of 55–70 nm were cut on a Leica Ultracut UCT microtome with a Reichert FCS cryo attachment and retrieved with a 1:1 mix of 2% methyl-cellulose – 2.3 M sucrose, placed on carbon/pioloform-coated EM support grids, floated upside down in PBS at 40°C before immunogold labeling.

Immunogold labeling on cryosections

Cryosections of different clones were incubated with specific primary antibodies, washed and then incubated with the secondary Goat anti-Rabbit IgG-6 nm Gold, (Jackson 111-195-144), 1:20 antibody. Sections for EM were contrasted in methyl cellulose/uranyl acetate, examined in a FEI Tecnai G2 Spirit TEM (FEI, Hillsboro, Oregon, USA) operating at 120 kV. Images were taken with a Gatan Ultrascan 4000 (Pleasanton, CA, USA) camera at maximum resolution using the manufacturer's software.

Fluorescence microscopy

Bacterial samples taken at OD_{578} of 1.0 were mixed with 1 µg ml^{-1} BODIPY® FL vancomycin (Invitrogen) and incubated for 5 min in dark. Five microliters of cell suspension was applied to glass slide covered with 1% agarose. Fluorescent microscopy was performed with Leica DM5500 B Upright microscope. Images were captured by Leica DFC360 FX high-sensitivity monochrome digital camera.

Acknowledgements

We thank Regine Stemmler for the expert technical help; Karl Forchhammer, Waldemar Hauf and Alexander Klotz for assistance in Leica fluorescence microscope. The German Research Foundation supported this work (SFB766 to F.G.)

References

Agarwal, V., Hammerschmidt, S., Malm, S., Bergmann, S., Riesbeck, K., and Blom, A.M. (2012) Enolase of *Streptococcus pneumoniae* binds human complement inhibitor C4b-binding protein and contributes to complement evasion. *J Immunol* **189:** 3575–3584.

Banning, N., Toze, S., and Mee, B.J. (2002) *Escherichia coli* survival in groundwater and effluent measured using a combination of propidium iodide and the green fluorescent protein. *J Appl Microbiol* **93:** 69–76.

Bateman, A., and Bycroft, M. (2000) The structure of a LysM domain from *E. coli* membrane-bound lytic murein transglycosylase D (MltD). *J Mol Biol* **299:** 1113–1119.

Berks, B.C., Palmer, T., and Sargent, F. (2005) Protein targeting by the bacterial twin-arginine translocation (Tat) pathway. *Curr Opin Microbiol* **8:** 174–181.

Biswas, R., Voggu, L., Simon, U.K., Hentschel, P., Thumm, G., and Götz, F. (2006) Activity of the major staphylococcal autolysin Atl. *FEMS Microbiol Lett* **259:** 260–268.

Boel, G., Pichereau, V., Mijakovic, I., Maze, A., Poncet, S., Gillet, S., *et al.* (2004) Is 2-phosphoglycerate-dependent automodification of bacterial enolases implicated in their export? *J Mol Biol* **337:** 485–496.

Bogsch, E.G., Sargent, F., Stanley, N.R., Berks, B.C., Robinson, C., and Palmer, T. (1998) An essential component of a novel bacterial protein export system with homologues in plastids and mitochondria. *J Biol Chem* **273:** 18003–18006.

Courtney, H.S., Dale, J.B., and Hasty, D.L. (1996) Differential effects of the streptococcal fibronectin-binding protein, FBP54, on adhesion of group A streptococci to human buccal cells and HEp-2 tissue culture cells. *Infect Immun* **64:** 2415–2419.

Dramsi, S., Bourdichon, F., Cabanes, D., Lecuit, M., Fsihi, H., and Cossart, P. (2004) FbpA, a novel multifunctional *Listeria monocytogenes* virulence factor. *Mol Microbiol* **53:** 639–649.

Driessen, A.J., and Nouwen, N. (2008) Protein translocation across the bacterial cytoplasmic membrane. *Annu Rev Biochem* **77:** 643–667.

Egea, L., Aguilera, L., Gimenez, R., Sorolla, M.A., Aguilar, J., Badia, J., and Baldoma, L. (2007) Role of secreted glyceraldehyde-3-phosphate dehydrogenase in the infection mechanism of enterohemorrhagic and enteropathogenic *Escherichia coli*: interaction of the extracellular enzyme with human plasminogen and fibrinogen. *Int J Biochem Cell Biol* **39:** 1190–1203.

Foulston, L., Elsholz, A.K., DeFrancesco, A.S., and Losick, R. (2014) The extracellular matrix of *Staphylococcus aureus* biofilms comprises cytoplasmic proteins that associate with the cell surface in response to decreasing pH. *mBio* **5:** e01667-14.

Frankel, M.B., Hendrickx, A.P., Missiakas, D.M., and Schneewind, O. (2011) LytN, a murein hydrolase in the cross-wall compartment of *Staphylococcus aureus*, is involved in proper bacterial growth and envelope assembly. *J Biol Chem* **286:** 32593–32605.

Gibson, D.G. (2009) Synthesis of DNA fragments in yeast by one-step assembly of overlapping oligonucleotides. *Nucleic Acids Res* **37:** 6984–6990.

Giesbrecht, P., Kersten, T., Maidhof, H., and Wecke, J. (1998) Staphylococcal cell wall: morphogenesis and fatal variations in the presence of penicillin. *Microbiol Mol Biol Rev* **62:** 1371–1414.

Glowalla, E., Tosetti, B., Kronke, M., and Krut, O. (2009) Proteomics-based identification of anchorless cell wall proteins as vaccine candidates against *Staphylococcus aureus*. *Infect Immun* **77:** 2719–2729.

Götz, F. (2002) *Staphylococcus* and biofilms. *Mol Microbiol* **43:** 1367–1378.

Götz, F., Yu, W., Dube, L., Prax, M., and Ebner, P. (2015) Excretion of cytosolic proteins (ECP) in bacteria. *Int J Med Microbiol* **305:** 230–237.

Heilmann, C., Hartleib, J., Hussain, M.S., and Peters, G. (2005) The multifunctional *Staphylococcus aureus* autolysin aaa mediates adherence to immobilized fibrinogen and fibronectin. *Infect Immun* **73:** 4793–4802.

Henderson, B., and Martin, A. (2013) Bacterial moonlighting proteins and bacterial virulence. *Curr Top Microbiol Immunol* **358:** 155–213.

Herbert, S., Ziebandt, A.K., Ohlsen, K., Schafer, T., Hecker, M., Albrecht, D., *et al.* (2010) Repair of global regulators in *Staphylococcus aureus* 8325 and comparative analysis with other clinical isolates. *Infect Immun* **78:** 2877–2889.

Hughes, M.J., Moore, J.C., Lane, J.D., Wilson, R., Pribul, P.K., Younes, Z.N., *et al.* (2002) Identification of major outer surface proteins of *Streptococcus agalactiae*. *Infect Immun* **70:** 1254–1259.

Iordanescu, S., and Surdeanu, M. (1976) Two restriction and modification systems in *Staphylococcus aureus* NCTC8325. *J Gen Microbiol* **96:** 277–281.

Jeffery, C.J. (1999) Moonlighting proteins. *Trends Biochem Sci* **24:** 8–11.

Jepras, R.I., Carter, J., Pearson, S.C., Paul, F.E., and Wilkinson, M.J. (1995) Development of a robust flow cytometric assay for determining numbers of viable bacteria. *Appl Environ Microbiol* **61:** 2696–2701.

de Jonge, B.L., Chang, Y.S., Gage, D., and Tomasz, A. (1992) Peptidoglycan composition of a highly methicillin-resistant *Staphylococcus aureus* strain. The role of penicillin binding protein 2A. *J Biol Chem* **267:** 11248–11254.

Kohler, T., Weidenmaier, C., and Peschel, A. (2009) Wall teichoic acid protects *Staphylococcus aureus* against antimicrobial fatty acids from human skin. *J Bacteriol* **191:** 4482–4484.

Kusch, H., and Engelmann, S. (2014) Secrets of the secretome in *Staphylococcus aureus*. *Int J Med Microbiol* **304:** 133–141.

Leibig, M., Liebeke, M., Mader, D., Lalk, M., Peschel, A., and Götz, F. (2011) Pyruvate formate lyase acts as a formate supplier for metabolic processes during anaerobiosis in *Staphylococcus aureus*. *J Bacteriol* **193:** 952–962.

Leo, J.C., Oberhettinger, P., Chaubey, M., Schutz, M., Kühner, D., Bertsche, U., *et al.* (2015) The Intimin periplasmic domain mediates dimerisation and binding to peptidoglycan. *Mol Microbiol* **95:** 80–100.

Li, M., Rosenshine, I., Tung, S.L., Wang, X.H., Friedberg, D., Hew, C.L., and Leung, K.Y. (2004) Comparative proteomic analysis of extracellular proteins of enterohemorrhagic and enteropathogenic *Escherichia coli* strains and their ihf and ler mutants. *Appl Environ Microbiol* **70:** 5274–5282.

McAleese, F.M., Walsh, E.J., Sieprawska, M., Potempa, J., and Foster, T.J. (2001) Loss of clumping factor B fibrinogen binding activity by *Staphylococcus aureus* involves cessation of transcription, shedding and cleavage by metalloprotease. *J Biol Chem* **276:** 29969–29978.

Monk, I.R., Shah, I.M., Xu, M., Tan, M.W., and Foster, T.J. (2012) Transforming the untransformable: application of direct transformation to manipulate genetically *Staphylococcus aureus* and *Staphylococcus epidermidis*. *mBio* **3:** e00277-11.

Oliveira, L., Madureira, P., Andrade, E.B., Bouaboud, A., Morello, E., Ferreira, P., *et al.* (2012) Group B streptococcus GAPDH is released upon cell lysis, associates with bacterial surface, and induces apoptosis in murine macrophages. *PLoS ONE* **7:** e29963.

Pancholi, V., and Fischetti, V.A. (1993) Glyceraldehyde-3-phosphate dehydrogenase on the surface of group A strep-

tococci is also an ADP-ribosylating enzyme. *Proc Natl Acad Sci USA* **90:** 8154–8158.
Pancholi, V., and Fischetti, V.A. (1998) Alpha-enolase, a novel strong plasmin(ogen) binding protein on the surface of pathogenic streptococci. *J Biol Chem* **273:** 14503–14515.
Pasztor, L., Ziebandt, A.K., Nega, M., Schlag, M., Haase, S., Franz-Wachtel, M., *et al.* (2010) Staphylococcal major autolysin (atl) is involved in excretion of cytoplasmic proteins. *J Biol Chem* **285:** 36794–36803.
Reed, S.B., Wesson, C.A., Liou, L.E., Trumble, W.R., Schlievert, P.M., Bohach, G.A., and Bayles, K.W. (2001) Molecular characterization of a novel *Staphylococcus aureus* serine protease operon. *Infect Immun* **69:** 1521–1527.
Rothfield, L., and Finkelstein, A. (1968) Membrane biochemistry. *Annu Rev Biochem* **37:** 463–496.
Schagger, H., and von Jagow, G. (1987) Tricine-sodium dodecyl sulfate-polyacrylamide gel electrophoresis for the separation of proteins in the range from 1 to 100 kDa. *Anal Biochem* **166:** 368–379.
Schlag, M., Biswas, R., Krismer, B., Köhler, T., Zoll, S., Yu, W., *et al.* (2010) Role of staphylococcal wall teichoic acid in targeting the major autolysin Atl. *Mol Microbiol* **75:** 864–873.
Schwarz, H., and Humbel, B.M. (2014) Correlative light and electron microscopy using immunolabeled sections. *Methods Mol Biol* **1117:** 559–592.
Shaw, L., Golonka, E., Potempa, J., and Foster, S.J. (2004) The role and regulation of the extracellular proteases of *Staphylococcus aureus*. *Microbiology* **150:** 217–228.
Sibbald, M.J., Ziebandt, A.K., Engelmann, S., Hecker, M., de Jong, A., Harmsen, H.J., *et al.* (2006) Mapping the pathways to staphylococcal pathogenesis by comparative secretomics. *Microbiol Mol Biol Rev* **70:** 755–788.
Sibbald, M.J., Winter, T., van der Kooi-Pol, M.M., Buist, G., Tsompanidou, E., Bosma, T., *et al.* (2010) Synthetic effects of secG and secY2 mutations on exoproteome biogenesis in *Staphylococcus aureus*. *J Bacteriol* **192:** 3788–3800.
Sloan, I.S., Horowitz, P.M., and Chirgwin, J.M. (1994) Rapid secretion by a non-classical pathway of overexpressed mammalian mitochondrial rhodanese. *J Biol Chem* **269:** 27625–27630.
Smith, E.J., Corrigan, R.M., van der Sluis, T., Grundling, A., Speziale, P., Geoghegan, J.A., and Foster, T.J. (2012) The immune evasion protein Sbi of *Staphylococcus aureus* occurs both extracellularly and anchored to the cell envelope by binding lipoteichoic acid. *Mol Microbiol* **83:** 789–804.
Strauss, A., Thumm, G., and Götz, F. (1998) Influence of Lif, the lysostaphin immunity factor, on acceptors of surface proteins and cell wall sorting efficiency in *Staphylococcus carnosus*. *J Bacteriol* **180:** 4960–4962.
Suvorov, A.N., Flores, A.E., and Ferrieri, P. (1997) Cloning of the glutamine synthetase gene from group B streptococci. *Infect Immun* **65:** 191–196.
Tjalsma, H., Antelmann, H., Jongbloed, J.D., Braun, P.G., Darmon, E., Dorenbos, R., *et al.* (2004) Proteomics of protein secretion by *Bacillus subtilis*: separating the 'secrets' of the secretome. *Microbiol Mol Biol Rev* **68:** 207–233.
Tokuyasu, K.T. (1973) A technique for ultracryotomy of cell suspensions and tissues. *J Cell Biol* **57:** 551–565.
Tunio, S.A., Oldfield, N.J., Berry, A., Ala'Aldeen, D.A., Wooldridge, K.G., and Turner, D.P. (2010) The moonlighting protein fructose-1, 6-bisphosphate aldolase of *Neisseria meningitidis*: surface localization and role in host cell adhesion. *Mol Microbiol* **76:** 605–615.
Uehara, T., Parzych, K.R., Dinh, T., and Bernhardt, T.G. (2010) Daughter cell separation is controlled by cytokinetic ring-activated cell wall hydrolysis. *EMBO J* **29:** 1412–1422.
Wang, G., Chen, H., Xia, Y., Cui, J., Gu, Z., Song, Y., *et al.* (2013) How are the non-classically secreted bacterial proteins released into the extracellular milieu? *Curr Microbiol* **67:** 688–695.
Weidenmaier, C., Kokai-Kun, J.F., Kristian, S.A., Chanturiya, T., Kalbacher, H., Gross, M., *et al.* (2004) Role of teichoic acids in *Staphylococcus aureus* nasal colonization, a major risk factor in nosocomial infections. *Nat Med* **10:** 243–245.
Wilkins, M.R., Gasteiger, E., Bairoch, A., Sanchez, J.C., Williams, K.L., Appel, R.D., and Hochstrasser, D.F. (1999) Protein identification and analysis tools in the ExPASy server. *Methods Mol Biol* **112:** 531–552.
Xia, X.X., Han, M.J., Lee, S.Y., and Yoo, J.S. (2008) Comparison of the extracellular proteomes of *Escherichia coli* B and K-12 strains during high cell density cultivation. *Proteomics* **8:** 2089–2103.
Yang, C.K., Ewis, H.E., Zhang, X., Lu, C.D., Hu, H.J., Pan, Y., *et al.* (2011) Nonclassical protein secretion by *Bacillus subtilis* in the stationary phase is not due to cell lysis. *J Bacteriol* **193:** 5607–5615.
Yang, C.K., Zhang, X.Z., Lu, C.D., and Tai, P.C. (2014) An internal hydrophobic helical domain of *Bacillus subtilis* enolase is essential but not sufficient as a non-cleavable signal for its secretion. *Biochem Biophys Res Commun* **446:** 901–905.
Ythier, M., Resch, G., Waridel, P., Panchaud, A., Gfeller, A., Majcherczyk, P., *et al.* (2012) Proteomic and transcriptomic profiling of *Staphylococcus aureus* surface LPXTG-proteins: correlation with agr genotypes and adherence phenotypes. *Mol Cell Proteomics* **11:** 1123–1139.
Zhang, L., Jacobsson, K., Vasi, J., Lindberg, M., and Frykberg, L. (1998) A second IgG-binding protein in *Staphylococcus aureus*. *Microbiology* **144** (Part 4): 985–991.
Ziebandt, A.K., Becher, D., Ohlsen, K., Hacker, J., Hecker, M., and Engelmann, S. (2004) The influence of agr and sigmaB in growth phase dependent regulation of virulence factors in *Staphylococcus aureus*. *Proteomics* **4:** 3034–3047.
Zoll, S., Schlag, M., Shkumatov, A.V., Rautenberg, M., Svergun, D.I., Götz, F., and Stehle, T. (2012) Ligand-binding properties and conformational dynamics of autolysin repeat domains in staphylococcal cell wall recognition. *J Bacteriol* **194:** 3789–3802.

Supporting information

Additional supporting information may be found in the online version of this article at the publisher's web-site.

AMERICAN SOCIETY FOR MICROBIOLOGY | Infection and Immunity

Excreted Cytoplasmic Proteins Contribute to Pathogenicity in *Staphylococcus aureus*

Patrick Ebner,[a] Janina Rinker,[a] Minh Thu Nguyen,[a] Peter Popella,[a] Mulugeta Nega,[a] Arif Luqman,[a] Birgit Schittek,[b] Moreno Di Marco,[c] Stefan Stevanovic,[c] Friedrich Götz[a]

Microbial Genetics, Interfaculty Institute of Microbiology and Infection Medicine, University of Tübingen, Tübingen, Germany[a]; Department of Dermatology, University of Tübingen, Tübingen, Germany[b]; Department of Immunology, Interfaculty Institute for Cell Biology, University of Tübingen, Tübingen, Germany[c]

Excretion of cytoplasmic proteins in pro- and eukaryotes, also referred to as "nonclassical protein export," is a well-known phenomenon. However, comparatively little is known about the role of the excreted proteins in relation to pathogenicity. Here, the impact of two excreted glycolytic enzymes, aldolase (FbaA) and glyceraldehyde-3-phosphate dehydrogenase (GAPDH), on pathogenicity was investigated in *Staphylococcus aureus*. Both enzymes bound to certain host matrix proteins and enhanced adherence of the bacterial cells to host cells but caused a decrease in host cell invasion. FbaA and GAPDH also bound to the cell surfaces of staphylococcal cells by interaction with the major autolysin, Atl, that is involved in host cell internalization. Surprisingly, FbaA showed high cytotoxicity to both MonoMac 6 (MM6) and HaCaT cells, while GAPDH was cytotoxic only for MM6 cells. Finally, the contribution of external FbaA and GAPDH to *S. aureus* pathogenicity was confirmed in an insect infection model.

Excretion of *c*ytosolic *p*roteins (ECP) has been reported in bacteria and eukaryotes. As none of the classical signal peptide (SP)-dependent or SP-independent pathways could be associated until now with ECP, it has also been referred to as "nonclassical protein export" (1). It is hotly debated whether the release of such proteins is due to cell lysis or whether they are exported by a presently unknown mechanism (2). One of the first reports that typical cytoplasmic proteins are found on the bacterial cell surface came from Pancholi and Fischetti (3). They found that the glyceraldehyde-3-phosphate dehydrogenase (GAPDH) is present not only at the cell surface of pathogenic streptococcal groups (3) but also in the supernatant of various bacteria, fungi, and even protozoans (4). GAPDH is a very "sticky" protein as it binds to various human proteins, including plasminogen (5–7), lysozyme, myosin, actin, fibronectin (3), and PAR/CD87 on pharyngeal cells (8). It also stimulates B lymphocytes and induces early interleukin-10 (IL-10) production that facilitates host colonization (9). In group B streptococci (GBS) GAPDH acts as an inducer of apoptosis of murine macrophages (10). Moreover, in enterohemorrhagic and enteropathogenic *Escherichia coli*, GAPDH was exposed on the surface, where it binds to human plasminogen and fibrinogen, suggesting a role in pathogenesis (11).

For ECP in eukaryotes, the term "moonlighting proteins" has also been coined (12). Moonlighting refers to a single protein that has multiple functions. For example, the mammalian thymidine phosphorylase catalyzes the intracellular dephosphorylation of thymidine but acts outside as a platelet-derived endothelial cell growth factor, which stimulates endothelial cell growth and chemotaxis (12). The glycolytic enzymes GAPDH and enolase and the cell stress proteins chaperonin 60, Hsp70, and peptidyl prolyl isomerase are among the most common of the bacterial moonlighting proteins. They play a role in bacterial virulence since they are involved in adhesion and modulation of cell signaling processes. An overview of moonlighting proteins deriving from bacteria and their role in bacterial virulence is given by Henderson and Martin (13). Such multifunctional proteins are typical for living cells and represent evolutionarily ancient proteins.

Secretome analysis of *Staphylococcus aureus* showed that there are also typical cytosolic proteins (CPs) in the culture supernatant (14–16). How these CPs are excreted is still not known. Cell lysis has been postulated, and indeed when the cell wall structure is altered in such a way that the cross-linking is affected, a higher release of CPs is observed (17); in a major autolysin (Atl) mutant there is almost no ECP (18). There are, however, good arguments speaking against the hypothesis that ECP is caused only by cell lysis. One of the main arguments is that only certain CPs were excreted, while others, although highly abundant in the cytoplasm, were not found extracellularly, suggesting that there is a selection principle at work (18). Studying the excretion pattern of cytoplasmic proteins using two glycolytic model enzymes, aldolase (FbaA) and enolase (Eno), showed that they are excreted mainly during the exponential growth phase in *S. aureus* and that the exit site is the septal cleft of dividing cells (19). Another typical excreted CP is the glyceraldehyde-3-phosphate dehydrogenase (GAPDH), which is, like FbaA, an essential enzyme in glycolysis of *S. aureus* (18, 20, 21).

Here, we investigated the role of the excreted glycolytic enzymes FbaA and GAPDH in staphylococci. Application of the two proteins enhanced adherence of *S. aureus* to host cells but the proteins also adhered to the staphylococcal cell surface via binding to the major autolysin, Atl. However, the most striking activity was their cyto-

Received 13 February 2016 **Returned for modification** 10 March 2016
Accepted 13 March 2016
Accepted manuscript posted online 21 March 2016
Citation Ebner P, Rinker J, Nguyen MT, Popella P, Nega M, Luqman A, Schittek B, Di Marco M, Stevanovic S, Götz F. 2016. Excreted cytoplasmic proteins contribute to pathogenicity in *Staphylococcus aureus*. Infect Immun 84:1672–1681. doi:10.1128/IAI.00138-16.
Editor: A. Camilli
Address correspondence to Friedrich Götz, friedrich.goetz@uni-tuebingen.de.
Supplemental material for this article may be found at http://dx.doi.org/10.1128/IAI.00138-16.

toxicity for monocytes and HaCaT cells and their contribution to the killing of worms in a *Galleria mellonella* infection model.

MATERIALS AND METHODS

Bacterial strains and growth conditions. The strains used in this study are listed in Table S1 in the supplemental material. Most of the studies were carried out with *S. aureus* USA300 JE2 (22), which is cured from the three plasmids present in the parent strain USA300 LAC (23), a highly characterized community-associated methicillin-resistant *S. aureus* (MRSA) strain isolated from the Los Angeles County jail. USA300 JE2 and mutants thereof from the Nebraska Transposon Mutant Library (NTML) were obtained from Ken Bayles, Department of Pathology and Microbiology, University of Nebraska Medical Center. Construction of *spa* (protein A) deletion mutants in *S. aureus* strains (Δ*spa* strains) was performed using allelic replacement as described by Bae and Schneewind (24). Briefly, ≈2 kb upstream and ≈1 kb downstream of *spa* were amplified by PCR and ligated to pBASE6 (25) using Gibson assembly (26). The strains of interest were then transformed with the resulting plasmid, pBASE-Δ*spa*. *Staphylococcal* strains and *Escherichia coli* strains DC10B and M15 (27) were cultivated at 37°C and with shaking in tryptic soy broth (TSB) and LB, respectively. When appropriate, the medium was supplemented with either 10 μg/ml chloramphenicol for staphylococcal species and 100 μg/ml ampicillin and 25 μg/ml kanamycin for *E. coli*.

Western blot analysis of cytoplasmic fractions, cell wall-associated proteins, and culture supernatant of staphylococcal strains. Cell wall-associated proteins were isolated by boiling SA113 Δ*spa* Δ*srtA* and SA113 Δ*spa* Δ*atlA* cells in sample buffer containing β-mercaptoethanol for 7 min. Subsequently cells were pelleted by centrifugation, and supernatant was applied to SDS-PAGE gels. Preparation of cytoplasmic proteins, enrichment of extracellular proteins, and Western blot analyses were performed as described by Ebner et al. (19).

Quantification of FbaA in the cytoplasm and supernatant of *S. aureus*. Staphylococcal cultures were grown in basic medium (BM) overnight at 37°C. The cells and supernatants were harvested by applying cells at the same optical densities (optical density at 578 nm [OD_{578}] of 9) and subsequent centrifugation. Supernatant proteins were enriched as described above and analyzed by Western blotting. A standard curve was performed with serial dilutions of purified FbaA, which was used as an internal standard on every blot. Quantification was carried out by comparing the band intensities using ImageJ software.

Purification of FbaA, GAPDH, mCherry, FbaA-mCherry, GAPDH-mCherry, AM, AM-R1/2, and GL. SA113 Δ*spa* containing the plasmids pCtufamp-*fbaA* and pCtufamp-*gapdh* and *E. coli* DC10B containing the plasmids pCtufamp-mCh (where mCh indicates mCherry), pCtufamp-*fbaA*-mCh, and pCtufamp-*gapdh*-mCh were inoculated to an OD_{578} of ≈0.1 and grown overnight at 37°C. The cells were harvested by centrifugation (7,000 × g for 10 min) and washed twice in phosphate-buffered saline (PBS; Biochrom). Pellets were resuspended in PBS containing complete protease inhibitor cocktail (Roche, Grenzach-Wyhlen, Germany), broken with glass beads (Roth, Karlsruhe, Germany) using a FastPrep FP120 instrument (Thermo Scientific, St. Leon-Rot, Germany), and then subjected to centrifugation (17000 × *g* for 15 min) to pellet the cell debris. The supernatant containing the cytoplasmic fractions was collected and mixed with preequilibrated Strep-Tactin Superflow resin (IBA, Goettingen, Germany) and incubated for 10 min at 4°C to allow the tagged protein to bind to the resin. The resin-protein mixture was then poured into an empty column and further treated as described by the manufacturer. The His-tagged Atl fragments were composed of the amidase and the two repeats R1 and R2 (AM-R1/2); R1/2 comprises only the repeat sequences R1 and R2, AM comprises only the amidase domain without repeats R1 and R2, and, finally, GL comprises the glucosaminidase domain (28, 29). These proteins were expressed in *E. coli* M15 using the isopropyl-β-D-thiogalactopyranoside (IPTG)-inducible plasmid pEQ30 and purified using Ni-nitrilotriacetic acid (NTA) Superflow resin (Qiagen, Hilden, Germany). Purification of the proteins was performed as described by the manufacturer.

Binding of mCherry, FbaA-mCherry, and GAPDH-mCherry to staphylococcal cells. To investigate the binding of excreted proteins to staphylococcal cells, 1-ml portions of overnight cultures (16 h) of *S. aureus* JE2, respective mutants, and *Staphylococcus carnosus* TM300 were adjusted to the same OD_{578} values and washed twice with PBS. For each strain, the remaining cell pellet was resuspended in 5 ml of fresh PBS. Subsequently, 0.5 ml of each strain was incubated with 30 μg of either mCherry, FbaA-mCherry, GAPDH-mCherry, or a mixture of 15 μg of FbaA-mCherry and 15 μg of GAPDH-mCherry for 15 min at 37°C. After incubation, the staphylococcal cells were pelleted (17,000 × *g* for 2 min), and the supernatant was discarded. The pellet was washed twice in 2 ml of PBS and resuspended in 400 μl of PBS. Measurements were carried out using 200 μl in a black F-bottom microtiter plate (Greiner, Frickenhausen, Germany) using a Tecan Infinite 200 (Tecan, Männedorf, Switzerland) plate reader with a constant gain of 193 and with unstained cells as blanks.

Purification of staphylococcal PGN and binding studies of GAPDH to PGN. The purification of *S. aureus* peptidoglycan (PGN) was performed essentially as described by de Jonge et al. (30), with modifications according to Ebner et al. (19), resulting in insoluble wall teichoic acid (WTA)-free polymeric PGN. A PGN pulldown assay was performed as described by Terrasse et al. (31), with modifications. Briefly, 20 μg of GAPDH was incubated with PGN for 2 h; subsequently, the unbound protein was removed by centrifugation, and the supernatant was collected. The remaining pellet was mixed with Laemmli buffer and boiled for 10 min to elute bound protein. Subsequently, all samples were loaded on a 12% SDS-PAGE gel and immunoblotted. Detection was carried out using an anti-GAPDH antibody.

Far-Western blot analysis to study interaction of GAPDH and FbaA with extracellular matrix proteins and Atl fragments. Far-Western blot analysis was performed as described by Wu et al. (32), with modification, using the extracellular matrix proteins plasminogen (Abcam), vitronectin, fibrinogen, fibronectin, human IgG, bovine serum albumin (BSA) (all from Sigma, Munich, Germany) AM-R1/2, AM, GL, and purified GAPDH and FbaA.

Protein digestion for mass analysis. Protein spots were excised from SDS-PAGE gels and washed with 100 μl of double-distilled H_2O (ddH_2O) for 5 min (Vibrax VXR; IKA). After the ddH_2O was removed, spots were ground with gel-loading pipette tips and destained by the addition of 100 μl of 50% acetonitrile (Merck) and shaking for 5 min. Solvent was removed, and samples were dried in a SpeedVac instrument (Bachofer). A destaining procedure was performed twice or until samples were completely destained. Reduction was carried out with 2.5 μl of dithiothreitol (DTT) solution (45 mM; Merck) in 20 μl of ammonium bicarbonate buffer (25 mM) by shaking for 20 min at 55°C (Thermomixer 5436; Eppendorf). Iodoacetamide (2.5 μl; 100 mM) (Merck) was added, and samples were shaken for 20 min at room temperature. After the supernatant was removed, samples were rinsed with 50 μl of ddH_2O and dried in a SpeedVac. Twenty microliters of ammonium bicarbonate buffer (25 mM) and 5 μl of trypsin (0.5 μg, Promega) were added, and samples were digested overnight at 37°C. Supernatants were transferred into protein LoBind tubes (Eppendorf). Peptide extractions were performed twice by adding 15 μl of 50% acetonitrile–1% trifluoroacetic acid (Merck) and transferring the supernatant into the LoBind tubes. Peptide extracts were concentrated down to 30 μl and were further purified and desalted using ZipTip C_{18} pipette tips (Millipore). Extracted peptides were eluted in 35 μl of 80% acetonitrile–0.1% trifluoroacetic acid, completely dried, and resuspended in 15 μl of 1% acetonitrile–0.05% trifluoroacetic acid. Samples were stored at 4°C until analysis by liquid chromatography-tandem mass spectrometry (LC-MS/MS).

Analysis of protein digests by LC-MS/MS. Peptides were separated by reversed-phase liquid chromatography (UltiMate 3000 RSLCnano nano-ultrahigh-performance liquid chromatograph [UHPLC]) (Dionex) and

subsequently analyzed in an online-coupled linear trap quadrupole (LTQ) Orbitrap XL hybrid mass spectrometer (ThermoFisher). Sample volumes of 5 μl were injected onto a 75-μm by 2-cm trapping column (Acclaim PepMap rapid separation LC [RSLC] column; Dionex) at 4 μl/min for 5.75 min. Peptide separation was subsequently performed at 50°C and a flow rate of 175 nl/min on a 50-μm by 25-cm separation column (Acclaim PepMap RSLC; Dionex) applying a 90-min gradient ranging from 2.4 to 32.0% acetonitrile. Eluting peptides were ionized by nanospray ionization and analyzed in the mass spectrometer, implementing a top-five collision-induced dissociation (CID) method which generates fragment spectra for the five most abundant precursor ions in the survey scans. Survey scans were acquired with a resolution of 60,000 and a mass range of 300 to 2,000 *m/z*, with charge states 2+ and 3+ selected for fragmentation.

Database search and spectral annotation. Data were processed against the *Staphylococcus aureus* strain NCTC8325 proteome as contained in the Swiss-Prot database (protein sequences downloaded October 2015; 2,892 reviewed protein sequences [www.uniprot.org]) using the Mascot search engine (Mascot, version 2.2.04; Matrix Science) integrated into the Proteome Discoverer software (version 1.3; ThermoFisher). The search was restricted to tryptic peptides. Precursor mass tolerance was set to 5 ppm, and fragment mass tolerance was set to 0.5 Da. Carbamidomethyl and oxidized methionine were allowed as dynamic modifications. False discovery rates (FDR) were determined by the Percolator algorithm (33) based on processing against a decoy database consisting of the shuffled target database. The FDR was set at a target *q* value of ≤0.05 (5% FDR). Peptide-spectrum matches (PSMs) with a *q* value of ≤0.05 were filtered according to additional, orthogonal parameters to ensure spectral quality and validity. Mascot scores were filtered to ≥20.

Adherence to HEK293 and HaCaT cells. The HaCaT cells, obtained from the Department of Dermatology, University of Tübingen, were cultured in Dulbecco's modified Eagle's medium (DMEM)–high-glucose medium supplied with 10% fetal bovine serum (FBS) and 1% ZellShield at 37°C with 5% CO_2. The HEK293 cells, purchased from Invivogen, were cultured in DMEM–high-glucose medium supplemented with 10% FBS (Biochrom GmbH, Berlin, Germany), 1% glutamine, and 1% ZellShield. Prior to stimulation, 5×10^5 cells per well were seeded in a 24-well microtiter plate in 1 ml of culture medium supplemented with antibiotics and grown until confluence at 37°C with 5% CO_2. The assay was performed at a multiplicity of infection (MOI) of 30 according to Nguyen et al. (34), with addition of the protein concentrations indicated in the legend for Fig. 3. For invasion, the same experimental procedure was performed, with additional killing of adhered JE2 cells by lysostaphin treatment for 1 h prior to lysis of HaCaT cells. The experiment at an MOI of 30 resulted in too few CFU, so the MOI was increased to 100.

Cytotoxicity assay. Cytotoxicity assays of JE2-derived FbaA and GAPDH were carried out separately on MonoMac 6 (MM6), a human monocytic leukemia cell line, obtained from the DSMZ (Braunschweig, Germany), and HaCaT cells. Prior to a cytotoxicity assay, 100 μl of HaCaT cells was seeded in a 96-well microtiter plate and incubated for 2 days until the cell number reached 10^5 cells per well; for MonoMac 6 cells, 10^5 cells were seeded in a 96-well microtiter plate in 100 μl of culture medium and incubated for 1 h. Both cell lines were incubated at 37°C in 5% CO_2. Final concentrations of FbaA and GAPDH (80, 40, 20, 10, 5, and 0 μg/ml) were added to the well, and then cytotoxicity assays were performed using Cell Proliferation Kit I (MTT [3-(4,5-dimethyl-2-thiazolyl)-2,5-diphenyl-2H-tetrazolium bromide]) (Roche, Germany). Wavelengths of 570 nm and 690 nm as references were used to measure the absorbance of formed formazan (36).

***Galleria mellonella* infection model.** Larvae of *Galleria mellonella* in the final stage (R. J. Mous Live Bait, EX Balk, Netherlands) weighing between 300 and 700 mg were infected with 1×10^6 cells of *S. aureus* JE2 either untreated or with exogenously applied GAPDH and FbaA at 20 μg/ml each (37, 38). For each experiment, 10 larvae weighing between 300 and 700 mg were infected. This experiment was repeated three times with a total of 30 larvae. Bacteria grown overnight were prepared by being washed twice with PBS (140 mM NaCl, 10 mM Na_2HPO_4, 2.7 mM KCl, 1.8 mM KH_2PO_4) and adjusted to an OD_{578} of 0.1 in PBS. The injection volume for each larva was 10 μl into the last left proleg. A 500-μl Hamilton HPLC syringe and a Hamilton PB600 repeating dispenser were used for injection. After injection, the larvae were incubated at 37°C for 5 days and counted every 24 h.

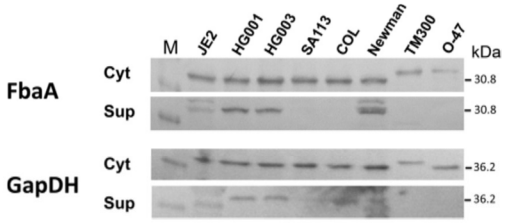

FIG 1 Immunoblotting of FbaA and GAPDH in various staphylococcal strains. Detection of FbaA and GAPDH (theoretical masses, 30.8 and 36.2 kDa, respectively) via specific anti-FbaA and anti-GAPDH antibodies in the cytoplasmic fraction (Cyt) and in the supernatant (Sup). The theoretical masses of FbaA of *S. aureus* and *S. carnosus* or *S. epidermidis* are the same; however, the migration rates are different. The same is true for GAPDH of *S. carnosus*. Lane M, molecular mass marker.

RESULTS

Excretion of FbaA and GAPDH shows a tendency to correlate with virulence. In this study, the glycolytic enzymes FbaA and GAPDH as model proteins for excreted CPs were used. We studied the excretion of these proteins in various staphylococcal strains to see whether the amount of excreted proteins correlates with the virulence of the strains. Since ECP occurs mainly during bacterial growth (19), samples were collected after 4 h (mid-exponential phase), and the relative amounts of FbaA and GAPDH in the cytoplasm (control) and culture supernatant were determined by Western blotting. The largest amounts of secreted FbaA and GAPDH were found in the Newman, HG001, HG003, and JE2 strains. FbaA was not detectable in the SA113 and COL strains or in *S. carnosus* TM300 and *S. epidermidis* O47 strains. GAPDH was highly excreted in COL and excreted to a lower extent in SA113. Like FbaA, GAPDH was hardly excreted in *S. carnosus* TM300 and *S. epidermidis* O47 (Fig. 1). There is a slight tendency that the levels of FbaA and GAPDH released are correlated with virulence. We quantified the amounts of FbaA in the culture supernatant of overnight cultures, which were 0.128 μg/ml in HG003 and 0.294 μg/ml in the Newman strain. However, in lysostaphin-lysed cells, the concentrations increased to 7.299 μg/ml in HG003 and 6.093 μg/ml in Newman (see Fig. S2 in the supplemental material).

GAPDH and FbaA bind to host matrix proteins and promote adherence to host cells. For better understanding of the role of excreted FbaA and GAPDH, we purified the proteins (Fig. 2A) and tested their binding activities to various matrix proteins, like plasminogen, vitronectin, fibrinogen, fibronectin, and BSA (Fig. 2B), by far-Western blot analyses (Fig. 2C). Both proteins bound to plasminogen and a subfragment of vitronectin and to specific fibrinogen chains, but there was no interaction with fibronectin and BSA (Fig. 2C). An overview of the binding specificity is shown in Fig. 2D.

Exogenously applied GAPDH and FbaA promote adherence to HaCaT and HEK293 cells. To investigate whether GAPDH and FbaA play a role in infection, we performed adherence and invasion assays of JE2 cells. To put the adhesion results on a broader basis, we used two different cell lines: HEK293, a human embry-

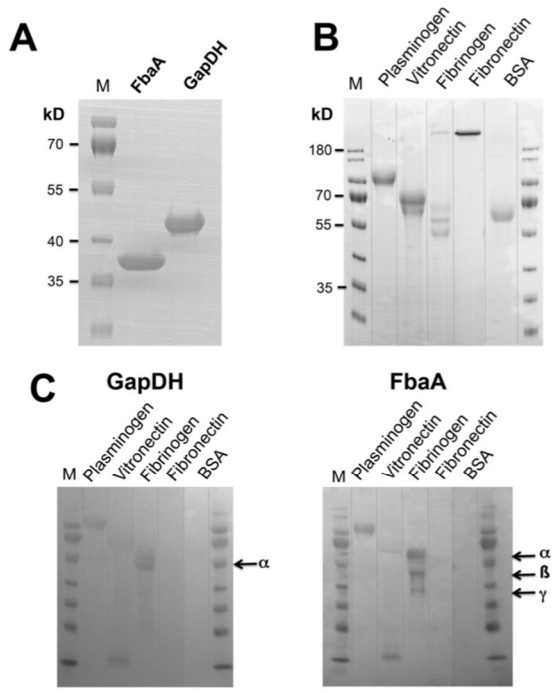

D

	Plasminogen	Vitronectin	Fibrinogen	Fibronectin	BSA
GapDH	++	-	++	-	-
FbaA	+++	+	+++	+	-

FIG 2 Interaction of FbaA and GAPDH with extracellular matrix proteins. (A) SDS-PAGE of the StrepTag-purified FbaA and GAPDH. (B) SDS-PAGE of plasminogen, vitronectin, fibrinogen, fibronectin, and BSA as a control. (C) Far-Western blot analyses of matrix proteins using purified GAPDH and FbaA as ligands. (D) Summary of the interactions between the matrix proteins and GAPDH and FbaA. The degree of interaction is indicated as follows: +++, strong; ++, intermediate; +, weak; − none. The theoretical masses of FbaA (30.8) and GAPDH (36.2 kDa) were lower than the estimated sizes in SDS-PAGE gels, which were 36 and 42 kDa, respectively. Arrows indicate the alpha, beta, and gamma chains of fibrinogen.

onic kidney cell line, and HaCaT cells, a keratinocyte cell line which has been widely used as a model of keratinocyte function (39). The adhesion assay was performed in the presence and absence of exogenously applied FbaA and GAPDH. As a basis for the adherence assays, we used H_2O, Strep-Tactin elution buffer, and BSA. The CFU count with H_2O was set to 1.0, and all CFU values were calculated relative to the H_2O control. The controls of elution buffer (1.04-fold) and BSA (0.97-fold) did not show any significant difference in adherence levels compared to the level of the H_2O control (Fig. 3A). However, in the presence of equal concentrations GAPDH and FbaA, adherence to HaCaT cells was 1.45- and 1.54-fold increased, respectively, and for HEK293 cells adherence was increased 1.23-fold with GAPDH, 1.45-fold with FbaA, and 1.63-fold with both proteins. The strongest increase in adherence, 1.78-fold, was observed in HaCaT cells in the presence of both proteins (Fig. 3A). The adherence of GAPDH and FbaA in a concentration range of 5, 10, 20, and 40 μg/ml was dose dependent (Fig. 3B); saturation was achieved with GAPDH at 40 μg/ml and with FbaA already at 10 μg/ml.

Exogenously applied FbaA and GAPDH decreased invasion into HaCaT cells. The effect of GAPDH and FbaA on invasion was investigated in HaCaT cells, an aneuploid immortal keratinocyte cell line from adult human skin. HaCaT cells were infected with JE2 (MOI of 100) in the absence and presence of GAPDH and FbaA (each, 10 μg/ml). An MOI of 100 is frequently used for *S. aureus* invasion into keratinocytes (40). While adherence to HaCaT cells was increased in the presence of both proteins (Fig. 3A), the invasion into HaCaT cells was decreased by more than 50% (Fig. 3C). We wondered why there was such a discrepancy between adherence and invasion and tried to find the reason. The primary mechanism by which *S. aureus* enters host cells is well characterized: staphylococcal fibronectin binding proteins (FnBPs) interact with cell surface α5β1 integrins via a fibronectin bridge (41). A second internalization mechanism involves the major autolysin, Atl, and heat shock cognate protein Hsc70 as a host cell receptor (42). In the following, we addressed the question of whether GAPDH and FbaA affect these two mechanisms.

Extracellular GAPDH and FbaA bind to staphylococcal cells. Above, we have shown that GAPDH and FbaA bind to plasminogen and fibrinogen but not to fibronectin and BSA (Fig. 2C), suggesting that the two proteins do not block fibronectin's interaction with the fibronectin binding proteins (FnbA and FnbB) of *S. aureus*. However, GAPDH and FbaA still might bind to the fibronectin binding proteins at the *S. aureus* surface. To investigate GAPDH and FbaA binding to the *S. aureus* surface, we constructed mCherry fusions of both proteins with mCherry as a control. The fluorescent proteins were expressed in *E. coli* and purified by Strep-Tactin resin (see Fig. S1B in the supplemental material). Their binding to the cell surface was investigated with both *S. aureus* JE2 and *S. carnosus* TM300; the two strains showed very similar binding patterns. mCherry as a control showed only low binding to the cells, while binding of the FbaA-mCherry and GAPDH-mCherry fusion proteins was on average increased 10 to 15 times (Fig. 4A). The question now was whether it was a surface protein or a cell wall component like peptidoglycan (PGN) to which FbaA-mCherry and GAPDH-mCherry fusion proteins were bound. To resolve this question, we compared binding of the proteins to JE2 cells with and without trypsin pretreatment for 2 h. Trypsin-treated cells showed a 4- to 5-fold lower binding than that of the untreated cells (Fig. 4C), suggesting that the binding partner is a surface protein.

Nevertheless, pulldown experiments with purified insoluble and WTA-free polymeric *S. aureus* peptidoglycan (PGN) were carried out. Neither FbaA nor GAPDH revealed significant binding to PGN. The amount of applied protein to PGN (Fig. 4B, load) and the amount remaining in the supernatant after 2 h of incubation (Fig. 4B, Sup) were essentially the same. When the proteins were extracted from the PGN pellet (eluate), only tiny amounts of GAPDH and FbaA were eluted (Fig. 4B). These results indicate that PGN is not the binding component, leaving the question open as to which surface protein could be the binding partner.

Extracellular GAPDH and FbaA bind to the major autolysin, Atl. To identify the staphylococcal surface protein(s) with which GAPDH and FbaA interact, far-Western blot assays were performed. The surface-associated proteins of *S. aureus* SA113 Δ*spa* Δ*srtA* were stripped off by boiling washed whole cells in sample buffer and separating the proteins by SDS-PAGE. The *srtA* deletion mutant was chosen because the surface proteins of this mu-

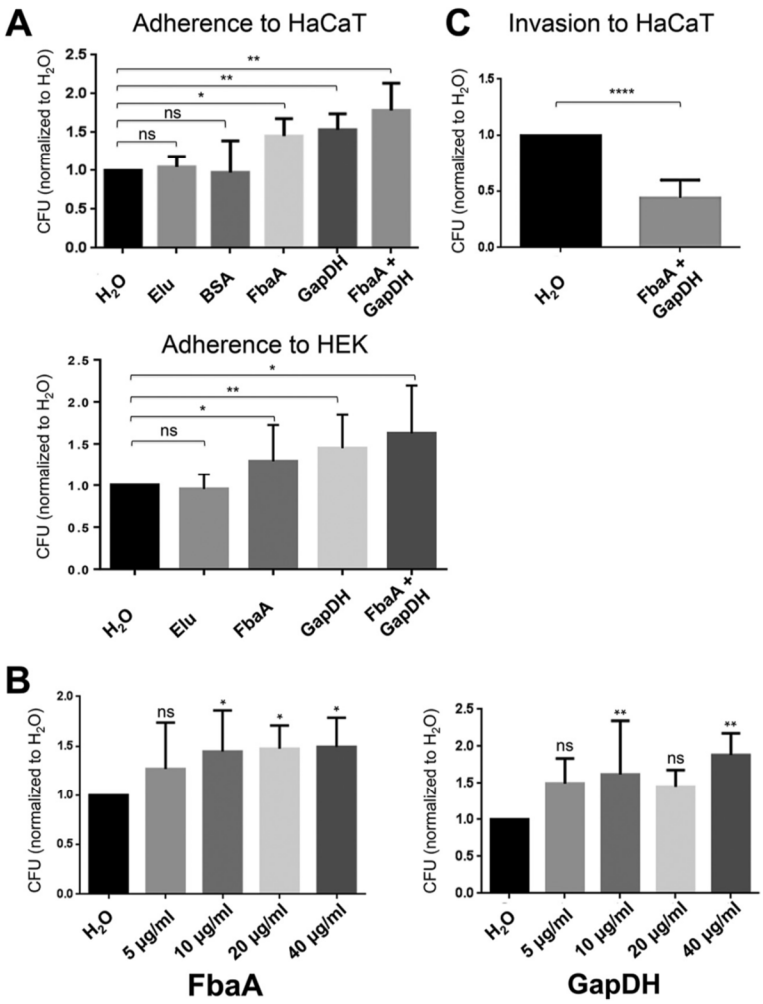

FIG 3 Impact of FbaA and GAPDH on adherence to and invasion of HaCaT cells. (A) Adherence of JE2 to HaCaT and HEK293 cells normalized to that of H_2O. Strep-Tactin elution (Elu) buffer or the addition of BSA (20 μg/ml) made no significant difference in adherence. Only the addition of GAPDH (20 μg/ml), FbaA (20 μg/ml), or GAPDH plus FbaA (each 10 μg/ml) enhanced adherence (*, $P < 0.05$; **, $P < 0.01$; Wilcoxon test). (B) Adherence of JE2 to HaCaT cells with increasing concentrations (5, 10, 20, and 40 μg/ml) of GAPDH or FbaA (*, $P < 0.05$; **, $P < 0.001$; ns, not significant, by one-way analysis of variance with a Bonferroni posttest). (C) Invasion into HaCaT cells, normalized to that of H_2O, in the presence of GAPDH and FbaA (each, 10 μg/ml) (****, $P < 0.0001$, by *t* test).

tant are not covalently bound and are therefore easier to extract from the cell wall. After the proteins were blotted, one could see in the far-Western blot with both GAPDH and FbaA bands of 65 and 55 kDa, and with GAPDH an additional weak band was visible at 130 kDa (Fig. 5A). The corresponding protein bands were cut from the SDS-PAGE gel and subjected to LC-MS/MS peptide analysis. The predominant protein found in the size range of 55, 65, and 130 kDa belonged to the major autolysin, Atl. Indeed, it has been previously shown that the approximately 130-kDa Atl precursor is processed to 60- and 52-kDa proteins (29).

To prove that Atl is the binding partner of GAPDH and FbaA, far-Western blotting was performed with surface proteins derived from the *atl* deletion mutant, SA113 Δ*atlA*. In this mutant no interaction was observed (Fig. 5A). Other evidence that Atl is the binding partner was the approximately 4-fold-decreased binding of GAPDH-mCherry to the surface of the *atl* mutant compared to that of JE2 and its *fnbA* and *fnbB* mutants (Fig. 5B).

Finally, we wondered to which Atl domain GAPDH and FbaA are binding. Again, we performed far-Western blot analysis with His-tagged Atl fragments heterologously expressed in *E. coli* and purified via Ni-NTA. The chosen Atl derivatives were AM-R1/2, composed of the amidase and the two repeats R1 and R2. R1/2 comprises only the repeat sequences R1 and R2, whereas AM is only the amidase domain without the repeats R1 and R2. Finally, GL is only the glucosaminidase domain. The far-Western blotting showed that GAPDH and FbaA bound to all Atl fragments; however, the binding to R1/2 was the strongest (Fig. 5C). The control without ligands showed no signals (see Fig. S1C in the supplemental material). Apparently, the repeats R1/2 are the major target structures of GAPDH and FbaA.

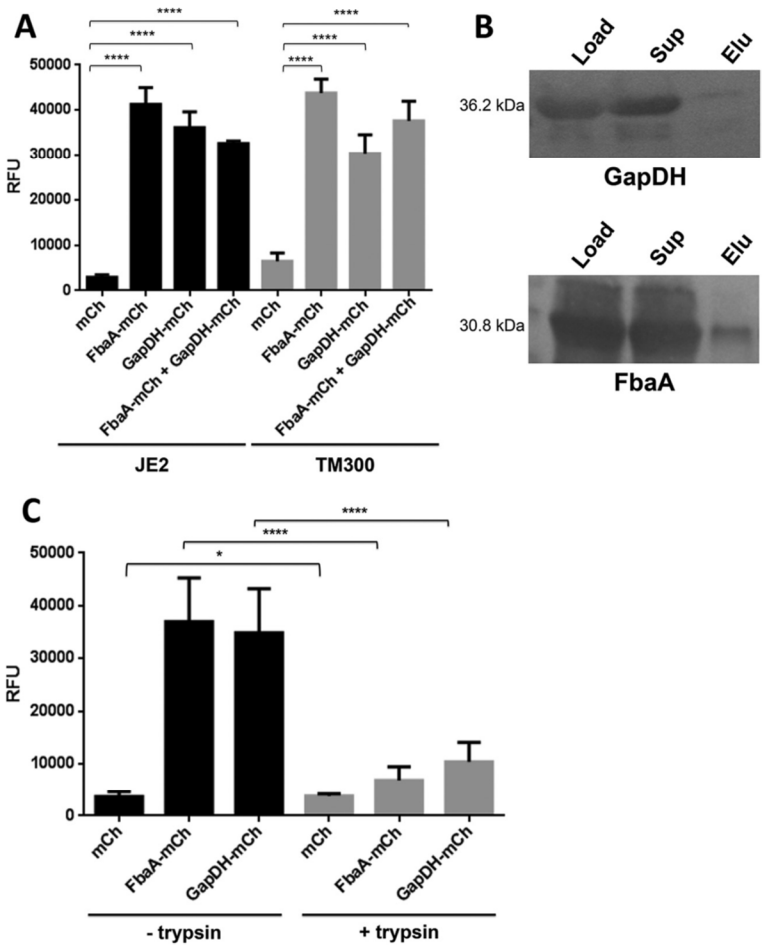

FIG 4 FbaA-mCherry and GAPDH-mCherry bind to staphylococci. (A) Binding of mCherry, FbaA-mCherry, and GAPDH-mCherry and the combination of both proteins to JE2 and *S. carnosus* TM300 cells and measurement of the relative fluorescence units (RFU) (****, $P < 0.0001$, by *t* test). (B) Binding of mCherry, FbaA-mCherry, and GAPDH-mCherry to JE2 with and without pretreatment with trypsin for 2 h and measurement of the relative fluorescence units (*, $P < 0.05$; ****, $P < 0.0001$, by *t* test). (C) Pulldown experiments for detection of the interaction between GAPDH and FbaA and staphylococcal PGN. Load, loading control (same amounts of GAPDH and FbaA as used for binding to PGN); Sup, unbound GAPDH and FbaA after incubation with PGN; Elu, GAPDH and FbaA bound to the insoluble PGN, eluted by boiling with Laemmli buffer.

FbaA and GAPDH are cytotoxic. To investigate whether the binding of FbaA and GAPDH to the matrix proteins has an effect on the host cells, we investigated cytotoxicity with the cell proliferation (MTT) assay in MonoMac 6 (MM6) cells and the keratinocyte cell line HaCaT. With MM6 cells, both proteins exerted a dose-dependent (5 to 80 μg/ml) cytotoxic effect; the toxicity of FbaA was more pronounced than that of GAPDH. At the highest concentrations of GAPDH and FbaA, viability of MM6 cells was decreased by 22% and 52%, respectively (Fig. 6A). With HaCaT cells, GAPDH had no cytotoxic effect; on the contrary, the viability of the cells even appeared increased with increasing concentrations. However, FbaA also showed a high cytotoxic effect with HaCaT cells in a range comparable to that with MM6 cells (Fig. 6B).

GAPDH and FbaA enhance virulence of *S. aureus* USA300 JE2 in a *Galleria mellonella* infection model. As external FbaA and GAPDH contribute to host cell adherence and are cytotoxic to host cells, we wondered whether exogenously applied FbaA and GAPDH also have an effect *in vivo*. To answer this question, we used a *Galleria mellonella* infection model to compare the virulence of JE2 with and without exogenously applied proteins. The percentage of survival was measured over a 5-day period. In the control group, which was injected with PBS containing FbaA and GAPDH, all larvae survived the 5-day period. The group of larvae infected with only JE2 survived the first day, with a percentage of 97%, followed by a high death rate at the second day, and after 5 days 10% still survived. Larvae infected with JE2 together with FbaA and GAPDH were significantly more rapidly killed. Only 73% survived the first day, and after 4 days 97% were killed; there was no survival after 5 days (Fig. 6C).

DISCUSSION

Excretion of cytoplasmic proteins (ECP) into the culture supernatant is a general phenomenon observed in both pro- and eukaryotes (43,

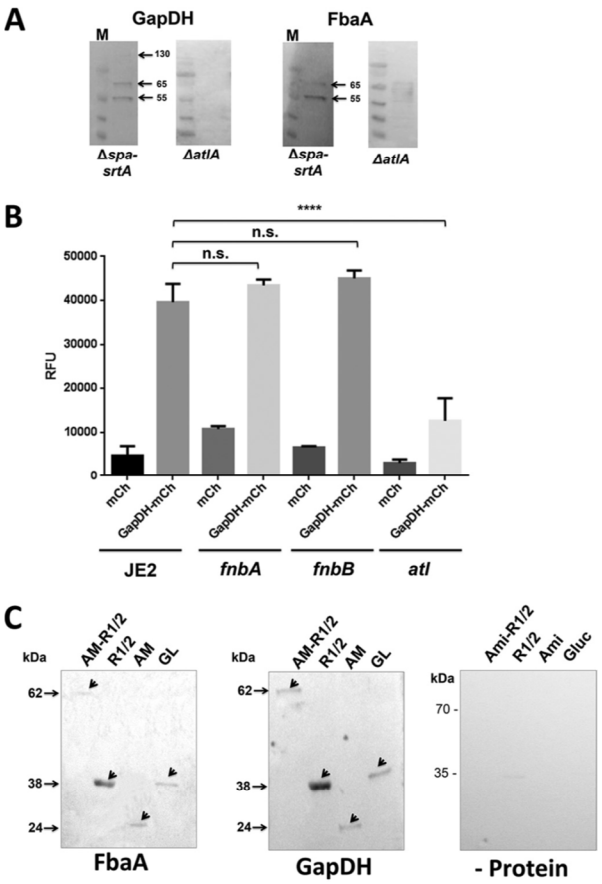

FIG 5 FbaA and GAPDH interact with subfragments of the major amidase (Atl). (A) Far-Western blotting of GAPDH and FbaA with SA113 Δ*spa* Δ*srtA* and SA113 Δ*atlA* cells. (B) Binding of mCherry and GAPDH-mCherry to JE2 as well as to its *fnbA*, *fnbB*, and *atl* transposon mutants; binding was quantified by measurement of relative fluorescence units (****, $P < 0.0001$, by *t* test). (C) Far-Western blot analyses of recombinant Atl fragments (AM-R1/2, R1/2, AM [amidase] and GL [glucosaminidase]) purified from *E. coli*. GAPDH and FbaA were used as ligands; for detection, specific anti-FbaA and anti-GAPDH antibodies were used. As a control, no bait protein was added.

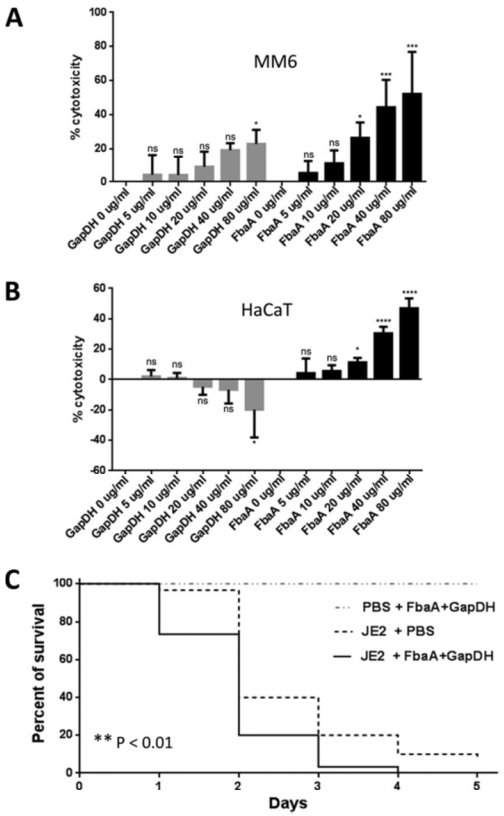

FIG 6 Cytotoxicity test of FbaA and GAPDH in MonoMac 6 and HaCaT cells and infection assay with *Galleria mellonella*. (A and B) Concentration-dependent cytotoxicity of GAPDH and FbaA in MonoMac 6 cells and HaCaT cells, as indicated. For toxicity testing Cell Proliferation Kit I (MTT) was used. ns, not significant; *, $P < 0.05$; ***, $P < 0.001$; ****, $P < 0.0001$, by one-way analysis of variance with a Bonferroni posttest. (C) Survival of *Galleria mellonella* treated with JE2 in the presence or absence of FbaA and GAPDH. Survival was followed over 5 days. Statistical significance was measured for JE2 treated with PBS and for JE2 treated with FbaA plus GAPDH (**, $P < 0.01$, by a Gehan-Breslow-Wilcoxon test; **, $P < 0.01$, by a Mantel-Cox test).

44). In particular, glycolytic enzymes, chaperones, translation factors, or enzymes involved in detoxification of reactive oxygen species (ROS) were found in the supernatants by secretome analysis (15, 45–48). However, proteome analysis alone does not reveal the potential role of excreted CPs in pathogenicity. Therefore, we concentrated here on two typical cytoplasmic proteins, the aldolase (FbaA) and the glyceraldehyde 3-phosphate dehydrogenase (GAPDH). Both proteins are glycolytic proteins, and their excretion into the supernatant has been observed in various microorganisms.

One of the first questions we asked was whether the amounts of excreted GAPDH and FbaA differ in various staphylococcal strains and species. For appropriate detection of the proteins in *S. aureus* by Western blotting, we first had to create protein A (*spa*) mutants in the corresponding strains, which is the reason why we tested only a limited number of *S. aureus* strains. However, one tendency can be seen already: the more virulent the strains, the larger the amounts of excreted proteins in the supernatant (Fig. 1).

The virulence of some of the strains has been previously investigated in a mouse sepsis model (49). In this study, *S. aureus* Newman, USA300, HG001, and HG003 showed the highest killing rates. Exactly these strains showed the largest amounts of FbaA and GAPDH in the supernatant; in JE2, a derivative of USA300, there was also a higher migrating band visible that we cannot explain at the moment. In SA113 FbaA and GAPDH were hardly detectable in the supernatant, and in COL only GAPDH was present. In the mouse sepsis model *S. aureus* COL was almost avirulent; SA113 has not been tested in this study, but it should also be attenuated as it is defective in the global regulators *agr* and *sigB* (49), which are involved in virulence. In the biofilm-forming *Staphylococcus epidermidis* O47 strain, a medium-pathogenic species, and in the nonpathogenic species representative *S. carnosus* TM300 (50), the two proteins were hardly excreted although the cytoplasmic counterparts were clearly visible. We are aware that this is only a preliminary study, but it suggests a correlation between ECP and virulence.

But how do FbaA and GAPDH contribute to virulence? We

showed that they bind to host matrix proteins like plasminogen, vitronectin, and fibrinogen, but they did not bind to fibronectin or BSA. This binding to matrix proteins is not unusual and has been observed in other microorganisms as well, such as the FbaA of mycobacteria or GAPDH and FbaA of *Candida albicans* that bind to plasminogen (51, 52). In contrast to the FbA of *S. aureus*, the *Neisseria meningitidis* FbaA is not essential for growth, but it is required for enhanced adhesion to host cells (21). This is what was also seen with FbaA and GAPDH; they increase adherence of JE2 to HaCaT and HEK293 cells by a factor of 1.5 to 1.8 (Fig. 3A and B). Surprisingly, however, in the presence of FbaA and GAPDH, invasion of JE2 into HaCaT cells was decreased by 50% (Fig. 3C). The mechanism for the enhanced adherence of FbaA and GAPDH to HaCaT and HEK293 cells is unknown. However, it was shown that the *Streptococcus pneumoniae* Fba directly interacts with the Flamingo cadherin receptor (41); maybe this interaction causes the increased adherence. Since Fba from *S. pneumoniae* shares 53% identity with the *S. aureus* FbaA, this interaction might also apply for the *S. aureus* FbaA.

We also wondered why there was such a discrepancy between adherence and invasion, and we tried to find the reason. The primary mechanism by which *S. aureus* enters host cells is well characterized: staphylococcal fibronectin binding proteins (FnBPs) interact with the host cell surface α5β1 integrin via a fibronectin bridge (41). A second internalization mechanism involves the major autolysin Atl and heat shock cognate protein Hsc70 as host cell receptors (42). In the following, the question of whether FbaA and GAPDH interfere with one of the two mechanisms was addressed. Neither FbaA nor GAPDH binds to fibronectin; therefore, one can rule out that either affects the interaction of the cell surface-bound fibronectin binding proteins (FnbA and FnbB) with fibronectin. However, neither FbaA nor GAPDH could bind to FnbA and FnbB, thus hampering binding to fibronectin. To answer this question, we investigated the binding of fluorescent GAPDH-mCherry and FbaA-mCherry to the cell surface of JE2 cells and of *S. carnosus* as a control. Both proteins showed strong binding to the cell surfaces of both bacteria. The interaction partner must be a surface protein as trypsin treatment significantly decreased binding, and peptidoglycan as a major cell wall component showed almost no interaction (Fig. 4). At this stage we also could exclude protein A and fibronectin binding proteins as interaction partners as the corresponding genes are absent in the genome of *S. carnosus* (53). Both far-Western blotting and LC-MS/MS showed that FbaA and GAPDH interact with the major autolysin, Atl, on the surface. Atl appears to be essential as in far-Western blotting with an *atl* mutant, there was no further binding partner visible. This result suggests that FbaA and GAPDH are partially excreted into the supernatant, but there is also a proportion bound to the cell wall by interaction particularly with the repeat domains of Atl (Fig. 7).

In staphylococci Atl is secreted in a *sec*-dependent manner as a bifunctional precursor that is composed of two distinct murein hydrolases, an *N*-acetylmuramyl-L-alanine amidase (AM) and a glucosaminidase (GL) (54, 55). The AM and GL domains are separated by three major repeats, R1 to R3. Following cleavage of the signal peptide, external Atl is proteolytically cleaved at two positions, after the propeptide (PP) and after repeat R2, leading to the formation of processed enzymes AM-R1-R2 and R3-GL (29). Both enzymes bind to the staphylococcal cell wall, particularly to the septum site of dividing cells (56, 57). The repeat sequences are responsible for the targeting of

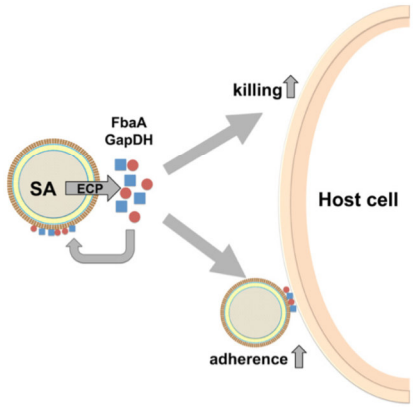

FIG 7 Model for the secondary role of FbaA and GAPDH after excretion. FbaA and GAPDH get excreted and bind to certain extracellular matrix proteins and also bind back to the staphylococcal cells via interaction with Atl and weak interaction with PGN. This affinity to both eucaryotic matrix proteins and staphylococcal surface proteins mediates adherence. SA, *S. aureus*.

the enzymes to the lipoteichoic acid (LTA) at the septum region, where amidase and a glucosaminidase catalyze the last step in cell division, the cell separation of the daughter cells, by resolving the intertwined murein sacculus (58, 59). By far-Western blotting, we could show that FbaA and GAPDH bound to all Atl fragments; however, the binding to repeat sequences R1/2 was by far the strongest (Fig. 5C). These results suggest that a fraction of FbaA and GAPDH is not excreted but is bound via interaction with Atl, particularly with its repeat domains R1-R2, at the cell surface. Atl is described as a second factor contributing to *S. aureus* and *S. epidermidis* internalization by nonprofessional phagocytes via interaction with the host heat shock cognate 71-kDa protein, Hsc70, receptor (42). Which Atl domain is interacting with Hsc70 is unknown; however, the repeat domains are likely candidates. The interaction of FbaA and GAPDH with Atl could occur during the excretion pathway and/or by back-binding of the excreted proteins to Atl. In any case, interference of FbaA and GAPDH with the Atl-Hsc70 internalization pathway is an explanation for the decreased host cell internalization.

Another question was whether excreted FbaA and GAPDH have an effect on host cells. To our great surprise, FbaA showed comparatively high cytotoxicity to both MM6 and HaCaT cells, while GAPDH was cytotoxic only for MM6 cells (Fig. 6A and B). For GAPDH of group B streptococci (GBS) and *S. pyogenes*, it has been previously described that they induce apoptosis in murine macrophages (10). How the two, seemingly harmless, glycolytic enzymes FbaA and GAPDH affect the viability of host cells is unclear. An explanation for the finding that GAPDH is toxic for MonoMac 6 but not for HaCaT cells could lie in an enhanced internalization (endocytosis-like?) of GAPDH, which might cause apoptosis, as reported for the *Streptococcus pyogenes* and *S. aureus* GAPDH proteins (10). However, this cytotoxic activity could contribute to the virulence of *S. aureus*, maybe not at the same high level as alpha-toxin but to a noticeable extent. It is quite difficult to mimic the *in vivo* situation exactly since quantification of excreted CPs in an *in vivo* model is not easily feasible. In a host organism, *S. aureus* is continuously challenged by the immune system, which makes it very likely that the amount of released CPs in an infection is by far

higher than that in an *in vitro* culture. Subsequently, cell lysis caused by immune cells is expected. The amount of bacteria in an abscess is strongly dependent on the inoculum and strain and was quantified to approximately 6.5×10^6 using 1×10^6 CFU for the Newman strain (40). However, the number of lysed *S. aureus* cells might be magnitudes higher. *In vitro*, lysostaphin-lysed *S. aureus* cells release roughly 7 μg/ml FbaA (see Fig. S2 in the supplemental material), which is already a concentration that exerts cytotoxic activity. Probably, such concentrations may be reached during abscess formation (23). Indeed, it has been shown that a number of cytoplasmic proteins were enriched in neutrophil-depleted abscesses, and among these enzymes was also GAPDH (60). So far, only toxins, binding proteins, cell wall polymers, and defensin or ROS resistance factors have been considered virulence molecules (61). Now we think, however, that the time has come to consider also excreted cytoplasmic proteins as serious virulence factors. Indeed, in a *Galleria mellonella* infection model, the addition of FbaA and GAPDH aggravated the virulence of JE2 (Fig. 6C). Although *Galleria mellonella* lacks the adaptive immune system of higher mammals, the results show that in the presence of FbaA and GAPDH, the survival of the larvae was significantly decreased.

ACKNOWLEDGMENTS

We thank Regine Stemmler for excellent technical assistance, Cordula Gekeler and Shideh Vatani Shamirzadi for assistance in cell culture, Sebastian Reichert and Lukas Mechler for useful discussion on the topic, and Daniela Eberhart for carefully reading the manuscript. In particular, we thank Kenneth W. Bayles for kindly providing the Nebraska Transposon Mutant Library.

FUNDING INFORMATION

This work, including the efforts of Patrick Ebner and Friedrich Götz, was funded by Deutsche Forschungsgemeinschaft (DFG) (SFB766). This work, including the efforts of Minh Thu Nguyen, was funded by Deutsche Forschungsgemeinschaft (DFG) (SFB TR34). This work, including the efforts of Birgit Schittek, was funded by Deutsche Forschungsgemeinschaft (DFG) (DFG Schi 510/8-1 and TRR156).

REFERENCES

1. **Nickel W.** 2003. The mystery of nonclassical protein secretion. A current view on cargo proteins and potential export routes. Eur J Biochem **270:** 2109–2119.
2. **Wang G, Chen H, Xia Y, Cui J, Gu Z, Song Y, Chen YQ, Zhang H, Chen W.** 2013. How are the non-classically secreted bacterial proteins released into the extracellular milieu? Curr Microbiol **67:**688–695. http://dx.doi.org/10.1007/s00284-013-0422-6.
3. **Pancholi V, Fischetti VA.** 1992. A major surface protein on group A streptococci is a glyceraldehyde-3-phosphate-dehydrogenase with multiple binding activity. J Exp Med **176:**415–426. http://dx.doi.org/10.1084/jem.176.2.415.
4. **Pancholi V, Chhatwal GS.** 2003. Housekeeping enzymes as virulence factors for pathogens. Int J Med Microbiol **293:**391–401. http://dx.doi.org/10.1078/1438-4221-00283.
5. **D'Costa SS, Boyle MD.** 2000. Interaction of group A streptococci with human plasmin(ogen) under physiological conditions. Methods **21:**165–177. http://dx.doi.org/10.1006/meth.2000.0988.
6. **Lottenberg R, Broder CC, Boyle MD, Kain SJ, Schroeder BL, Curtiss R, III.** 1992. Cloning, sequence analysis, and expression in *Escherichia coli* of a streptococcal plasmin receptor. J Bacteriol **174:**5204–5210.
7. **Winram SB, Lottenberg R.** 1996. The plasmin-binding protein Plr of group A streptococci is identified as glyceraldehyde-3-phosphate dehydrogenase. Microbiology **142:**2311–2320. http://dx.doi.org/10.1099/13500872-142-8-2311.
8. **Jin H, Song YP, Boel G, Kochar J, Pancholi V.** 2005. Group A streptococcal surface GAPDH, SDH, recognizes uPAR/CD87 as its receptor on the human pharyngeal cell and mediates bacterial adherence to host cells. J Mol Biol **350:**27–41. http://dx.doi.org/10.1016/j.jmb.2005.04.063.
9. **Madureira P, Baptista M, Vieira M, Magalhaes V, Camelo A, Oliveira L, Ribeiro A, Tavares D, Trieu-Cuot P, Vilanova M, Ferreira P.** 2007. *Streptococcus agalactiae* GAPDH is a virulence-associated immunomodulatory protein. J Immunol **178:**1379–1387. http://dx.doi.org/10.4049/jimmunol.178.3.1379.
10. **Oliveira L, Madureira P, Andrade EB, Bouaboud A, Morello E, Ferreira P, Poyart C, Trieu-Cuot P, Dramsi S.** 2012. Group B streptococcus GAPDH is released upon cell lysis, associates with bacterial surface, and induces apoptosis in murine macrophages. PLoS One **7:**e29963. http://dx.doi.org/10.1371/journal.pone.0029963.
11. **Egea L, Aguilera L, Gimenez R, Sorolla MA, Aguilar J, Badia J, Baldoma L.** 2007. Role of secreted glyceraldehyde-3-phosphate dehydrogenase in the infection mechanism of enterohemorrhagic and enteropathogenic *Escherichia coli*: interaction of the extracellular enzyme with human plasminogen and fibrinogen. Int J Biochem Cell Biol **39:**1190–1203. http://dx.doi.org/10.1016/j.biocel.2007.03.008.
12. **Jeffery CJ.** 1999. Moonlighting proteins. Trends Biochem Sci **24:**8–11. http://dx.doi.org/10.1016/S0968-0004(98)01335-8.
13. **Henderson B, Martin A.** 2013. Bacterial moonlighting proteins and bacterial virulence. Curr Top Microbiol Immunol **358:**155–213. http://dx.doi.org/10.1007/82_2011_188.
14. **Sibbald MJ, Winter T, van der Kooi-Pol MM, Buist G, Tsompanidou E, Bosma T, Schafer T, Ohlsen K, Hecker M, Antelmann H, Engelmann S, van Dijl JM.** 2010. Synthetic effects of *secG* and *secY2* mutations on exoproteome biogenesis in *Staphylococcus aureus*. J Bacteriol **192:**3788–3800. http://dx.doi.org/10.1128/JB.01452-09.
15. **Tjalsma H, Antelmann H, Jongbloed JD, Braun PG, Darmon E, Dorenbos R, Dubois JY, Westers H, Zanen G, Quax WJ, Kuipers OP, Bron S, Hecker M, van Dijl JM.** 2004. Proteomics of protein secretion by *Bacillus subtilis*: separating the "secrets" of the secretome. Microbiol Mol Biol Rev **68:**207–233. http://dx.doi.org/10.1128/MMBR.68.2.207-233.2004.
16. **Ziebandt AK, Becher D, Ohlsen K, Hacker J, Hecker M, Engelmann S.** 2004. The influence of *agr* and σ^B in growth phase dependent regulation of virulence factors in *Staphylococcus aureus*. Proteomics **4:**3034–3047. http://dx.doi.org/10.1002/pmic.200400937.
17. **Nega M, Dube L, Kull M, Ziebandt AK, Ebner P, Albrecht D, Krismer B, Rosenstein R, Hecker M, Götz F.** 2015. Secretome analysis revealed adaptive and non-adaptive responses of the *Staphylococcus carnosus femB* mutant. Proteomics **15:**1268–1279. http://dx.doi.org/10.1002/pmic.201400343.
18. **Pasztor L, Ziebandt AK, Nega M, Schlag M, Haase S, Franz-Wachtel M, Madlung J, Nordheim A, Heinrichs DE, Götz F.** 2010. Staphylococcal major autolysin (Atl) is involved in excretion of cytoplasmic proteins. J Biol Chem **285:**36794–36803. http://dx.doi.org/10.1074/jbc.M110.167312.
19. **Ebner P, Prax M, Nega M, Koch I, Dube L, Yu W, Rinker J, Popella P, Flötenmeyer M, Götz F.** 2015. Excretion of cytoplasmic proteins (ECP) in *Staphylococcus aureus*. Mol Microbiol **97:**775–789. http://dx.doi.org/10.1111/mmi.13065.
20. **Ling E, Feldman G, Portnoi M, Dagan R, Overweg K, Mulholland F, Chalifa-Caspi V, Wells J, Mizrachi-Nebenzahl Y.** 2004. Glycolytic enzymes associated with the cell surface of *Streptococcus pneumoniae* are antigenic in humans and elicit protective immune responses in the mouse. Clin Exp Immunol **138:**290–298. http://dx.doi.org/10.1111/j.1365-2249.2004.02628.x.
21. **Tunio SA, Oldfield NJ, Berry A, Ala'Aldeen DA, Wooldridge KG, Turner DP.** 2010. The moonlighting protein fructose-1, 6-bisphosphate aldolase of *Neisseria meningitidis*: surface localization and role in host cell adhesion. Mol Microbiol **76:**605–615. http://dx.doi.org/10.1111/j.1365-2958.2010.07098.x.
22. **Fey PD, Endres JL, Yajjala VK, Widhelm TJ, Boissy RJ, Bose JL, Bayles KW.** 2013. A genetic resource for rapid and comprehensive phenotype screening of nonessential *Staphylococcus aureus* genes. mBio **4:**e00537-12. http://dx.doi.org/10.1128/mBio.00537-12.
23. **Cheng AG, DeDent AC, Schneewind O, Missiakas D.** 2011. A play in four acts: *Staphylococcus aureus* abscess formation. Trends Microbiol **19:** 225–232. http://dx.doi.org/10.1016/j.tim.2011.01.007.
24. **Bae T, Schneewind O.** 2006. Allelic replacement in *Staphylococcus aureus* with inducible counter-selection. Plasmid **55:**58–63. http://dx.doi.org/10.1016/j.plasmid.2005.05.005.
25. **Geiger T, Francois P, Liebeke M, Fraunholz M, Goerke C, Krismer B,**

Schrenzel J, Lalk M, Wolz C. 2012. The stringent response of *Staphylococcus aureus* and its impact on survival after phagocytosis through the induction of intracellular PSMs expression. PLoS Pathog **8:**e1003016. http://dx.doi.org/10.1371/journal.ppat.1003016.

26. **Gibson DG, Young L, Chuang RY, Venter JC, Hutchison CA, III, Smith HO.** 2009. Enzymatic assembly of DNA molecules up to several hundred kilobases. Nat Methods **6:**343–345. http://dx.doi.org/10.1038/nmeth.1318.
27. **Monk IR, Shah IM, Xu M, Tan MW, Foster TJ.** 2012. Transforming the untransformable: application of direct transformation to manipulate genetically *Staphylococcus aureus* and *Staphylococcus epidermidis*. mBio **3:**e00277-11. http://dx.doi.org/10.1128/mBio.00277-11.
28. **Biswas R, Voggu L, Simon UK, Hentschel P, Thumm G, Götz F.** 2006. Activity of the major staphylococcal autolysin Atl. FEMS Microbiol Lett **259:**260–268. http://dx.doi.org/10.1111/j.1574-6968.2006.00281.x.
29. **Heilmann C, Hussain M, Peters G, Götz F.** 1997. Evidence for autolysin-mediated primary attachment of *Staphylococcus epidermidis* to a polystyrene surface. Mol Microbiol **24:**1013–1024. http://dx.doi.org/10.1046/j.1365-2958.1997.4101774.x.
30. **de Jonge BL, Chang YS, Gage D, Tomasz A.** 1992. Peptidoglycan composition of a highly methicillin-resistant *Staphylococcus aureus* strain. The role of penicillin binding protein 2A. J Biol Chem **267:**11248–11254.
31. **Terrasse R, Amoroso A, Vernet T, Di Guilmi AM.** 2015. *Streptococcus pneumoniae* GAPDH Is released by cell lysis and interacts with peptidoglycan. PLoS One **10:**e0125377. http://dx.doi.org/10.1371/journal.pone.0125377.
32. **Wu Y, Li Q, Chen XZ.** 2007. Detecting protein-protein interactions by Far Western blotting. Nat Protoc **2:**3278–3284. http://dx.doi.org/10.1038/nprot.2007.459.
33. **Kall L, Canterbury JD, Weston J, Noble WS, MacCoss MJ.** 2007. Semi-supervised learning for peptide identification from shotgun proteomics datasets. Nat Methods **4:**923–925. http://dx.doi.org/10.1038/nmeth1113.
34. **Nguyen MT, Kraft B, Yu W, Demicrioglu DD, Hertlein T, Burian M, Schmaler M, Boller K, Bekeredjian-Ding I, Ohlsen K, Schittek B, Götz F.** 2015. The νSaα specific lipoprotein like cluster (*lpl*) of *Staphylococcus aureus* USA300 contributes to immune stimulation and invasion in human cells. PLoS Pathog **11:**e1004984. http://dx.doi.org/10.1371/journal.ppat.1004984.
35. **Yu W, Götz F.** 2012. Cell wall antibiotics provoke accumulation of anchored mCherry in the cross wall of *Staphylococcus aureus*. PLoS One **7:**e30076. http://dx.doi.org/10.1371/journal.pone.0030076.
36. **Barlow M.** 2009. What antimicrobial resistance has taught us about horizontal gene transfer. Methods Mol Biol **532:**397–411. http://dx.doi.org/10.1007/978-1-60327-853-9_23.
37. **Mechler L, Herbig A, Paprotka K, Fraunholz M, Nieselt K, Bertram R.** 2015. A novel point mutation promotes growth phase-dependent daptomycin tolerance in *Staphylococcus aureus*. Antimicrob Agents Chemother **59:**5366–5376. http://dx.doi.org/10.1128/AAC.00643-15.
38. **Peleg AY, Jara S, Monga D, Eliopoulos GM, Moellering RC, Jr, Mylonakis E.** 2009. *Galleria mellonella* as a model system to study *Acinetobacter baumannii* pathogenesis and therapeutics. Antimicrob Agents Chemother **53:**2605–2609. http://dx.doi.org/10.1128/AAC.01533-08.
39. **Olaru F, Jensen LE.** 2010. Chemokine expression by human keratinocyte cell lines after activation of Toll-like receptors. Exp Dermatol **19:**e314–e316. http://dx.doi.org/10.1111/j.1600-0625.2009.01026.x.
40. **Weidenmaier C, McLoughlin RM, Lee JC.** 2010. The zwitterionic cell wall teichoic acid of *Staphylococcus aureus* provokes skin abscesses in mice by a novel $CD4^+$ T-cell-dependent mechanism. PLoS One **5:**e13227. http://dx.doi.org/10.1371/journal.pone.0013227.
41. **Blau K, Portnoi M, Shagan M, Kaganovich A, Rom S, Kafka D, Chalifa Caspi V, Porgador A, Givon-Lavi N, Gershoni JM, Dagan R, Mizrachi Nebenzahl Y.** 2007. Flamingo cadherin: a putative host receptor for *Streptococcus pneumoniae*. J Infect Dis **195:**1828–1837. http://dx.doi.org/10.1086/518038.
42. **Hirschhausen N, Schlesier T, Schmidt MA, Götz F, Peters G, Heilmann C.** 2010. A novel staphylococcal internalization mechanism involves the major autolysin Atl and heat shock cognate protein Hsc70 as host cell receptor. Cell Microbiol **12:**1746–1764. http://dx.doi.org/10.1111/j.1462-5822.2010.01506.x.
43. **Götz F, Yu W, Dube L, Prax M, Ebner P.** 2015. Excretion of cytosolic proteins (ECP) in bacteria. Int J Med Microbiol **305:**230–237. http://dx.doi.org/10.1016/j.ijmm.2014.12.021.
44. **Jeffery CJ.** 2003. Moonlighting proteins: old proteins learning new tricks. Trends Genet **19:**415–417. http://dx.doi.org/10.1016/S0168-9525(03)00167-7.
45. **Sibbald MJ, Ziebandt AK, Engelmann S, Hecker M, de Jong A, Harmsen HJ, Raangs GC, Stokroos I, Arends JP, Dubois JY, van Dijl JM.** 2006. Mapping the pathways to staphylococcal pathogenesis by comparative secretomics. Microbiol Mol Biol Rev **70:**755–788. http://dx.doi.org/10.1128/MMBR.00008-06.
46. **Trost M, Wehmhoner D, Karst U, Dieterich G, Wehland J, Jansch L.** 2005. Comparative proteome analysis of secretory proteins from pathogenic and nonpathogenic *Listeria* species. Proteomics **5:**1544–1557. http://dx.doi.org/10.1002/pmic.200401024.
47. **Xia XX, Han MJ, Lee SY, Yoo JS.** 2008. Comparison of the extracellular proteomes of *Escherichia coli* B and K-12 strains during high cell density cultivation. Proteomics **8:**2089–2103. http://dx.doi.org/10.1002/pmic.200700826.
48. **Li M, Rosenshine I, Tung SL, Wang XH, Friedberg D, Hew CL, Leung KY.** 2004. Comparative proteomic analysis of extracellular proteins of enterohemorrhagic and enteropathogenic *Escherichia coli* strains and their *ihf* and *ler* mutants. Appl Environ Microbiol **70:**5274–5282. http://dx.doi.org/10.1128/AEM.70.9.5274-5282.2004.
49. **Herbert S, Ziebandt AK, Ohlsen K, Schäfer T, Hecker M, Albrecht D, Novick R, Götz F.** 2010. Repair of global regulators in *Staphylococcus aureus* 8325 and comparative analysis with other clinical isolates. Infect Immun **78:**2877–2889. http://dx.doi.org/10.1128/IAI.00088-10.
50. **Rosenstein R, Götz F.** 2013. What distinguishes highly pathogenic staphylococci from medium- and non-pathogenic? Curr Top Microbiol Immunol **358:**33–89. http://dx.doi.org/10.1007/82_2012_286.
51. **Crowe JD, Sievwright IK, Auld GC, Moore NR, Gow NA, Booth NA.** 2003. *Candida albicans* binds human plasminogen: identification of eight plasminogen-binding proteins. Mol Microbiol **47:**1637–1651. http://dx.doi.org/10.1046/j.1365-2958.2003.03390.x.
52. **Puckett S, Trujillo C, Eoh H, Marrero J, Spencer J, Jackson M, Schnappinger D, Rhee K, Ehrt S.** 2014. Inactivation of fructose-1,6-bisphosphate aldolase prevents optimal co-catabolism of glycolytic and gluconeogenic carbon substrates in *Mycobacterium tuberculosis*. PLoS Pathog **10:**e1004144. http://dx.doi.org/10.1371/journal.ppat.1004144.
53. **Rosenstein R, Nerz C, Biswas L, Resch A, Raddatz G, Schuster SC, Götz F.** 2009. Genome analysis of the meat starter culture bacterium *Staphylococcus carnosus* TM300. Appl Environ Microbiol **75:**811–822. http://dx.doi.org/10.1128/AEM.01982-08.
54. **Albrecht T, Raue S, Rosenstein R, Nieselt K, Götz F.** 2012. Phylogeny of the staphylococcal major autolysin and its use in genus and species typing. J Bacteriol **194:**2630–2636. http://dx.doi.org/10.1128/JB.06609-11.
55. **Götz F, Heilmann C, Stehle T.** 2014. Functional and structural analysis of the major amidase (Atl) in *Staphylococcus*. Int J Med Microbiol **304:**156–163. http://dx.doi.org/10.1016/j.ijmm.2013.11.006.
56. **Komatsuzawa H, Sugai M, Nakashima S, Yamada S, Matsumoto A, Oshida T, Suginaka H.** 1997. Subcellular localization of the major autolysin, ATL and its processed proteins in *Staphylococcus aureus*. Microbiol Immunol **41:**469–479. http://dx.doi.org/10.1111/j.1348-0421.1997.tb01880.x.
57. **Yamada S, Sugai M, Komatsuzawa H, Nakashima S, Oshida T, Matsumoto A, Suginaka H.** 1996. An autolysin ring associated with cell separation of *Staphylococcus aureus*. J Bacteriol **178:**1565–1571.
58. **Schlag M, Biswas R, Krismer B, Köhler T, Zoll S, Yu W, Schwarz H, Peschel A, Götz F.** 2010. Role of staphylococcal wall teichoic acid in targeting the major autolysin Atl. Mol Microbiol **75:**864–873. http://dx.doi.org/10.1111/j.1365-2958.2009.07007.x.
59. **Zoll S, Schlag M, Shkumatov AV, Rautenberg M, Svergun DI, Götz F, Stehle T.** 2012. Ligand-binding properties and conformational dynamics of autolysin repeat domains in staphylococcal cell wall recognition. J Bacteriol **194:**3789–3802. http://dx.doi.org/10.1128/JB.00331-12.
60. **Attia AS, Cassat JE, Aranmolate SO, Zimmerman LJ, Boyd KL, Skaar EP.** 2013. Analysis of the *Staphylococcus aureus* abscess proteome identifies antimicrobial host proteins and bacterial stress responses at the host-pathogen interface. Pathog Dis **69:**36–48. http://dx.doi.org/10.1111/2049-632X.12063.
61. **Kobayashi SD, Malachowa N, DeLeo FR.** 2015. Pathogenesis of *Staphylococcus aureus* abscesses. Am J Pathol **185:**1518–1527. http://dx.doi.org/10.1016/j.ajpath.2014.11.030.